PB85-185890

Bench-Scale Process Evaluation of Reburning and Sorbent Injection for In-Furnace NOx/SOx Reduction

Energy and Environmental Research Corp.
Irvine, CA

Prepared for

Environmental Protection Agency
Research Triangle Park, NC

Mar 85

U.S. Department of Commerce
National Technical Information Service
NTIS

PB85-185890

EPA/600/7-85/012
March 1985

BENCH-SCALE PROCESS EVALUATION OF REBURNING AND SORBENT INJECTION FOR IN-FURNACE NO_x/SO_x REDUCTION

by

S.B. Greene, S.L. Chen, W.D. Clark, M.P. Heap,
D.W. Pershing, and W.R. Seeker

Energy and Environmental Research Corporation
18 Mason
Irvine, CA 92718

EPA Contract: 68-02-3925

EPA Project Officer: Robert E. Hall
Air and Energy Engineering Research Laboratory
Research Triangle Park, NC 27711

AIR AND ENERGY ENGINEERING RESEARCH LABORATORY
OFFICE OF RESEARCH AND DEVELOPMENT
U.S. ENVIRONMENTAL PROTECTION AGENCY
RESEARCH TRIANGLE PARK, NC 27711

REPRODUCED BY
NATIONAL TECHNICAL
INFORMATION SERVICE
U.S. DEPARTMENT OF COMMERCE
SPRINGFIELD, VA. 22161

TECHNICAL REPORT DATA
(Please read Instructions on the reverse before completing)

1. REPORT NO.
EPA/600/7-85/012

2.

3. RECIPIENT'S ACCESSION NO.
PB85 185890/AS

4. TITLE AND SUBTITLE
Bench-scale Process Evaluation of Reburning and Sorbent Injection for In-furnace NOx/SOx Reduction

5. REPORT DATE
March 1985

6. PERFORMING ORGANIZATION CODE

7. AUTHOR(S)
S. B. Greene, S. L. Chen, W. D. Clark, M. P. Heap, D. W. Pershing, and W. R. Seeker

8. PERFORMING ORGANIZATION REPORT NO.

9. PERFORMING ORGANIZATION NAME AND ADDRESS
Energy and Environmental Research Corporation
18 Mason
Irvine, California 92714

10. PROGRAM ELEMENT NO.

11. CONTRACT/GRANT NO.
68-02-3925

12. SPONSORING AGENCY NAME AND ADDRESS
EPA, Office of Research and Development
Air and Energy Engineering Research Laboratory
Research Triangle Park, NC 27711

13. TYPE OF REPORT AND PERIOD COVERED
Task Final; 10/83 - 10/84

14. SPONSORING AGENCY CODE
EPA/600/13

15. SUPPLEMENTARY NOTES AEERL project officer is Robert E. Hall, Mail Drop 65, 919/541-2477.

16. ABSTRACT The report gives results of combining reburning with the injection of calcium-based sorbents to investigate the potential for combined NOx and SOx reduction. Reburning, applied to pulverized-coal-fired utility boilers, involves injecting a secondary fuel above the main firing zone to produce a reducing zone where NOx is converted to molecular nitrogen. Overfire air is added above the reburn reducing zone to complete the combustion. Bench-scale evaluations of reburning, carried out in a plug-flow furnace at 23 kWt, have indicated that NOx reductions of up to 70% can be achieved depending on a number of process variables, dominant of which are the initial NOx level that is to be reduced, the reburning fuel type (pulverized coal type or natural gas), and the stoichiometry, residence time, and temperature in the reducing zone. Combining the two processes indicates that the optimum sorbent injection location in a reburning system is with the burnout air because of the increased reactivity of the calcined sorbent. Dolomite consistently produces higher capture than calcitic limestone for a wide spectrum of combustion conditions. It is possible to relate sulfur capture directly to sorbent reactivity as characterized by surface area after calcination. Sulfur capture in a coal-fired system is similar to that obtained with doped propane. Sulfur capture is most dependent on injection temperature.

17. KEY WORDS AND DOCUMENT ANALYSIS

a. DESCRIPTORS		b. IDENTIFIERS/OPEN ENDED TERMS	c. COSATI Field/Group
Pollution	Calcium	Pollution Control	13B
Sulfur Oxides		Stationary Sources	07B
Nitrogen Oxides		Reburning	
Combustion		Secondary Fuels	21B
Pulverized Coal			21D
Sorbents			11G

18. DISTRIBUTION STATEMENT
Release to Public

19. SECURITY CLASS *(This Report)*
Unclassified

20. SECURITY CLASS *(This page)*
Unclassified

21. NO. OF PAGES
269

22. PRICE

EPA Form 2220-1 (9-73)

NOTICE

This document has been reviewed in accordance with U.S. Environmental Protection Agency policy and approved for publication. Mention of trade names or commercial products does not constitute endorsement or recommendation for use.

ABSTRACT

Reburning, as applied to pulverized-coal-fired utility boilers, involves the injection of a secondary fuel above the main firing zone to produce a reducing zone which acts to convert NO_x to molecular nitrogen. Overfire air is added above the reburn reducing zone to complete the combustion. Bench-scale evaluations of the process carried out in a plug-flow furnace at 23 kWt have indicated that NO_x reductions of up to 70% can be achieved depending on a number of process variables. The dominant variables include the initial NO_x level that is to be reduced, the reburning fuel type (pulverized coal type or natural gas), and the stoichiometry, residence time, and temperature in the reducing zone. The reburning process has been combined with the injection of calcium-based sorbents to investigate the potential for combined NO_x and SO_x reduction. The results obtained indicate that the optimum sorbent injection location in a reburning system is with the burnout air because of the increased reactivity of the calcined sorbent. Dolomite consistently produces higher capture than calcitic limestone for a wide spectrum of combustion conditions. It is possible to relate sulfur capture directly to sorbent reactivity as characterized by surface area after calcination. Sulfur capture in a coal-fired system is similar to that obtained with doped propane. Surface area after calcination, and therefore sulfur capture, is most dependent on injection temperature.

TABLE OF CONTENTS

Section Page

Figures ix
Tables xv

Part I--Process Parameter Definition Studies--NO_x

1.0 INTRODUCTION 1-1
  1.1 Background 1-1
  1.2 Purpose and Scope 1-4
2.0 EXPERIMENTAL FACILITIES 2-1
  2.1 Furnace System 2-1
    2.1.1 Control Temperature Tower 2-1
    2.1.2 Main Burner 2-3
  2.2 Measurement Systems and Analytical Methods 2-3
    2.2.1 Flue Gas Sampling 2-3
    2.2.2 Detailed Measurements 2-6
    2.2.3 Temperature Measurements 2-6
3.0 FUEL COMPOSITION 3-1
4.0 EXPERIMENTAL APPROACH 4-1
  4.1 Structure of Parametric Studies 4-1
  4.2 Baseline Conditions 4-3
  4.3 Data Reduction 4-4
5.0 PRELIMINARY MIXING STUDIES 5-1
  5.1 Influence of Primary Effluent Velocity and Reburning Fuel Jet Velocity 5-1
  5.2 Reburning Fuel Injection 5-3
  5.3 Burnout Air Injection 5-10
  5.4 Effects of Reburning Transport Fuel Transport Medium. . 5-15
  5.5 Fuel/Air Premixing 5-18
  5.6 Summary--Baseline Mixing Conditions 5-23
6.0 PRIMARY ZONE PARAMETERS 6-1

Preceding page blank

TABLE OF CONTENTS (Continued)

Section Page

6.1 Primary Zone Stoichiometry 6-1
6.2 Primary Zone NO_x Concentration 6-1
6.3 Primary Fuel Effects 6-4
6.4 Summary 6-10

7.0 REBURNING ZONE PARAMETERS 7-1

7.1 Reburning Zone Stoichiometry 7-1
7.2 Influence of Reburning Fuel Composition 7-1
7.2.1 Hydrocarbon Content 7-1
7.2.2 Fuel Nitrogen Content/Fuel Type 7-5
7.2.3 Coal Composition 7-11
7.2.4 Summary 7-17

7.3 Influence of Residence Time 7-18
7.3.1 Overall Effects 7-20
7.3.2 Fuel Hydrocarbon Content 7-30
7.3.3 Coal Type Dependence 7-30
7.3.4 Summary 7-30
7.4 Impacts of Thermal History 7-35

8.0 BURNOUT ZONE STOICHIOMETRY 8-1

8.1 Burnout Zone Stoichiometry 8-1
8.2 Influence of Thermal Environment 8-1

9.0 CONCLUSIONS ON NO_x CONTROL BY REBURNING 9-1

Part II--Process Parameter Definition Studies--NO_x/SO_x

10.0 INTRODUCTION 10-1

11.0 EXPERIMENTAL FACILITIES 11-1

TABLE OF CONTENTS (Continued)

Section Page

11.1 Furnace Configuration--Experimental Approach 11-1
11.2 Measurement Systems and Analytical Methods 11-3
11.2.1 SO_2 Measurement 11-3
11.2.2 Sorbent Surface Area Measurement 11-3

12.0 SORBENT PROPERTIES 12-1

12.1 Sorbent Composition 12-1
12.2 Sorbent Surface Area 12-1

13.0 PARAMETRIC SCREENING STUDIES 13-1

13.1 Impact on Reburning Effectiveness 13-1
13.2 Reburning Zone Stoichiometry 13-1
13.3 SO_2 Partial Pressure 13-1
13.4 Sulfur Speciation 13-6
13.5 Burnout Zone Stoichiometry 13-6

14.0 SORBENT COMPOSITION EFFECTS 14-1

14.1 Injection Location and Calcination Temperature . . . 14-1
14.2 Influence of Reaction Time/Temperature 14-6

15.0 FUEL COMPOSITION EFFECTS 15-1

15.1 Injection Location 15-1
15.2 Thermal Effects 15-1
15.3 Comparison of Coal and Gas 15-1

16.0 CONCLUSIONS ON NO_x/SO_x STUDIES 16-1

17.0 REFERENCES 17-1

TABLE OF CONTENTS (Concluded)

Section Page

APPENDIX A: QUALITY ASSURANCE A-1

APPENDIX B: DILUTION CORRECTION CALCULATIONS B-1

APPENDIX C: PROCESS MODEL FOR NO_x REDUCTION BY REBURNING C-1

APPENDIX D: SULFUR CAPTURE MODEL D-1

LIST OF FIGURES

Figure Page

1-1 The Reburning Process 1-3

2-1 Cross-Sectional Views of the Control Temperature Tower . 2-2

2-2 Multi-Layer Design of the CTT 2-4

2-3 Premixed Burner 2-5

2-4 Continuous Monitoring Flue Gas Sampling System 2-7

2-5 HCN and NH_3 Sampling Train 2-8

2-6 N_2O Sampling Train 2-9

2-7 Gas Temperature Measurement System 2-10

4-1 Experimental Approach to Reburning Process 4-2

4-2 Time/Temperature Profiles at Baseline Conditions 4-5

4-3 Examples of Data Reduction 4-6

5-1 Fast and Slow Primary Effluent Velocity Configurations . 5-2

5-2 Influence of Primary Velocity 5-4

5-3 Influence of Reburning Fuel Jet Velocity 5-5

5-4 Comparison of Extreme Reburning Zone Mixing Conditions . 5-6

5-5 Influence of Primary Velocity 5-7

5-6 Reburning Fuel Injection Methods 5-8

5-7 Influence of Reburning Fuel Injector 5-9

5-8 Influence of Reburning Fuel Injector at Elevated Levels of $(NO_x)_p$ and Reduced Values of SR_1 5-11

5-9 Burnout Air Injection Methods 5-12

5-10 Influence of Mixing Conditions in the Burnout Zone . . . 5-13

5-11 Influence of Mixing Conditions in the Burnout Zone . . . 5-14

5-12 Influence of Reburning Fuel Transport Medium 5-16

LIST OF FIGURES (Continued)

Figure Page

5-13 Influence of Transport Medium--Axial Fuel Injector . . . 5-17

5-14 Influence of Transport Medium--Radial Fuel Injector . . . 5-19

5-15 Influence of Transport Medium in Coal Reburning at High $(NO_x)_p$ 5-20

5-16 Effect of Fuel/Air Premixing 5-21

5-17 Effect of Fuel/Air Premixing 5-22

6-1 Influence of Primary Zone Stoichiometry 6-2

6-2 Influence of $(NO_x)_p$ 6-3

6-3 Detailed Measurements at Two $(NO_x)_p$ Concentrations . . . 6-5

6-4 TFN at Two $(NO_x)_p$ Concentrations 6-6

6-5 Conversions of $(NO_x)_p$ to TFN and TFN to $(NO_x)_{ex}$ 6-7

6-6 Effectiveness Depends on Primary NO_x 6-8

6-7 Influence of Primary Fuel Type 6-9

7-1 Influence of Reburning Zone Stoichiometry 7-2

7-2 Detailed Measurements, Variable SR_2 7-3

7-3 Hydrocarbon vs. Non-Hydrocarbon Reburning Fuels 7-4

7-4 XN Species Concentrations at the Exit of the Reburning Zone 7-6

7-5 Conversion in Different Zones 7-7

7-6 XN Species Concentrations at the Exit of the Reburning Zone 7-8

7-7 Conversion in Different Zones 7-9

7-8 Influence of Reburning Fuel Nitrogen Content 7-10

7-9 Influence of Fuel Type 7-12

7-10 Detailed Measurements 7-13

LIST OF FIGURES (Continued)

Figure Page

7-11 Conversions in the Reburning and Burnout Zones 7-14

7-12 Conversion of Inlet Nitrogen Species to NO_x 7-15

7-13 Comparison of Different Coals 7-16

7-14 Conversion of Inlet Nitrogen to $(NO_x)_{ex}$ 7-18

7-15 Reburning Zone Entrance (T_1) and Exit (T_2) Temperatures at Two Residence Times 7-19

7-16 Influence of Residence Time 7-21

7-17 Influence of Residence Time 7-22

7-18 Reburning Effectiveness as a Function of Residence Time . 7-23

7-19 Detailed Measurements at Two Residence Times 7-24

7-20 Conversion at Different Residence Times 7-25

7-21 Detailed Measurements at Two Residence Times 7-26

7-22 Conversions at Different Residence Times 7-27

7-23 Detailed Measurements at Two Residence Times 7-28

7-24 Conversions at Two Residence Times 7-29

7-25 Residence Time effects 7-31

7-26 Residence Time effects 7-32

7-27 Influence of Residence Time 7-33

7-28 Influence of Residence Time 7-34

7-29 Reburning Zone Temperatures, Baseline and High T_1 7-36

7-30 Influence of Reburning Zone Temperature 7-37

7-31 Influence of Reburning Zone Temperature 7-38

7-32 Effects of Reburning Zone Time/Temperature 7-39

8-1 Influence of Burnout Zone Stoichiometry 8-2

LIST OF FIGURES (Continued)

Figure		Page
8-2	Influence of Auxiliary Heating on Burnout Zone Temperatures	8-3
8-3	Emissions at Two Burnout Zone Temperatures	8-4
8-4	Emissions at Two Burnout Zone Temperatures	8-5
8-5	Effect of Burnout zone Cooling	8-6
11-1	CTT Configuration for SO_x Studies	11-2
11-2	Time-Temperature Profile at Baseline Conditions	11-4
11-3	Continuous Monitoring Gas Sampling System	11-5
11-4	Sorbent Sampling System	11-7
12-1	Vicron Surface Area as a Function of Residence Time and Cooling Rate	12-3
12-2	Limestone Surface Area as a Function of Peak Calcination Temperature	12-4
12-3	Sorbent Surface Area as a Function of Peak Calcination Temperature	12-6
13-1	Influence of Reburning Zone Stoichiometry on SO_2 Capture	13-3
13-2	Time/Temperature Histories at Three SR_2 Values	13-4
13-3	Sulfur Captures as a Function of Initial SO_2 Concentrations	13-5
13-4	Model Predictions	13-7
13-5	Impact of Initial Forms of Sulfur	13-8
13-6	Impact of Initial Forms of Sulfur	13-9
13-7	Effect of Burnout Zone Stoichiometry	13-10
14-1	Influence of Sorbent Injection Location	14-2
14-2	Time/Temperature Profile at Baseline Condition	14-3

LIST OF FIGURES (Continued)

Figure Page

14-3 Comparison of Sorbent Type 14-4

14-4 Capture vs. Sorbent Surface Area 14-5

14-5 Model Predictions 14-7

14-6 Reaction Zone Temperature Profiles 14-8

14-7 Reaction Zone Temperature Effects 14-9

14-8 Comparison of Model Predictions with Observed SO_2 Captures 14-10

15-1 Influence of Sorbent Injection Location 15-2

15-2 Reaction Zone Temperature Effects 15-3

15-3 Comparison of Coal and Gas 15-4

15-4 Time Temperature Profiles of Propane and Indiana Coal . . 15-5

15-5 Comparison Between Coal and Gas 15-7

A-1 Continuous Monitoring Sampling System A-6

A-2 SO_2 Continuous Monitoring System A-7

A-3 HCN and NH_3 Sampling Train A-9

A-4 Schematic of Water-Spray Probe A-10

A-5 N_2O Sampling Train A-11

A-6 Solids Sampling System A-12

A-7 Gas Temperature Measurement System A-14

A-8 Suction Pyrometer Aspirator Pressure Calibration A-15

A-9 Replicate Coal Size Distributions A-26

A-10 Size Distribution of Vicron 45-3 . . . . A-28

A-11 Precision of Gas Temperature Measurements A-30

A-12 Calculation of HCN and NH_3 Results A-32

A-13 XN Concentrations at Exit of Reburning Zone A-33

LIST OF FIGURES (Concluded)

Figure		Page
A-14	NO_x Emissions with Reburning	A-34
A-15	SO_2 Capture Data	A-36
B-1	Conceptual Layout of the Reburning Process	B-2
C-1	Composite Process Model	C-2
C-2	Composite Model Verification	C-8
C-3	Effect of SR_2	C-9
C-4	Effect of Primary NO Concentration	C-11
C-5	Effect of Fuel N Content	C-12
C-6	Effect of Secondary Residence Time	C-13
D-1	Zone Approach to Sulfur Capture Model	D-2
D-2	Effect of Peak Temperature on Sorbent Surface Area . . .	D-4
D-3	Conceptual Illustration of Pore Model for CaO/SO_2 Reaction	D-6
D-4	Application of Random Pore Model to Data Of Borgwardt . .	D-8
D-5	Model Comparison	D-10
D-6	Predicted Effect of Pore Structure Parameters	D-12
D-7	Predicted Effect of Temperature	D-13
D-8	Predicted Effect of Ca/S Ratio	D-15
D-9	Predicted Effect of SO_2 Concentration	D-16
D-10	Effect of SO_2 Concentration	D-17
D-11	Predicted Effect of Intrinsic Rate Constant	D-18
D-12	Predicted Effect of Product Layer Diffusivity	D-19
D-13	Predicted Effect of Particle Density	D-20
D-14	Predicted Effect of Particle CaO Content	D-21
D-15	Predicted Effect of Particle Size	D-22

LIST OF TABLES

Table — Page

3-1 Fuel Analysis 3-2

3-2 Relative Composition of Coals Tested 3-3

11-1 Sorbent Sampling System Shakedown Results 11-8

12-1 Sorbent Properties 12-2

13-1 Influence of SO_2 and Sorbent on Reburning Effectiveness in NO_x Reduction 13-2

A-1 Program Objectives for Measurement Precision, and Accuracy A-2

A-2 Sampling Procedures A-4

A-3 Calibration Procedures A-16

A-4 Calibration Gases A-19

A-5 Analytical Procedures A-20

A-6 Continuous Gas Analysis Instruments A-23

A-7 Comparison of Measurement Precision and Accuracy with Program Goals A-37

A-8 Comparison of Continuous Monitoring Instrumentation with EPA Reference Methods A-38

C-1 Fenimore Homogeneous Kinetics C-4

C-2 De Soete Heterogeneous Kinetics C-5

C-3 Test Conditions C-7

D-1 Baseline Conditions D-11

Part I--Process Parameter Definition Studies--NO_x

1.0 INTRODUCTION

Since it was first recognized that nitrogen oxides (NO_x) emitted by stationary sources made a significant contribution to the degradation of air quality, there have been considerable advances in control technology to reduce emissions. NO_x control technologies fall into two categories: those which prevent the formation of nitric oxide (NO) and those which remove NO from the products of combustion. Nitric oxide is formed during combustion either from molecular nitrogen or from nitrogen contained in the fuel. Modification of the combustion process to change peak temperatures and maximize residence times under fuel-rich conditions minimize NO formation from both of these sources. Consequently, provided the process requirements are satisfied combustion modification provides a cost effective method of controlling NO_x emissions. However, when the process is not tolerant to combustion modification or very low emission levels are required it may be necessary to use flue gas cleaning techniques to remove NO_x from the combustion products. This report addresses a technology which removes NO from combustion products using fuel as the reducing agent and involves similar kinetic processes to those involved in combustion modification techniques. This technology is variously referred to as:

- In-furnace NO_x reduction
- Reburning
- Staged fuel injection
- "MACT"

Reburning can be considered as the process which allows "in-furnace NO_x reduction" to take place.

1.1 Background

The basic concepts associated with in-furnace NO_x reduction by reburning are not new. The reduction of NO by flames has been appreciated for over a decade. A flue gas NO_x incinerator was developed by the John Zinc Company (Reed, 1969). The term "reburning" was coined by Wendt, Sternling and

Matovich (1973) who reduced NO produced in a laboratory scale flat flame by adding methane or ammonia to the combustion products. Recently, Japanese investigators have reported the application of reburning to large test furnaces (Takahash, 1981). The MACT (Mitsubishi Advanced Combustion Technology) in-furnace NO_x removal process applies the concept of reburning to a boiler. Part of the fuel bypasses the main heat release zone and is injected above the main burners to provide the fuel for reburning. It is claimed that the NO_x produced by the main firing system can be reduced "to half at any level of concentration," (Takahashi, 1981). However, recent results obtained under EPA Fundamental Combustion Research program indicate that the effectiveness of the reburning concept depends heavily on the fuel rich zone stoichiometry and the reburning fuel nitrogen content (Chen et al. 1982)

The reburning process can be divided into three zones as shown in Figure 1-1:

- Primary Zone. This main heat release zone accounts for approximately 90 percent of the total heat input to the system. Operating under fuel lean conditions, the primary zone produces the initial NO_x species.

- Reburning Zone. Reburning fuel is injected downstream of the primary zone to create a fuel-rich mixture. Three major general reactions take place in the reburning zone which affect the reburning process:

  1. NO reacts with hydrocarbon radicals by reactions such as

     $$\begin{aligned} NO + CH &\longrightarrow N + CHO \\ &\longrightarrow HCN + O \end{aligned}$$

     which increases the nitrogen radical pool.

  2. Interconversion of nitrogen species among different fixed nitrogen compounds (NO, HCN, or NH_3). (In this report, the expression XN is used to refer generically to any of these three fixed nitrogen species.)

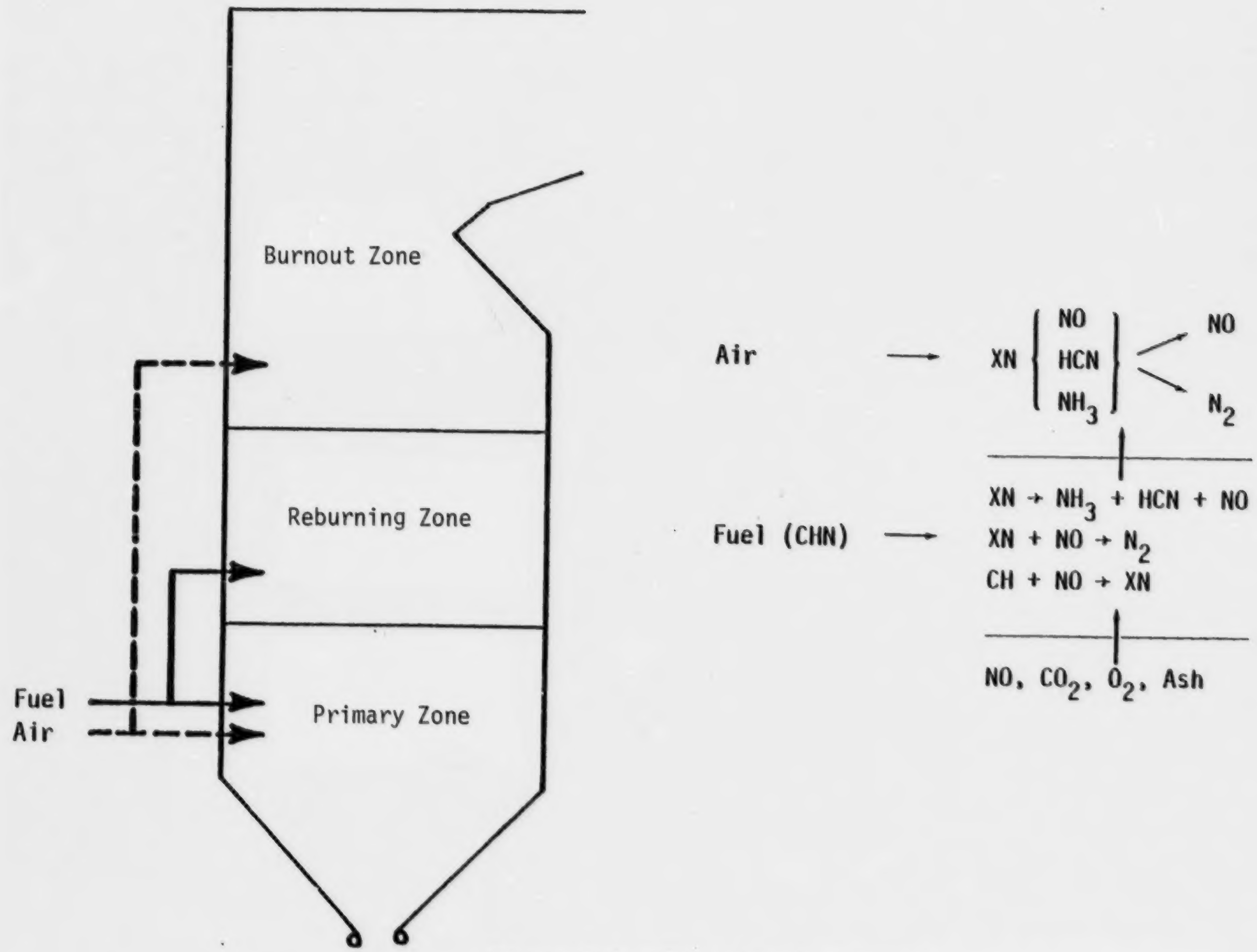
Burnout Zone
Reburning Zone
Primary Zone
Fuel
Air
Air
Fuel (CHN)
XN
NO
HCN
NH_3
NO
N_2
XN → NH_3 + HCN + NO
XN + NO → N_2
CH + NO → XN
NO, CO_2, O_2, Ash

Figure 1-1. The reburning process.

3. The formation of molecular nitrogen by the reaction of nitrogen radicals with NO. The reaction

$$NO + N \longrightarrow N_2 + O$$

sometimes referred to as the "back-Zeldovich" reaction mechanism, is the most probable path although reactions with NH_i species are possible.

Consequently, the nitrogen oxide formed in the primary zone is converted either to N_2, NH_3, HCN, or retained as NO. When the reburning fuel contains nitrogen (e.g., if the reburning fuel is coal), coal nitrogen could remain with the char or form NO, HCN, and NH_3. Thus, the products of this zone contain nitrogen species which can be converted to NO, namely char nitrogen, NH_3, and HCN, as well as NO. The sum of these gas-phase species is referred to as total fixed nitrogen (TFN).

- Burnout Zone. In the burnout zone, air is added to produce overall fuel-lean conditions which oxidize all the remaining fuel. The TFN or char nitrogen is either converted to NO or partially to N_2. Emissions are minimized if the TFN conversion is minimized and this zone is analogous to the second stage of a staged combustion process. Combustion must be completed efficiently, but the ultimate NO_x levels must be minimized.

Appendix C describes a composite process model for prediction of NO_x reduction by reburning.

1.2 Purpose and Scope

The purpose of the Task 2 experimental study was to define the parameters which influence the fate of nitrogen species in these three zones. The parameters of principle interest were:

- The level of NO in the primary zone.

- The temperature, stoichiometry and residence time in the reburning and burnout zones.

- The properties of the reburning fuel, particularly the fuel nitrogen content, the nitrogen volatility and the carbon/hydrogen ratio.

This report summarizes all of the results from the bench scale experiments. Various fuels, including H_2, CO, C_3H_8, C_3H_8 doped with NH_3, and coals, were tested in the bench scale furnace (Control Temperature Tower) with well-defined conditions in each of the three zones. Exhaust and in-flame measurements were made to quantify the influence of process parameters on the effectiveness of reburning.

2.0 EXPERIMENTAL FACILITIES

2.1 Furnace System

The design objective for the bench scale combustor was to simulate combustion conditions typical of United States designed pulverized coal-fired boilers. In addition, the combustor system must exhibit sufficient flexibility such that specific combustion conditions may be varied. Specific design considerations included:

- Duplication of typical furnace zone time/temperature histories of utility boilers and the ability to change the thermal profiles.
- Variation of reburning fuel and air addition techniques.
- Ability to fire either gaseous or solid fuels as primary and reburning fuels.
- Ability to make both in-combustor and exhaust measurements of solids and gaseous composition.

2.1.1 Control Temperature Tower

An overall diagram of the control temperature tower furnace (CTT) is presented in Figure 2-1. The reactor entry (top section) includes a 45.7 cm long quarl that diverges from 5.1 cm to 20.3 cm. The long quarl provided flame stabilization as well as established a one-dimensional flow pattern. Numerous ports located along the axis of the reactor enabled supplementary equipment; i.e., zone seperation chokes, fuel and air injectors, and cooling coils.

The CTT had the capability of manipulating the time/temperature profile by firing one or both of the back-fired heating sections (second and fourth sections from the top). The back-fired sections employed natural gas burners which fired in the direction opposite to the main combustion gas. The back

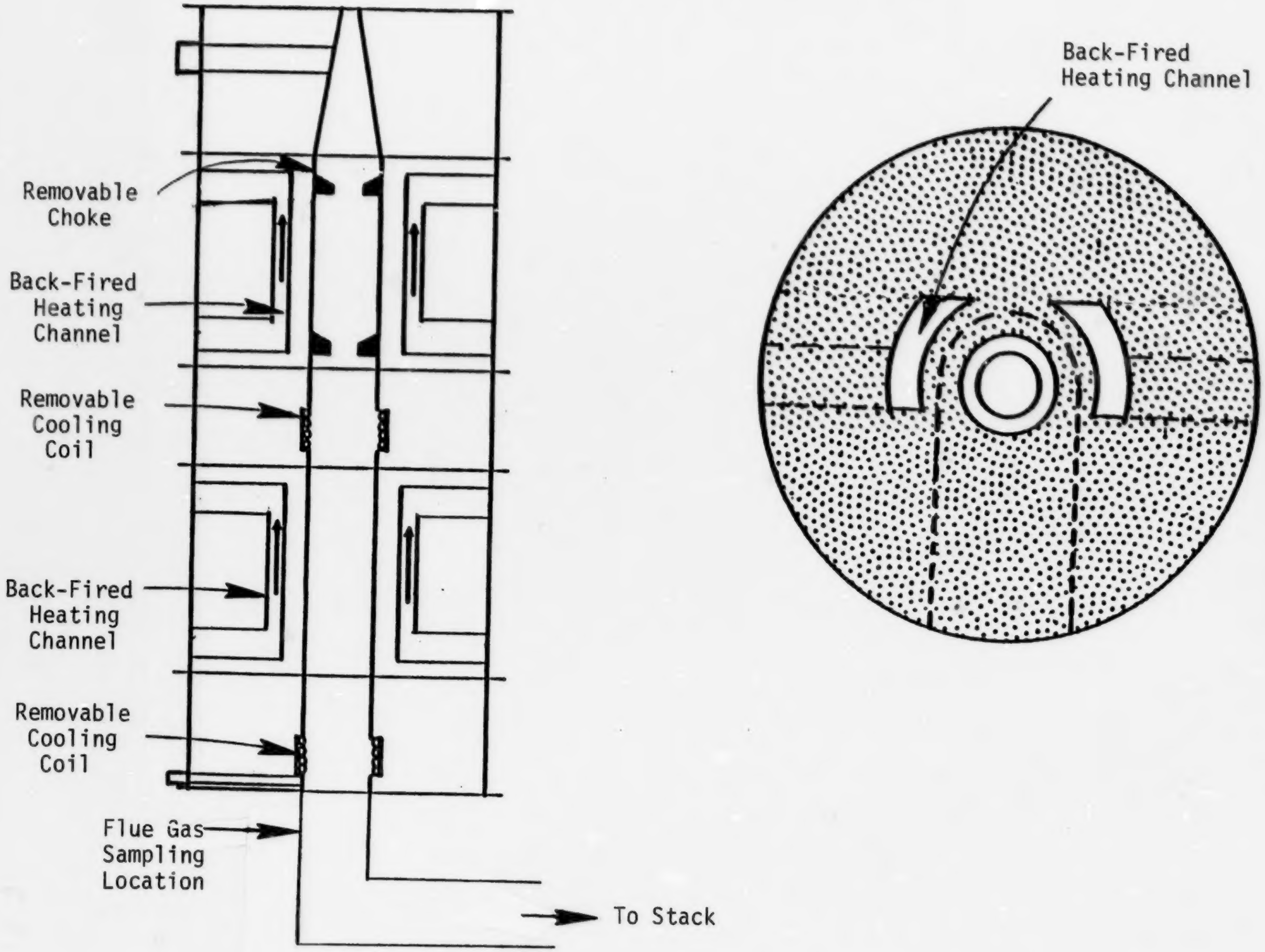
Removable Choke
Back-Fired Heating Channel
Removable Cooling Coil
Back-Fired Heating Channel
Removable Cooling Coil
Flue Gas Sampling Location
To Stack
Back-Fired Heating Channel

Figure 2-1. Cross-sectional views of the control temperature tower.

fired effluent passed through channels in the refractory walls surrounding the main combustion zone (see the radial cross-sectional view in Figure 2-1). Backfiring in this manner minimized the temperature decay of the combustion products in the main combustion zone. Additional alteration of the temperature profile could be accomplished by inserting cooling coils in the main combustion chamber.

Each section of the CTT was fabricated from a 91.4 cm diameter steel shell (0.32 cm thick), two layers of castable insulation and two layers of castable refractory. The multi-layer design of the CTT is illustrated in Figure 2-2.

2.1.2 Main Burner

The cross-sectional layout of the premixed burner used on the CTT is shown in Figure 2-3. The primary air and fuel (propane or coal) were injected radially outward through six 0.32 cm holes into a mixing chamber. The preheated secondary air is injected radially inward into the mixing chamber where the air and fuel are uniformly mixed. The premixed burner produced essentially a one-dimensional, plug-flow flame with no backmixing. Preignition of the fuel/air mixture in the mixing chamber was prevented by the cooling matrix located at the exit of the burner.

2.2 Measurement Systems and Analytical Methods

2.2.1 Flue Gas Sampling

Flue gas sampling was conducted with a stainless-steel, water-cooled probe (jacketed with cooling water) and the following gas species were continuously measured by the method indicated:

- NO_x-chemiluminescence
- O_2-paramagnetism

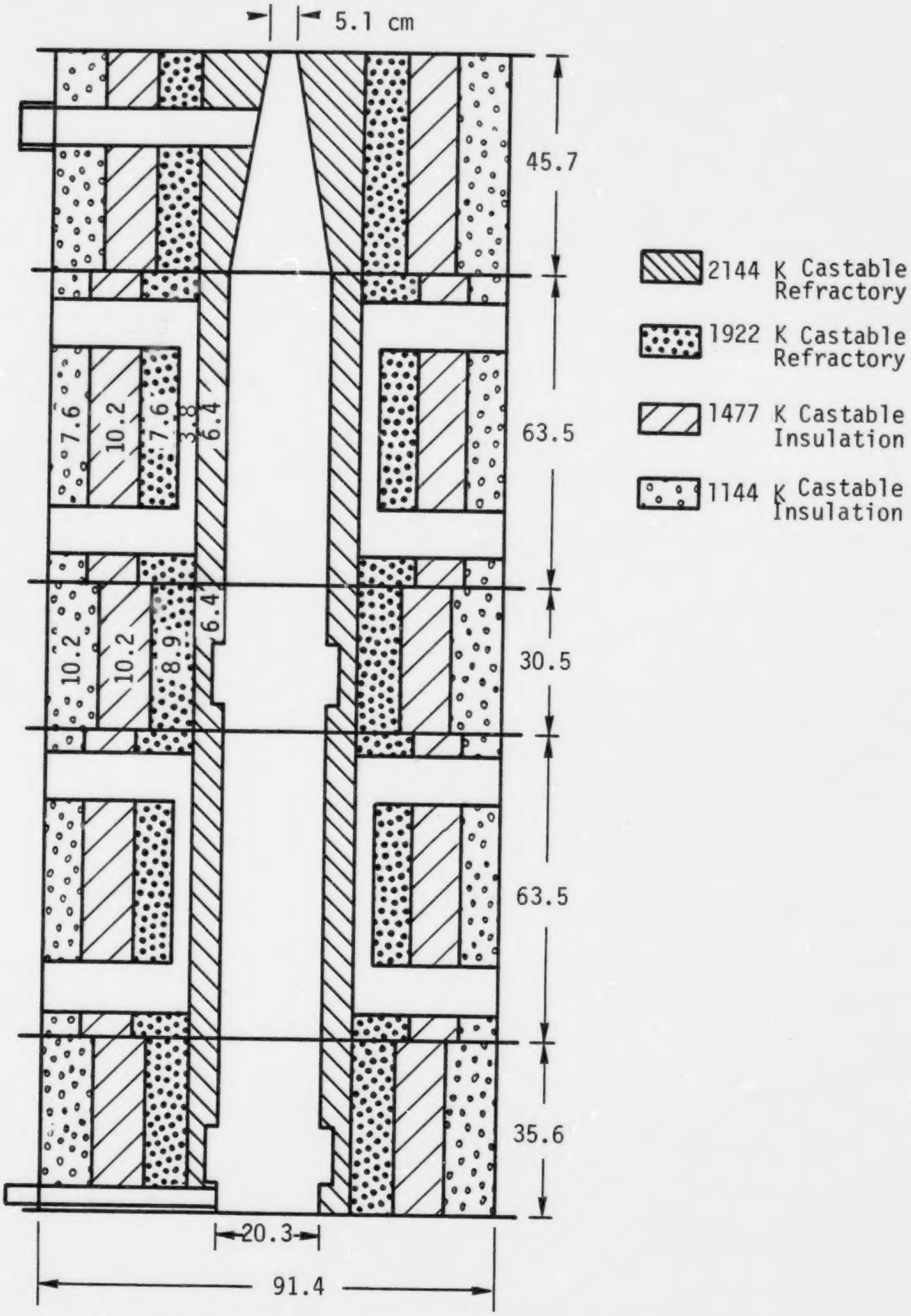
5.1 cm
45.7
63.5
30.5
63.5
35.6
7.6
10.2
7.6
3.8
6.4
10.2
10.2
8.9
6.4
20.3
91.4
2144 K Castable Refractory
1922 K Castable Refractory
1477 K Castable Insulation
1144 K Castable Insulation

Figure 2-2. Multi-layer design of the C.T.T.

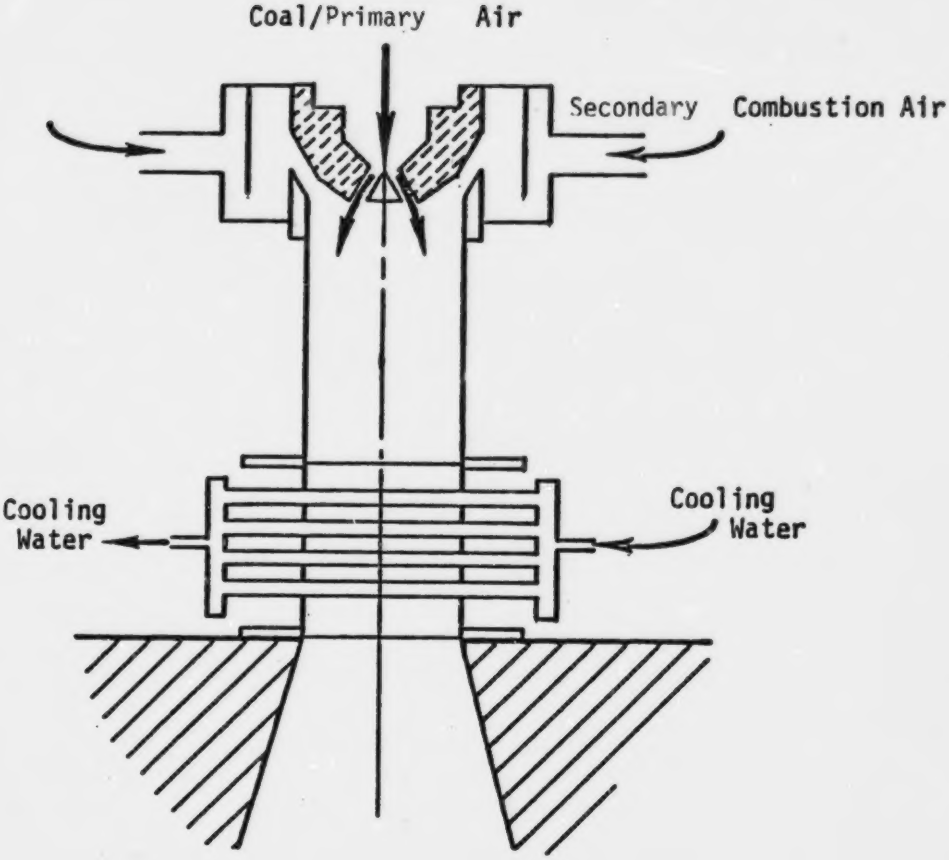
Coal/Primary Air
Secondary Combustion Air
Cooling Water
Cooling Water

Figure 2-3. Premixed burner.

- CO/CO_2 nondispersive infrared

The schematic of the sampling system is shown in Figure 2-4. Precision and accuracy data for the sampling techniques described in this report are presented in Appendix A.

2.2.2 Detailed Measurements

Sampling of HCN and NH_3 at exit of the reburning zone was performed with the sampling train represented in Figure 2-5. A water quench probe was used to "freeze" any reactions at the probe tip. The gas sample was withdrawn through a gas washing impinger and bubbler to remove any HCN and NH_3 in the gas stream. The concentrations of CN^- and dissolved ammonia in the sample solutions were analyzed with specific ion electrodes. Measurement of N_2O was made with the sampling train shown in Figure 2-6. After the gas sample was transferred to the Tedlar bag, the concentration of N_2O was determined by syringe injection into a gas chromatograph.

2.2.3 Gas Temperature Measurement

Gas temperatures were measured with a B-type thermocouple in a suction pyrometer jacket as shown in Figure 2-7. The pyrometer was placed in the flue gas stream with the opening in the alumina sheath pointing downstream. A sufficient gas sample was drawn around the thermocouple tip such that the convective heat transfer of the gas to the thermocouple dominated over the radiation heat loss of the thermocouple tip to the surroundings.

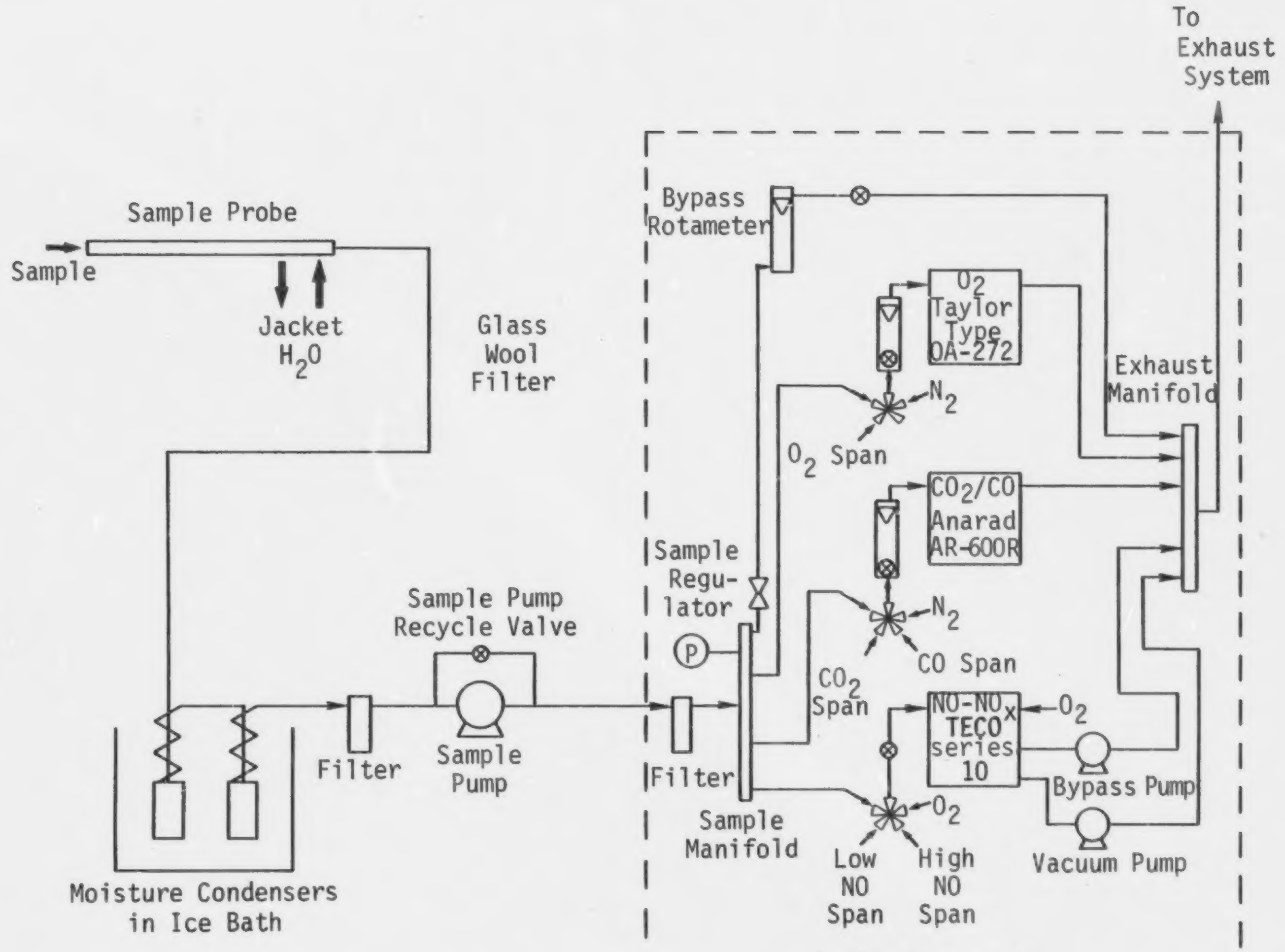
To Exhaust System
Sample Probe
Sample
Jacket H_2O
Glass Wool Filter
Bypass Rotameter
O_2 Taylor Type OA-272
N_2
O_2 Span
Exhaust Manifold
CO_2/CO Anarad AR-600R
N_2
CO Span
CO_2 Span
Sample Regu-lator
P
Sample Pump Recycle Valve
Sample Pump
Filter
Filter
Sample Manifold
NO-NO_x TECO series 10
O_2
O_2
Bypass Pump
Vacuum Pump
Low NO Span
High NO Span
Moisture Condensers in Ice Bath
Analysis Console

Figure 2-4. Continuous monitoring flue gas sampling system.

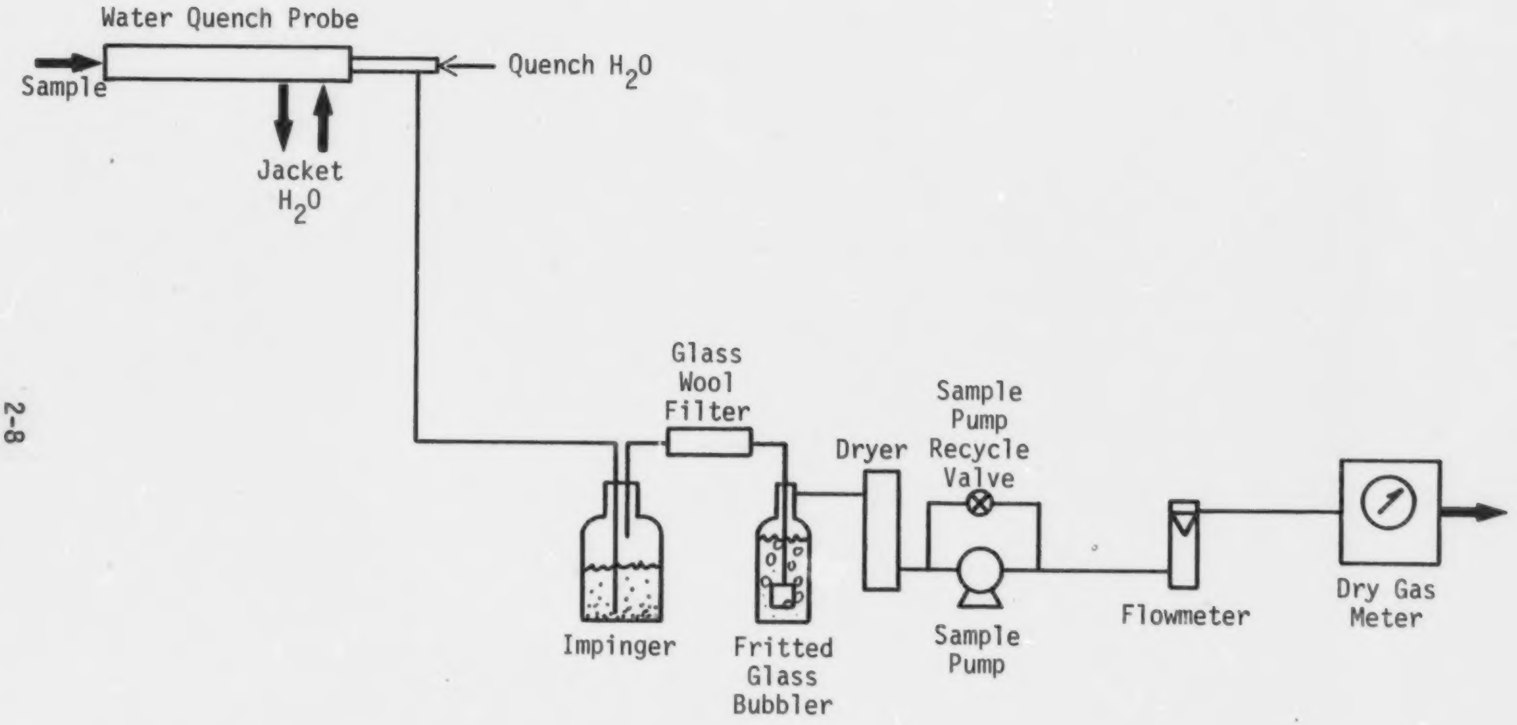
Water Quench Probe
Sample
Quench H_2O
Jacket H_2O
Glass Wool Filter
Sample Pump Recycle Valve
Dryer
Impinger
Fritted Glass Bubbler
Sample Pump
Flowmeter
Dry Gas Meter

Figure 2-5. HCN and NH_3 sampling train.

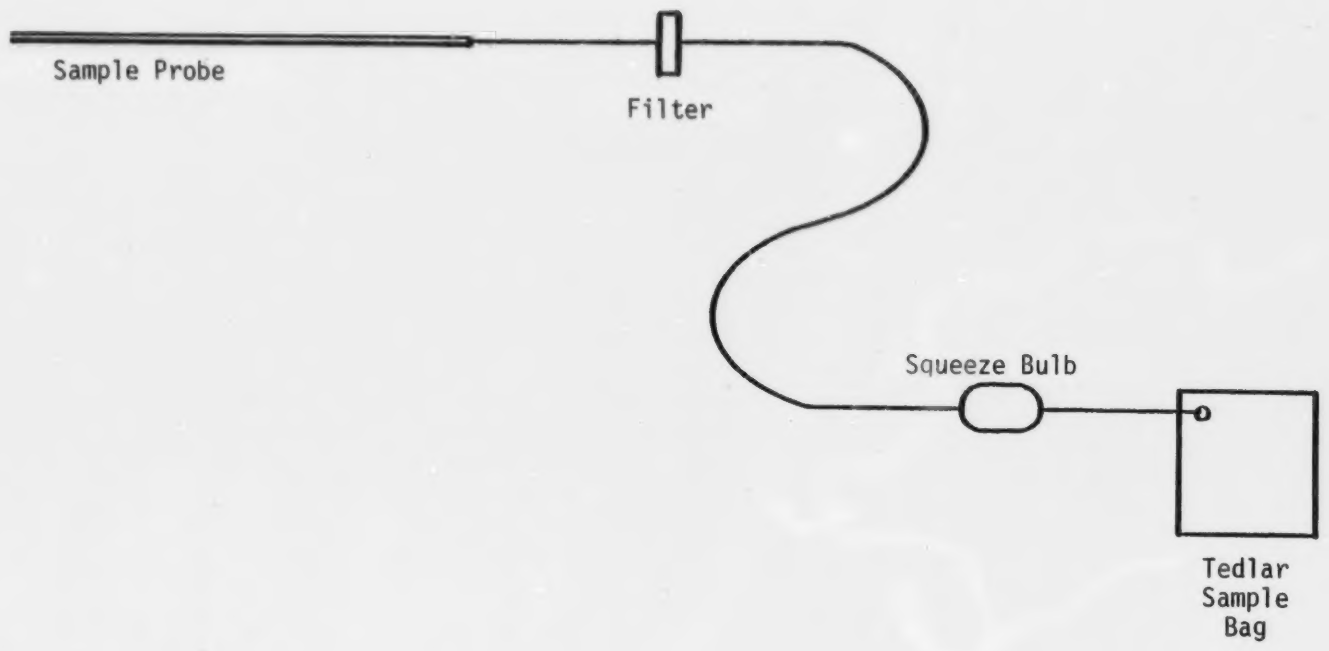
Sample Probe
Filter
Squeeze Bulb
Tedlar
Sample
Bag

Figure 2-6. N_2O sampling train.

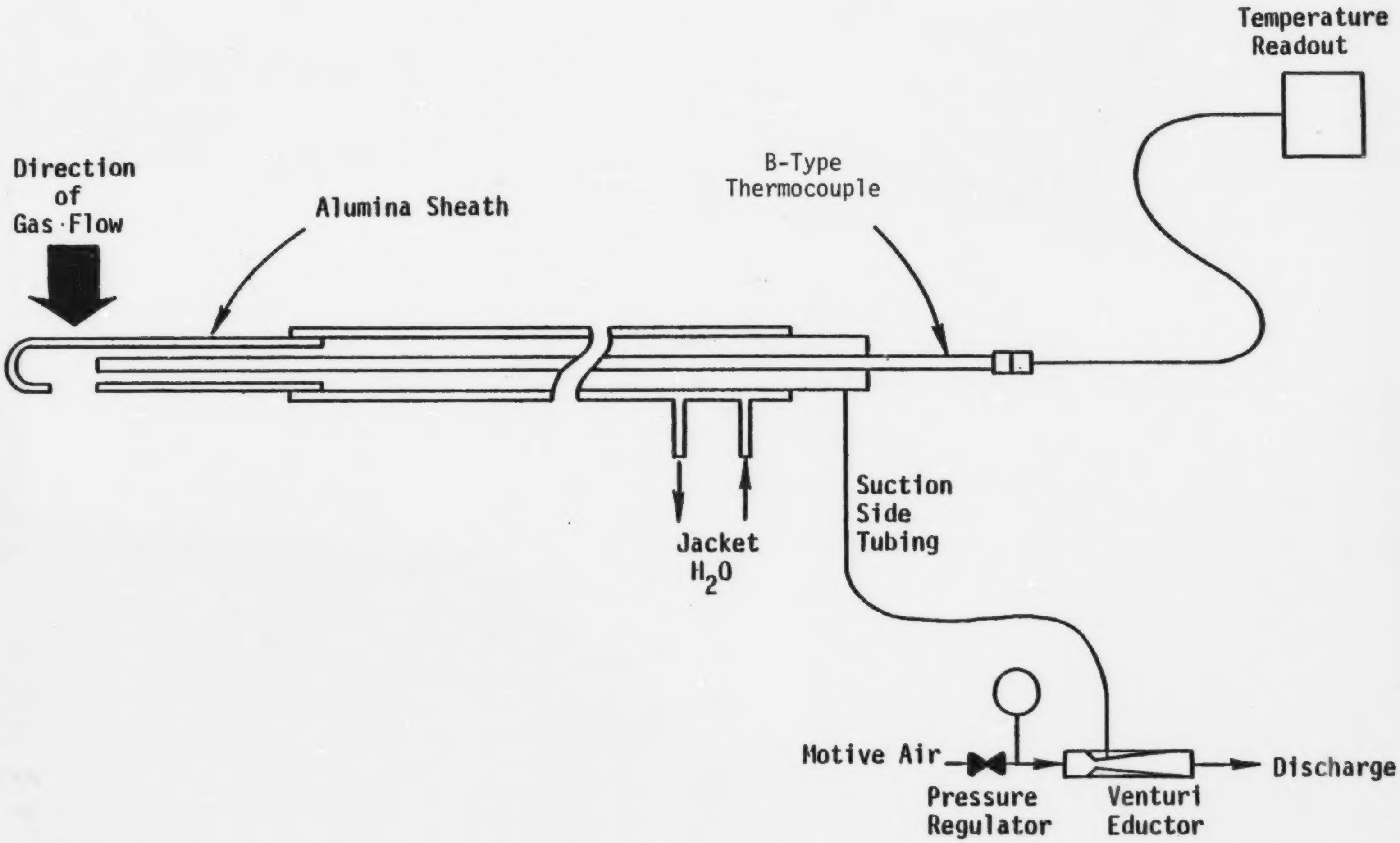
Direction
of
Gas·Flow
Alumina Sheath
B-Type
Thermocouple
Temperature
Readout
Jacket
H_2O
Suction
Side
Tubing
Motive Air
Pressure
Regulator
Venturi
Eductor
Discharge

Figure 2-7. Gas temperature measurement system.

3.0 FUEL COMPOSITION

Some of the testing reported here was performed using NO-doped propane as the primary fuel, and utilizing a gas-propane, H_2, CO, or propane doped with ammonia as the reburning fuel. This was done in order to enable an understanding of the process, separating out any coal-related effects, and to provide an indication of the performance that might be achieved if gas were used as the reburning fuel commercially.

A number of coals were also tested as the reburning fuel (and sometimes as the primary fuel), since coal might be a logical reburning fuel for use in a commercial coal-fired boiler. The coals investigated as reburning fuels are listed in Table 3-1 with their respective ultimate and proximate analyses. Coals from each classification were chosen, ranging from anthracitic to brown coals. Table 3-2 summarizes the specific fuel properties of interest: fuel nitrogen content, volatile matter content, and the inert pyrolysis HCN yield. The solid fuels were prepared for use by pulverization to an average size of 80 weight percent passing 200 mesh screen.

T 3-1
T 3-2

TABLE 3-1. FUEL ANALYSIS

Property \ Fuel	Yallourn, Australia	Beulah, ND	Coalstrip, MT	Indiana	Pennsylvania	Rosa AL	Utah
Rank	Brown	Lig A	Sub B	HVB	Anthracite	MV	HVB
Proximate Analysis (Percent, as received)							
Moisture	13.97	33.10	21.27	4.54	5.13	8.02	6.39
Ash	1.26	7.12	9.58	8.96	5.74	6.79	7.40
Volatile Matter	45.20	28.65	30.82	37.73	4.39	21.81	38.89
Fixed Carbon	39.57	31.13	38.33	48.77	84.74	63.38	47.32
Calorific Value MJ/kg	21.93	16.86	21.34	28.42	30.54	31.17	28.72
Sulfur	0.20	0.76	0.50	1.87	0.44	0.96	0.64
Ultimate Analysis (Percent, dry)							
C	66.03	65.29	67.52	71.17	88.45	81.23	73.17
H	4.55	3.96	4.36	4.75	2.14	4.73	5.55
N	0.55	0.99	1.38	1.44	0.79	1.74	1.54
S	0.23	1.14	0.63	1.96	0.47	1.04	1.54
Ash	1.46	10.64	12.17	9.39	6.05	7.38	7.90
O	27.18	17.98	13.94	11.29	2.10	3.88	11.39

TABLE 3-2. RELATIVE COMPOSITION OF COALS TESTED.

	Rank	Volatile Matter (%) (daf)	Fuel Nitrogen (%) (daf)	Pyrolysis HCN Yield (%)
Pennsylvania	Anthracite	4.9	0.84	2.8
Rosa, AL	MV	25.6	1.88	18.8
Utah	HVB	45.1	1.67	38.1
Colstrip, MT	Sub B	44.6	1.57	
Beulah, ND	Lig A	44.7	1.11	21.1
Australia	Brown	55.7	0.68	45.7

4.0 EXPERIMENTAL APPROACH

The experimental approach to the reburning process is outlined in Figure 4-1. Conceptually, the process can be divided into three zones: a fuel lean primary zone in which the majority of the total fuel is burned, a fuel-rich secondary or reburning zone, and a final tertiary or burnout zone operated at lean conditions. The characteristic stoichiometries of the primary, reburning, and burnout zones are referred to as SR_1, SR_2, and SR_3, respectively.

The experimental conditions investigated were all performed as a function of variable reburning zone stoichiometry. The reburning zone stoichiometry was varied by varying the feed rate of reburning fuel while the primary zone firing rate was held constant. By running the experiment in this manner, the following operating characteristics were obtained:

- Approximately constant reburning zone residence time.
- Variable total load (primary plus reburning fuel input).

4.1 Structure of Parametric Studies

The process variables investigated in the parametric studies were grouped into three categories: primary zone, reburning zone, and burnout zone parameters. The specific variables addressed in these categories were as follows:

Primary Zone

- Stoichiometry (SR_1)
- Primary NO_x concentration $(NO_x)_p$

Reburning Zone

- Mixing rate of reburning fuel

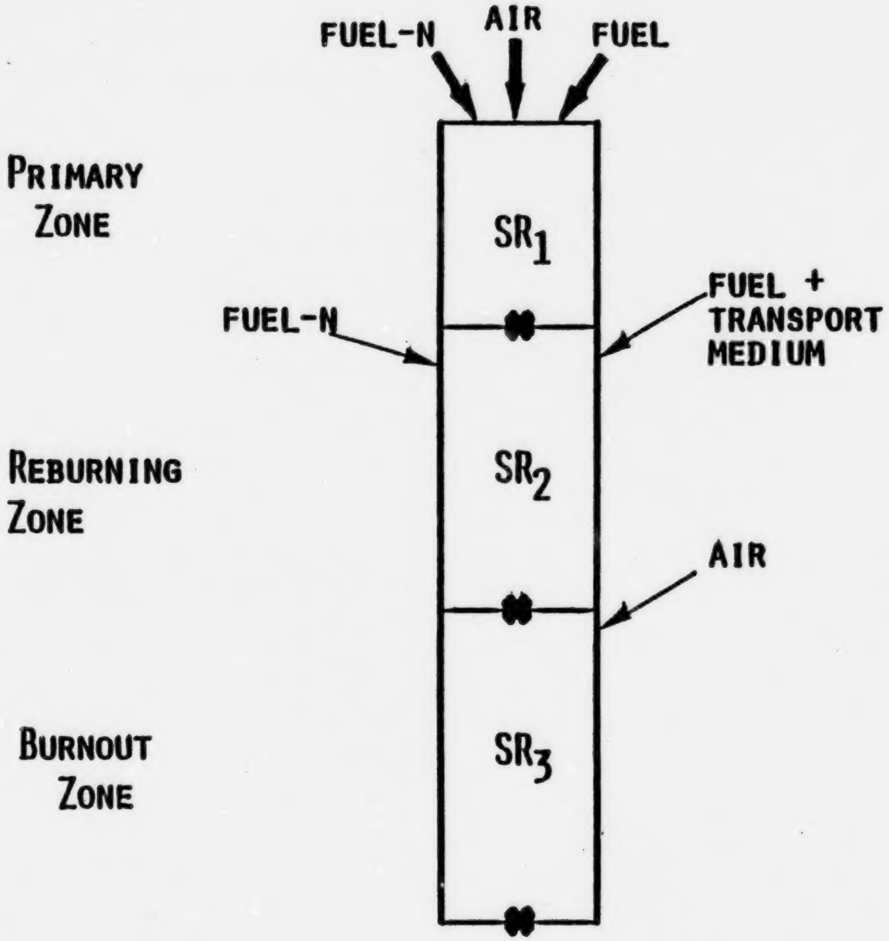
FUEL-N
AIR
FUEL
PRIMARY ZONE
SR_1
FUEL-N
FUEL + TRANSPORT MEDIUM
REBURNING ZONE
SR_2
AIR
BURNOUT ZONE
SR_3

Figure 4-1. Experimental approach to reburning process.

- Reburning fuel type and nitrogen content
- Stoichiometry (SR_2)
- Residence time (τ_2)
- Thermal history (T_1, primary zone exit temperature)

Burnout Zone

- Mixing rate of burnout air
- Overall stoichiometry (SR_3)
- Thermal history (T_2, reburning zone exit temperature)

The overall approach in the parametric studies was to begin the work with brief examination on the importance of diffusional mixing effects. Based upon these injector/mixing results, the appropriate fuel and air mixing conditions were selected for the investigation of the parameters in each of the three zones in the reburning process, in order to assure that the results of the remaining testing would be free of mixing effects.

4.2 Baseline Conditions

The baseline combustor operating conditions were as follows:

Primary Zone

- Propane fired at 17.6 kW (60×10^3 Btu/hr)
- $SR_1 = 1.10$
- $(NO_x)_p = 190$ ppm (dry, 0% O_2)*

Reburning Zone

- $\tau_2 = 400$ms
- $T_1 = 1700$ K (2600°F), with auxiliary lower burners off

---

*All gas concentrations reported are on a dry basis, corrected to 0 percent O_2 unless otherwise stated.

Burnout Zone

- $SR_3 = 1.25$
- T_2 1505 K (2250°F) with lower auxiliary burners off

Refractory chokes were placed at the reburning fuel and burnout air injection locations (see Figure 2-1). The chokes seperated the zones by preventing any backmixing between the zones. The primary fuel (propane) was doped with NO to the desired concentrations. Figure 4-2 shows the time/temperature profile in the reburning zone at baseline conditions.

4.3 Data Reduction

There are several schemes currently employed to represent NO_x emission data from combustion sources. Three methods of data interpretation for the same set of data obtained from a reburning experiment in the CTT are illustrated in Figure 4-3. The data were taken at the baseline firing conditions. Radial reburning fuel and burnout air injection was used. The data illustrates the effects of two different reburning fuels, propane and Utah coal, at several reburning zone stoichiometric ratios.

The plots on the left of Figure 4-3 show conventional means of NO_x data interpretation, the measured NO_x concentration in ppm (volume) and pounds of NO_x formed per million Btu of heat released, both as a function of SR_2. Both methods focus on the levels of NO_x emissions from the exhaust when reburning was applied to the system. As the reburning fuel rate (propane or coal) was increased, the SR_2 was reduced and additional air was required to ensure complete burnout. Adding the reburning fuel and the burnout air, in particular, to the system would naturally lower the primary NO_x concentrations due to dilution effect. Therefore, exhaust emissions on either a volumetric (ppm) or a heat-release (lbs $NO_2/10^6$ Btu) basis failed to represent the reduction of initial NO_x $[(NO_x)_p]$ by chemical means with reburning.

In order to assess the effectiveness of the process (reburning) on reducing primary NO_x, the measured NO_x concentrations in the exhaust need to

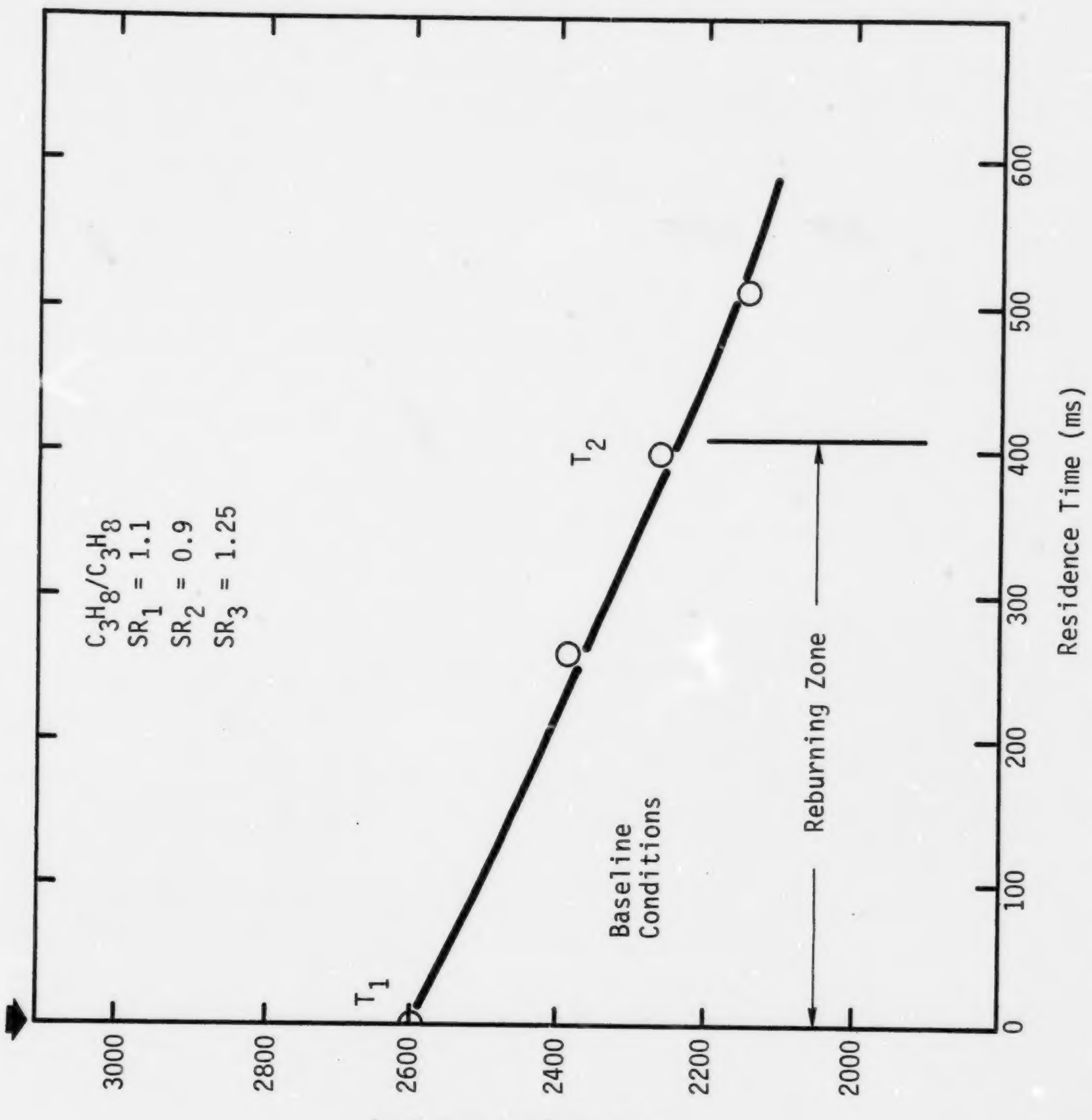

Figure 4-2. Time/temperature profiles at baseline conditions.

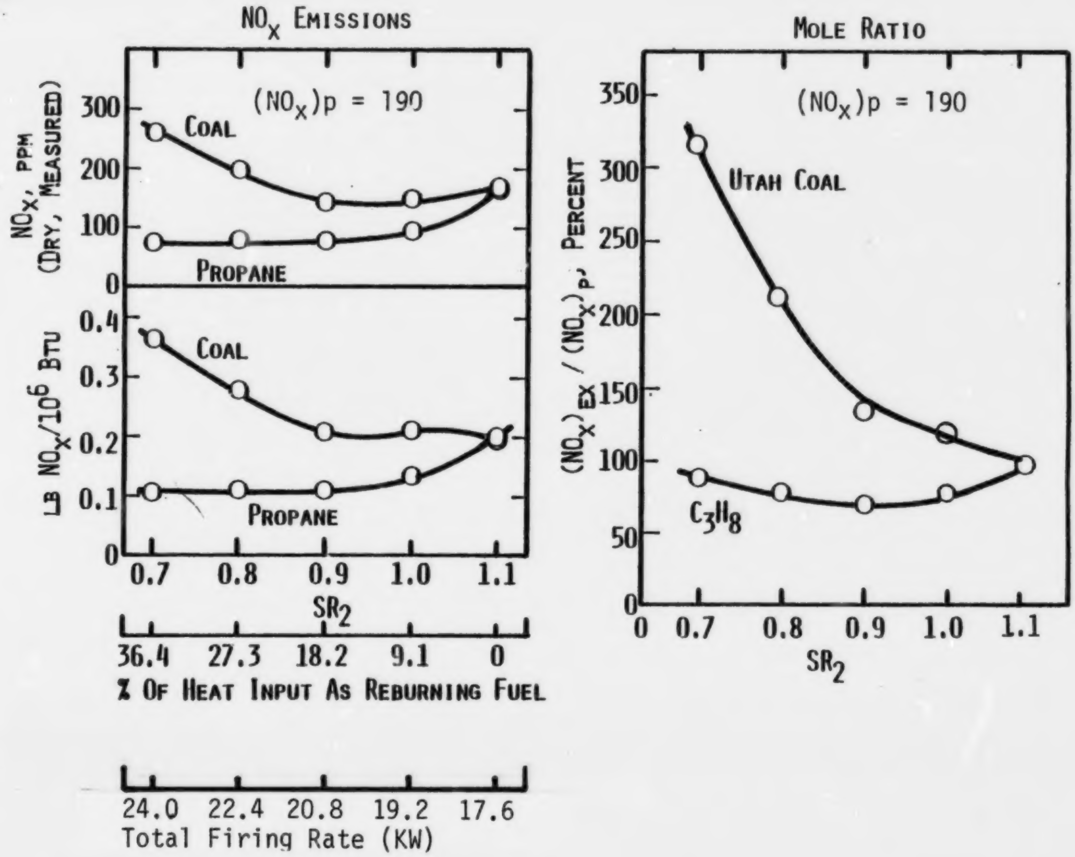

Figure 4-3. Examples of data reduction.

be corrected to exclude dilution effects. Figure 4-3 illustrates the method of data interpretation which takes into account the dilution effect. In this plot the data are reported in terms of the molar ratio of NO_x at the exit of the primary zone in percent. Utilizing this method of data reduction, the data are related to the "break even" value of 100 percent; i.e., at 100 percent the pound moles of NO_x in the exhaust is identical to that at the exit of the primary zone. Clearly, for reburning to be chemically effective, the molar ratio must be below 100 percent. The data in this report will be presented in the form of mole ratios. Detailed calculations on converting measured concentrations to mole ratios are given in Appendix B.

It should be noted that the chemical reduction is not the only reduction that will occur when reburning is applied to a furnace. The actual level of reduction would be significantly lower depending on how reburning is applied. For example, dropping load in the lower furnace may reduce the main zone NO_x and burning out the reburning fuel would result in dilution reduction. These studies were designed to define the chemical reduction while consideration must be given to the actual system before an assessment of performance can be made. Levels of NO_x reduction will typically be 30-50% higher when these other factors are taken into account.

5.0 PRELIMINARY MIXING STUDIES

Initially, a series of experiments were carried out to assess the role of fuel and air mixing in the reburning process. The goals of these studies were to:

- Provide a preliminary assessment of the influence of mixing rate on reburning effectiveness.
- Establish the importance of diffusion flame phenomena in the reburning process.
- Ensure that the data collected on process parameters was not complicated by first-order mixing effects.

Variations in the mixing rate of both the reburning fuel and the burnout air were investigated. The influence of primary velocity and fuel jet velocity will be first considered in the beginning of this section. Next, the effect of fuel injector design will be examined, followed by a discussion of the influence of burnout air injection method. This section concludes with results comparing the impact of fuel transport media (either oxidative or inert). All of the experiments in the mixing studies were performed at the baseline combustor operating conditions as outlined in Section 4.2.

5.1 Influence of Primary Effluent Velocity and Reburning Fuel Jet Velocity

A series of experiments was first performed with propane as the reburning fuel and N_2 as the transport medium to investigatethe impact of the velocities of primary effluent and reburning fuel jets. Figure 5-1 shows the furnace configuration. In these experiments, a water-cooled radial fuel injector was used for injecting the reburning fuel (propane) and the burnout air was added through a ring which injected the air radially inward, thus, well-defined fuel-rich and fuel-lean zones were created. The velocity of the

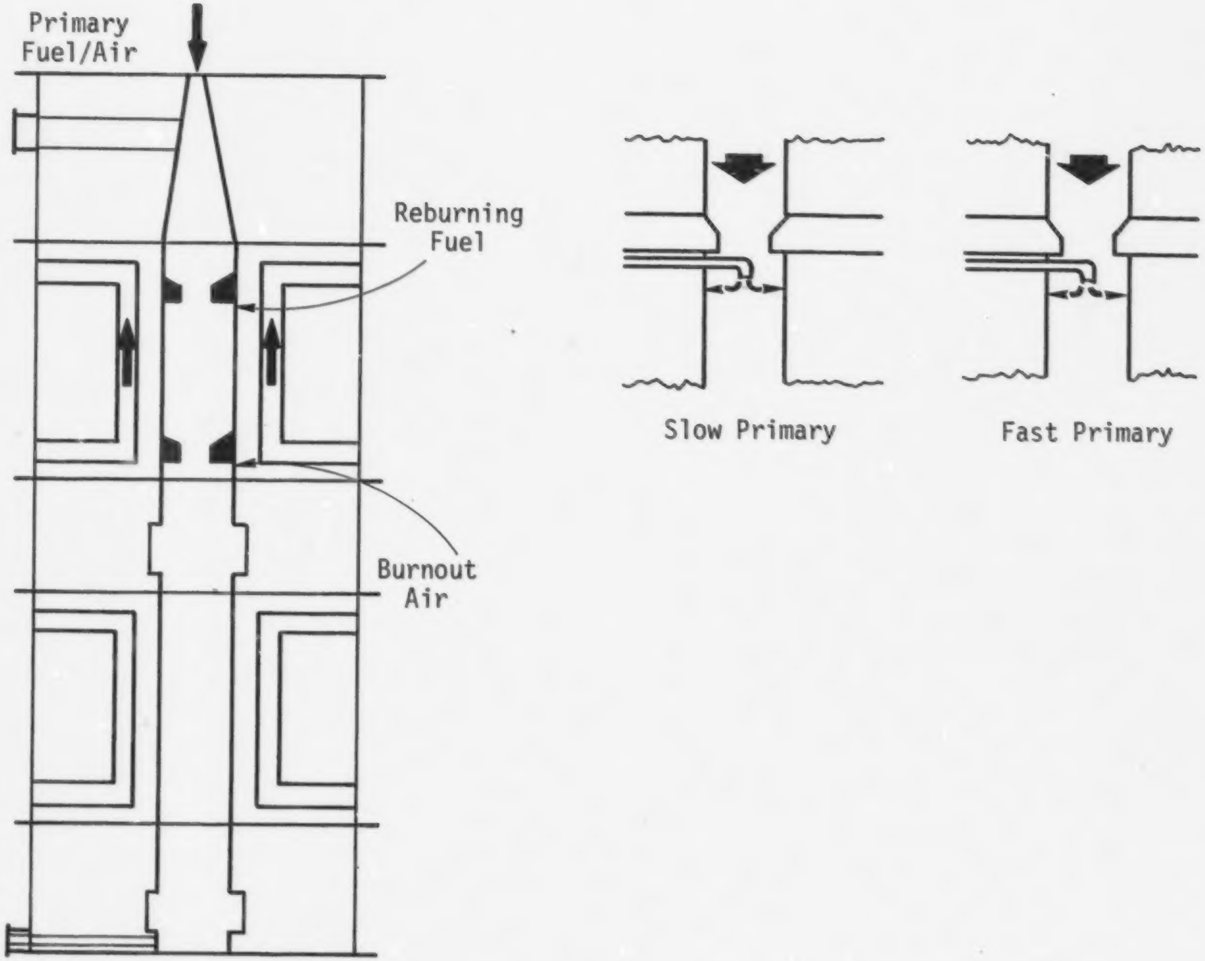
Primary
Fuel/Air
Reburning
Fuel
Burnout
Air
Slow Primary
Fast Primary

Figure 5-1. Fast and slow primary effluent velocity configurations.

primary effluent was varied by changing the diameter of the choke which separated the secondary zone from the primary zone, while the fuel jet velocity was controlled with the amount of transport medium. The effect of two different primary effluent velocities at two reburning fuel jet velocities is presented in Figure 5-2 (the notation at the top of Figure 5-2 denotes reburning with propane fired in the primary zone, propane injected as the reburning fuel, and the primary NO_x concentration, i.e. 190 ppm dry at 0% O_2). The same data crossplotted to show the effect of two different fuel jet velocities at two primary effluent velocities is presented in Figure 5-3. No significant effect of either parameter was observed. To further relax the mixing of the reburning fuel, an axial injector was used to inject propane parallel with the primary flow. Figure 5-4 compares results of the extreme reburning zone mixing conditions. At fuel-rich stoichiometries, mixing conditions had little influence on exhaust NO_x emissions. However, at a stoichiometry near unity ($SR_2 = 1.0$), lower emissions were obtained with higher fuel mixing rates.

The effect of primary velocity when coal was used as the reburning fuel is illustrated in Figure 5-5. A slight increase in the NO_x reduction occurred at the higher primary velocity over the entire range of SR_2. These observations indicated that the reburning effectiveness of an ideal (totally volatile) fuel, such as propane, did not strongly depend on the primary effluent or reburning fuel injection velocities. However, it was beneficial to mix a nitrogen containing fuel, such as coal, as rapidly as possible. Evidently, under fuel-rich conditions, maximum NO_x reduction was obtained when the reburning coal was immediately well-mixed upon injection.

5.2 Reburning Fuel Injection

Two types of reburning fuel injector designs (axial and radial) were investigated in this test. Figure 5-6 illustrates the two modes of fuel injection. The results for three reburning fuels (propane, coal, and propane doped with ammonia to the same nitrogen content as the coal) are presented in Figure 5-7. Little difference between fuel injection modes for propane was observed. The axial injection did shift the minimum to the richer

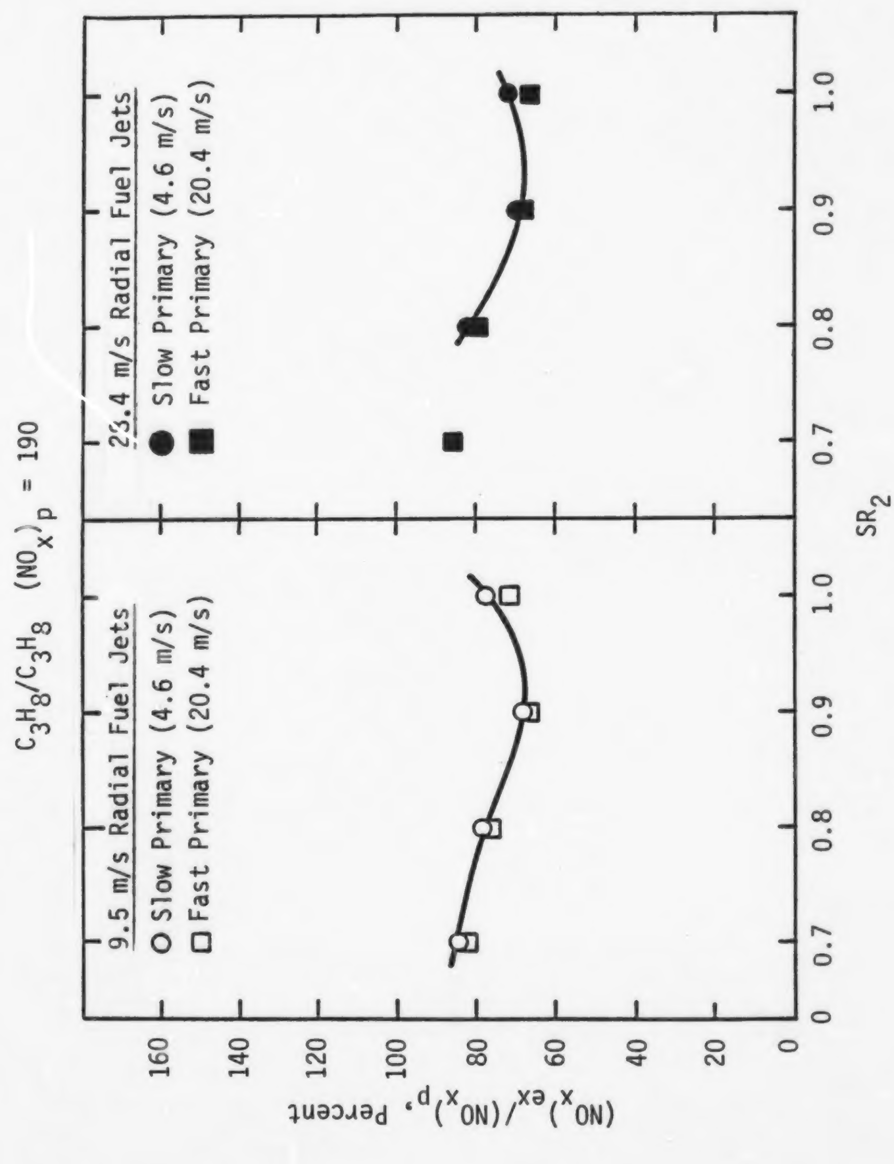

Figure 5-2. Influence of primary velocity.

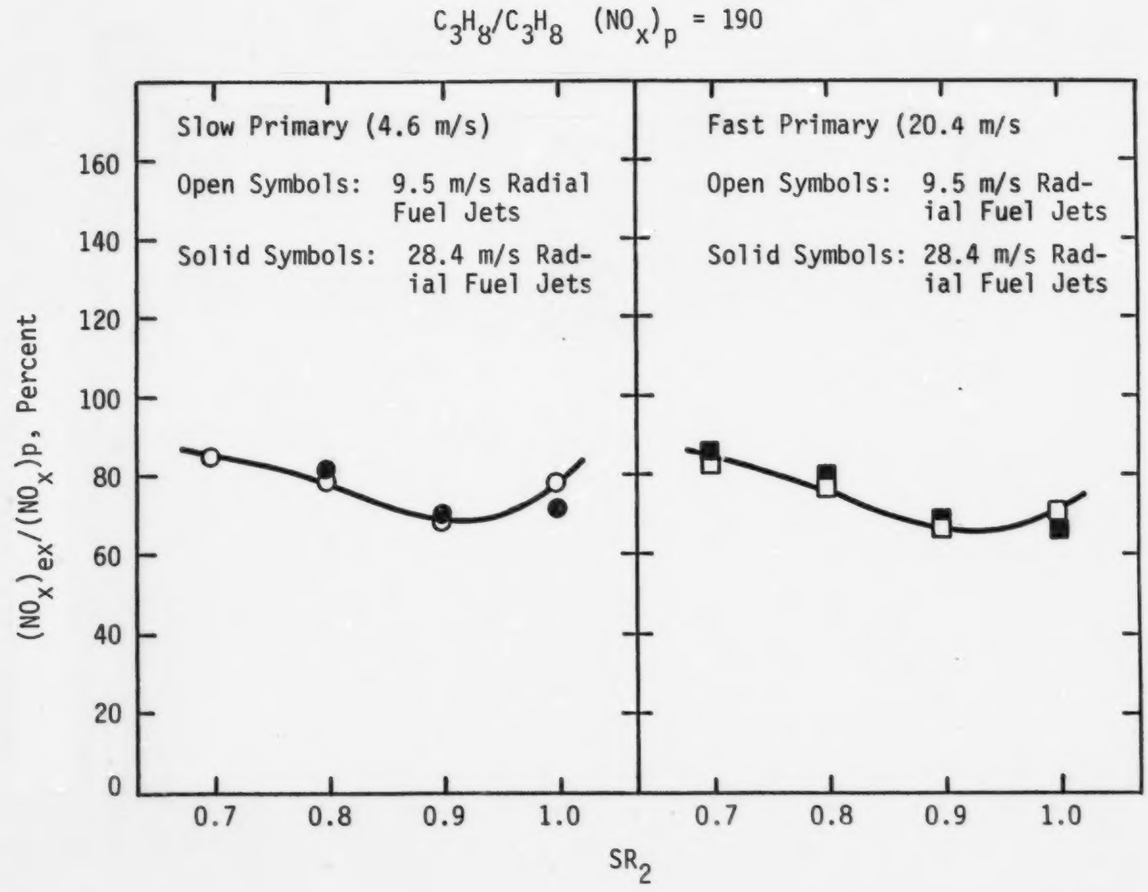

Figure 5-3. Influence of reburning fuel jet velocity

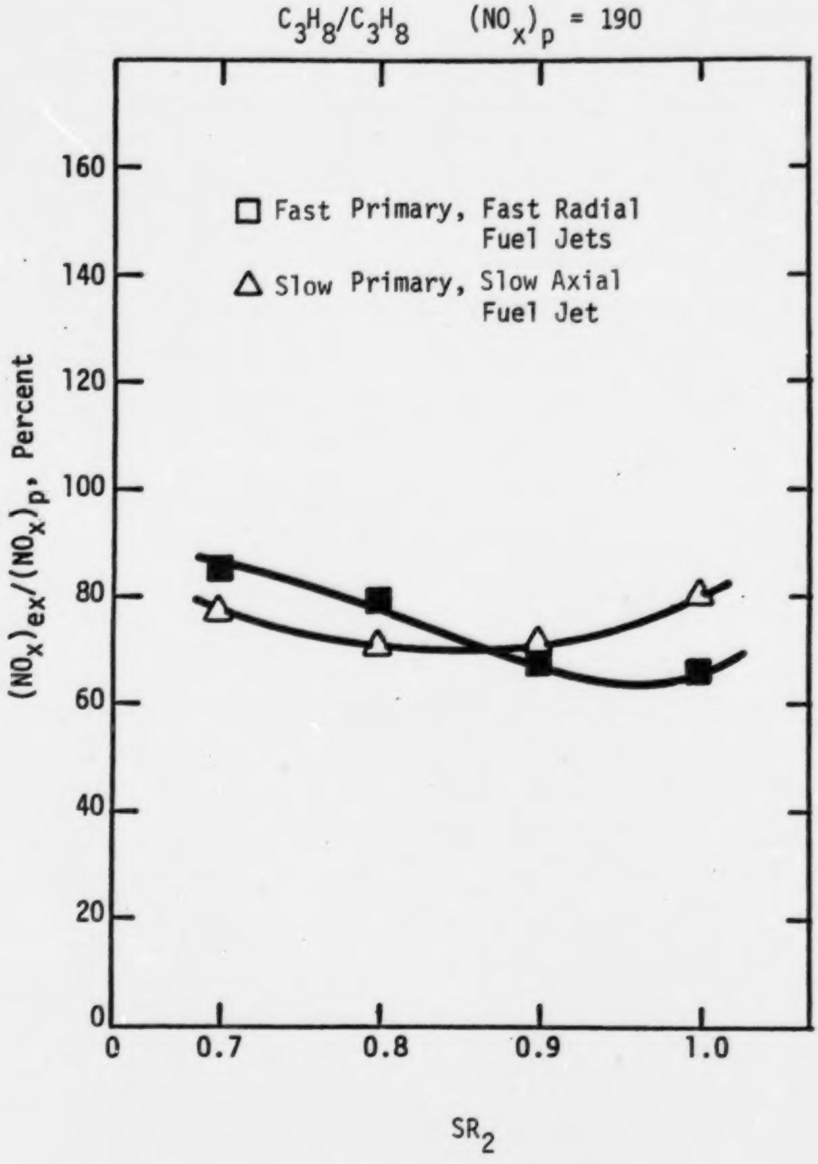

Figure 5-4. Comparison of extreme reburning zone mixing conditions.

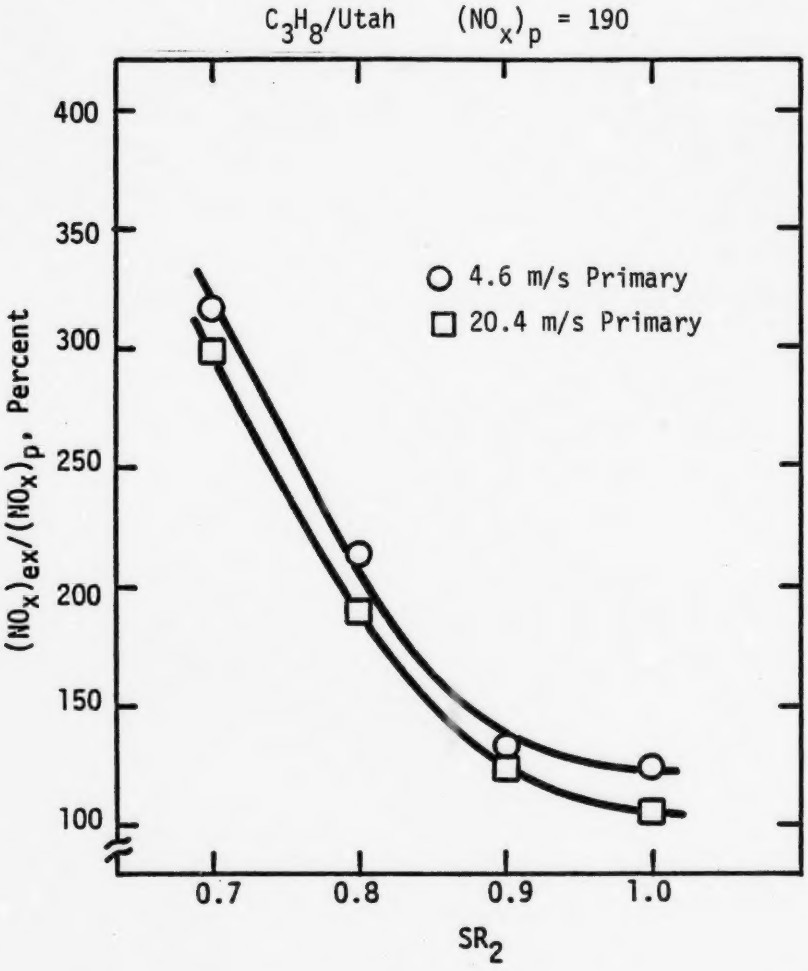

Figure 5-5. Influence of primary velocity.

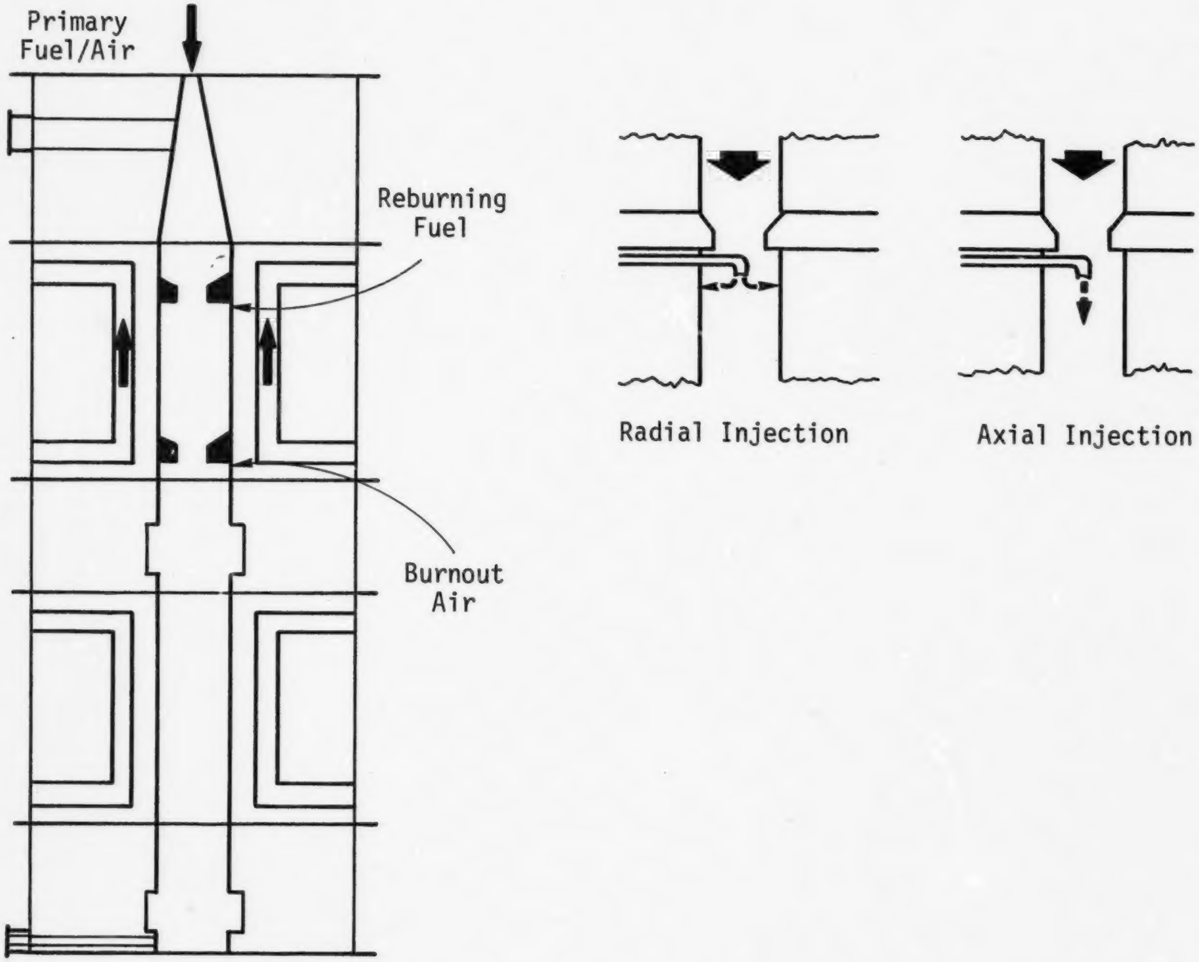
Primary
Fuel/Air
Reburning
Fuel
Burnout
Air

Radial Injection

Axial Injection

Figure 5-6. Reburning fuel injection methods.

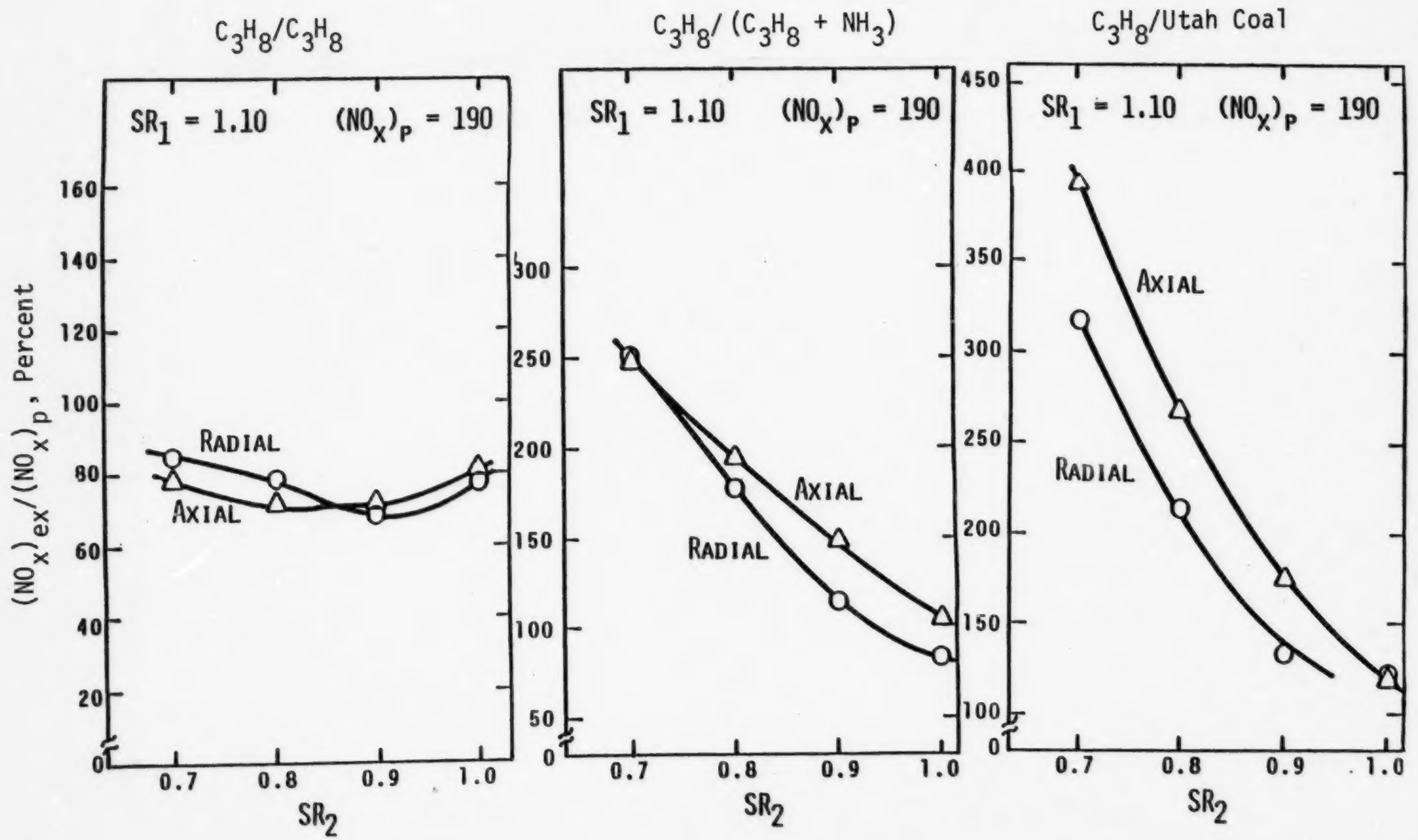

Figure 5-7. Influence of reburning fuel injector.

stoichiometries for propane. For the propane doped with NH_3 fuel, a significant increase in the NO reduction was obtained with the radial injector at leaner stoichiometries. When injecting Utah coal as the reburning fuel, consistently lower NO_x emissions were obtained with the radial injector. Injecting the coal radially increased the fuel/oxygen contacting and probably resulted in higher flame temperatures. It also effectively increased the rich zone residence time due to rapid radial dispersion of the particles. Higher flame temperature and longer residence time both were found to enhance the evolution of the coal nitrogen (see Sections 7.3 and 7.4). As a result, less solid nitrogen was carried into the fuel-lean burnout zone and lower exhaust emissions were observed.

To investigate the importance of the initial NO_x-to-hydrocarbon ratio (NO_x/HC) at the reburning fuel injection location, the reburning fuel injector experiments were conducted at a higher $(NO_x)_p$ concentration and lower SR_1 value, $(NO_x)_p$ = 605 ppm and SR_1 = 1.05, respectively. The results, plotted in Figure 5-8, indicate the same trends as Figure 5-7 (with significantly better overall NO_x reduction due to increased $(NO_x)_p$, see Section 6.2).

5.3 Burnout Air Injection

The influence of burnout air mixing techniques were investigated with two injection methods, radial and axial, as illustrated in Figure 5-9. Comparison between the two burnout air injection methods at the extreme reburning fuel mixing conditions is presented in Figure 5-10. Little difference in reburning effectiveness was noted with propane as the reburning fuel. Experiments were also carried out with Utah coal as the reburning fuel. Figure 5-11 shows data comparing the two methods of air injection for a case with an axial fuel injector and the other with a radial fuel injector. In both cases, it appears that the conversion of all nitrogen species exiting the reburning zone (TXN) was not sensitive to the rate at which the burnout air was added.

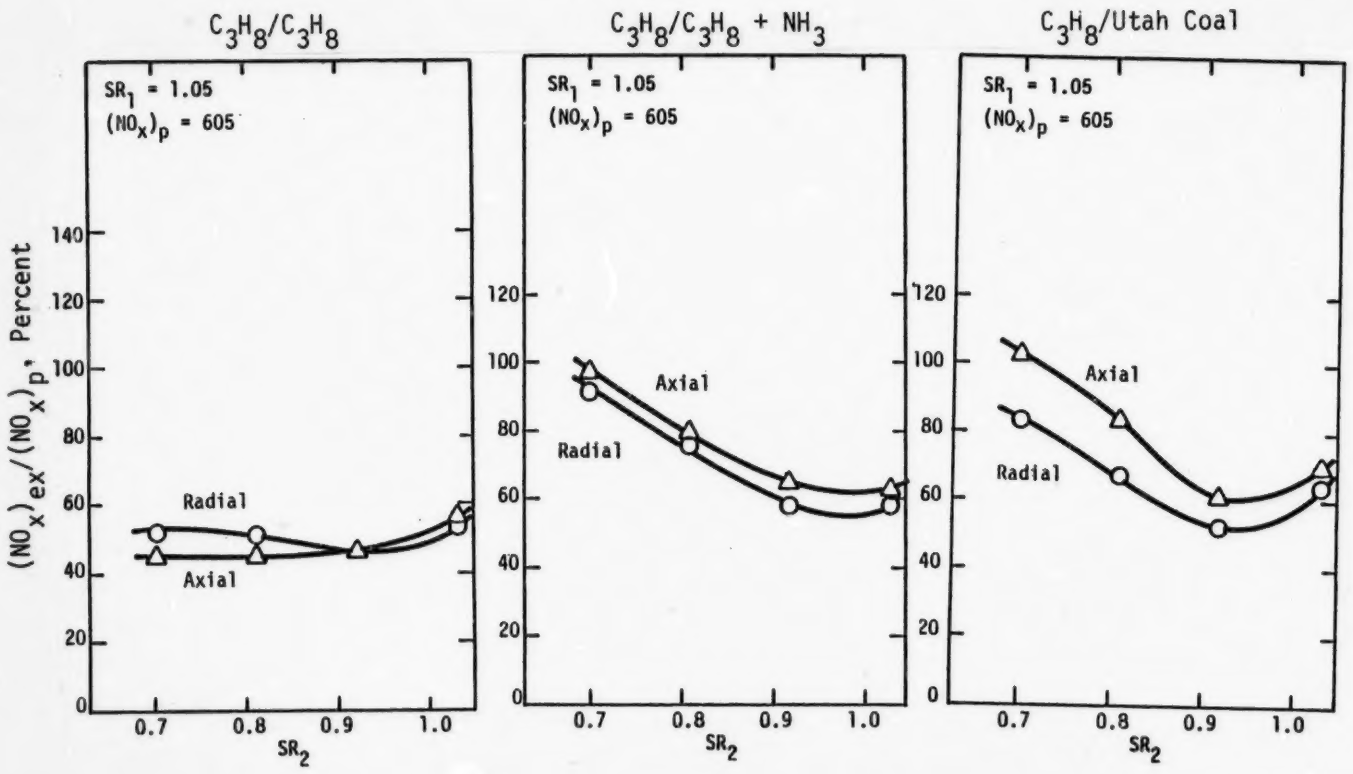

Figure 5-8. Influence of reburning fuel injector at elevated levels of $(NO_x)_p$ and reduced values of SR_1.

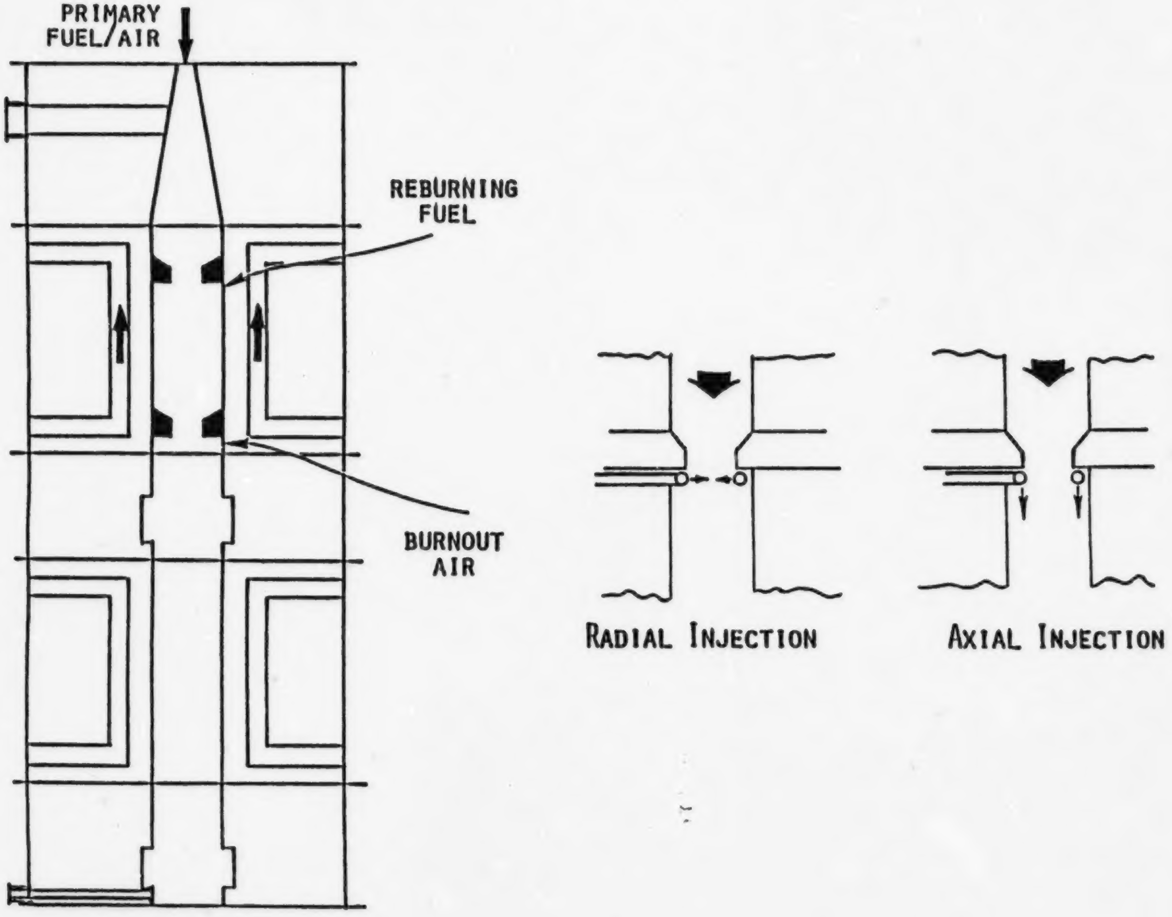
PRIMARY
FUEL/AIR
REBURNING
FUEL
BURNOUT
AIR
RADIAL INJECTION
AXIAL INJECTION

Figure 5-9. Burnout air injection methods.

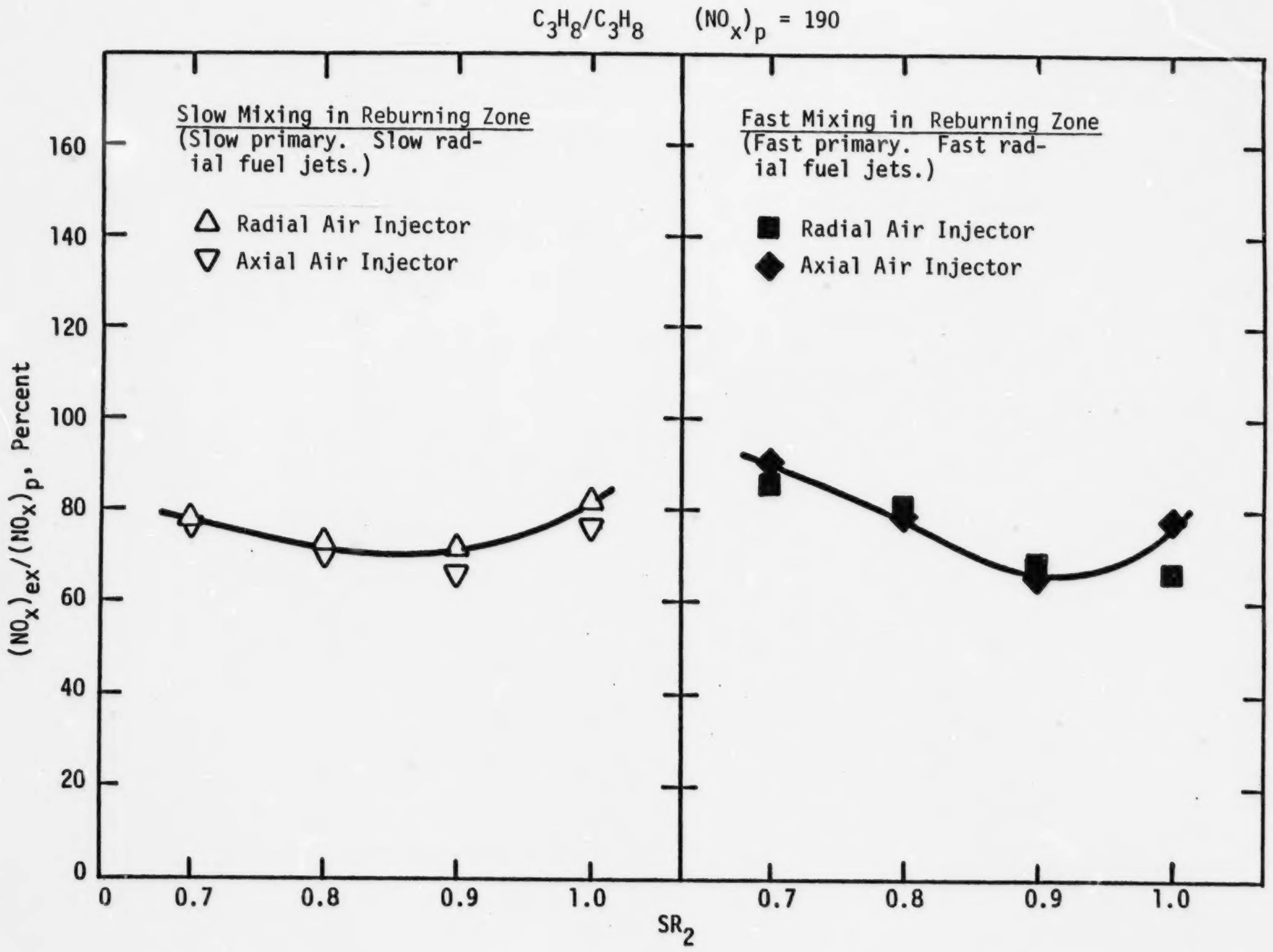

Figure 5-10. Influence of mixing conditions in the burnout zone.

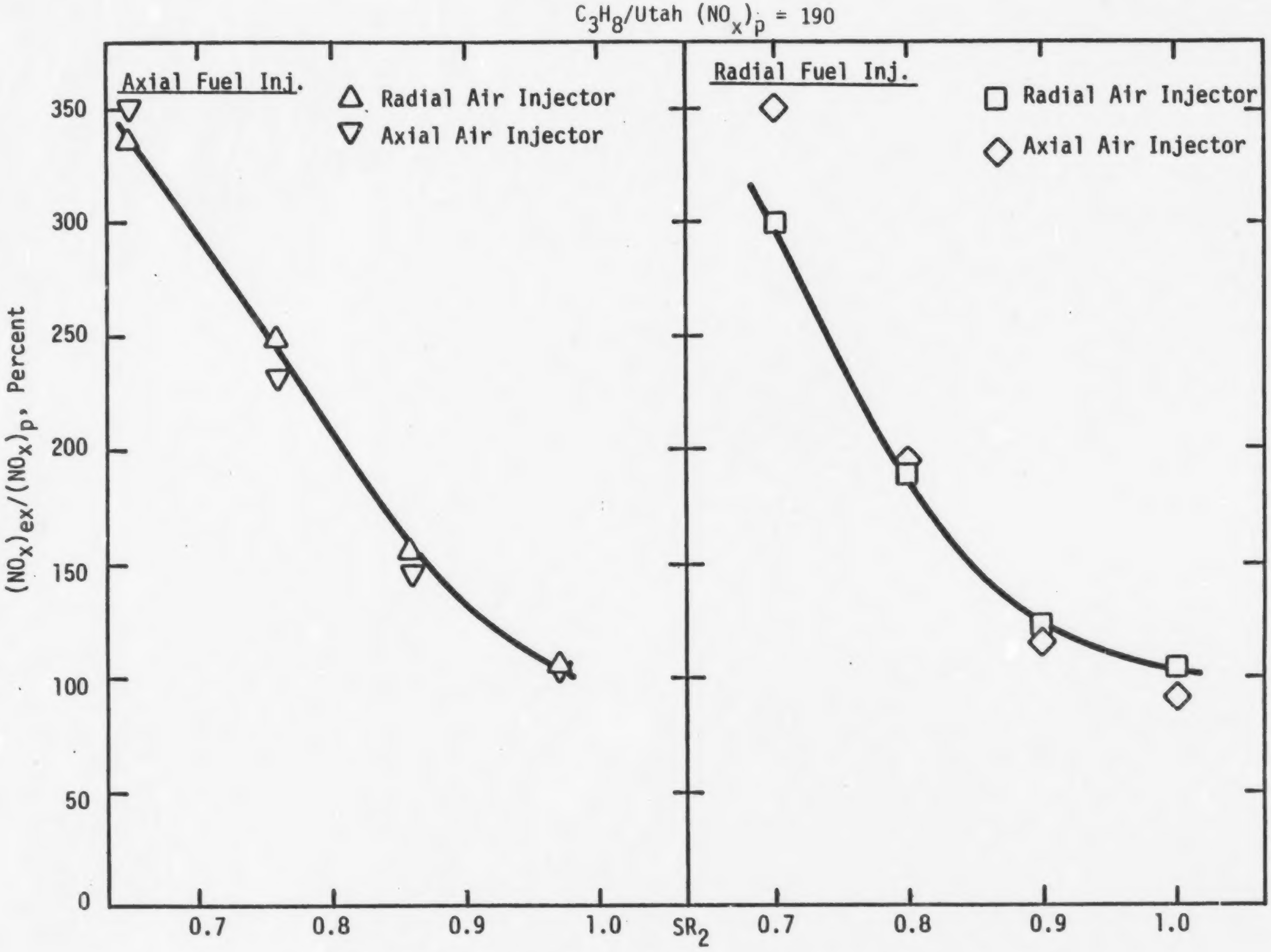

Figure 5-11. Influence of mixing conditions in the burnout zone.

5.4 Effects of Reburning Fuel Transport Medium

In the discussion presented thus far, all experiments were performed with an inert transport medium (N_2) for the reburning fuel. A series of tests were carried out with air as the transport medium to determine if a reactive carrier gas influenced the effectiveness of the reburning process. Figure 5-12 compares results obtained with the identical amounts of N_2 and air as the transport medium for propane and propane doped with ammonia. Using air instead of N_2 as the transport medium required that more reburning propane be added to achieve a given reburning zone stoichiometries. The amounts of ammonia, nevertheless, were purposely kept constant while the transport medium was changed from N_2 to air. It appeared that the transport medium had little impact on the effectiveness of reburning except at the leaner stoichiometries, specifically at an SR_2 of 1.0. By using air as the transport medium, a premixing of the reburning fuel and transport air occurred prior to injection into the combustor. This premixing, plus an overall higher fuel input probably enhanced the formation of thermal NO_x. In addition, premixing propane and air was found to reduce the efficiencies of NO_x destruction by hydrocarbon radicals at leaner stoichiometries (see Section 5.5). Therefore, higher NO_x emissions were obtained with air as the transport medium at an SR_2 of 1.0.

For reburning with real fuels, such as coal, replacing N_2 with air required more fuel and thus more fuel nitrogen to be added in the reburning zone. Figure 5-13 shows the impact of using air as the transport medium for Utah coal with axial injection. Higher emissions were obtained with air as the transport medium at all stoichiometries as can be seen from the plot on the left of Figure 5-13. These data were replotted and shown on the right of Figure 5-13 in terms of the molar flow rates of reactive nitrogen (primary NO_x plus nitrogen added with the coal) at the entrance of the reburning zone and the molar flow rates of NO_x in the exhaust. Evidently the conversion of the available reactive nitrogen was independent of the transport medium used and independent of the stoichiometry. The increase in emissions observed was attributable only to the increased fuel nitrogen input for using air as the transport medium.

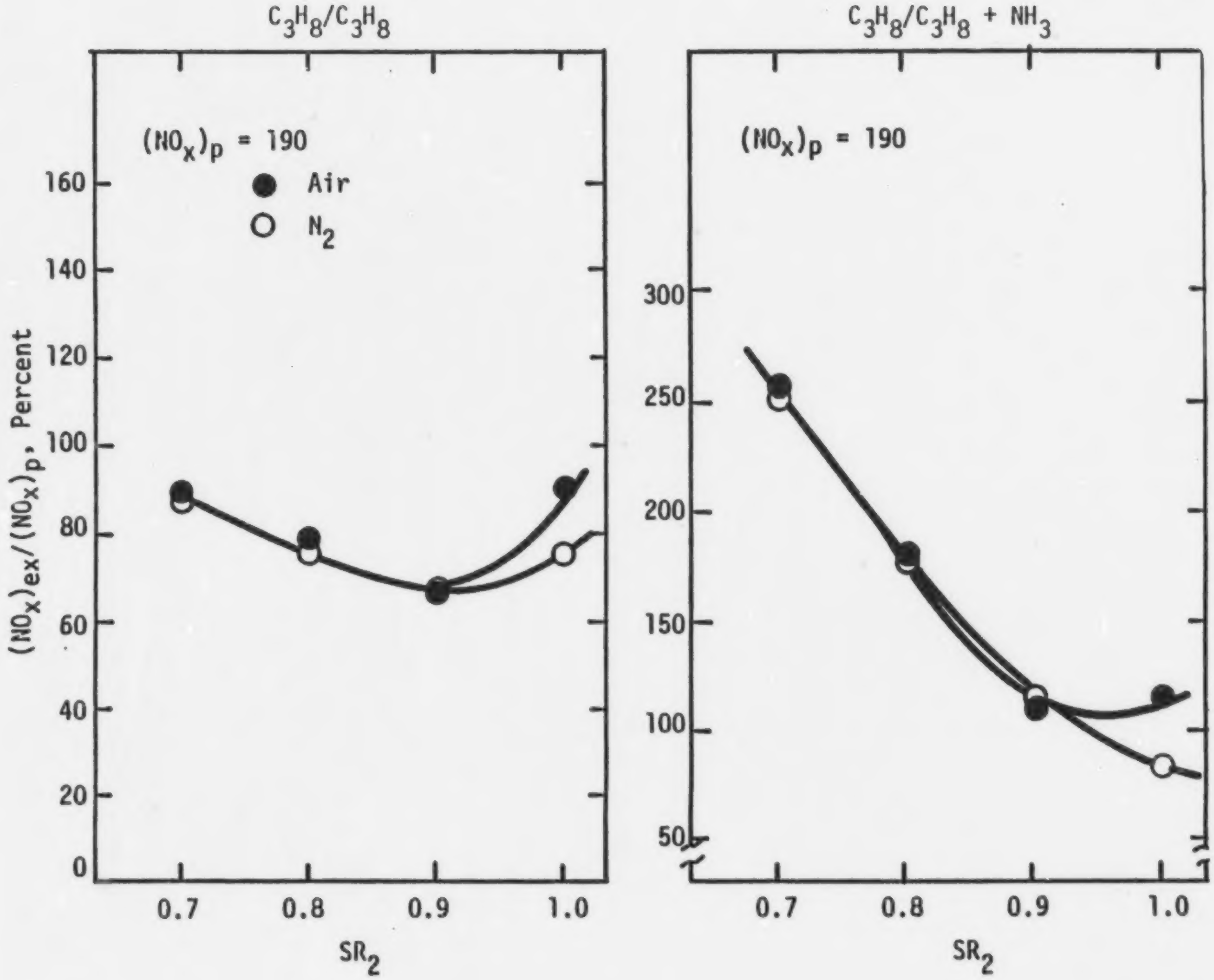

Figure 5-12. Influence of reburning fuel transport medium.

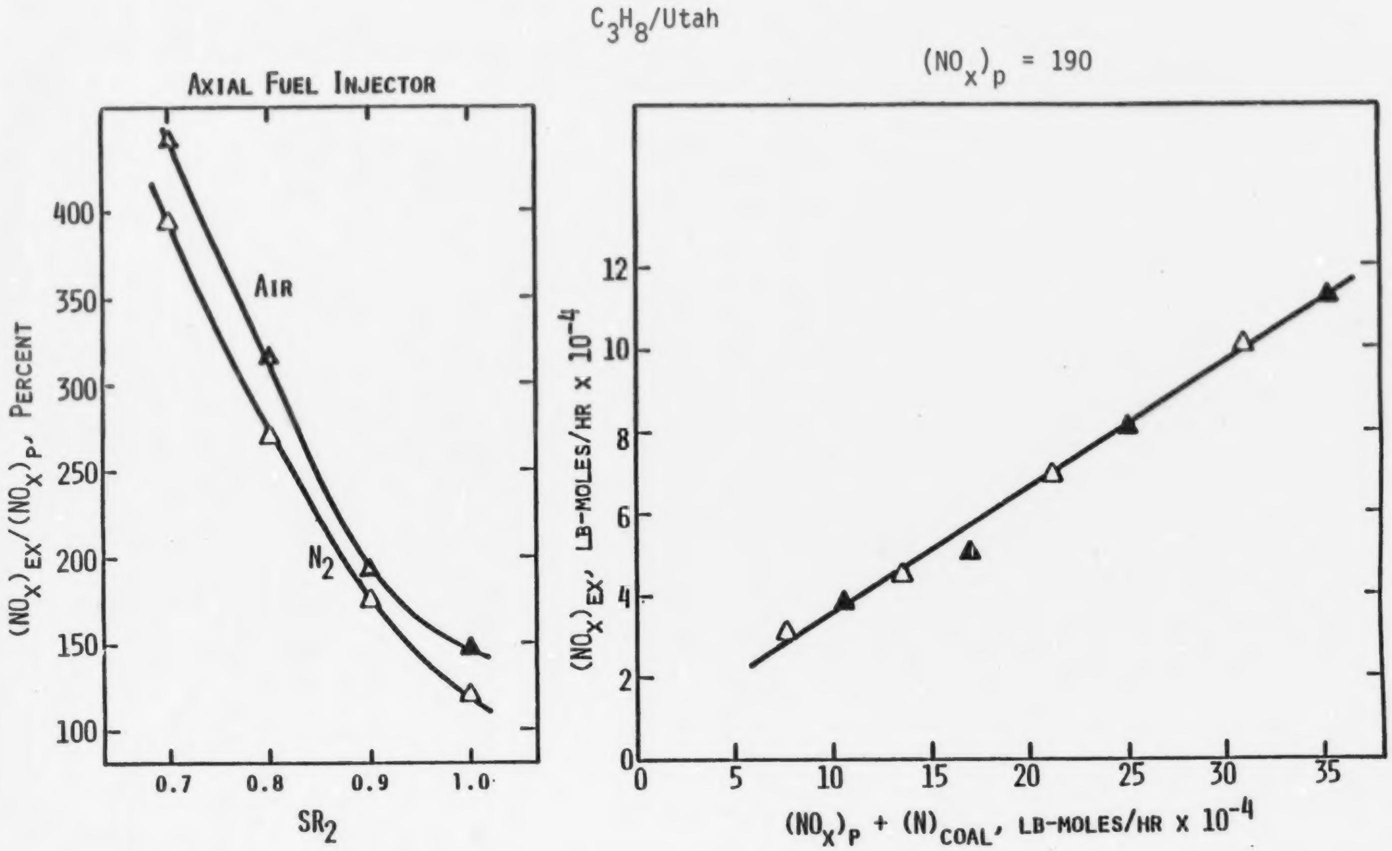

Figure 5-13. Influence of transport medium--axial fuel injector.

Figure 5-14 shows the corresponding data obtained with the radial fuel injector. Again, using air as the transport medium produced higher emissions when the reburning zone was relatively lean. As the SR_2 was progressively reduced, however, differences in emissions diminished. The molar flow plot shown in Figure 5-14 indicates that the percentage conversion of the reactive nitrogen was actually lower with air as the transport medium. It appeared that the impact of increased fuel nitrogen input was somewhat offset by the increased flame temperatures (see Section 7.4) due to the additional fuel input and the fuel/air premixing. Similar fuel injector effects were observed at higher primary NO_x levels as shown in Figure 5-15.

5.5 Fuel/Air Premixing

As discussed in the last section, using air as the transport medium required more reburning fuel input to achieve a given reburning zone stoichiometry. On the other hand, premixing the reburning fuel with the transport air increased the fuel mixing rate which can increase the flame temperature. To further investigate the effects of fuel/air premixing, experiments were carried out by premixing various amounts of air with a constant amount of reburning fuel (propane). Figure 5-16 shows the comparison of these results (closed symbols) with those obtained with N_2 as the transport medium (no premixing). At an SR_2 of 0.8, the reburning fuel flow was identical in both cases. In the premixing experiments, the SR_2 was increased by increasing the transport air flow and decreasing the burnout air flow by the same amount while the reburning fuel flow was held constant (constant overall firing rate). As shown in Figure 5-16, under fuel-rich conditions, there was little difference in NO_x emissions between the two cases. However, at leaner stoichiometries the premixed reburning flame produced higher emissions. This observation is attributed to lack of locally fuel-rich "pockets" and increased thermal NO_x formation from premixing with air.

When the reburning fuel contained nitrogen, the effects of premixing became more pronounced at leaner stoichiometries. As illustrated in Figure 5-17, premixing propane doped with ammonia with the transport air resulted in

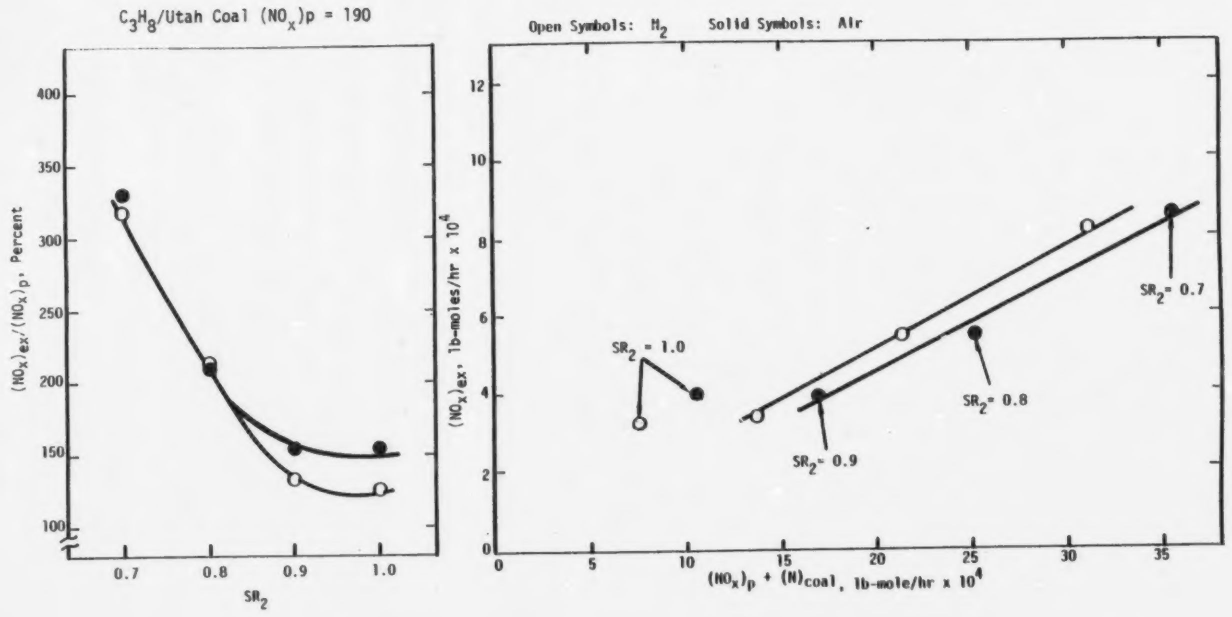

Figure 5-14. Influence of transport medium--radial fuel injector.

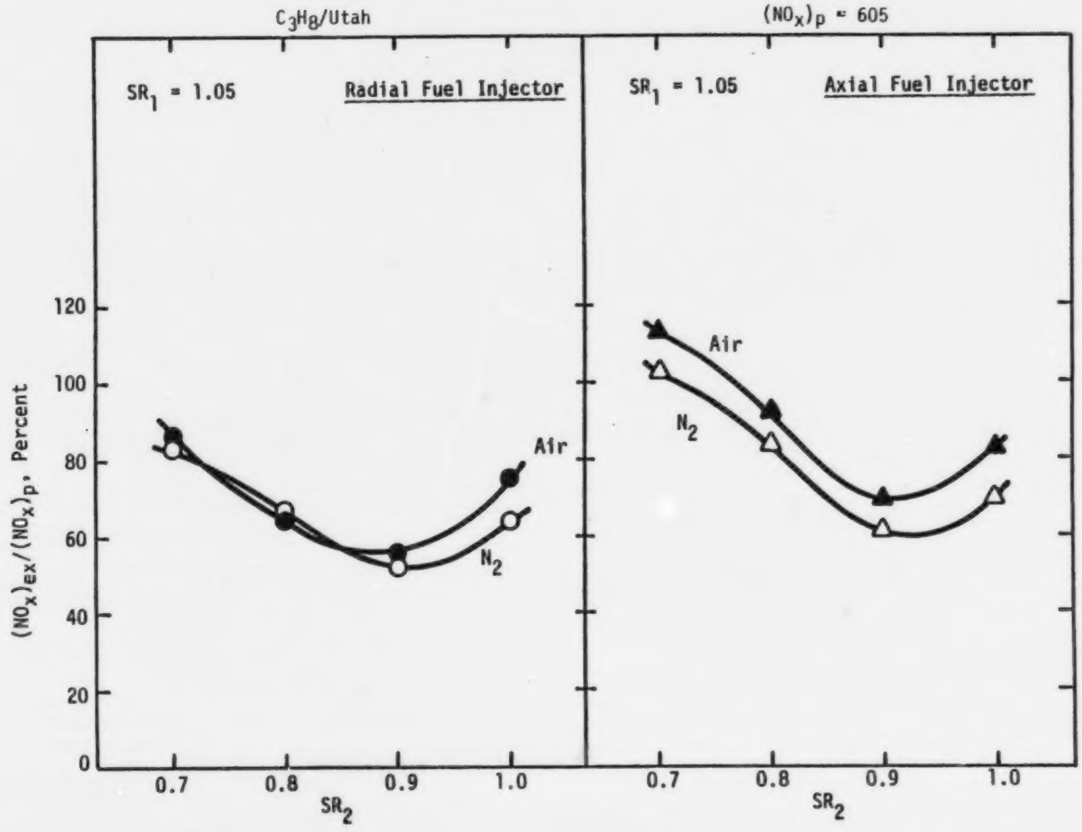

Figure 5-15. Influence of transport medium in coal reburning at high $(NO_x)_p$.

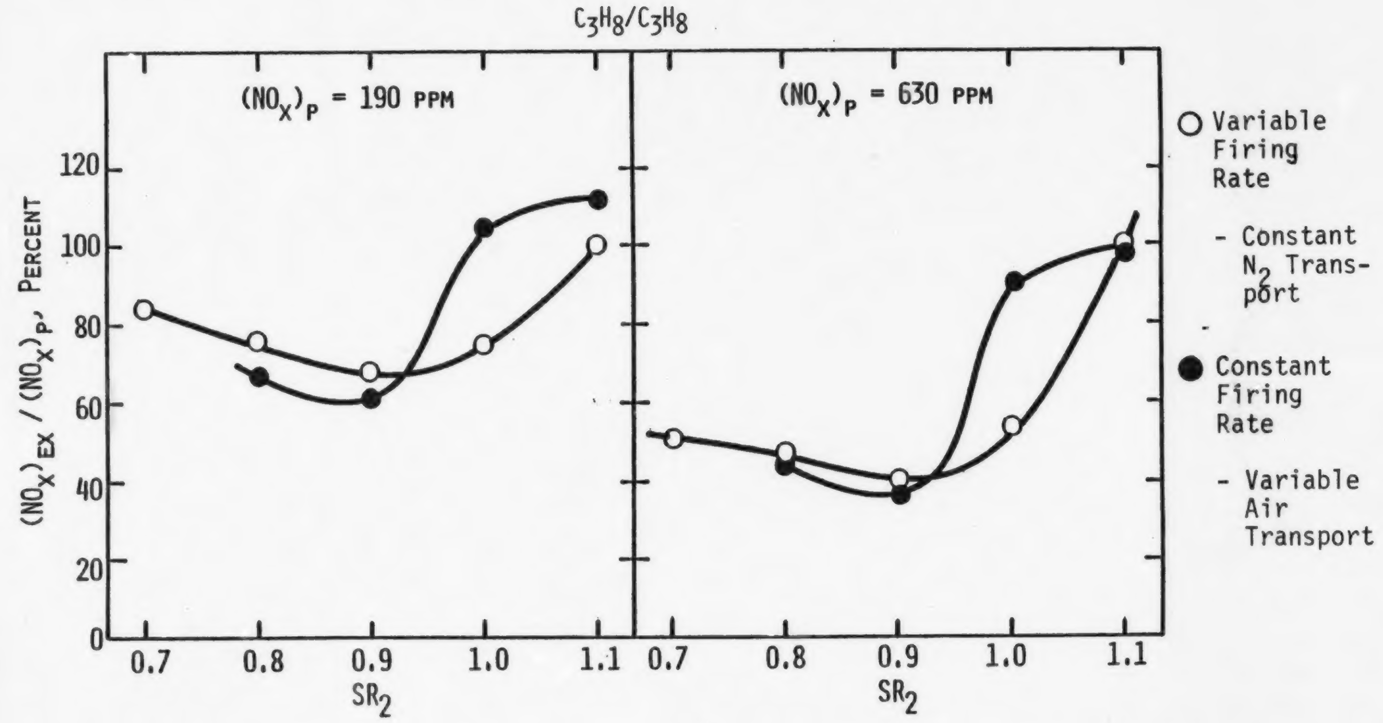

Figure 5-16. Effect of fuel/air premixing.

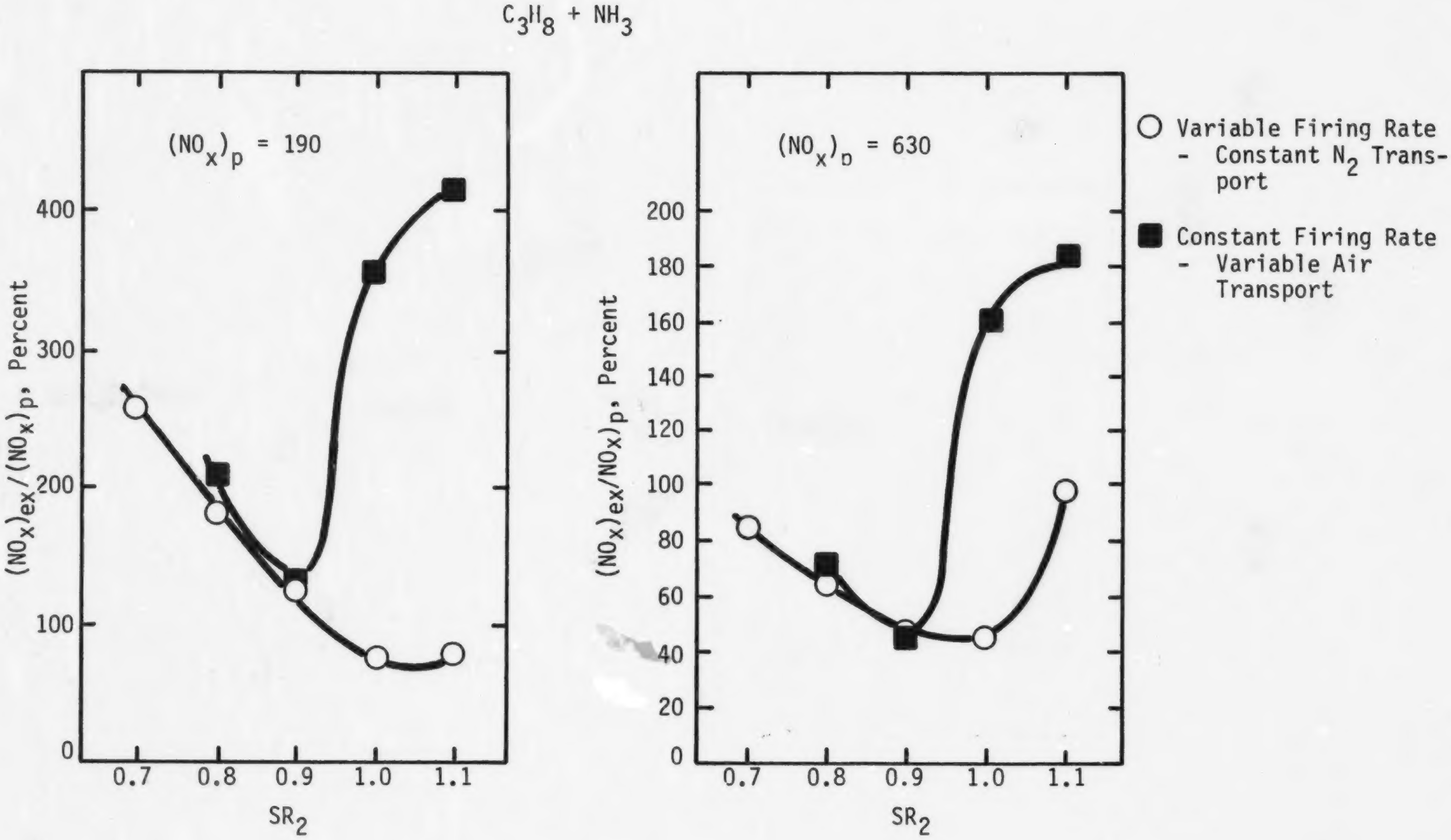

Figure 5-17. Effect of fuel/air premixing.

significantly higher NO_x emissions. Under fuel-rich conditions, there was very little effect at both primary NO_x levels, similar to the findings for reburning with propane.

5.6 Summary--Baseline Mixing Conditions

For reburning with gaseous fuels, the effectiveness of reburning was relatively insensitive to the injection methods for the reburning fuel and burnout air. For coal reburning, increasing the fuel mixing rate lowered exhaust NO_x emissions by increasing the evolution of fuel nitrogen in the rich zone, therefore minimizing the nitrogen carryover into the burnout zone. The coal reburning effectiveness was also insensitive to burnout air mixing.

Use of an inert transport medium increased reburning effectiveness for nitrogen bearing reburning fuels. When an oxidizing transport medium was used, more reburning fuel was required to react with the additional oxygen present. Therefore, more fuel nitrogen was present which increased TXN ($NO + NH_3 + HCN$ + char N) production in the rich zone. Use of an inert transport medium also avoided excess thermal NO_x formation due to premixing and allowed a locally fuel-rich environment necessary for the reduction of NO_x at overall lean stoichiometries.

Mixing conditions for the subsequent parametric studies were chosen to be slow primary effluent (4.6 m/s), slow radial reburning fuel injection (9.5 m/s) with nitrogen as the reburning fuel transport medium, and radial burnout air injection. These conditions allowed for maximum flexibility of combustor operation as well as simplification of data interpretation, since the radial injectors (fuel and air) provided well defined zones and residence times. These selected conditions should reduce the effects of mixing upon the subsequent results.

6.0 PRIMARY ZONE PARAMETERS

6.1 Primary Zone Stoichiometry

Results from experiments conducted to investigate the influence of primary zone stoichiometry on the reburning process are presented in Figure 6-1. The experiment was performed such that the total volumetric flowrate of primary effluent was held constant (at the $SR_1 = 1.1$ flowrate) for all SR_1 values tested. This was accomplished by varying load and holding the baseline air input constant. Performing the experiment in this manner enabled SR_1 to be varied without changing the residence time of the reburning zone, thus direct comparison of the reburning effectiveness was made between successive SR_1 values. The C_3H_8/C_3H_8 data in Figure 6-1 indicates that the primary stoichiometry has little influence on the reburning effectiveness for two $(NO_x)_p$ concentrations. However, as the primary stoichiometry is increased, the amount of reburning fuel must be increased proportionally to maintain a constant SR_2. In practice it would not be desirable to operate the reburning process at a high SR_1. The C_3H_8/Utah coal data in Figure 6-1 depicts a similar trend as the C_3H_8/C_3H_8 data.

With the Utah coal as reburning fuel, increasing the reburning fuel feedrate (to maintain a constant SR_2) as SR_1 is increased also increases the fuel nitrogen available. Therefore, operating the reburning process at low SR_1 will not only minimize the amount of reburning fuel needed, but also minimize the amount of fuel nitrogen available to react (in the case of a nitrogen containing fuel.) This finding is most apparent at high SR_2 values, particularly at $SR_2 = 1.0$ where lower NO_x emissions were measured at low $SR_1 = 1.05$.

6.2 Primary Zone NO_x Concentration

For C_3H_8/C_3H_8 reburning, the influence of variable primary zone NO_x concentration on the reburning process is illustrated in Figure 6-2. This figure indicates that the reburning effectiveness $[1-(NO_x)_{EX}(NO_x)_p]$ increased with increasing $(NO_x)_p$ even though the actual exhaust emissions were higher

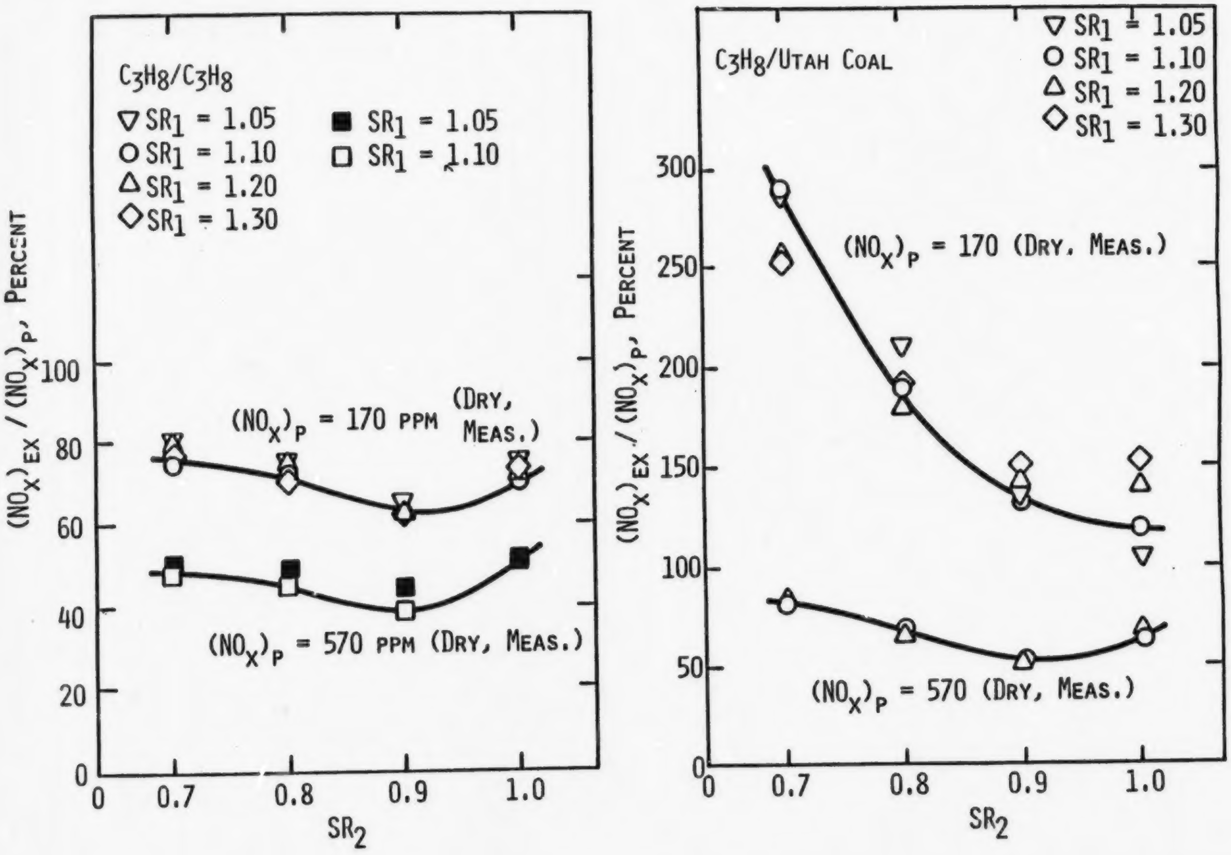

Figure 6-1. Influence of primary zone stoichiometry.

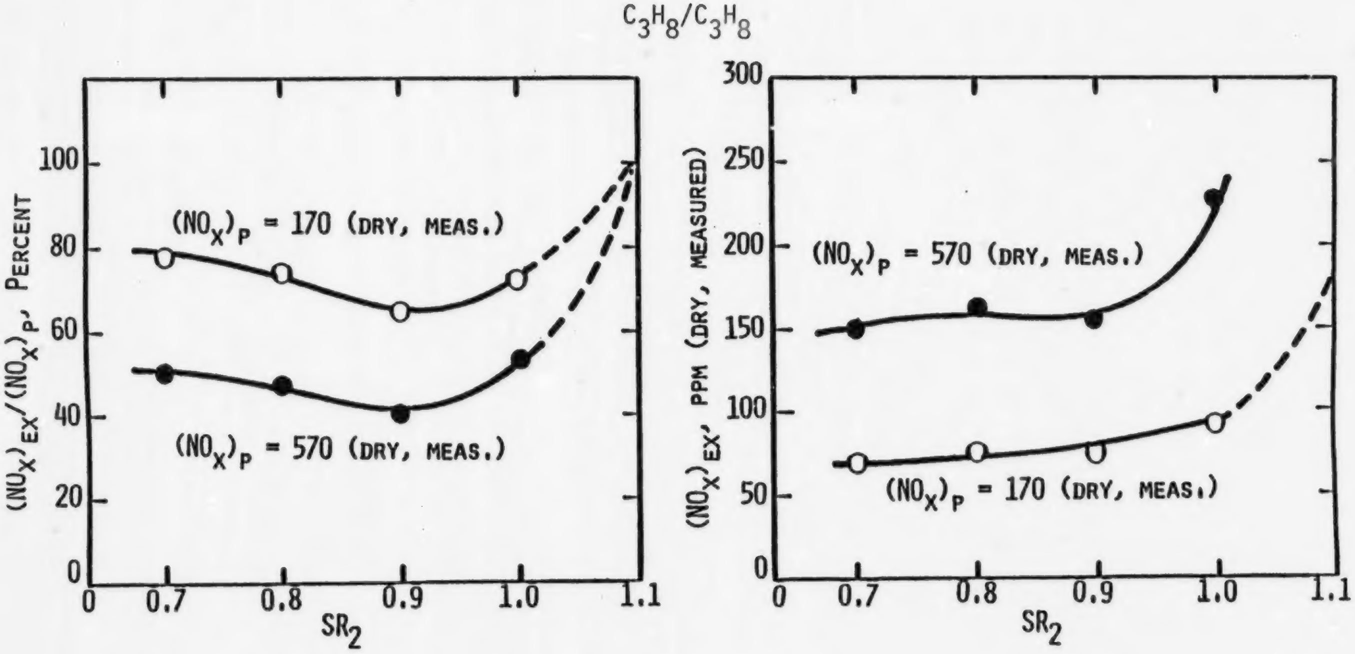

Figure 6-2. Influence of $(NO_x)_p$.

at the higher $(NO_x)_p$ levels. To understand this effect, detailed nitrogen species measurements were made at the exit of the fuel-rich reburning zone. These results (see Figure 6-3) indicated that increasing $(NO_x)_p$ increased the amounts of XN species (NO, NH_3, HCN) leaving the reburning zone. As a result, higher levels of TFN (NO + NH_3 + HCN) were obtained at all stoichiometries, as shown in Figure 6-4. However, the percent conversion of $(NO_x)_p$ to TFN was actually lower at higher values of $(NO_x)_p$, as illustrated in Figure 6-5. Figure 6-5 also indicates that the conversion of TFN to $(NO)_{Ex}$ in the burnout zone was about the same for both levels of $(NO_x)_p$. Therefore, a lower overall conversion of the (NOx)p to (NOx)Ex was observed at higher (NOx)p concentrations.

Figure 6-6 summarizes the effectiveness of reburning at the optimum reburning zone stoichiometry (SR_2 = 0.9) for the various primary NO_x concentrations. At high levels of primary NO_x, the reburning effectiveness was relatively independent of NO_x concentrations. At lower levels of $(NO_x)_p$ (<600 ppm), the reduction efficiency decreased with decreasing NO_x and the reduction was less for nitrogen containing reburning fuels.

6.3 Primary Fuel Effect

The majority of the reburning experimental work was conducted with propane as the primary fuel. The $(NO_x)_p$ levels were set by doping various amounts of NO with the primary fuel. This method provided experimental flexibility and simplified data acquisition. To investigate the validity of this method, reburning with Indiana coal as both primary and reburning fuels was compared to reburning with propane fired in the primary (with NO_x doping to the Indiana coal level) and Indiana coal as the reburning fuel. The results in Figure 6-7 indicate that no difference in reburning effectiveness was observed by substituting propane doped with NO_x for the Indiana coal as the primary fuel. Previous studies by Pershing et al (1982) have shown that coal fired in the primary gave similar results as propane with NO_x doping (to the same NO_x concentration) fired in the primary.

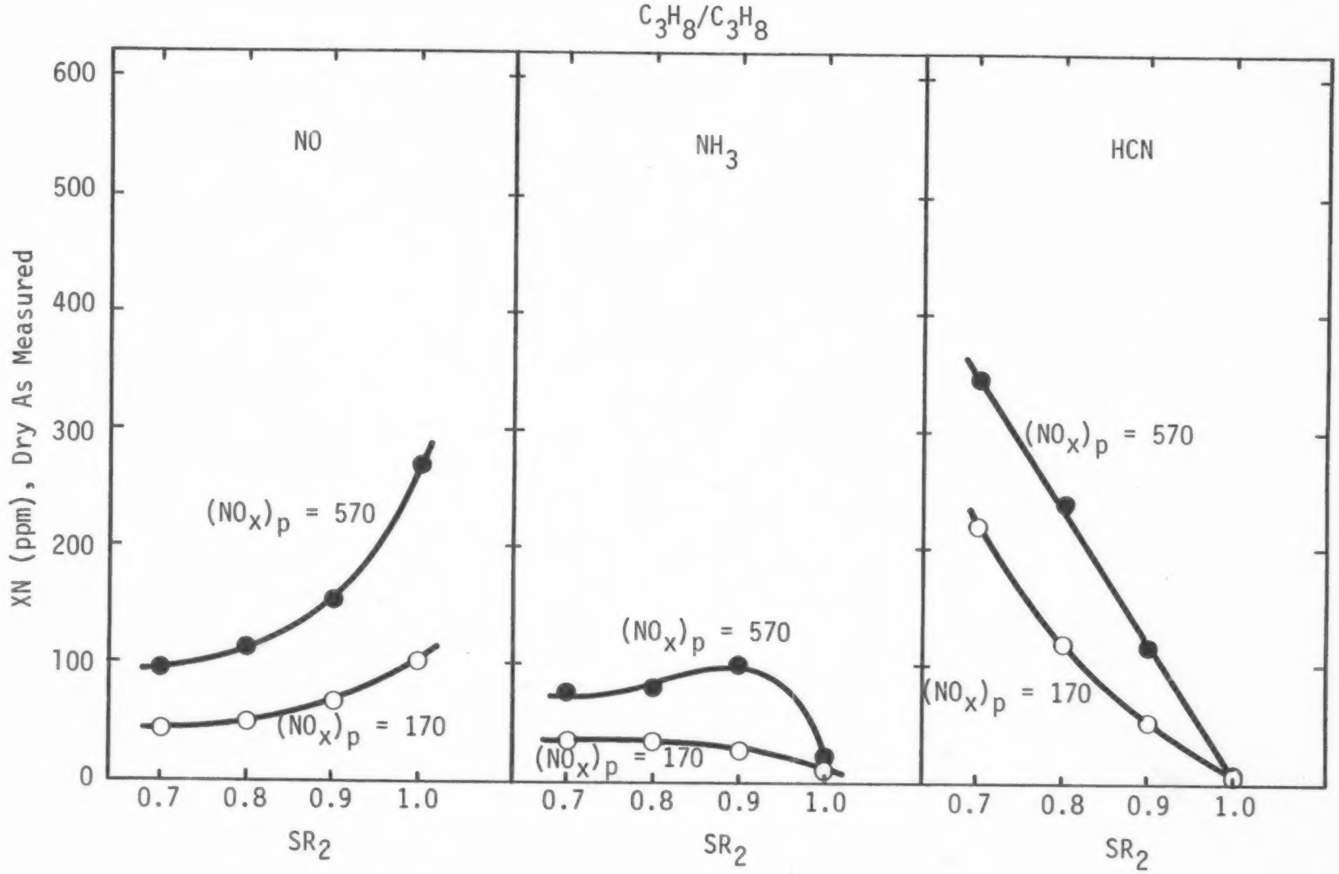

Figure 6-3. Detailed measurements at two $(NO_x)_p$ concentrations.

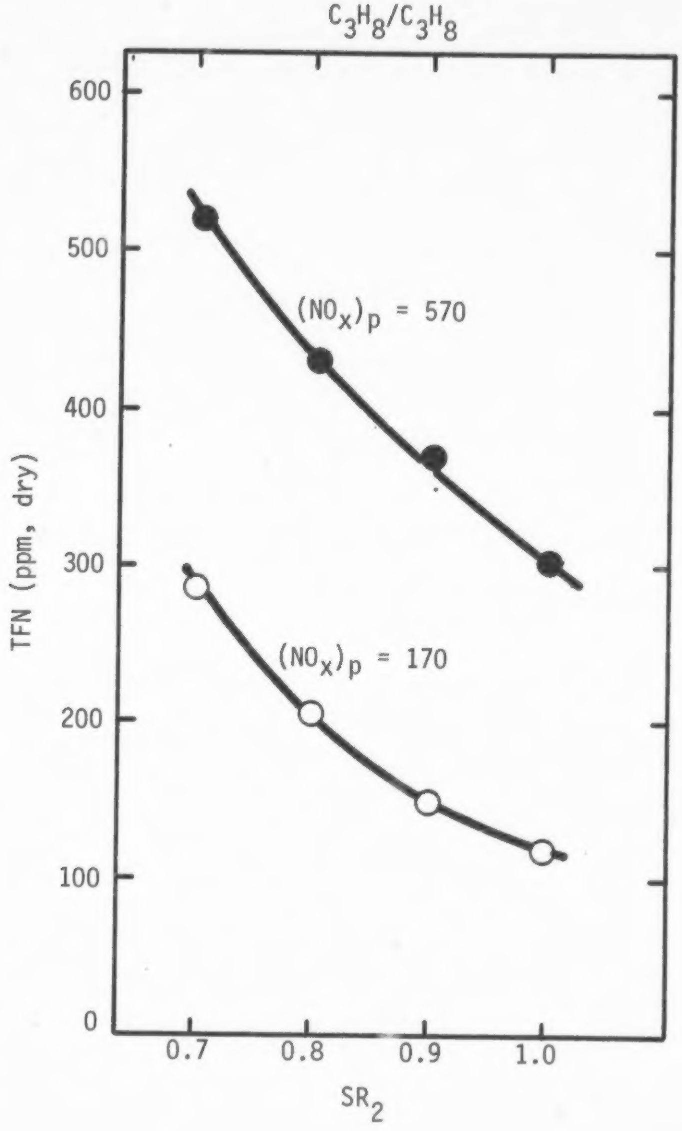

Figure 6-4. TFN at two $(NO_x)_p$ concentrations.

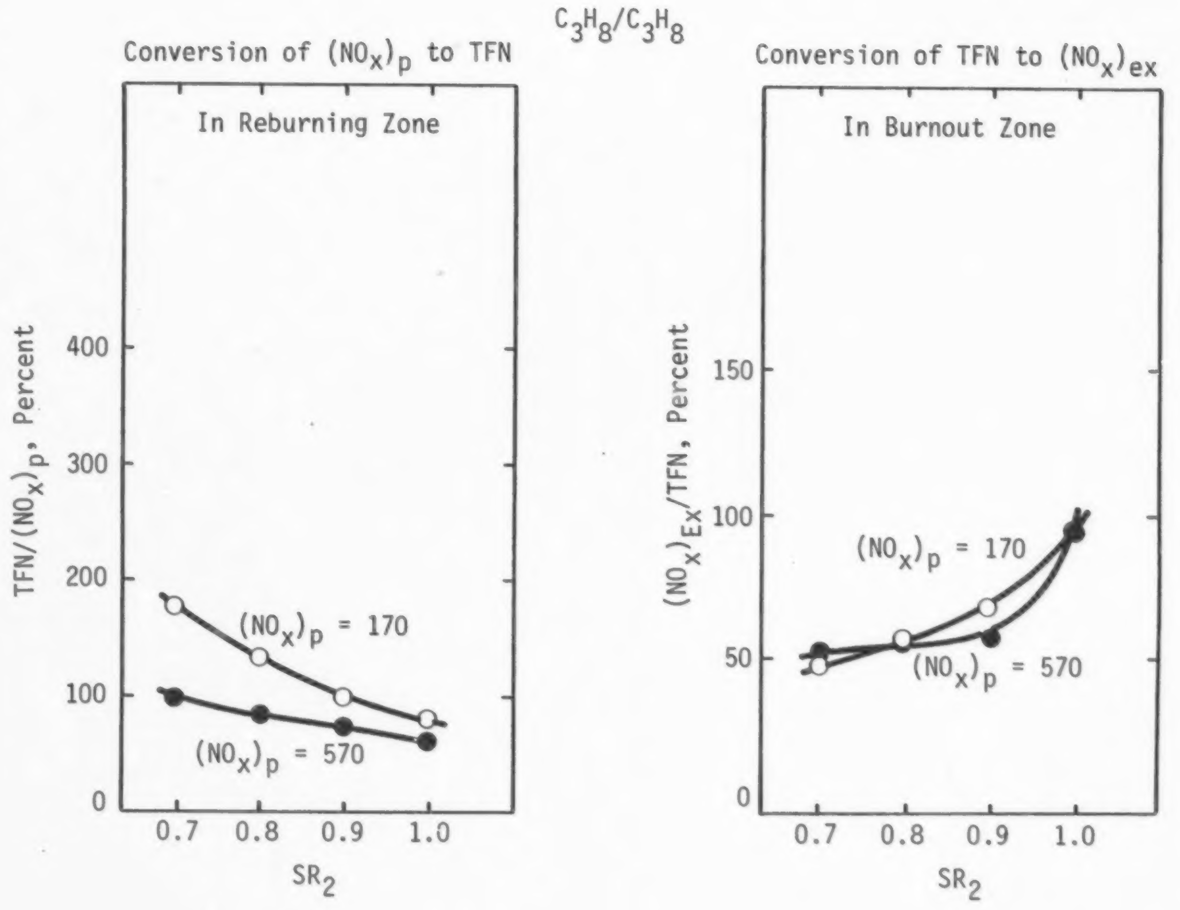

Figure 6-5. Conversions of $(NO_x)_p$ to TFN and TFN to $(NO_x)_{ex}$.

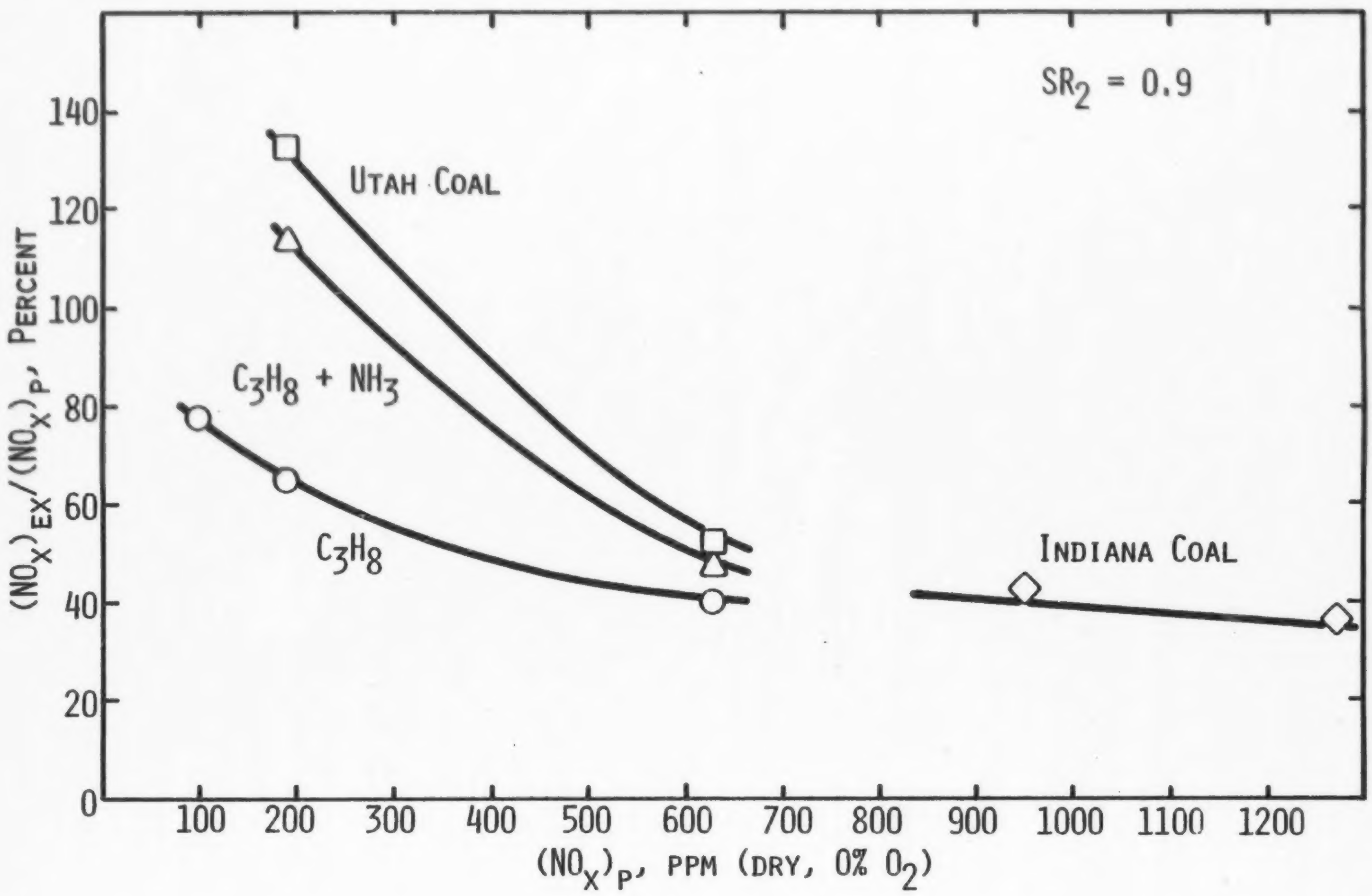

Figure 6-6. Effectiveness depends on primary NO_x.

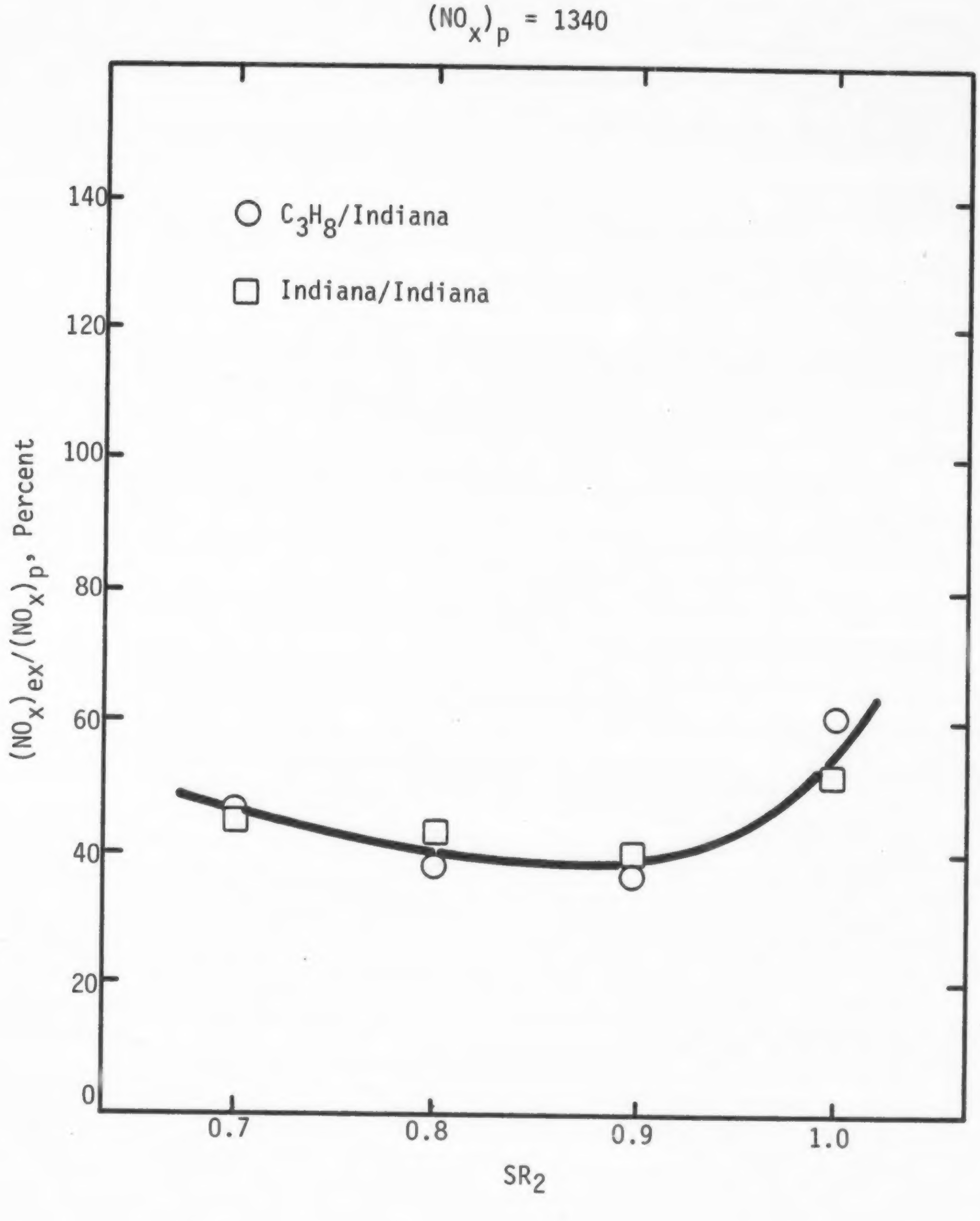

Figure 6-7. Influence of primary fuel type.

6.4 Summary

The conclusions formulated from the primary zone parametric studies are as follows:

- The primary zone stoichiometry did not alter the overall reburning efficiency. However, it was desirable to operate the primary zone at the lowest possible excess air level in order to minimize the amount of reburning fuel required to obtain the fuel-rich reburning zone. Minimizing the amount of reburning fuel also minimized the amount of fuel nitrogen present, for nitrogen bearing reburning fuels.

- The reburning effectiveness decreased dramatically at lower primary NO_x concentrations. Furthermore, at low primary NO_x levels, reburning with a nitrogen-containing fuel may lead to an overall formation of NO_x in the system. The effectiveness of the reburning process were clearly dependent on reburning fuel nitrogen concentration.

7.0 REBURNING ZONE PARAMETERS

7.1 Reburning Zone Stoichiometry

The effects of reburning zone stoichiometry on reburning effectiveness is presented in Figure 7-1. These results were obtained from a C_3H_8/C_3H_8 reburning experiment with $SR_1 = 1.30$. For both $(NO_x)_p$ curves, the minimums occurred simultaneously at $SR_2 = 0.9$. Detailed measurements (Figure 7-2) indicated that the minimum was a result of changes in the XN nitrogen speciation. Specifically, the middle plot showed that as SR_2 decreased, the NO also decreased, but the concentrations of other XN species (which could be partially converted to NO in the burnout zone) increased.

Figure 7-1 also indicates that an overall fuel-rich environment is not mandatory to reduce (NO_x) by reburning. At lean stoichiometries for the high $(NO_x)_p$ data, reduction up to 20 percent was obtained at $SR_2 = 1.2$. This overall lean reduction occurred mainly because of the diffusion nature of the reburning fuel flame. The flame developed a locally rich region around the fuel jets which was responsible for the overall lean reductions in Figure 7-1. for overall lean conditions. This phenomenon (reduction under overall fuel-lean conditions) was also observed with Utah coal as the reburning fuel (Overmoe, et al, 1984).

7.2 Influence of Reburning Fuel Composition

7.2.1 Hydrocarbon Content

Experiments were carried out to investigate the effectiveness of reburning with nonhydrocarbon fuels. Results of these tests with propane, H_2, and CO at two $(NO_x)_p$ levels are presented in Figure 7-3. At low $(NO_x)_p$, no difference in reburning effectiveness was noted between the H_2 and CO fuels, also the nonhydrocarbon fuels were as effective as propane at rich stoichiometries (SR_2 = 0.8 and 0.7). As the stoichiometry became leaner, higher reburning efficiency was attained with propane. As the $(NO_x)_p$ increased, the reburning efficiency of propane was better over the entire

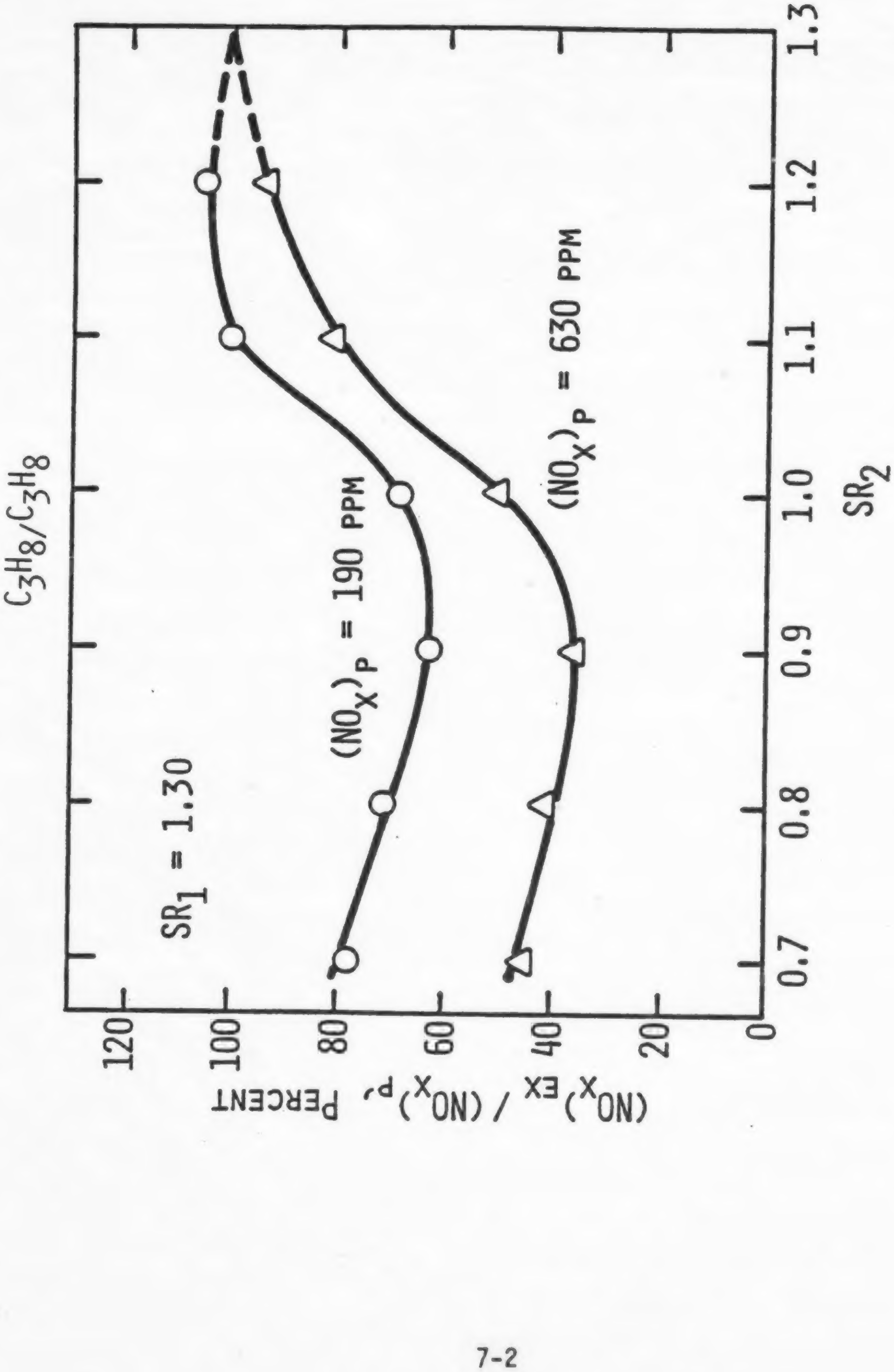

Figure 7-1. Influence of reburning zone stoichiometry.

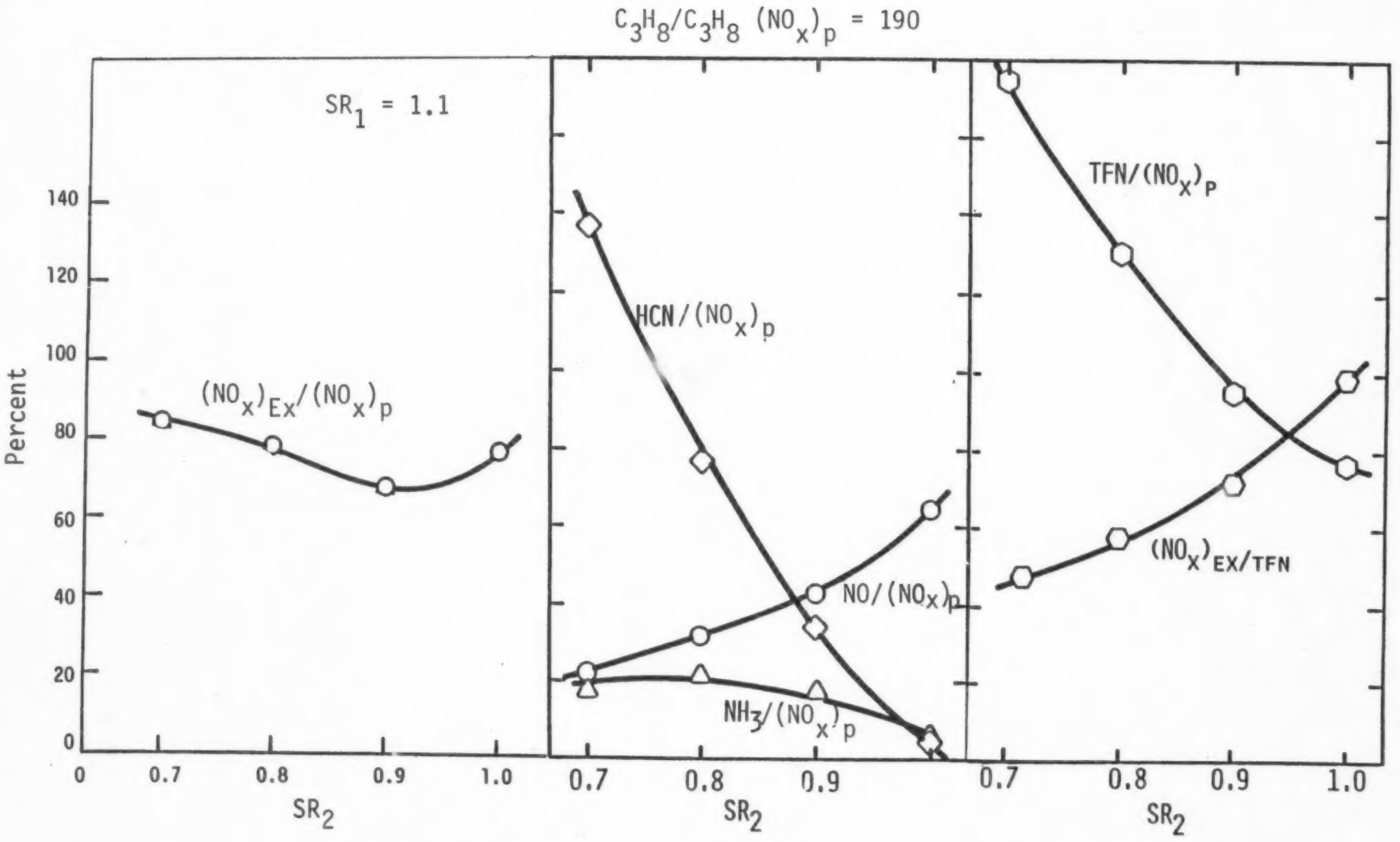

Figure 7-2. Detailed measurements, variable SR_2.

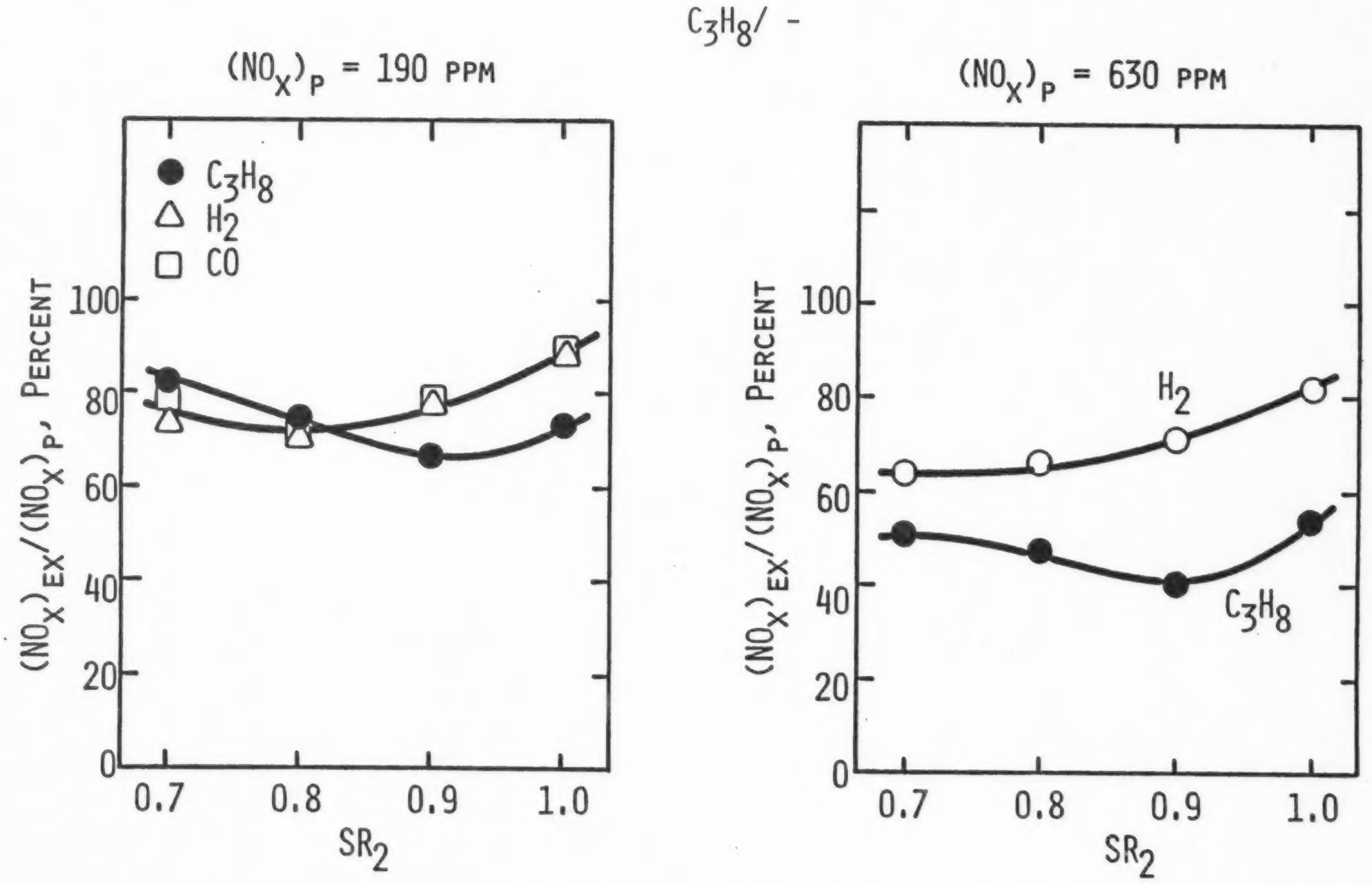

Figure 7-3. Hydrocarbon vs. non-hydrocarbon reburning fuels.

range of SR_2. This could be attributed to the generation of hydrocarbon radicals with propane reburning (See Section 1.1).

XN species concentrations were measured at the exit of the reburning zone for H_2 as the reburning fuel. These measurements compared to those taken with propane as the reburning fuel are presented in Figures 7-4 through 7-7. As shown, at low $(NO_x)p$ the H_2 reburning did not reduce NO in the reburning zone and little NH_3 and HCN were measured compared with propane reburning (see Figure 7-4). Figure 7-5 shows the conversions of $(NO_x)_p$ to TFN, of TFN to $(NO_x)_{ex}$, and the overall conversion of $(NO_x)_p$ to $(NO_x)_{ex}$. At leaner stoichiometries (SR_2 = 1.0 and 0.9), reburning with propane was more effective than with H_2. As the stoichiometry became richer, little difference in effectiveness was observed with respect to both fuels because the decreased NO in the reburning zone with propane was offset by the increased HCN species. For propane reburning, most of the reduction occurred in the burnout zone except at SR_2 = 1.0 where almost all the reduction took place in the reburning zone. With H_2 the majority of the reduction occurred in the burnout zone.

At high $(NO_x)_p$, identical trends were observed for both fuels with respect to the low $(NO_x)_p$ case (see Figure 7-6). The relative conversion data (Figure 7-7) indicated that even though more reduction occurs in the reburning zone at higher $(NO_x)_p$ (see Section 6-2) with propane, the relative reduction in the reburning zone does not increase for H_2 as $(NO_x)_p$ is increased. The reduction in the burnout zone was unaffected by $(NO_x)_p$ concentration for H_2 as the reburning fuel.

7.2.2 Reburning Fuel Nitrogen Content/Fuel Type

Pershing et al (1982) has shown that reburning efficiency increased as the fuel nitrogen content of the reburning fuel was decreased. Figure 7-8 illustrates the results from this previous experimental study where propane doped with NO was reburned with propane doped with variable amounts of NH_3. The data clearly indicated that optimum NO_x reduction occurred with no fuel

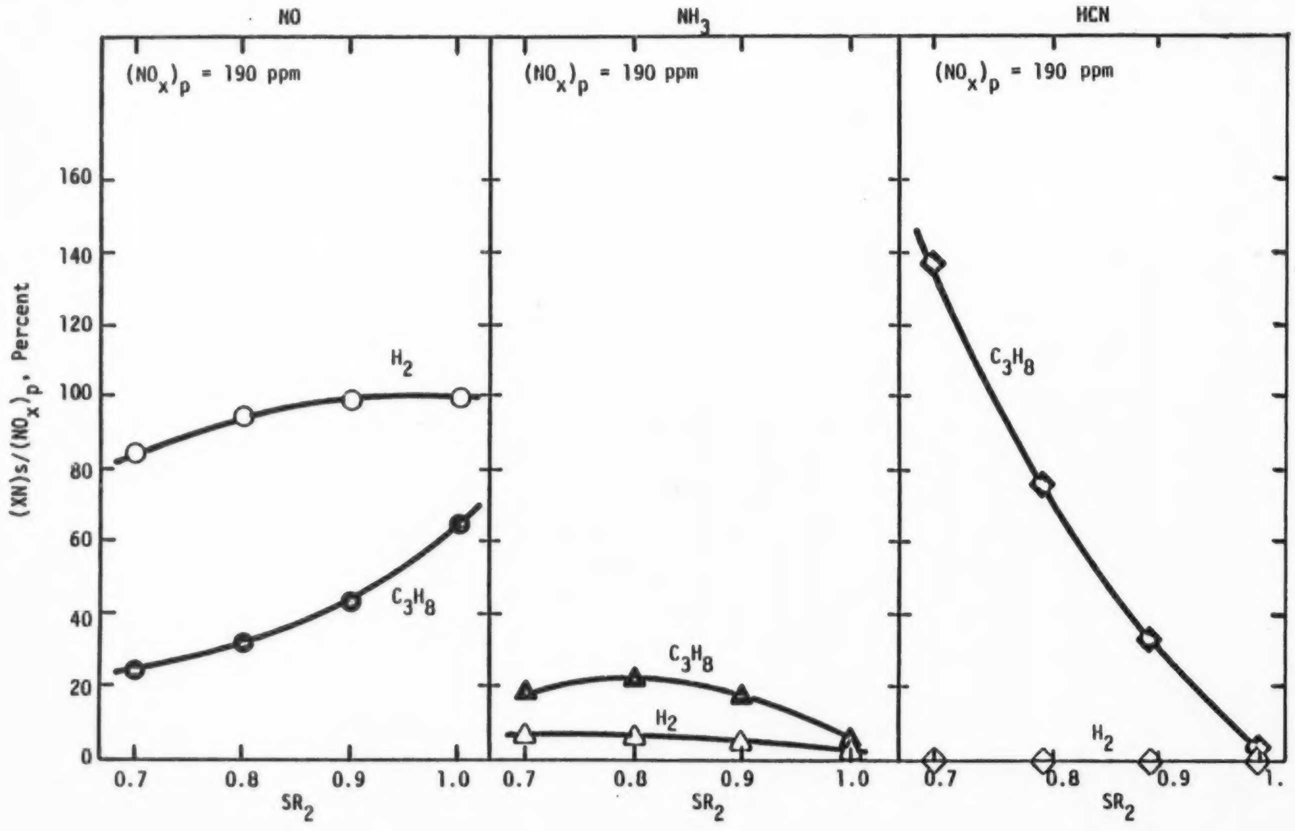

Figure 7-4. XN species concentrations at the exit of the reburning zone.

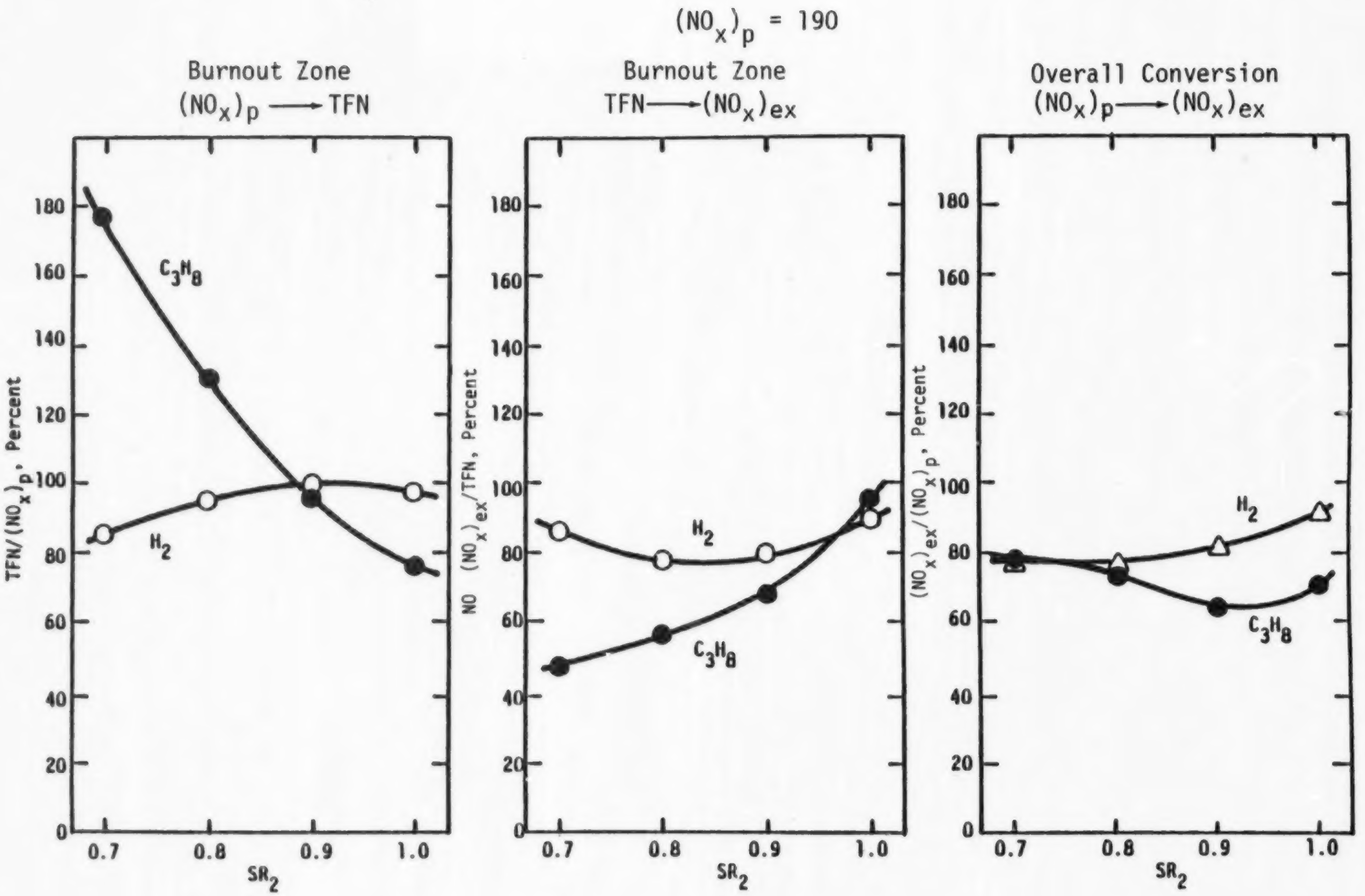

Figure 7-5. Conversion in different zones.

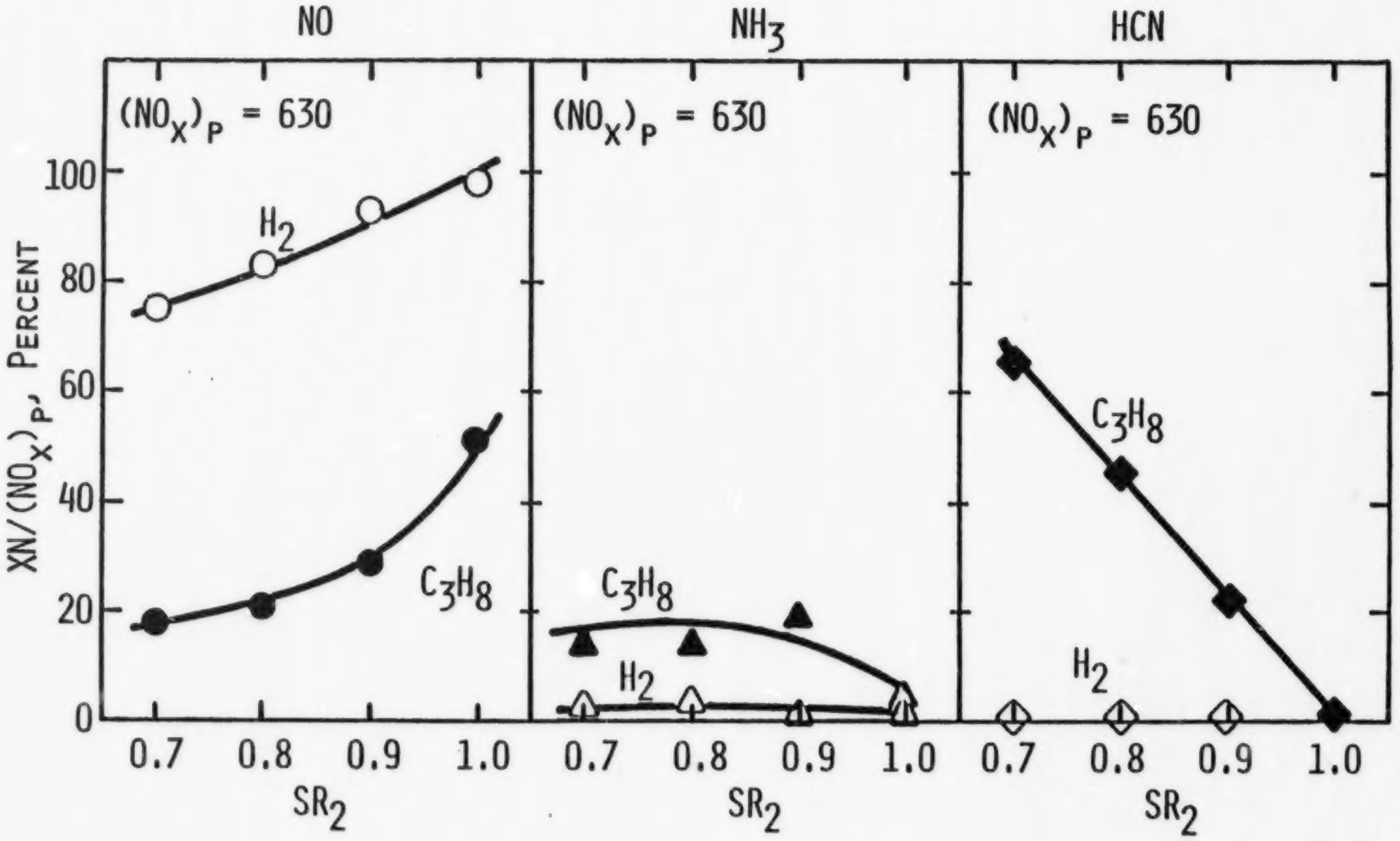

Figure 7-6. XN species concentrations at the exit of the reburning zone.

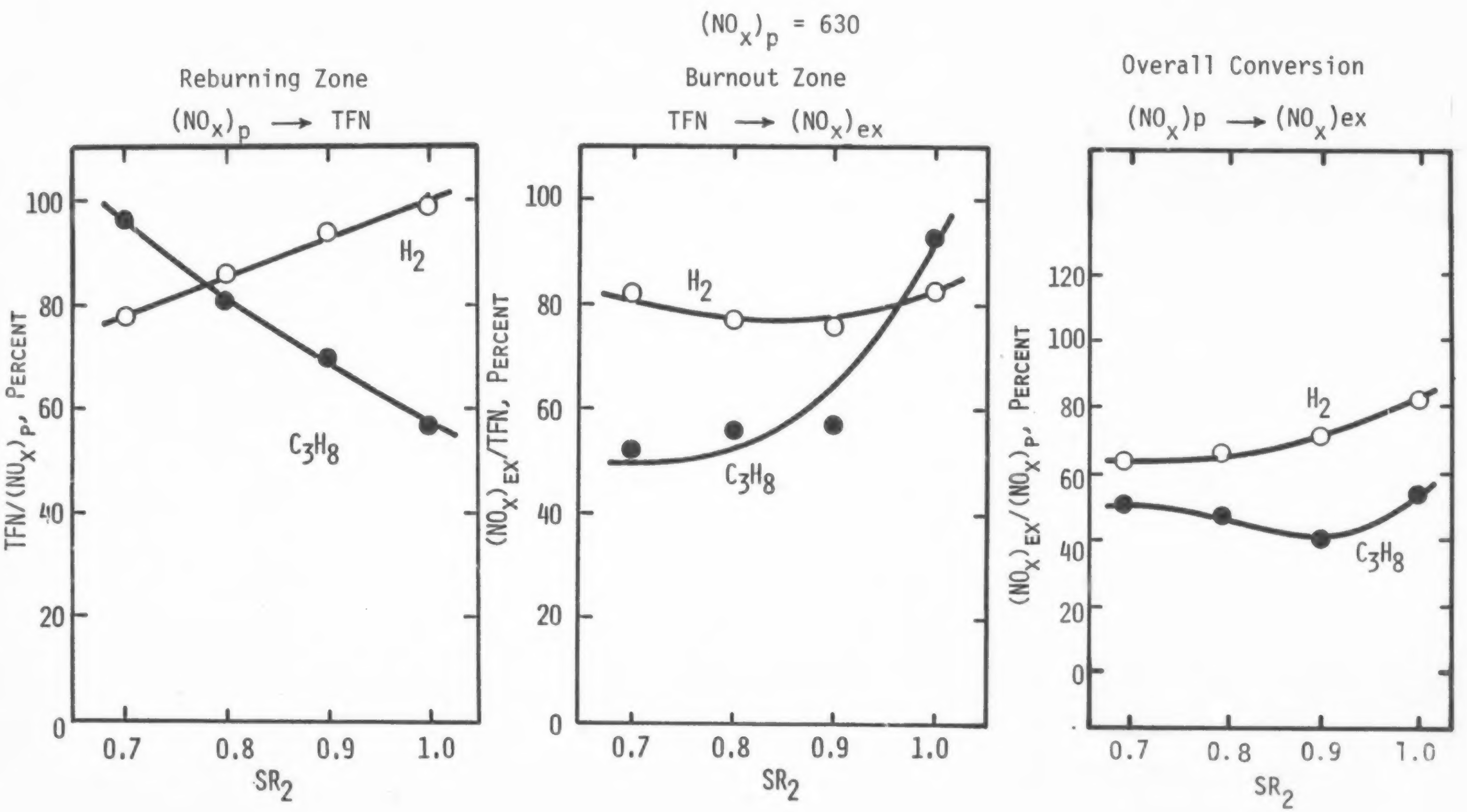

Figure 7-7. Conversion in different zones.

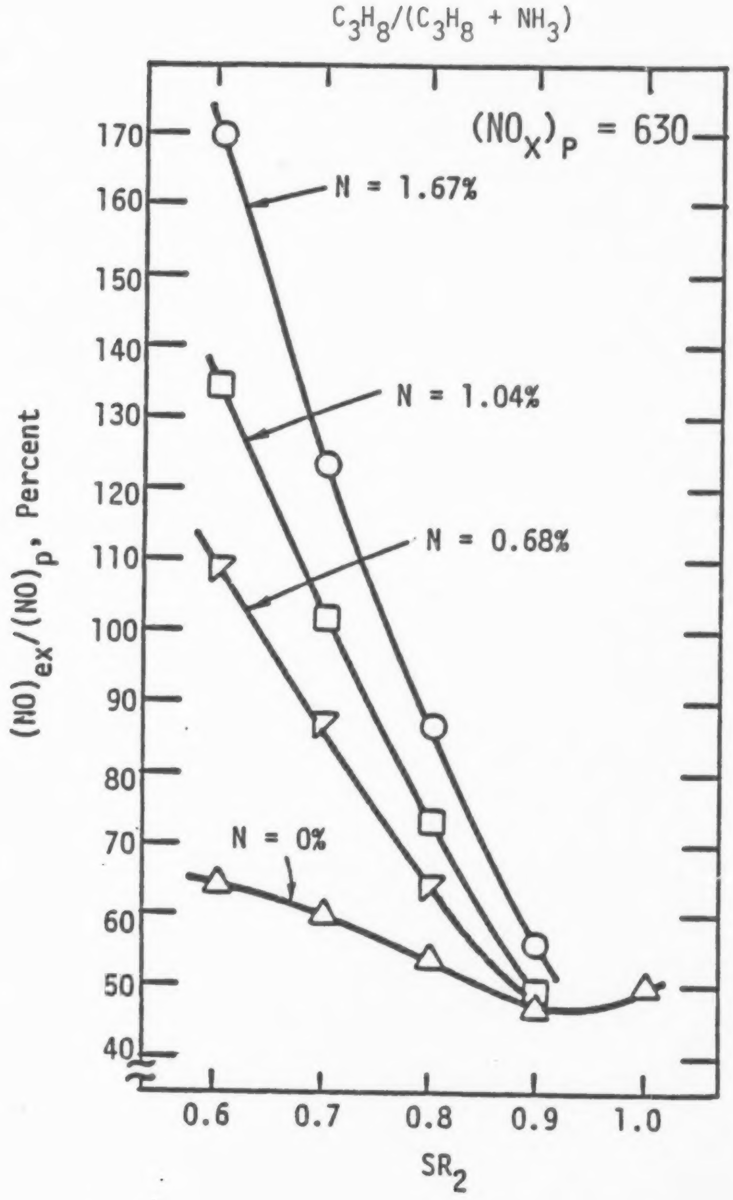

Figure 7-8. Influence of reburning fuel nitrogen content.

nitrogen in the reburning fuel and as nitrogen content increased, reburning efficiency decreased.

The effect of reburning fuel type is presented in Figure 7-9. This plot indicates that increased nitrogen content in the reburning fuel had an adverse effect on the reburning efficiency. Comparison between Utah and propane doped with ammonia (to the same nitrogen percentage as Utah coal) indicated that the fuel with totally volatile nitrogen had somewhat better reburning effectiveness. The detailed XN measurements, taken at the exit of the rich zone, indicated that the Utah coal did not reduce NO as well as the two propane fuels (see Figure 7-10). While the Utah and C_3H_8 + NH_3 fuels produced similar NH_3 and HCN yields, the Utah coal produced significantly higher TXN, due to the char nitrogen, as indicated in Figure 7-11. Even though the conversion of TXN to $(NO_x)_{ex}$ was lower for the Utah coal, higher exhaust emissions were measured with the Utah coal. For all three fuels, it appeared that the burnout zone predominated in the overall NO_x reduction mechanism.

A composite plot illustrating the overall conversion of the fixed nitrogen species (primary NO_x plus fuel nitrogen) to NO_x is presented in Figure 7-12. This figure contains all reburning data acquired, during this project, in an attempt to determine the range of reduction efficiencies for reburning. The bulk of the reburning data fell within the range of 20 percent to 40 percent conversion.

7.2.3 Coal Composition

Reburning effectivenesses for the coals fired as reburning fuels are presented in Figure 7-13. As anticipated, the Yallourn brown coal was the most efficient reburning coal, chiefly due to its low fuel nitrogen content and high volatility. By increasing the $(NO_x)_p$ the efficiency of the process increased (see Section 6.2) but the overall ranking of the coals, from best to worst, was unaffected.

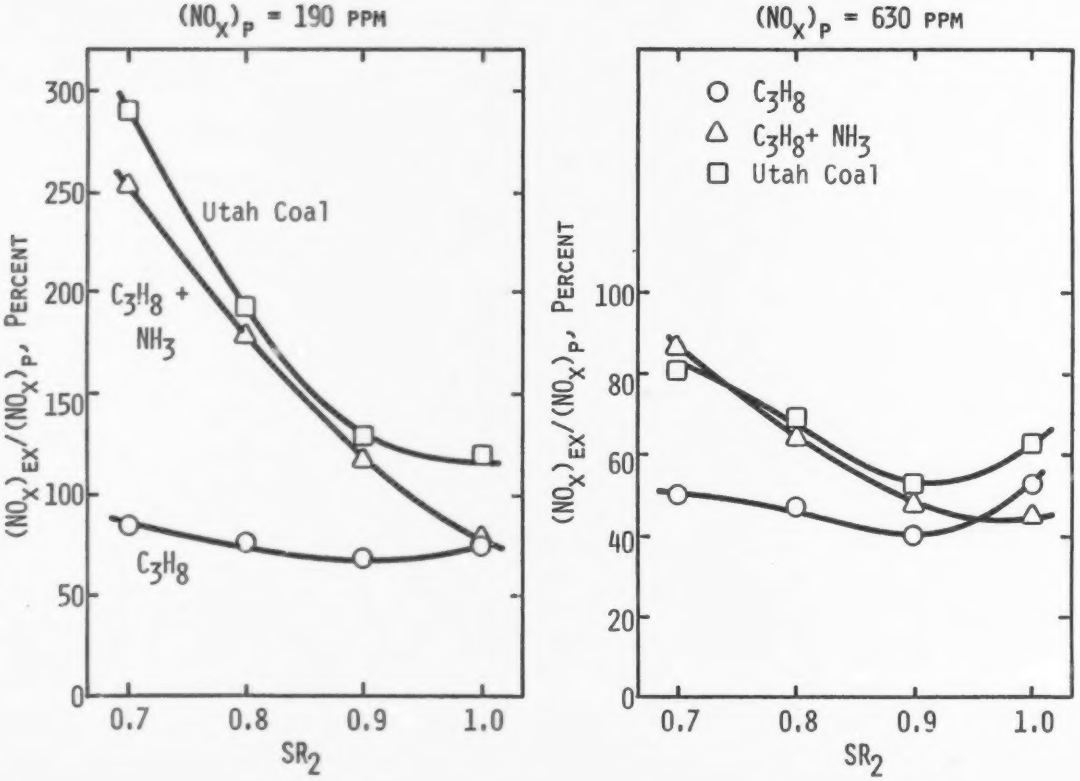

Figure 7-9. Influence of fuel type.

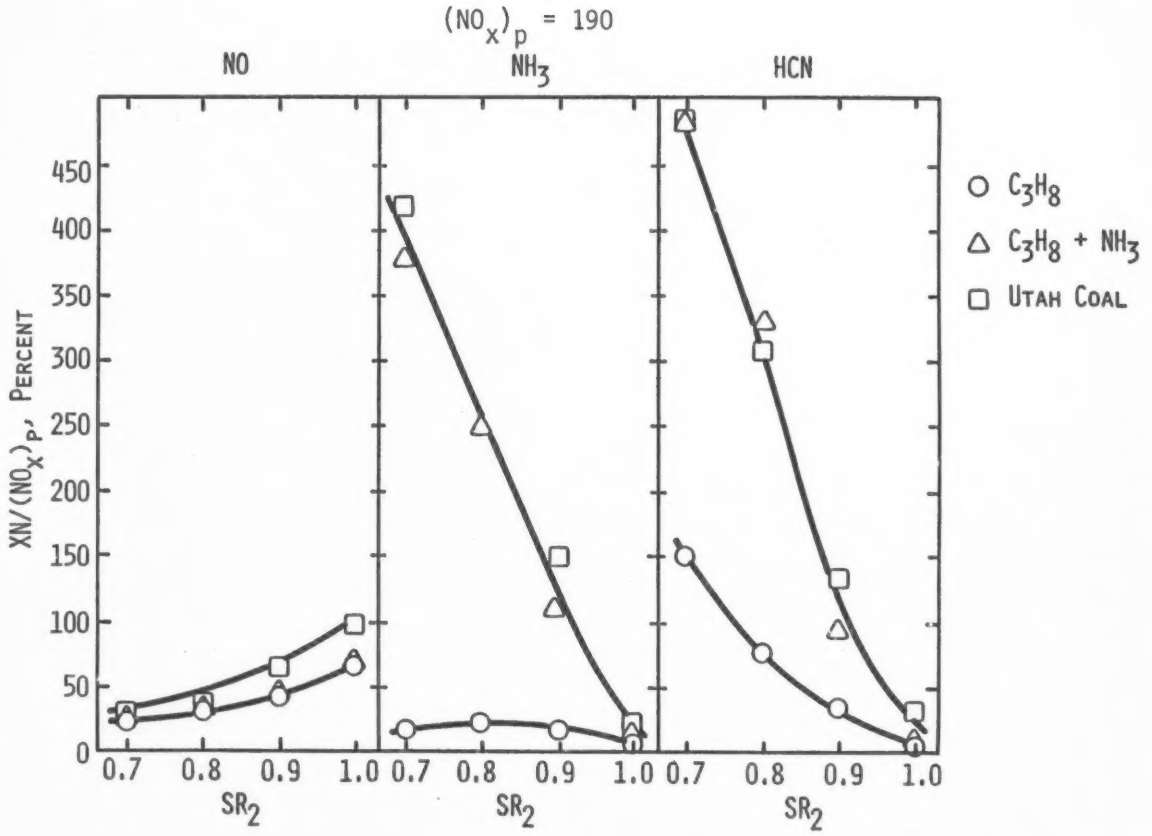

Figure 7-10. Detailed measurements.

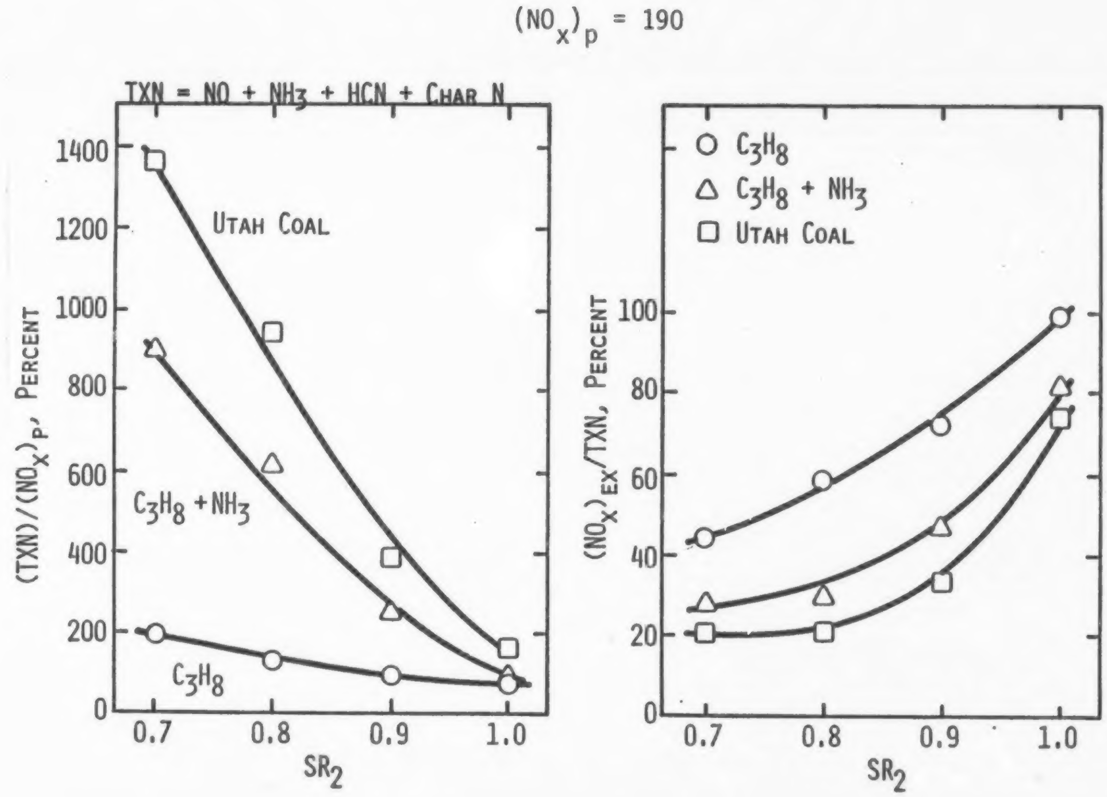

Figure 7-11. Conversions in the reburning and burnout zones.

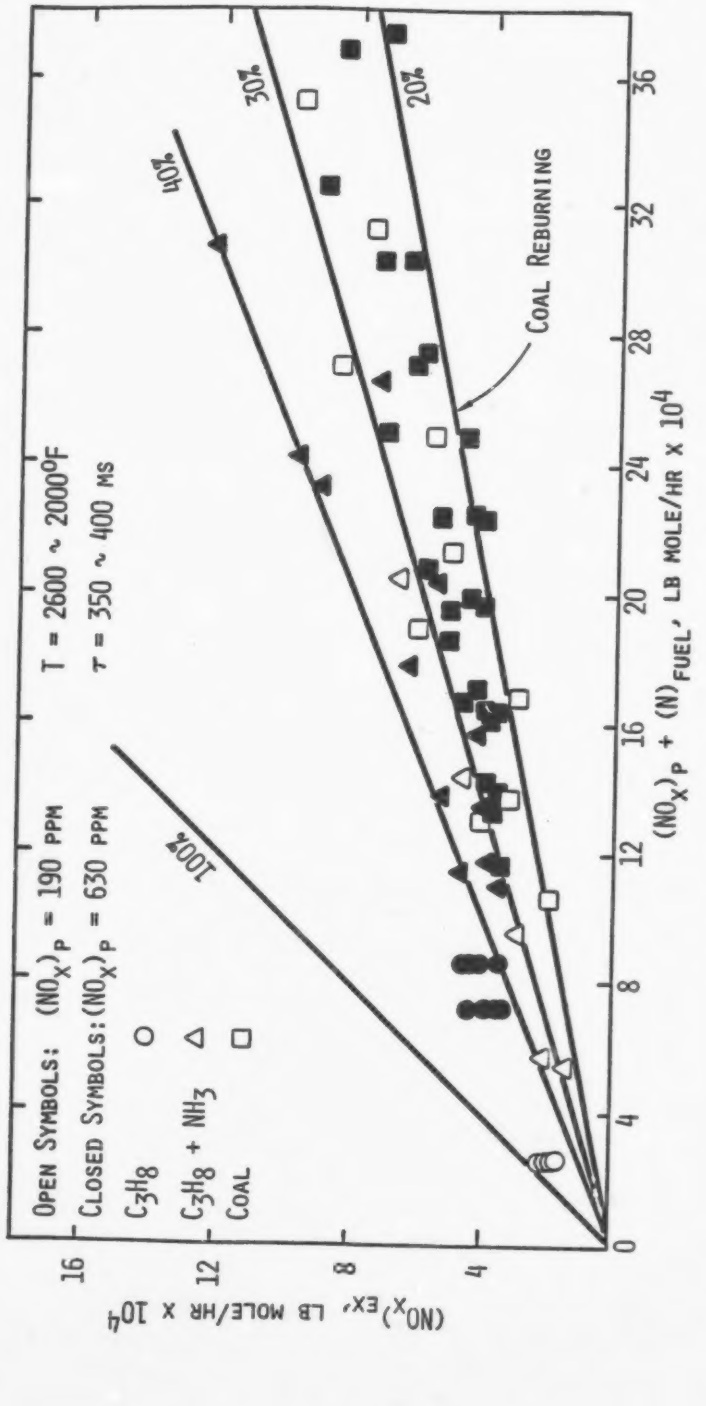

Figure 7-12. Conversion of inlet nitrogen species to NO_X.

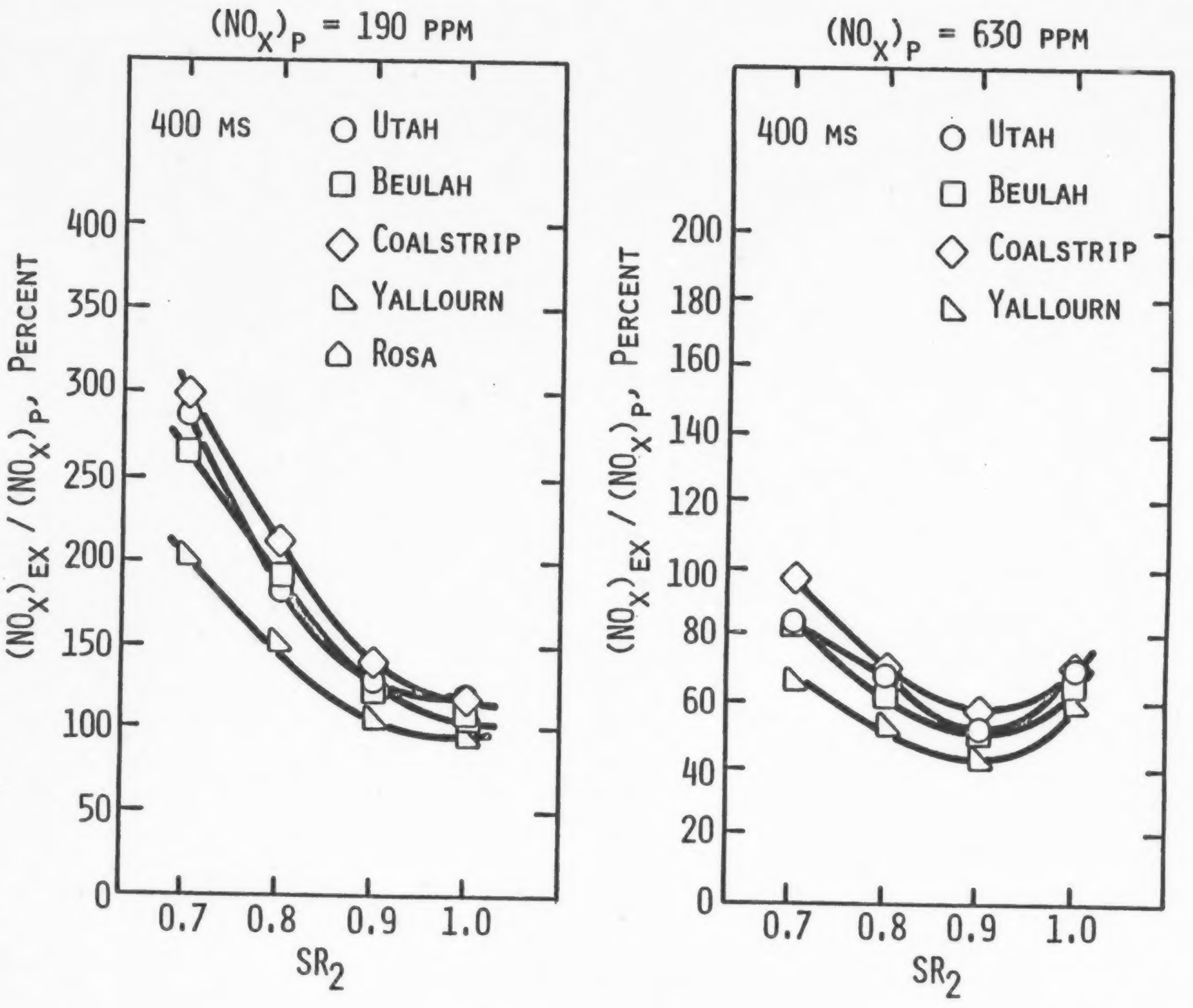

Figure 7-13. Comparison of different coals.

The coal reburning data replotted in terms of conversion of total nitrogen species [$(NO_x)_P$ plus coal nitrogen] is presented in Figure 7-14. This plot indicates that the percent conversion of the fuel nitrogen remained constant regardless of which coal was used as the reburning fuel. For rich stoichiometries ($SR_2<1.0$) approximately 24 percent of the primary NO_x plus the coal nitrogen appeared as $(NO_x)_{Ex}$ for all coals. At $SR_2 = 1.0$, 45 percent conversion was obtained.

Only the coals which completely burned out were included in the data set. Rosa coal burned out only at lean stoichiometries and the Pennsylvania anthracite did not burn completely at any conditions.

7.2.4 Summary

The following conclusions were made pertaining to the influence of reburning fuel composition.

- Hydrocarbon fuels are more effective than nonhydrocarbon fuels.
- Fuel nitrogen increases exhaust NO_x.
- Conversion of fuel nitrogen in coals is constant if the coals completely burn out.
- Low volatile coals have burnout problems.

7.3 Influence of Residence Time

The influence of reburning zone residence time was investigated by physically changing the location at which the burnout air was injected. Experimental work at three residence times (140 ms, 400 ms, 750 ms) was performed. By executing the experimental work in this manner, the primary zone exit temperature (T_1) was held constant while the reburning zone exit temperature (T_2) decreased as residence time was increased. Figure 7-15

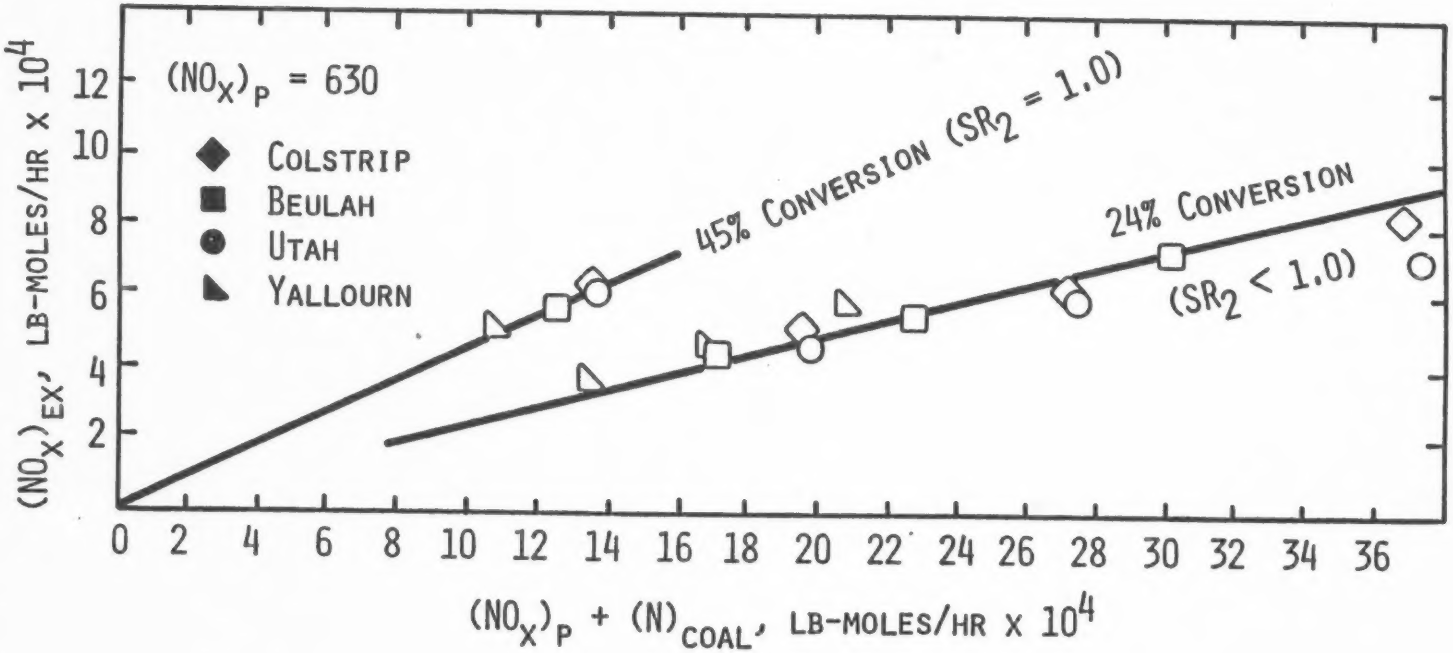

Figure 7-14. Conversion of inlet nitrogen to $(NO_x)_{Ex}$.

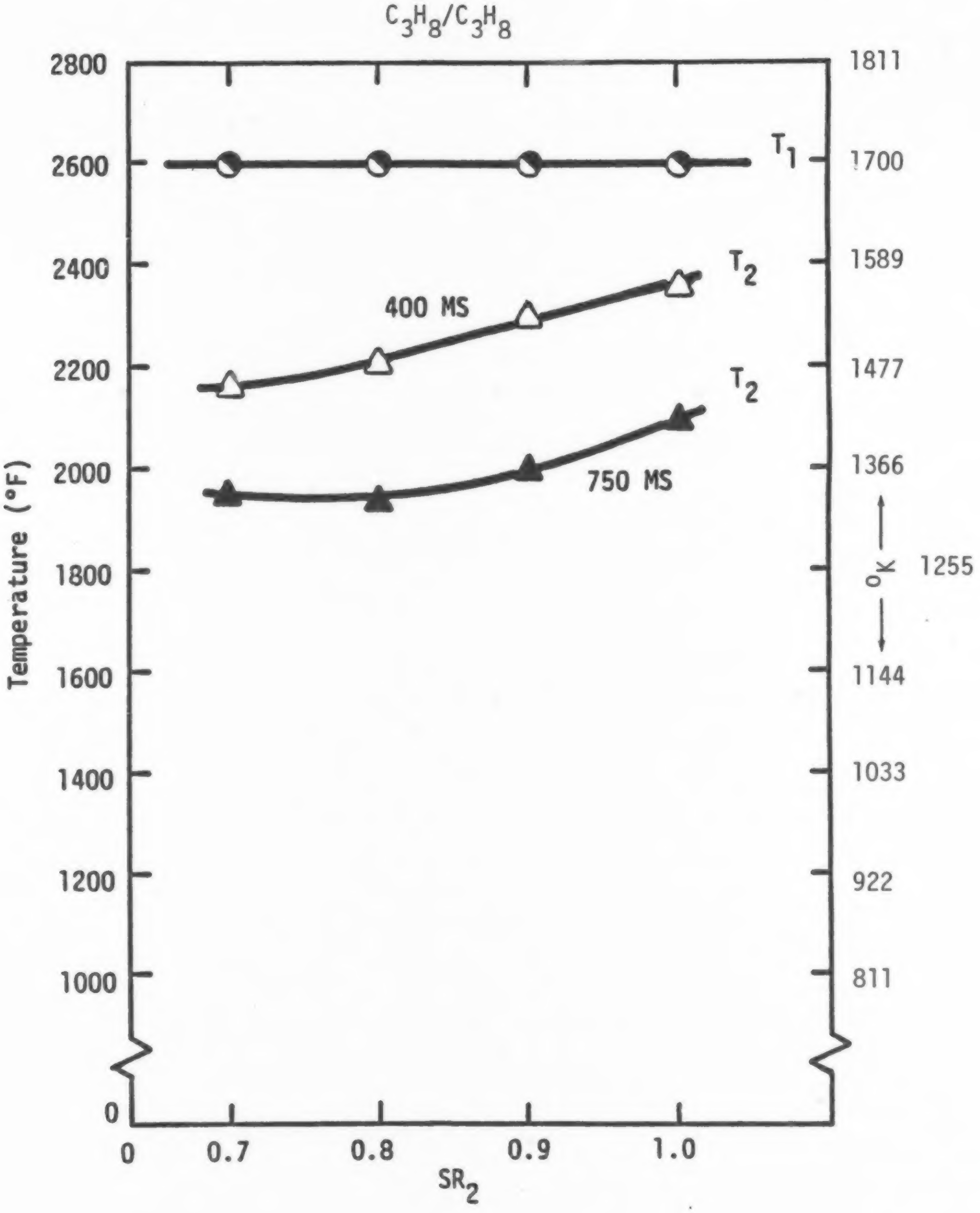

Figure 7-15. Reburning zone entrance (T_1) and exit (T_2) temperatures at two residence times.

shows the thermal characteristics for the test conditions at the 400 ms and 750 ms residence times. As indicated in Section 8.2, the reburning zone exit temperature does not affect reburning efficiency as long as thermal conditions are above the "de-NO_x" temperature window of about 1700°F.

7.3.1 Overall Effects

The influence of variable reburning zone residence time, at low $(NO_x)_p$, for three reburning fuels is presented in Figure 7-16. For all three reburning fuels, a significant improvement in the reburning efficiency was observed at longer residence times. Similar trends were observed at high $(NO_x)_p$ levels (see Figure 7-17). Figure 7-18 summarizes the effect of residence time on reburning effectiveness at optimum reburning zone stoichiometry. For all the fuels tested, the reburning process was enhanced by increasing the residence time.

Detailed measurements of the XN species exiting the reburning zone were performed for the three reburning fuels at residence times of 400 ms and 750 ms. For C_3H_8/C_3H_8 reburning, the increased residence time allowed the NO to decay further under the fuel-rich conditions (see Figure 7-19). This reduction of NO was observed at stoichiometries richer than 1.0. Although the formation of TFN did not change with time at SR_2 of 1.0, 0.9, and 0.8 (see Figure 7-20), the conversion of TFN to $(NO_x)_{ex}$ was lower at longer residence time due to the lower amount of NO present in the reactive nitrogen pool. At SR_2 = 0.7 the decrease in TFN formation and increase in TFN to NO_x conversion at the longer residence time resulted in a net destruction of NO with increased residence time. Figures 7-21 through 7-24 summarize the XN data with C_3H_8 + NH_3 and Utah coal as the reburning fuels. Similar NO decay was observed with both C_3H_8 + NH_3 and Utah coal as was noted with C_3H_8 as the reburning fuel. With nitrogen in the reburning fuel, the conversion of $(NO_x)_p$ to TFN was constant at leaner stoichiometries (SR_2 = 1.0, 0.9) and the conversion of TFN to $(NO_x)_{ex}$ decreased with increasing residence time. As the reburning zone became richer (SR_2 = 0.8, 0.7), the conversion of $(NO_x)p$ to TFN declined and the conversion of TFN to (NOx)ex became constant. This observation suggested that the presence of nitrogen in the reburning fuel shifts the cross-over point in these curves to leaner stoichiometries.

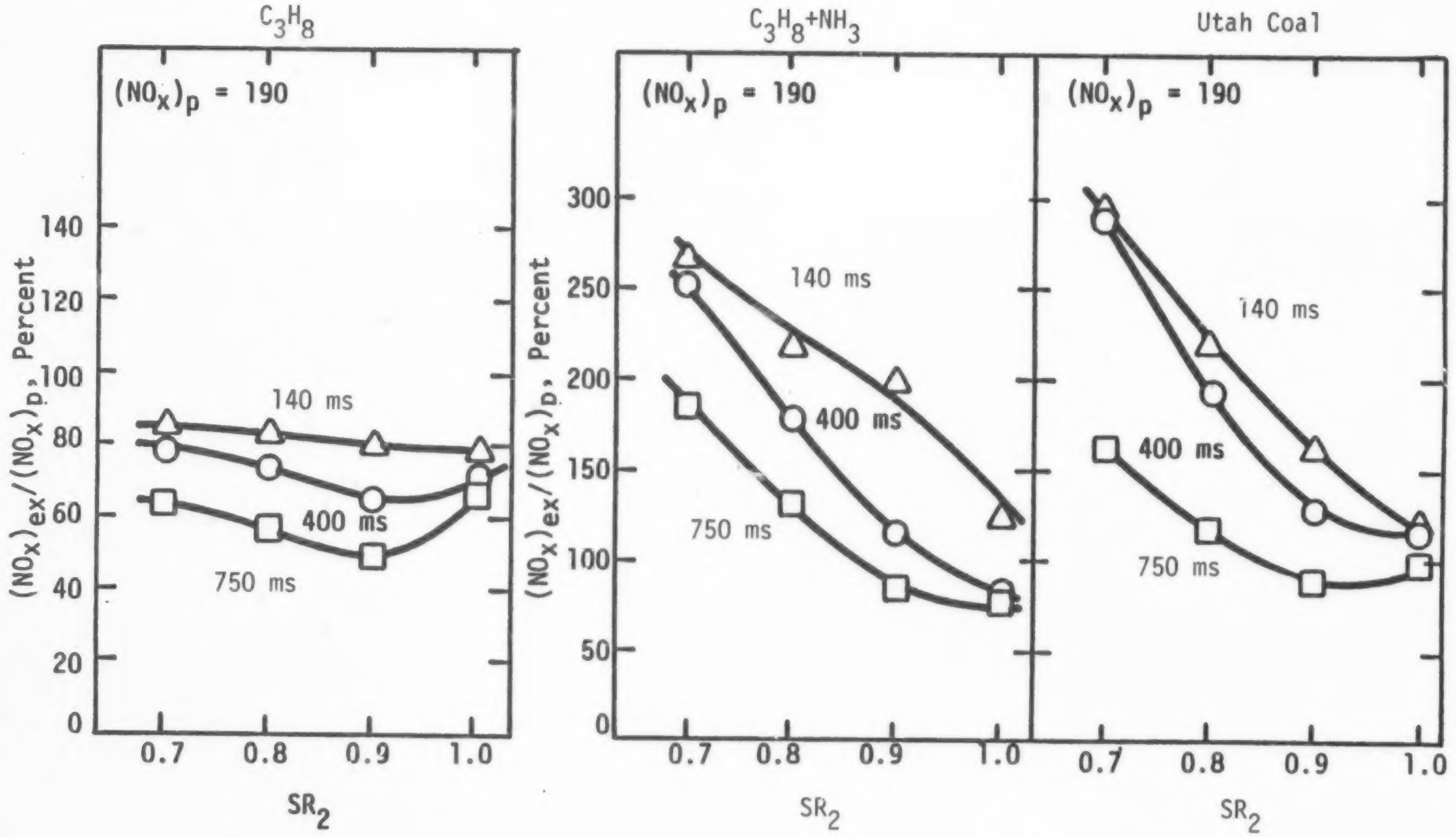

Figure 7- 16. Influence of residence time.

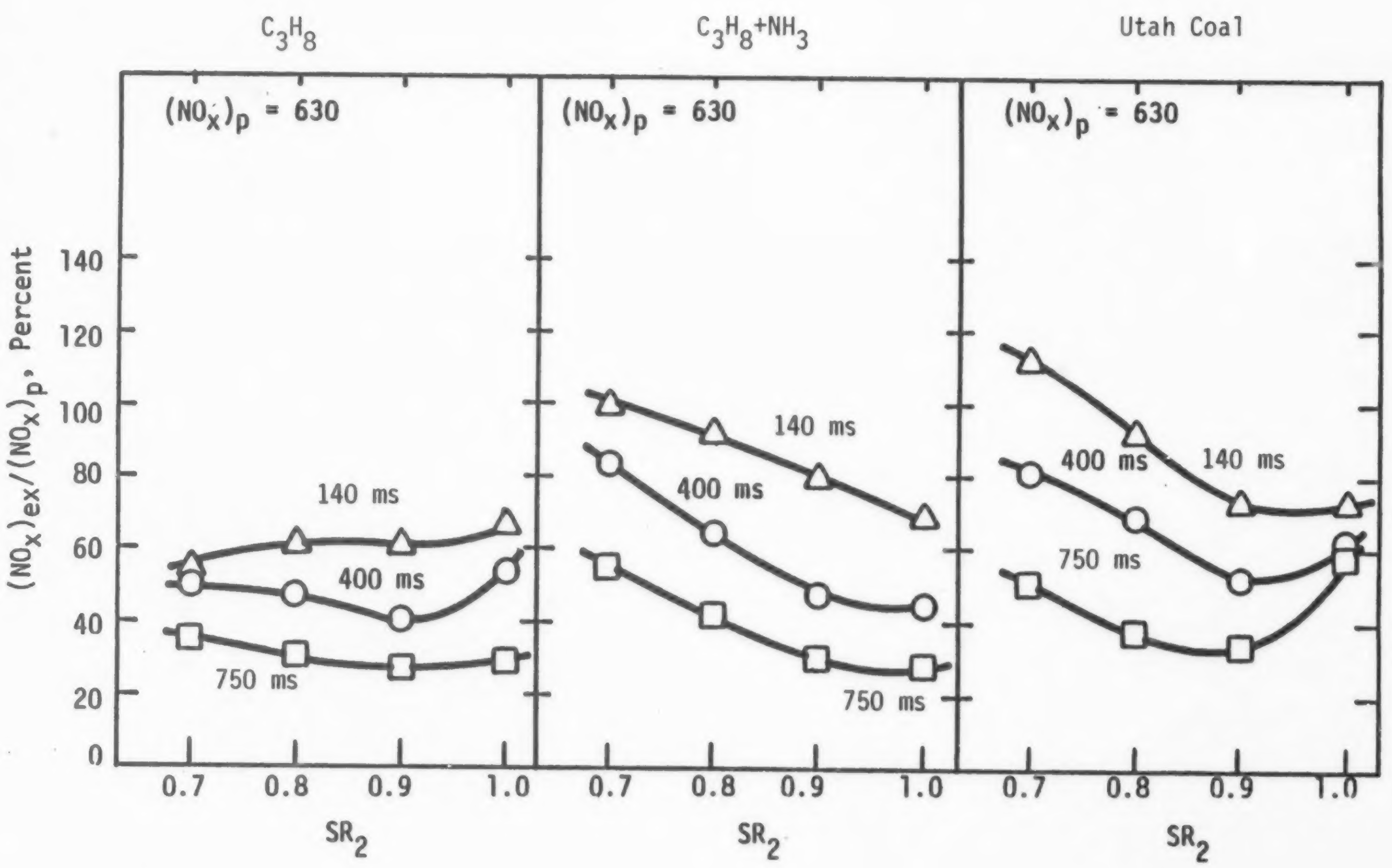

Figure 7- 17. Influence of residence time.

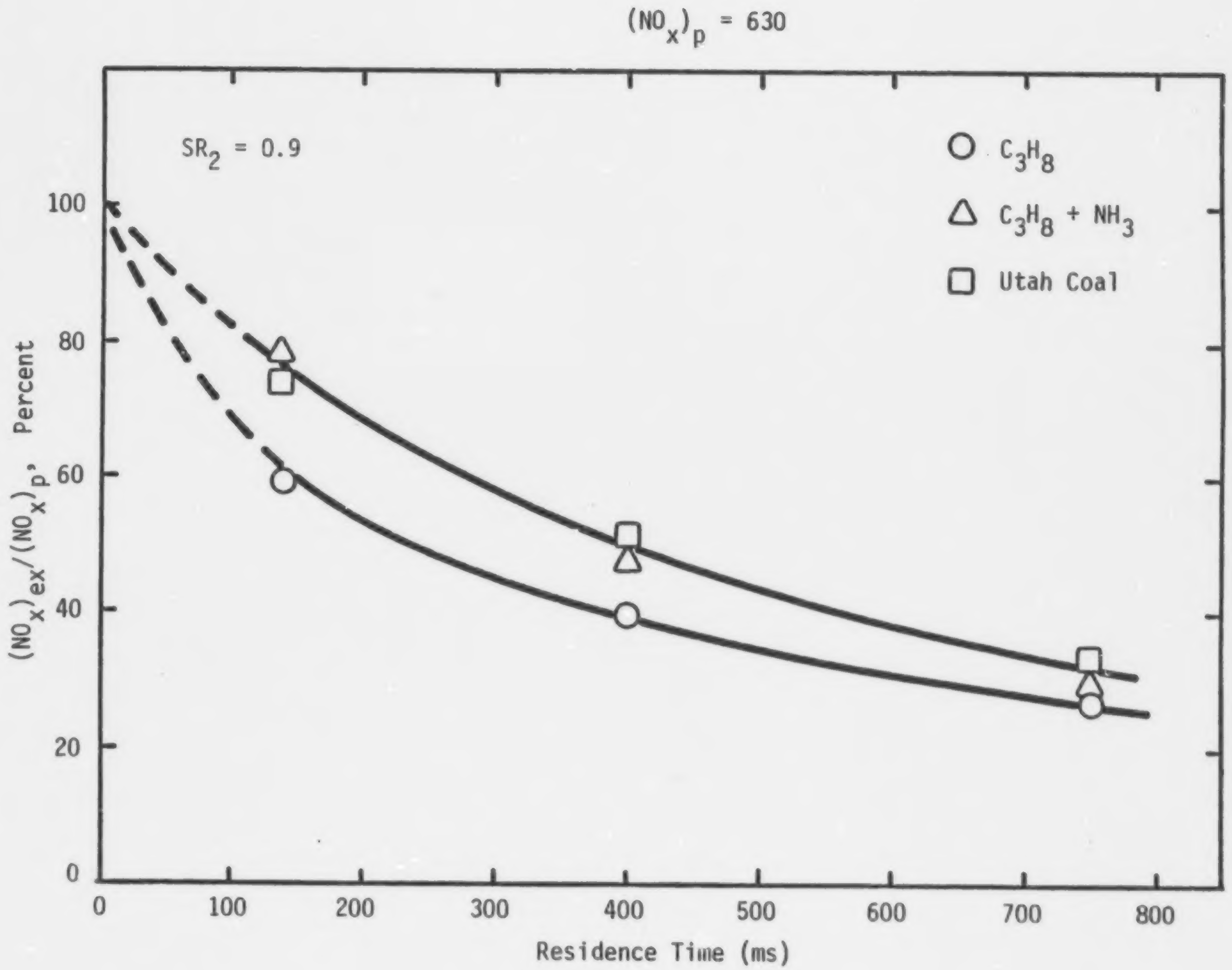

Figure 7-18. Reburning effectiveness as a function of residence time.

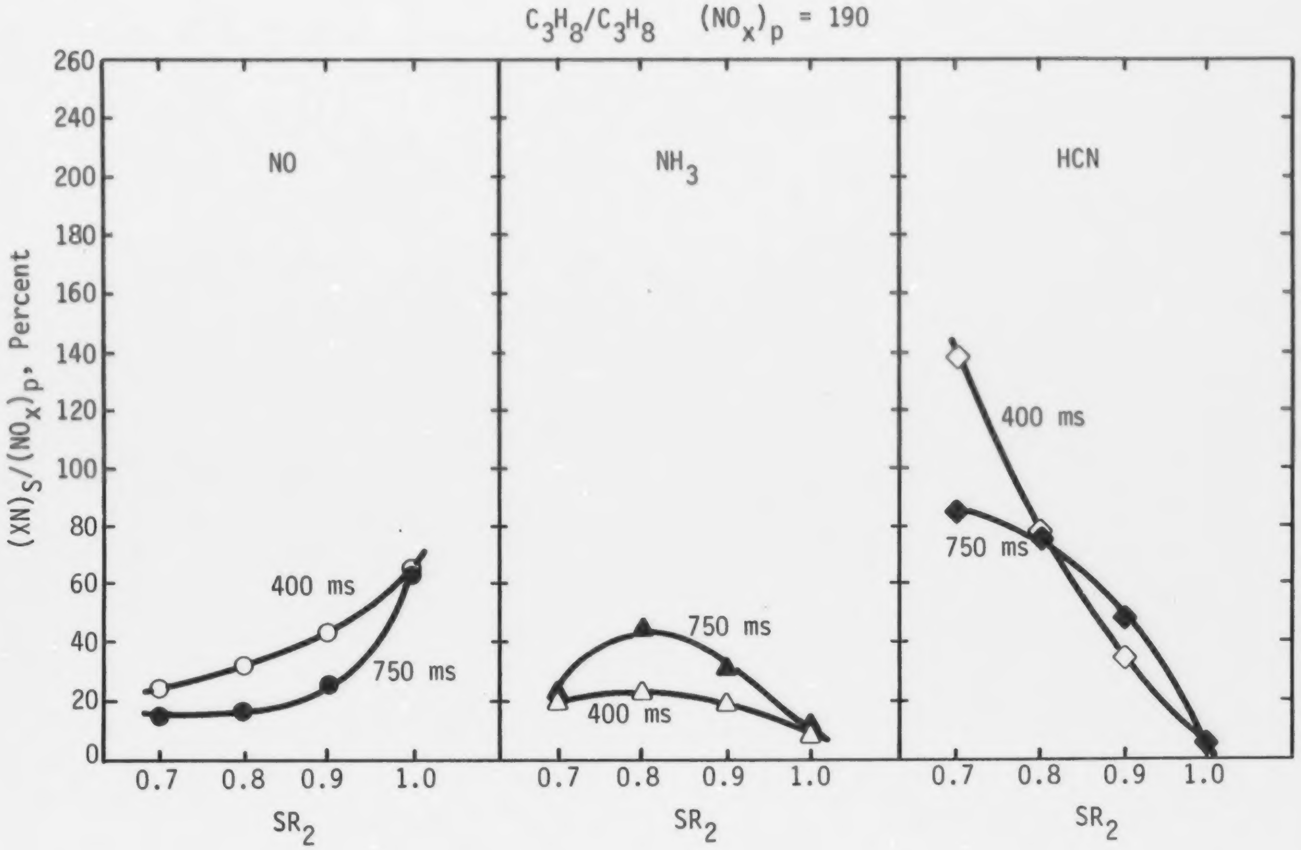

Figure 7-19. Detailed measurements at two residence times.

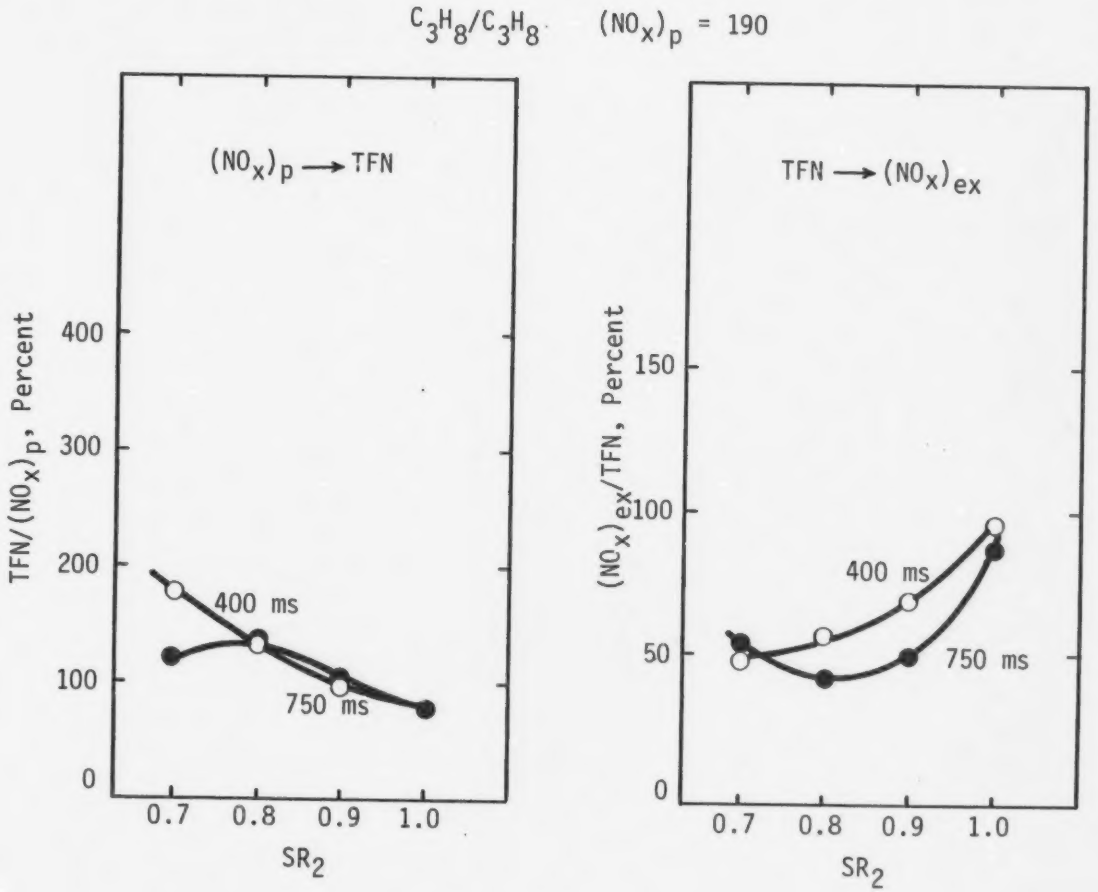

Figure 7- 20. Conversion at different residence times.

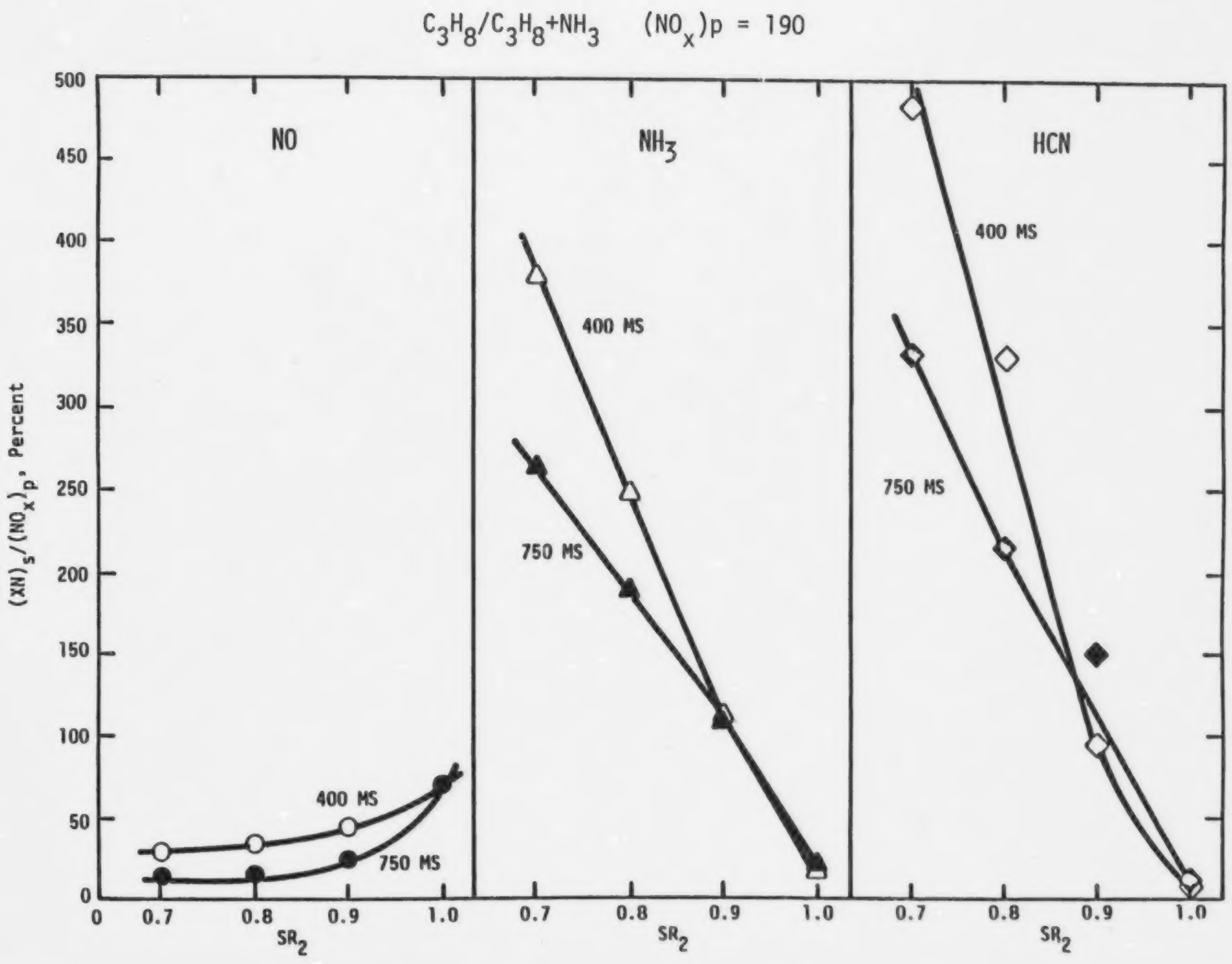

Figure 7- 21. Detailed measurements at two residence times.

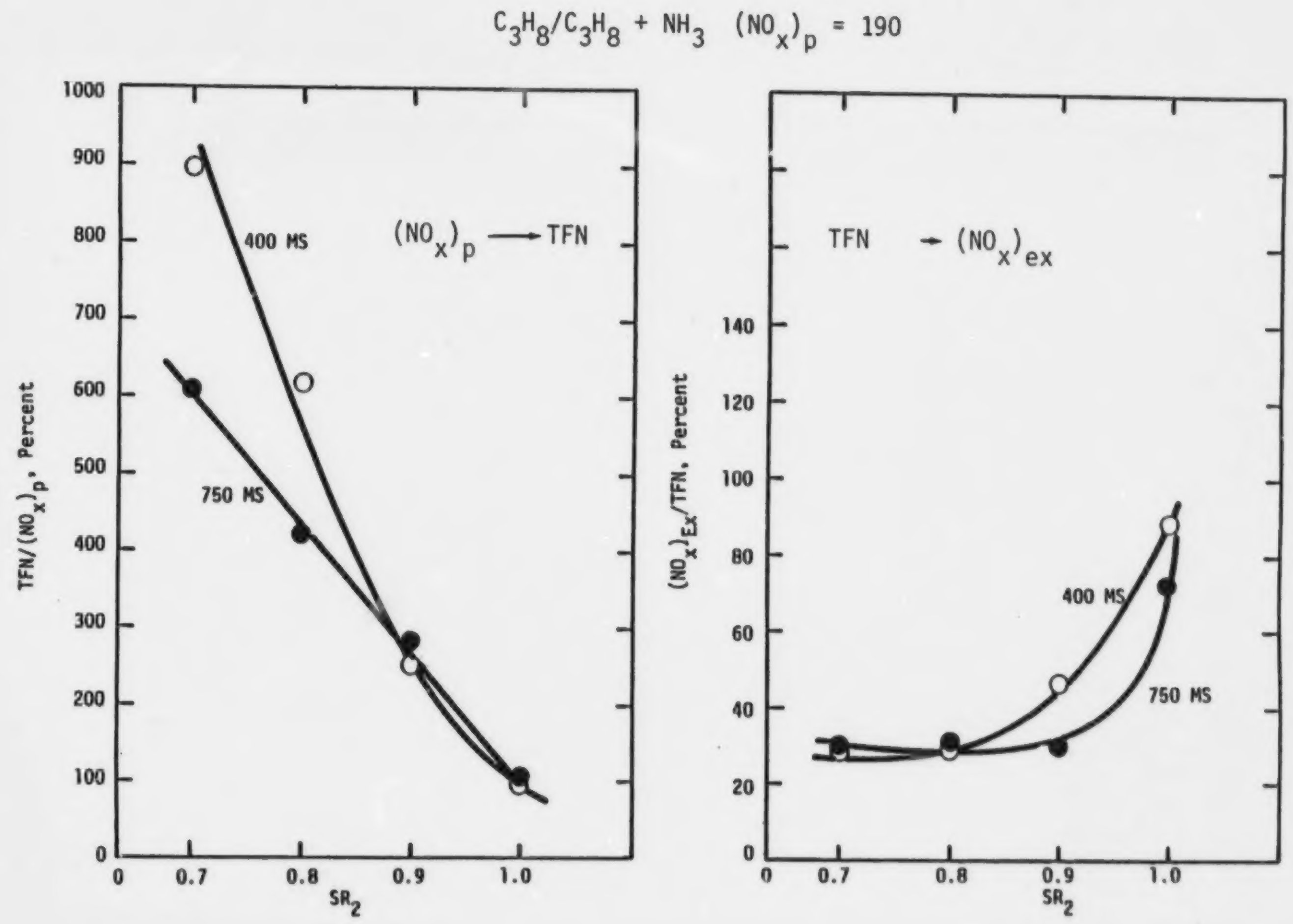

Figure 7-22. Conversions at different residence times.

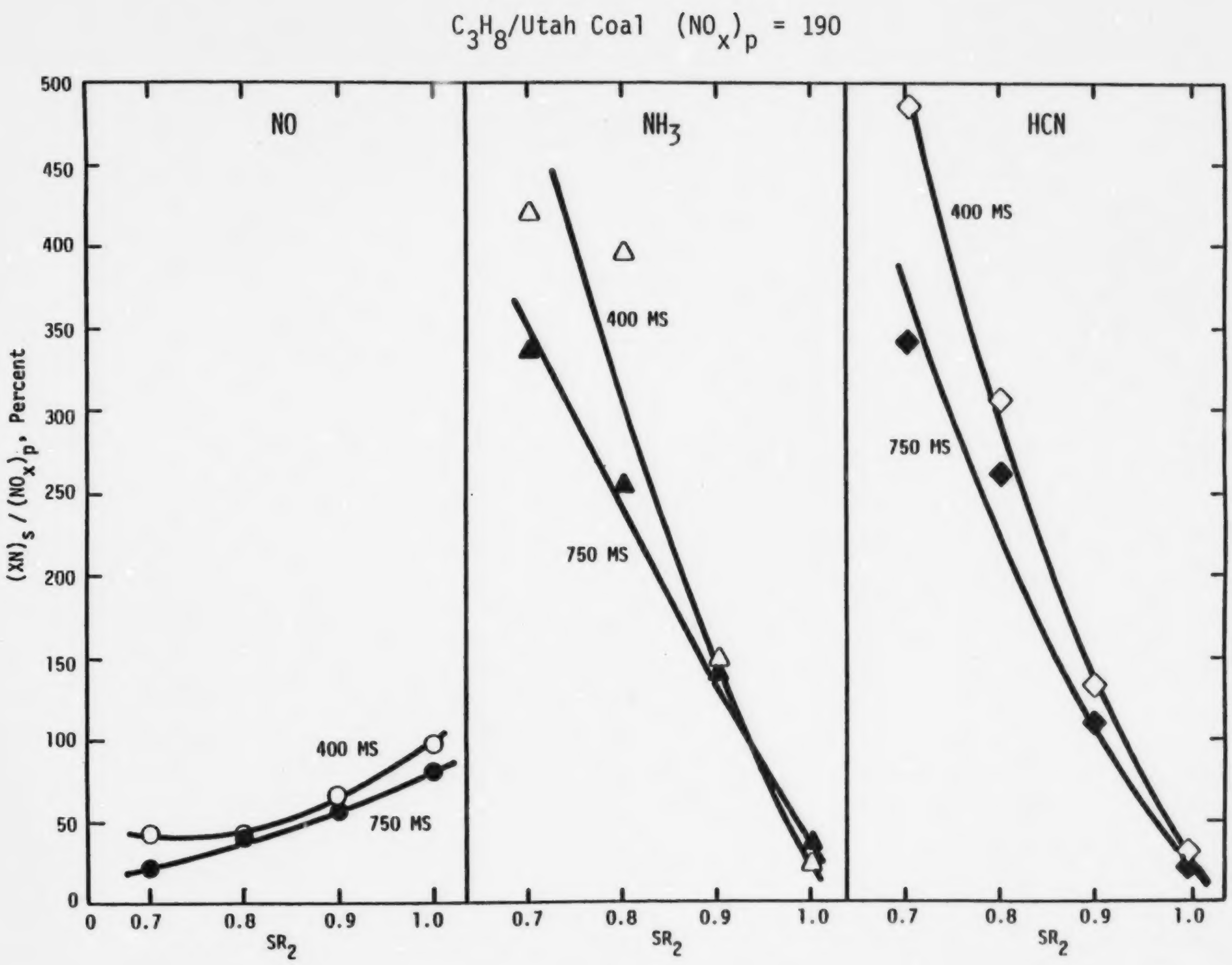
C_3H_8/Utah Coal $(NO_x)_p = 190$

Figure 7- 23. Detailed measurements at two residence times.

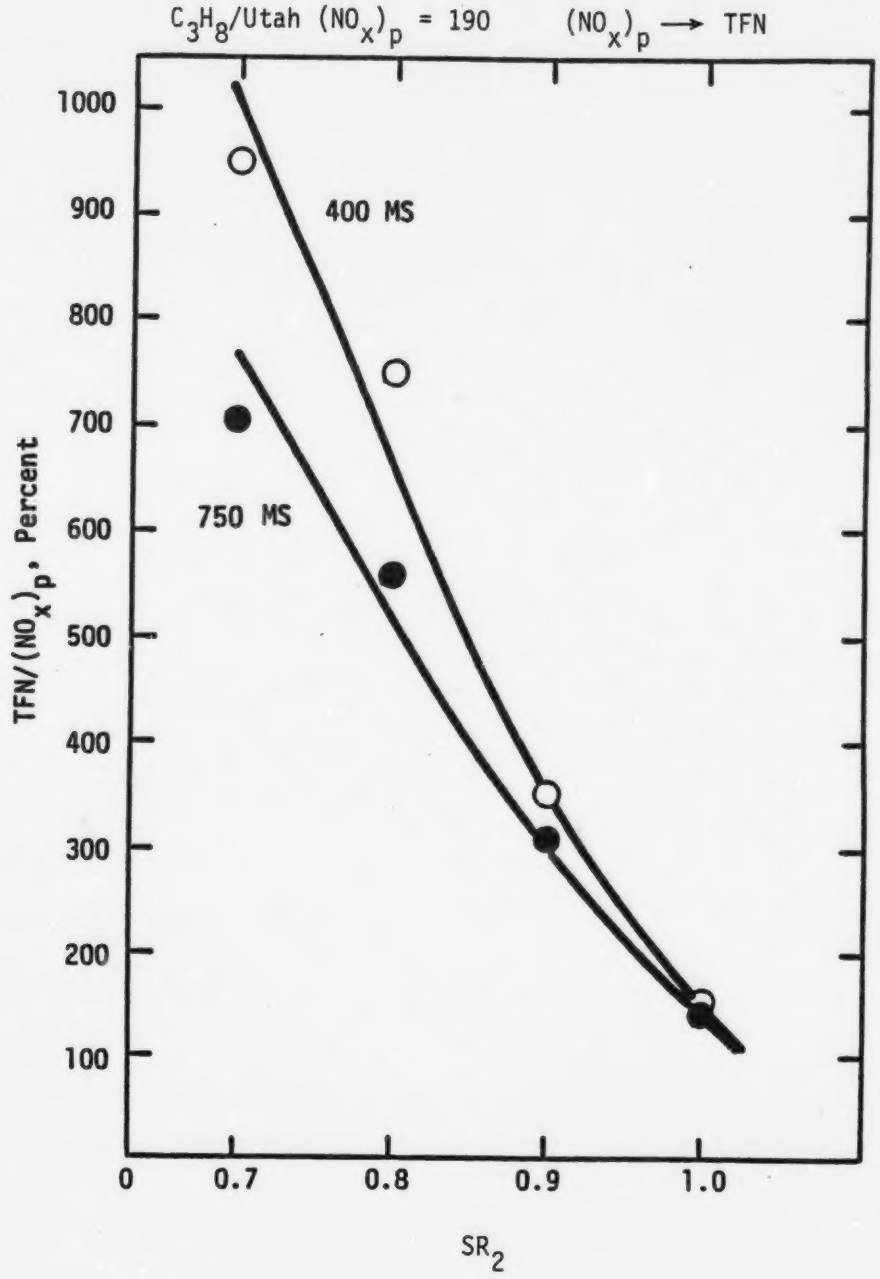

Figure 7- 24. Conversions at two residence times.

7.3.2 Fuel Hydrocarbon Content

The gas phase kinetic mechanisms responsible for the continued decay of NO with time are not completely understood. It apparently involves the reactions of NO and hydrocarbons such as described in Appendix C. NO was found to continue to decay even for times longer than 750 msec when the entire reactor was operated under rich conditions. The predominant mechanism for this reduction is related to the presence of hydrocarbons. Experiments with non-hydrocarbon fuels (H_2) indicate that reburning zone residence time had no effect on NO_x reduction. As shown in Figures 7-25 and 7-26 the insensitivity to residence time was independent of the initial NO_x level for non-hydrocarbon fuels.

7.3.3 Coal Type Dependence

A total of four coals were fired as reburning fuels during the residence time variation experiments. Different magnitudes of the residence time effect were observed for the four coals. The largest effects were observed with Utah and Coalstrip coals (see Figure 7-27) and the smallest effects were noted with Yallourn and Beulah coals (Figure 7-28). Seeker et al (1981) has shown that the Utah and Coalstrip coals both produced a sootier flame with respect to the combustion characteristics of Yallourn and Beulah. The maximum improvement in NO_x reduction occurred at rich stoichiometries (SR_2 = 0.7) at which the formation of soot was most pronounced. These data suggest that a combination of heterogeneous (soot + NO) and homogeneous (NO + HC) reduction is involved in the reburning process.

7.3.4 Summary

Conclusions obtained from the variable reburning zone residence time experiments were as follows:

- Increased NO_x reduction was attained at longer reburning zone residence times when firing hydrocarbon reburning fuels. The mechanism believed to be responsible for this conclusion was a

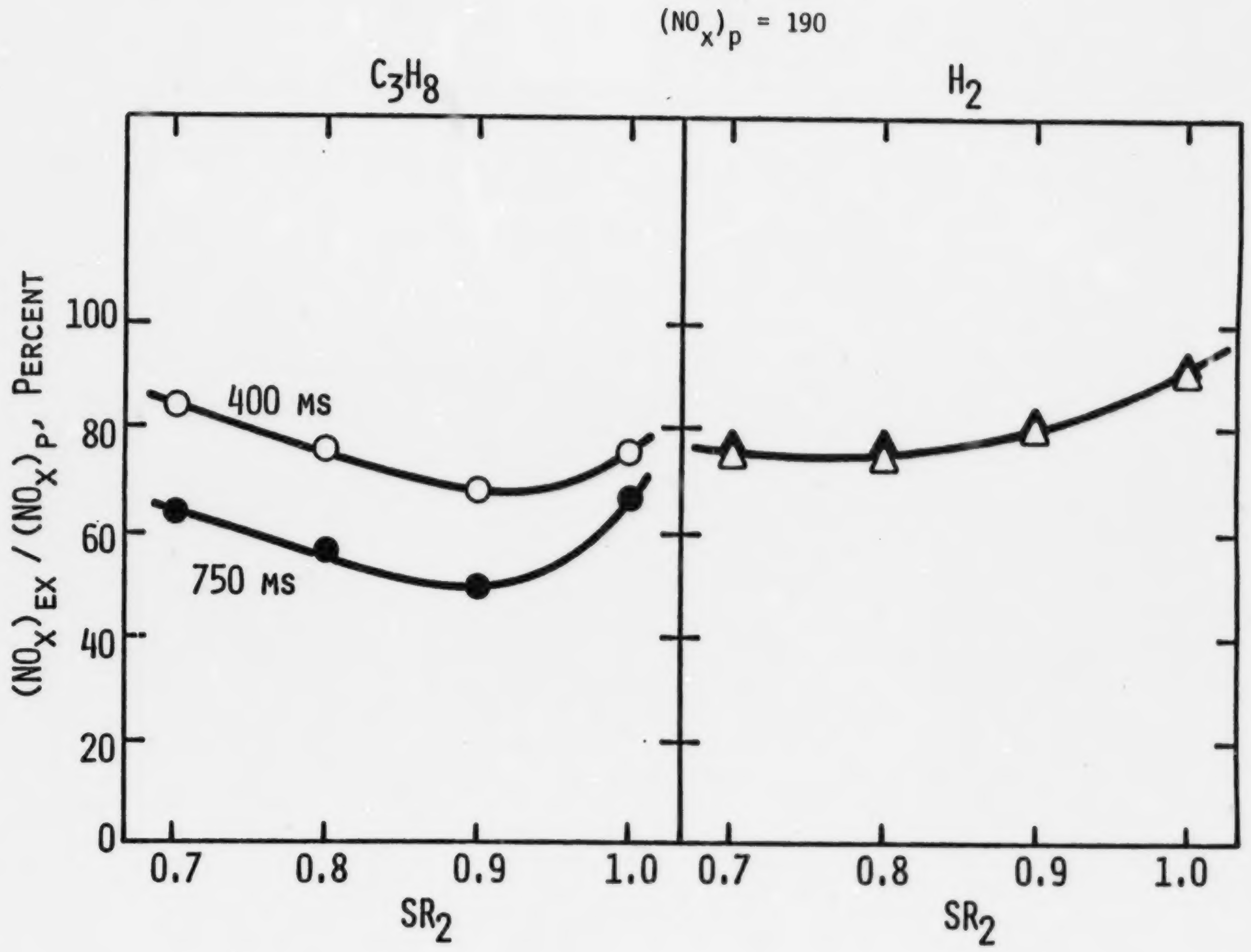

Figure 7-25. Residence time effects.

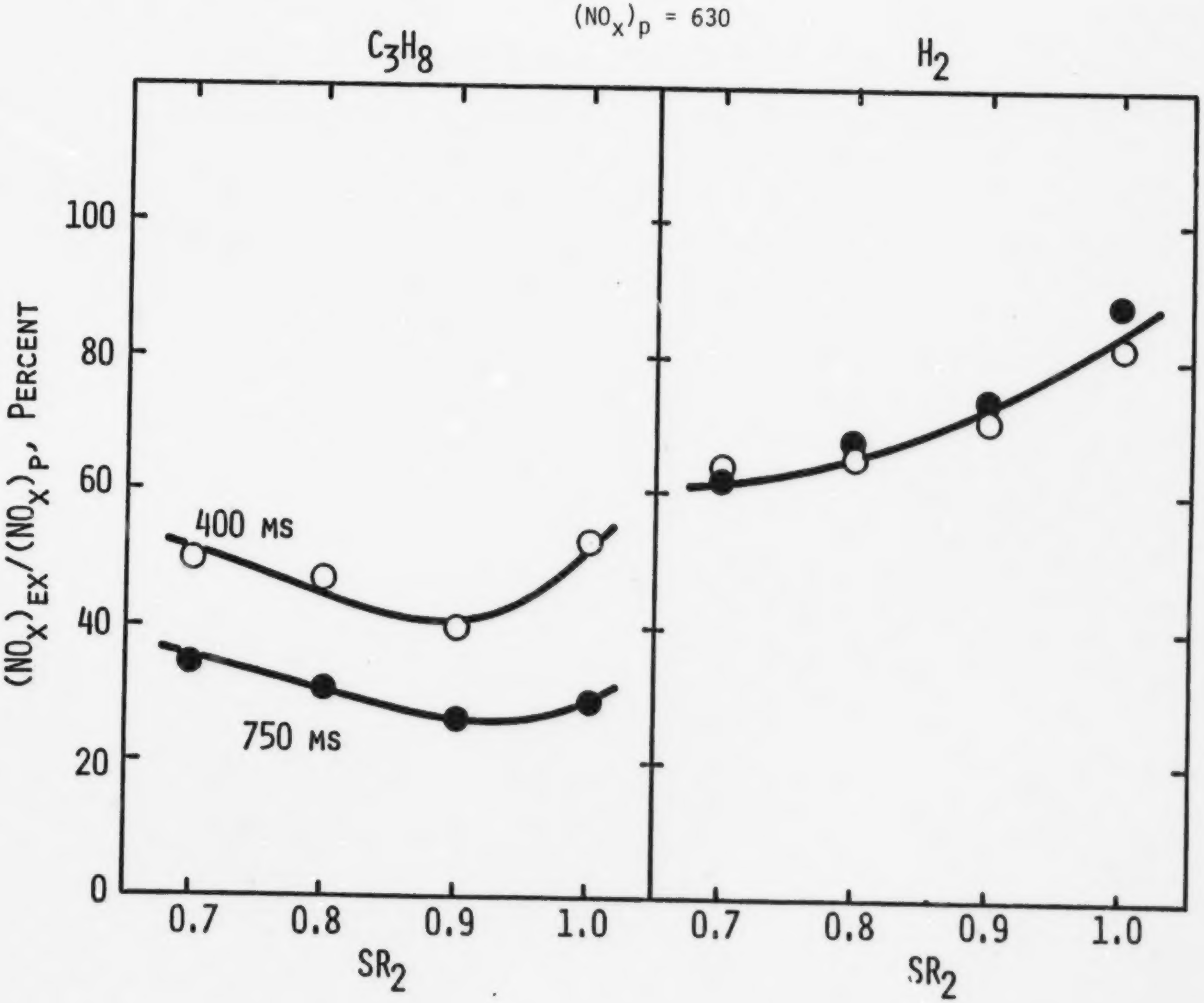

Figure 7- 26. Residence time effects.

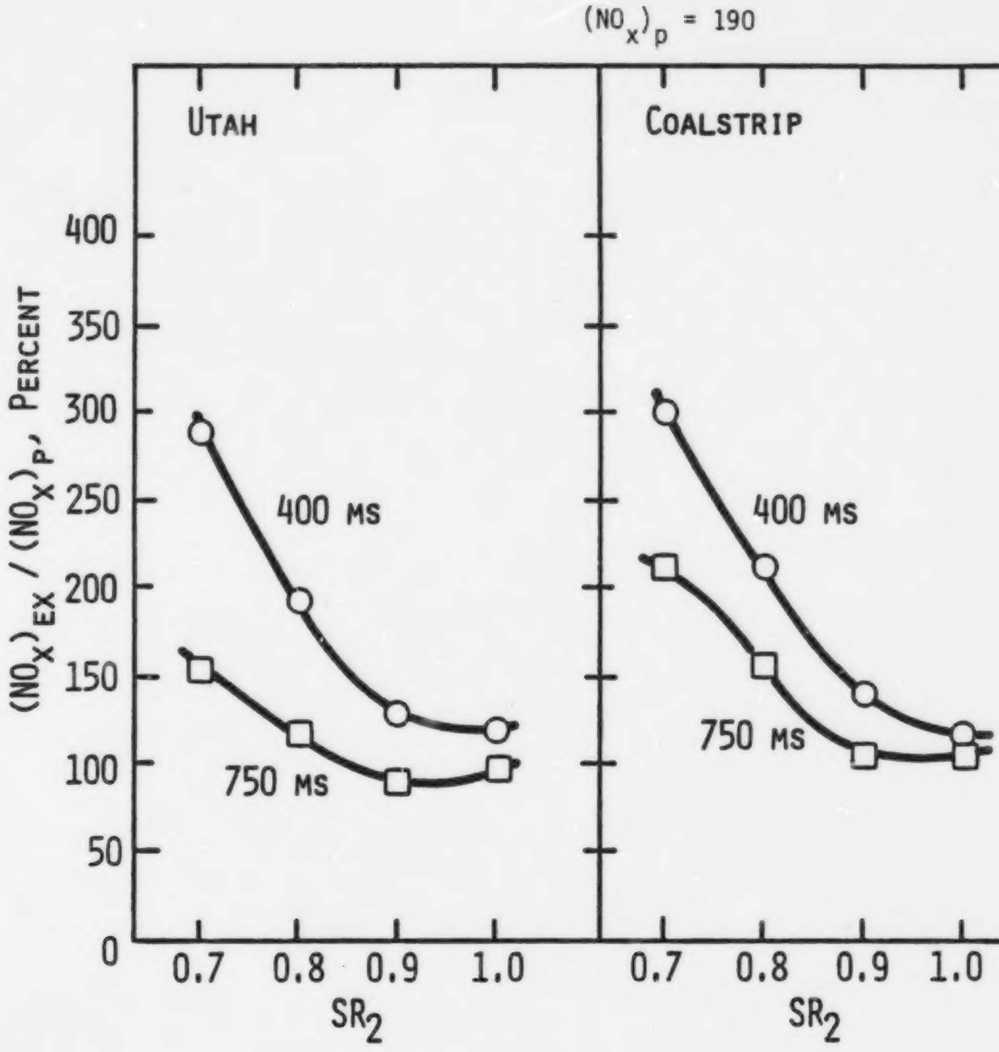

Figure 7-27. Influence of residence time.

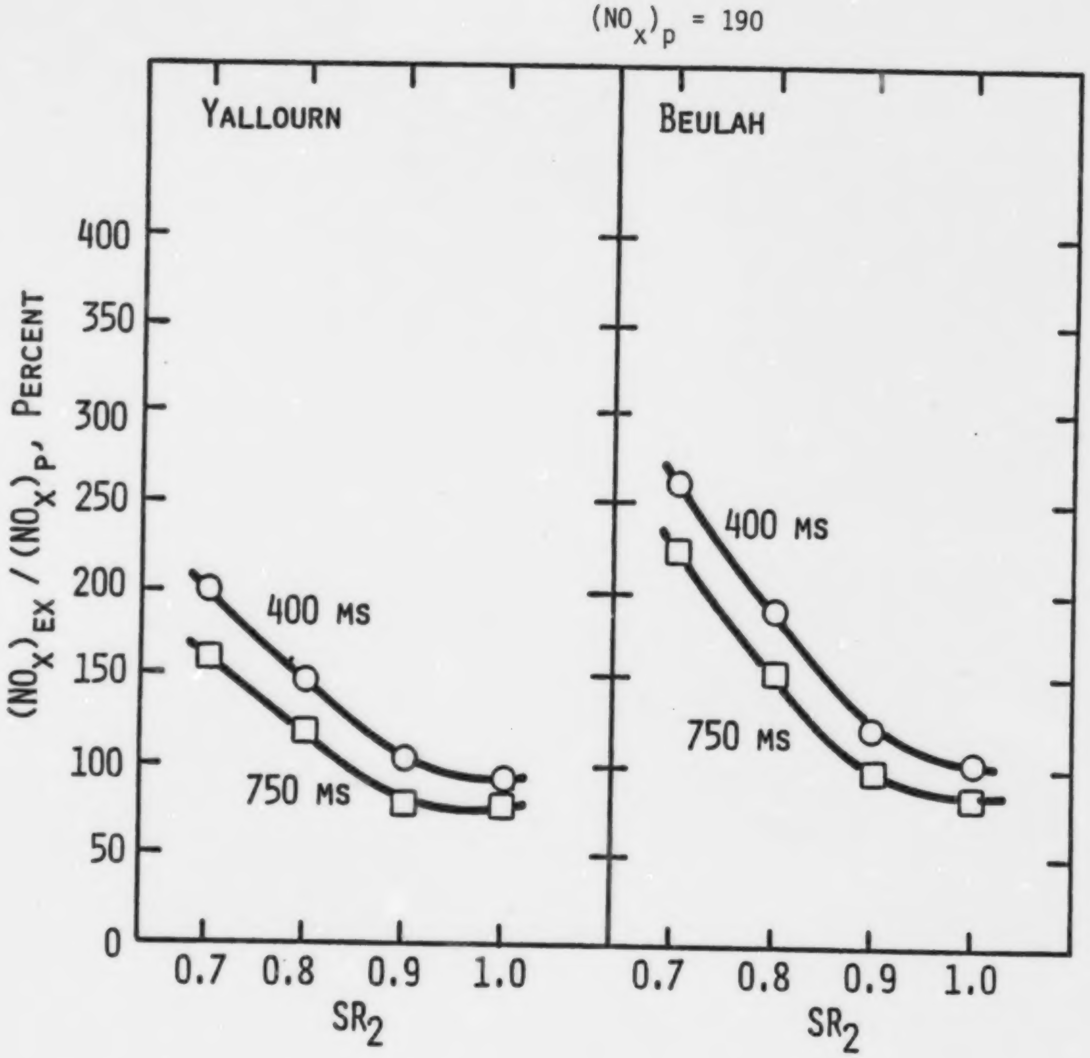

Figure 7- 28. Influence of residence time.

hydrocarbon reduction of NO in the fuel-rich reburning zone. This reduction of NO depleted the reactive nitrogen pool entering the burnout zone which lowered the conversion of TFN to $(NO_x)_{ex}$ in the burnout zone.

- There was no impact of reburning zone residence time for nonhydrocarbon fuels.
- For coal reburning, the impact of residence time depends upon coal type and the results suggest a combination of homogeneous and heterogeneous reduction.

7.4 Impacts of Thermal Environment

The influence of higher reburning zone temperature was examined by increasing the primary firing rate from 17.6 kW (60 x 10^3 Btu/hr) to 24.3 kW (83 x 10^3 Btu/hr). By increasing load, the primary zone exit temperature (T_1) as well as the bulk temperature of the reburning zone was increased. The reburning zone exit temperature (T_2) and residence time were held nearly constant by moving the burnout air injection further downstream of the baseline burnout air injection location. Figure 7-29 illustrates the baseline and high T_1 temperature profiles with their respective reburning zone residence times.

Increasing the reburning zone inlet temperature increased the reduction of NO_x significantly for the gaseous reburning fuels, but only slightly for Utah coal (see Figure 7-30). Additional experiments were performed at a higher $(NO_x)_p$ level with similar improvement in NO_x reduction, as noted in Figure 7-31.

A composite plot illustrating the effects of reburning zone residence time and inlet temperature is presented in Figure 7-32. The trends clearly indicated that in order to optimize the reburning process, the reburning fuel was to be injected at the hottest possible location and the injection of the burnout air should be delayed as long as practicality permits.

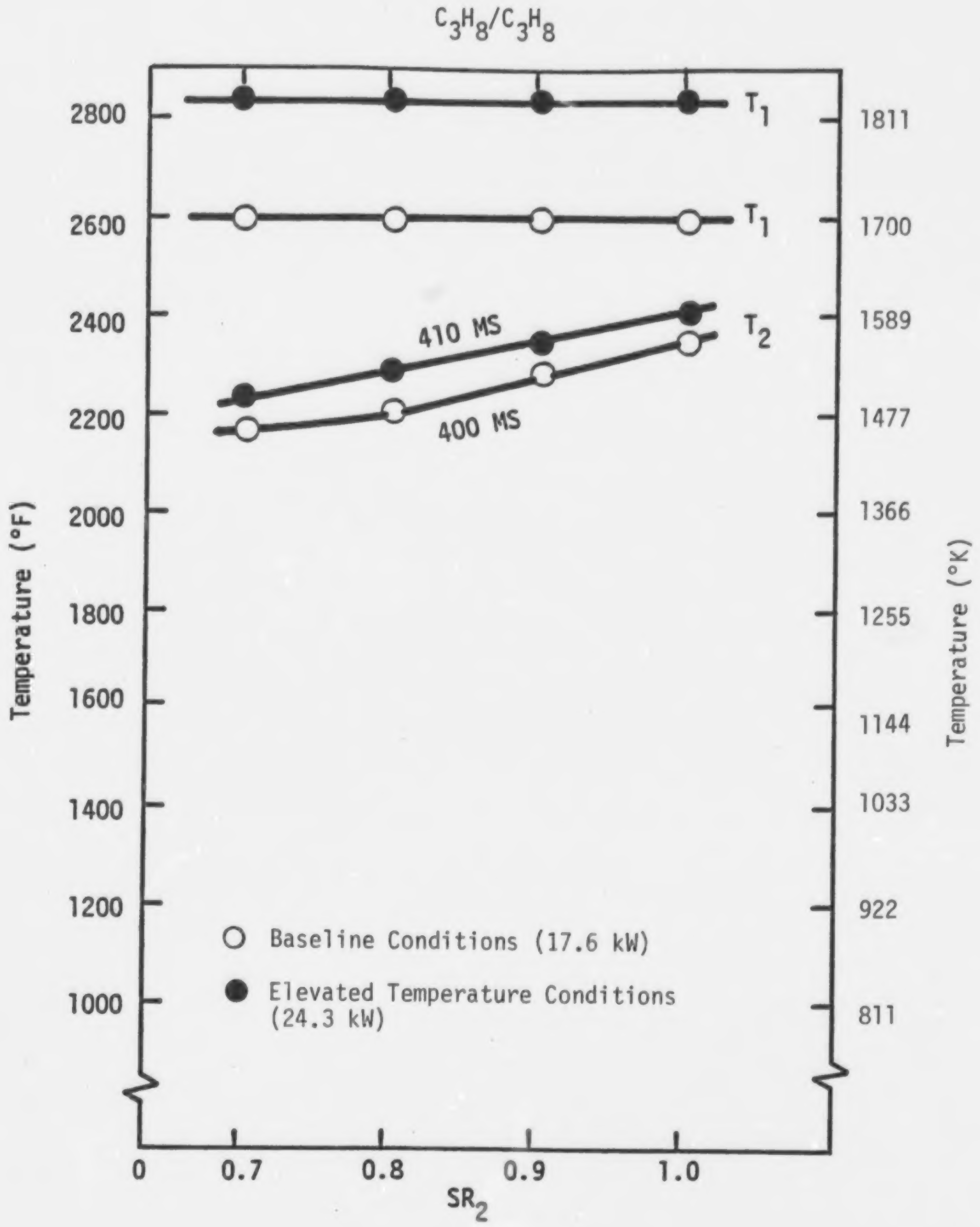

Figure 7-29. Reburning zone temperatures, baseline and high T_1.

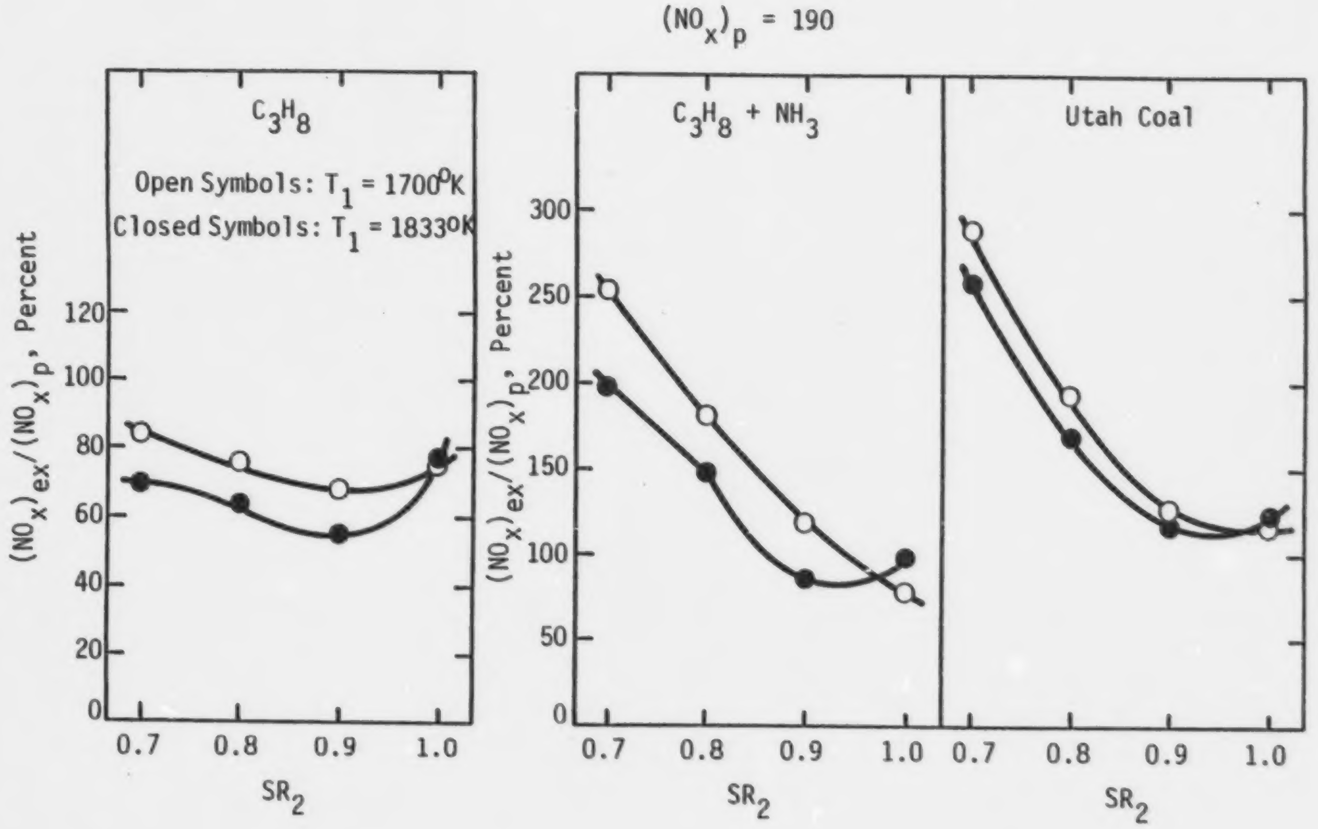

Figure 7-30. Influence of reburning zone temperature.

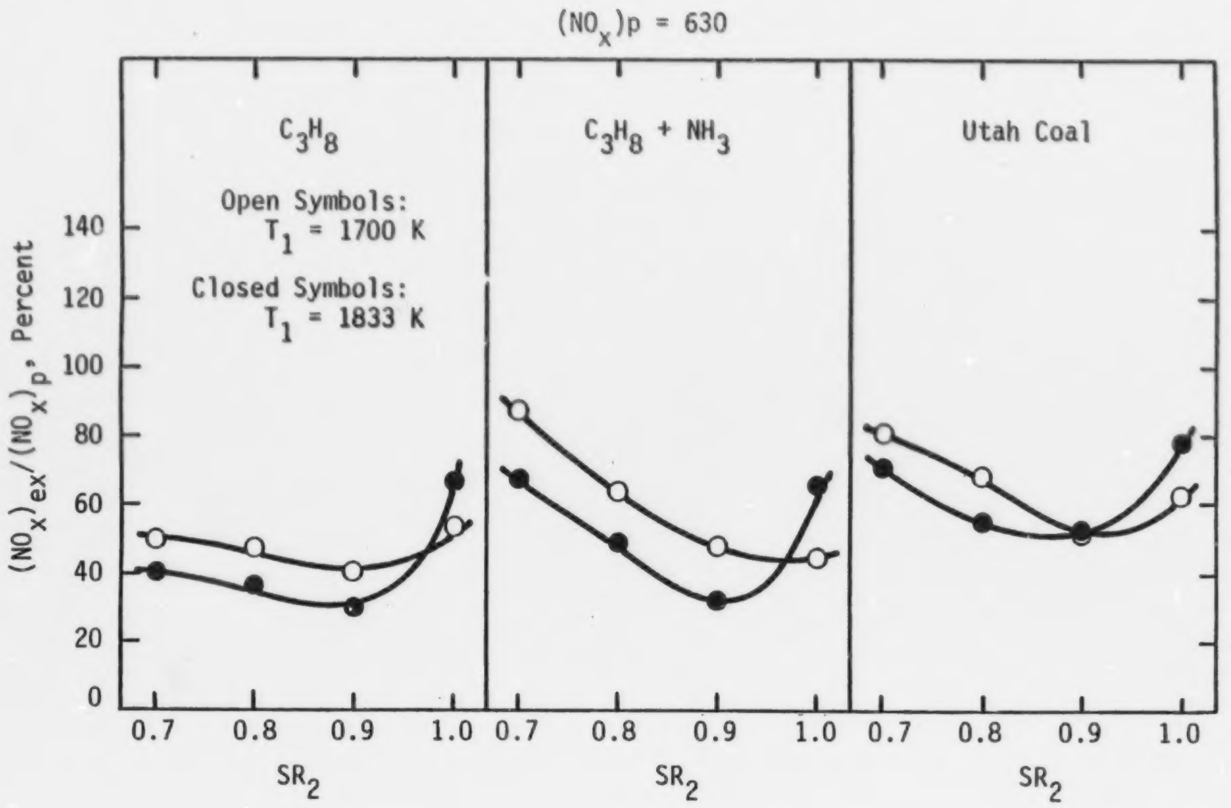

Figure 7-31. Influence of reburning zone temperature.

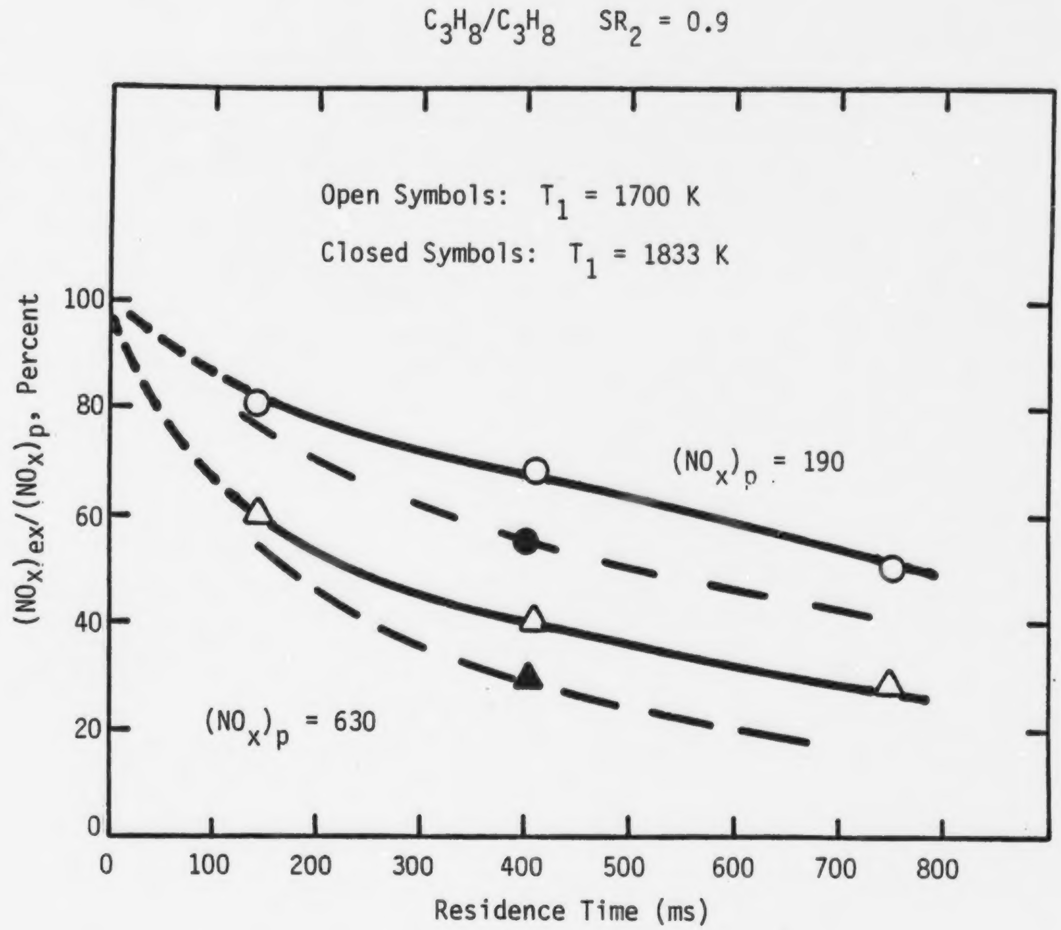

Figure 7- 32. Effects of reburning zone time/temperature.

8.0 BURNOUT ZONE PARAMETERS

8.1 Burnout Zone Stoichiometry

The influence of burnout zone stoichiometry on the effectiveness of reburning is shown in Figure 8-1. No effects of SR_3 was noted which is consistent with results obtained from previous reburning studies (Pershing, et al 1982).

8.2 Influence of Thermal Environment

To determine the influence of the burnout zone thermal environment upon the reburning process, experiments were performed with the lower auxiliary burners on. Figure 8-2 shows the resultant temperature profiles for the reburning and burnout zones with the lower auxiliary burners on. The lower burners predominantly affected the temperature profile of the burnout zone. The results of the experiments, presented in Figures 8-3 and 8-4, indicated that for reburning with either propane, propane and ammonia, or Indiana coal no effect of a hotter burnout zone was observed. The same conclusion was made at high and low $(NO_x)_p$ levels.

To investigate effects of a colder burnout zone, several attempts were made to cool the burnout zone with water cooled coils. For the furnace configurations that allowed for complete burnout of the rich-zone effluent (not all configurations experienced complete burnout), no improvement in the reburning process was noted. This observation was made for both gaseous and real (coal) fuels.

The most successful results for the burnout zone cooling experiments were obtained by placing the water cooled coil immediately upstream of the burnout air injection point. Results for reburning with Beulah coal at a residence time of 750 ms are presented in Figure 8-5. These results showed a significant improvement in the NO_x reduction due to the cooling effect. The temperature profile indicated that in order to obtain this effect the temperature of the reburning zone effluent must be within the so-called "de-NO_x"

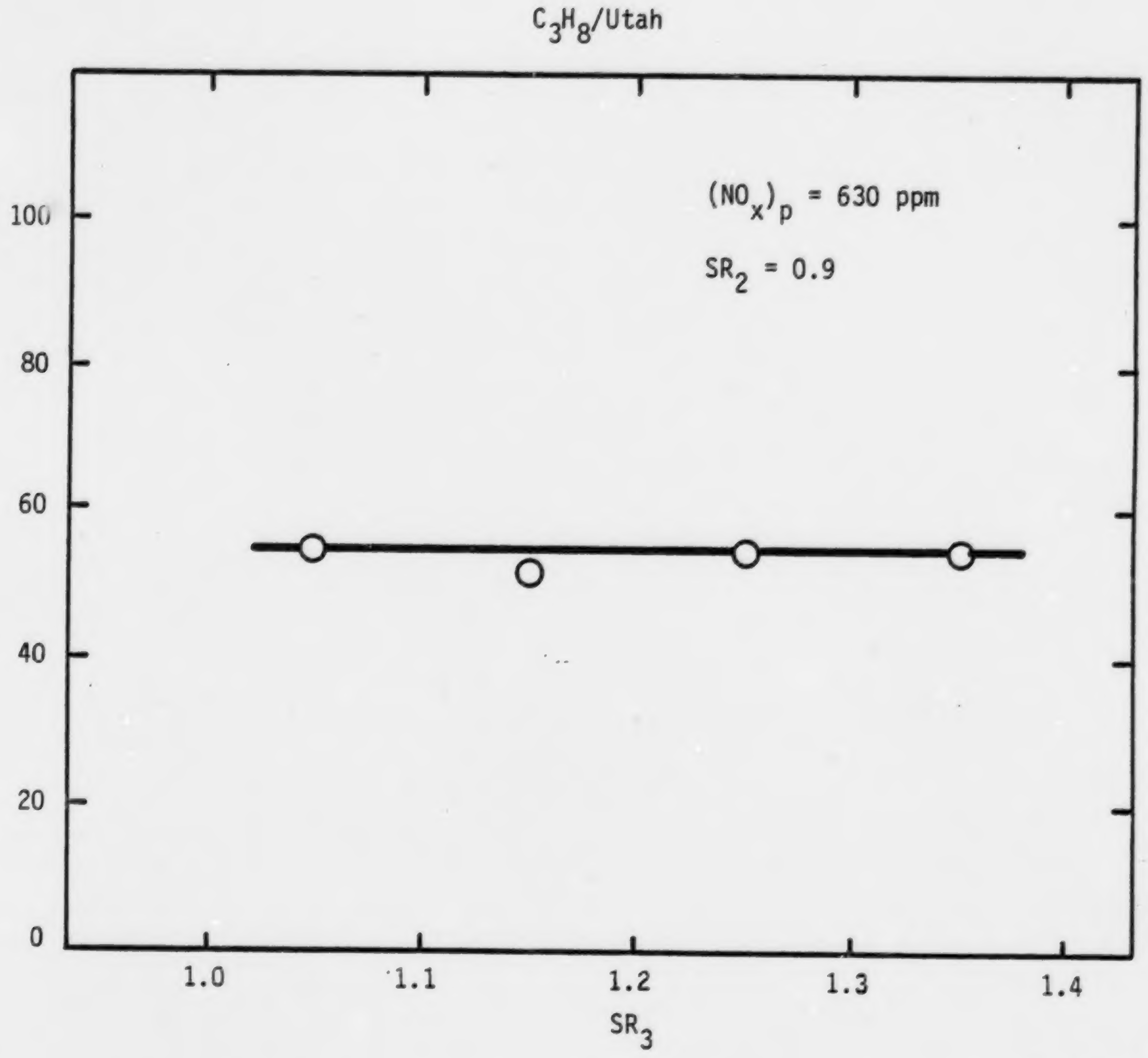

Figure 8-1. Influence of burnout zone stoichiometry.

C_3H_8/C_3H_8

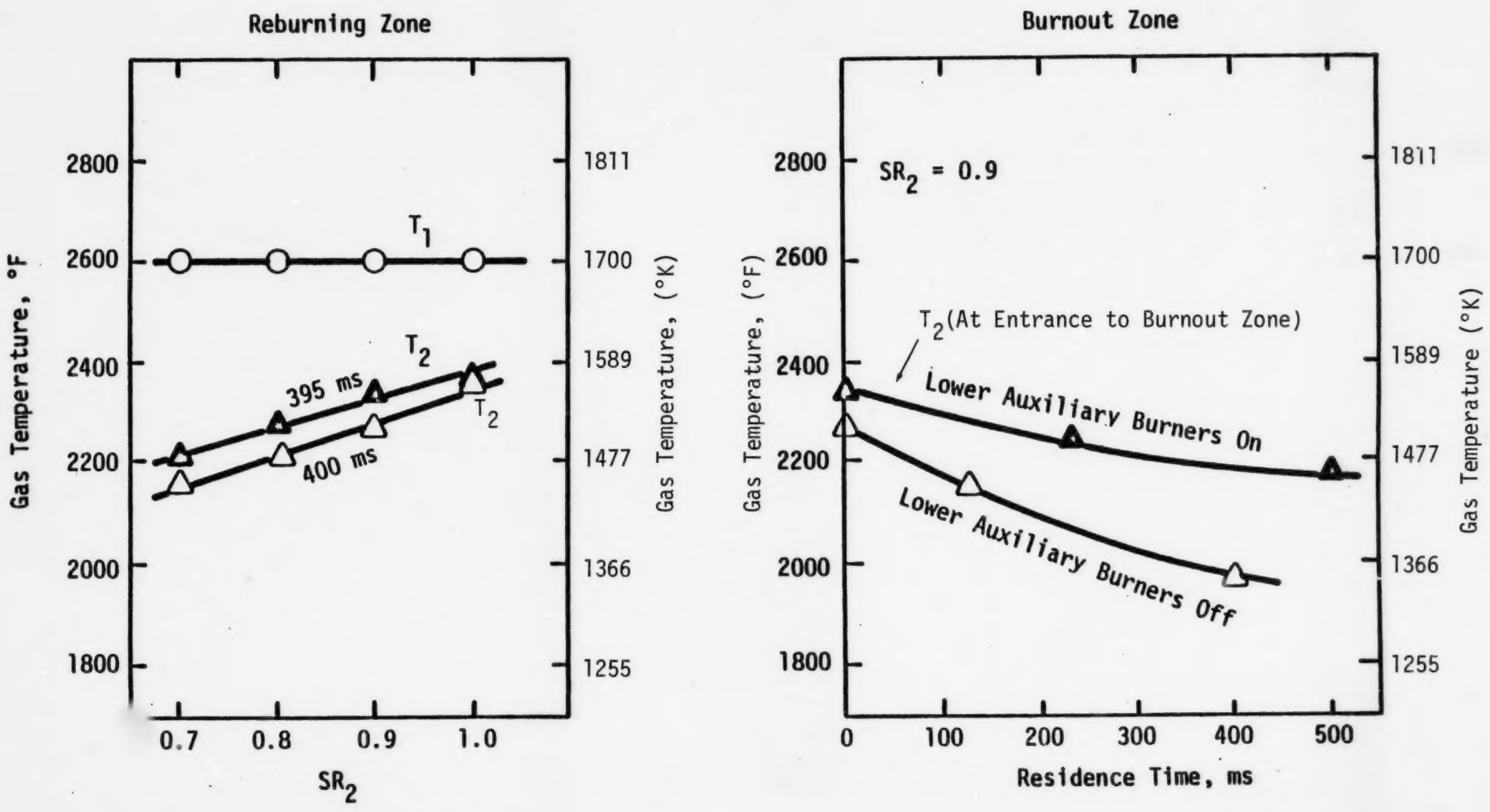

Figure 8-2. Influence of auxiliary heating on burnout zone temperatures.

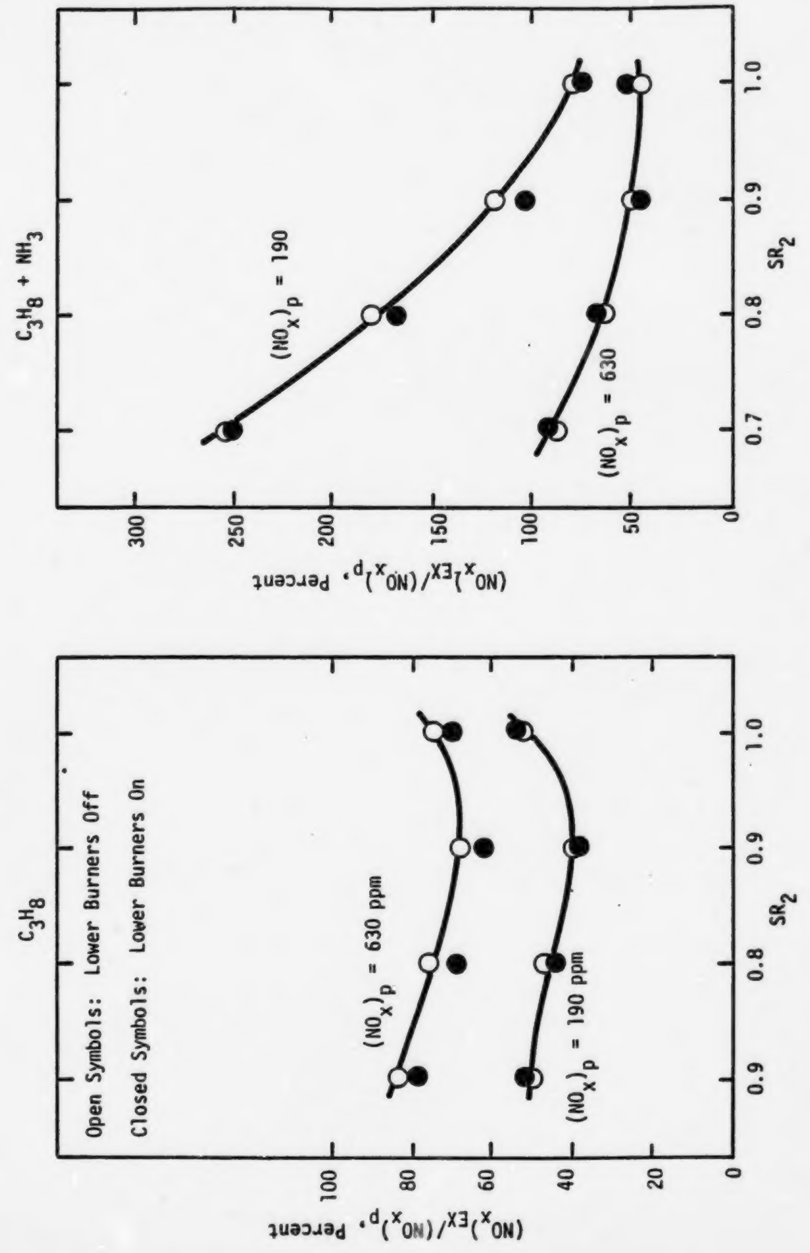

Figure 8-3. Emissions at two burnout zone temperatures.

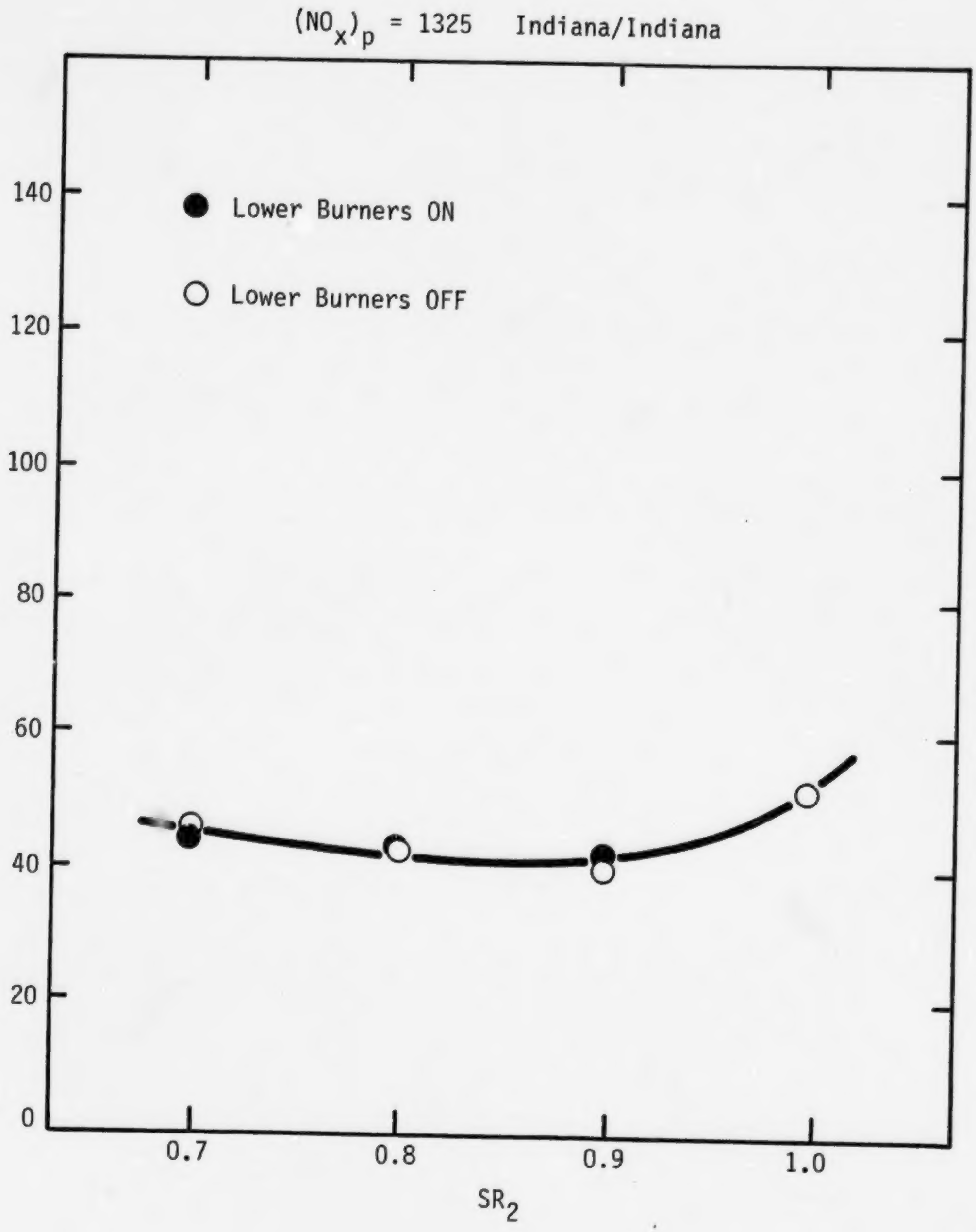

Figure 8-4. Emissions at two burnout zone temperatures.

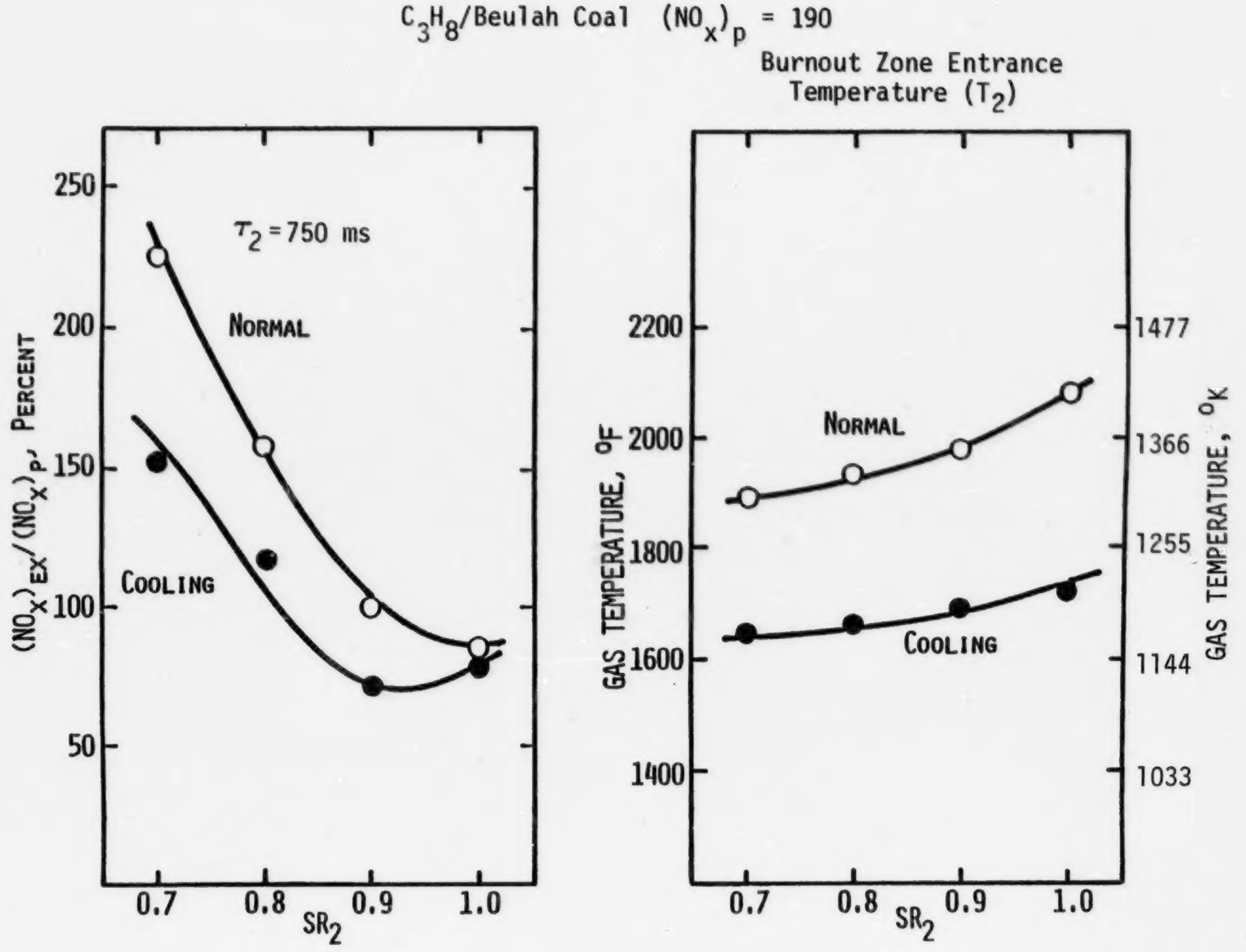

Figure 8-5. Effect of burnout zone cooling.

regime, believed to be approximately 1200 K as reported by Lyon, et al (1976). In addition to lowering the temperature in the burnout zone, an ammonia producing fuel must be used to supply ammonia for the de-NO_X reaction. Chen, et al (1982) has shown that low rank coals such as Beulah, were strong ammonia producers under rich conditions. Although the lower burnout zone temperature influenced the reburning performance, any significant improvement was obtained at temperatures outside the range of practical operating conditions for reburning.

9.0 CONCLUSIONS

The conclusions obtained from reburning experiments conducted in the CTT were as follows:

Major Parameters of Importance

- Reburning zone stoichiometry was optimized at 0.9.
- Reburning became less effective at low primary NO_x levels.
- Kinetically controlled reduction processes were favored by longer reburning zone residence time and higher reburning fuel injection temperature.
- Reburning fuels.
  - Hydrocarbon fuels were better than nonhydrocarbon fuels.
  - Nitrogen-free fuels were best.
  - Nitrogen-containing fuels were not as effective due to conversion of fuel nitogen to NO_x in the exhaust.
  - Percent conversion of nitrogen in coals was constant, and hence differences between coals were due to level of coal nitrogen.
  - Low volatile coals had burnout problems.

Minor Parameters of Importance

- Mixing reburning fuels rapidly was more effective (for coals).

- Low primary stoichiometry lessened the amount of reburning fuel input.

- An inert reburning fuel transport medium was desirable.

- Burnout zone stoichiometry and thermal history was not important, unless burnout zone temperature was reduced to "de-NO " levels which were probably too low for commercial reburning application.

Part II--Process Parameter Definition Studies--NO_x/SO_x

10.0 INTRODUCTION--NO_x/SO_x

The overall purpose of this task was to focus on the utilization of dry sorbent materials for SO_x control in conjunction with reburning systems. The basic concept of this SO_2 control process is that a pulverized sorbent (probably limestone, $CaCO_3$) is injected into the reburning system (either with the reburning fuel or with the final burnout air). The limestone then flash-calcines to lime (CaO) and begins to react with the sulfur dioxide (SO_2) and oxygen (O_2) to form calcium sulfite ($CaSO_3$) and/or calcium sulfate ($CaSO_4$). The reactivity of the calcined sorbent is a strong function of both its surface area and the pore size distribution which are dependent upon the crystaline structure of the original stone and the thermal history it experiences during the calcination process. If it attains too high a temperature, the surface area can be reduced by sintering and the stone will lose reactivity. If the sorbent particle is not heated strongly enough, it will not calcine completely and, therefore, will also be partially unreactive.

Combustion systems with reburning may be especially suitable for dry sorbent injection because of the following potential advantages:

- All of the sulfur from the main combustion zone is in the gas phase, giving the maximum driving force for sulfur capture.
- The temperatures in the reburning and final burnout zones are lower than in the main combustion zone, thus reducing the potential for loss of surface area via sintering and for deactivation of the sorbent by mineral matter constituents.
- The reburning and final burnout zones might offer a thermal environment desirable for effective sorbent activation and sulfation.

- The reburning fuel and air streams must be well mixed with the main combustion zone products, and hence, provide an ideal vehicle for transport of the sorbent across the combustion system.

The major emphasis of the task is on the role of thermal environment and local residence time on sorbent utilization. Specifically, the objectives were to:

- Verify the effectiveness of sorbent injection with temperatures, stoichiometries, and residence times typical of reburning systems.

- Investigate the role of thermal environment and local residence time on sorbent utilization.

- Define the overall potential for NO_x/SO_x reduction using sorbent injection with reburning.

11.0 EXPERIMENTAL FACILITIES

11.1 Furnace Configuration--Experimental Approach

The baseline CTT conditions for the SO_x capture experiments consisted of the following:

Primary Zone

- Propane fired at 17.6 KW (60×10^3 Btu/hr)
- $SR_1 = 1.1$
- $(SO_2)_p = 1940$ ppm (dry, 0% O_2)

Reburning Zone

- ${}_2 = 400$ ms
- $SR_2 = 0.9$
- $T_1 = 1700$ K ($2600^{o}F$) upper auxiliary burners on

Burnout Zone

- $SR_3 = 1.25$
- $T_2 = 1444$ K($2140^{o}F$) lower auxiliary burners on

All of the capture testing was conducted at these baseline conditions, except as stated otherwise.

Fuel mixing conditions for the SO_x studies were similar to conditions for the NO_x studies. The premixed burner was used to mix the primary fuel, transport air, and main combustion air. The elbow-shaped radial injector was used for injecting the reburning fuel. The sorbent was either injected together with the reburning fuel or through another radial injector (identical to the reburning fuel injector) at the burnout location. Both levels of auxiliary burners were fired (see Figure 11-1 for combustor

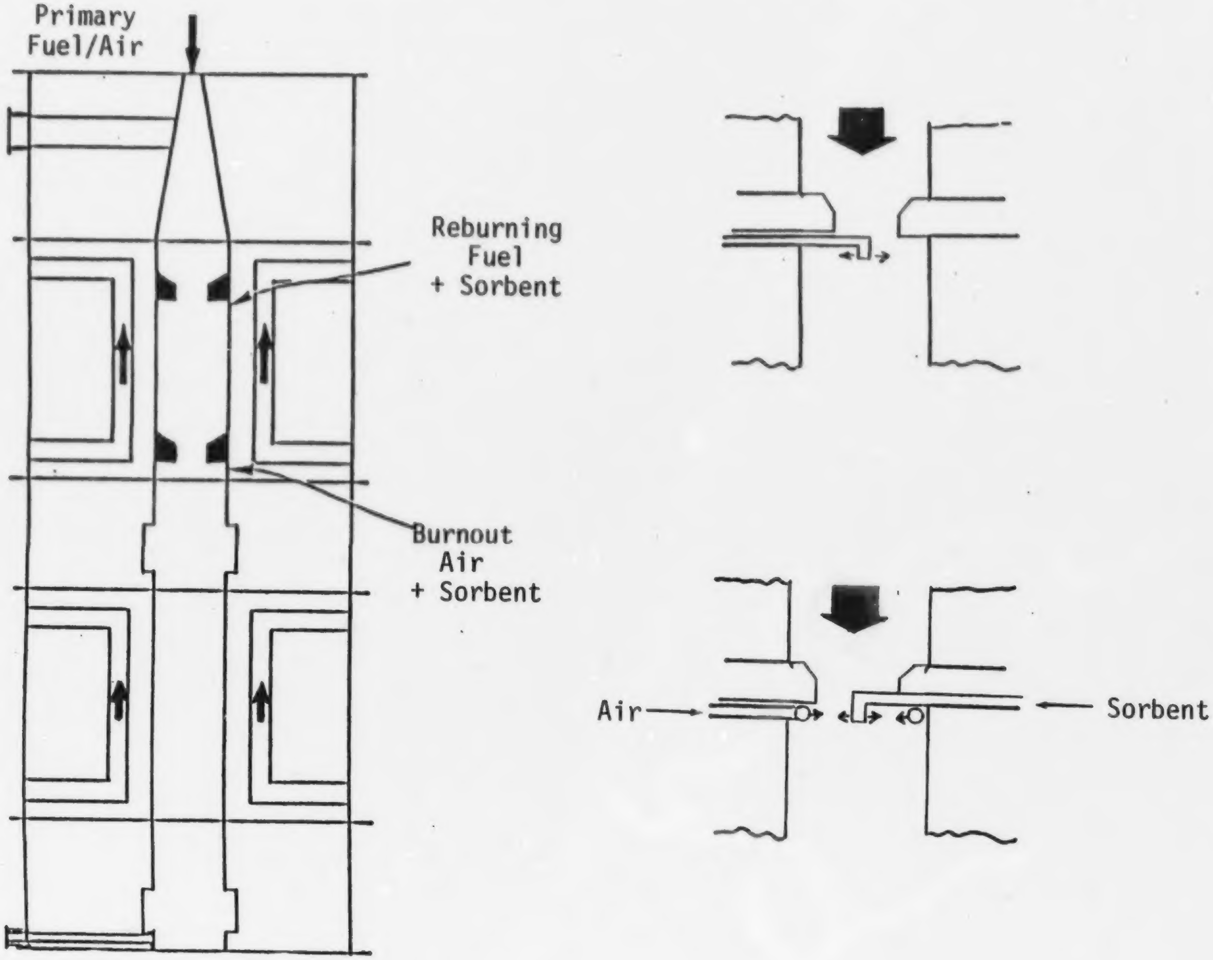
Primary
Fuel/Air
Reburning
Fuel
+ Sorbent
Burnout
Air
+ Sorbent
Air
Sorbent

Figure 11-1. CTT configuration for SO_x studies.

configuration). The time-temperature profile at these conditions is shown in Figure 11-2.

The experimental work was conducted by establishing reburning conditions with no sorbent being injected into the combustor. Sorbent was then added, first at the burnout air injection location then premixed with the reburnhing fuel. At each sorbent injection location, two calcium-to-sulfur ratios (Ca/S) were implemented.

11.2 Measurement Systems and Analytical Methods

11.2.1 SO_2 Measurement

The continuous monitoring flue gas sampling train used during the SO_2 capture experiments is illustrated in Figure 11-3. The exclusive feature of this system was the ability to sample SO_2 without any sulfuric acid condensation occurring, which would severely impede the accuracy of the measurements. The gas sample was taken from the combustor via a phases discrimination probe. This probe was designed such that a relatively particulate-free gas sample was obtained by extraction of a slip stream from the total gas sample. The slip stream was pulled through several openings in the probe tip oriented perpendicularly to the bulk gas sample flow. The particulate-free sample was transferred through a heated sample line and filter to a permeation tube dryer. The dryer selectively removed water from the gas stream by contacting the wet gas with an extrudible dessicant in tubular form. Sampling moist gases in this manner enabled a continuous monitoring of the SO_2 concentration. The particulate-laden sample taken from the probe was used for the continuous monitoring of O_2, CO_2, and NO_x.

11.2.2 Sorbent Surface Area Measurement

At the time of this report, no standardized method of sampling calcined sorbent for surface area analysis had been developed. For accurate interpretation of the SO_2 capture data, a method of obtaining precise surface area information about the sorbents used in the CTT testing was essential.

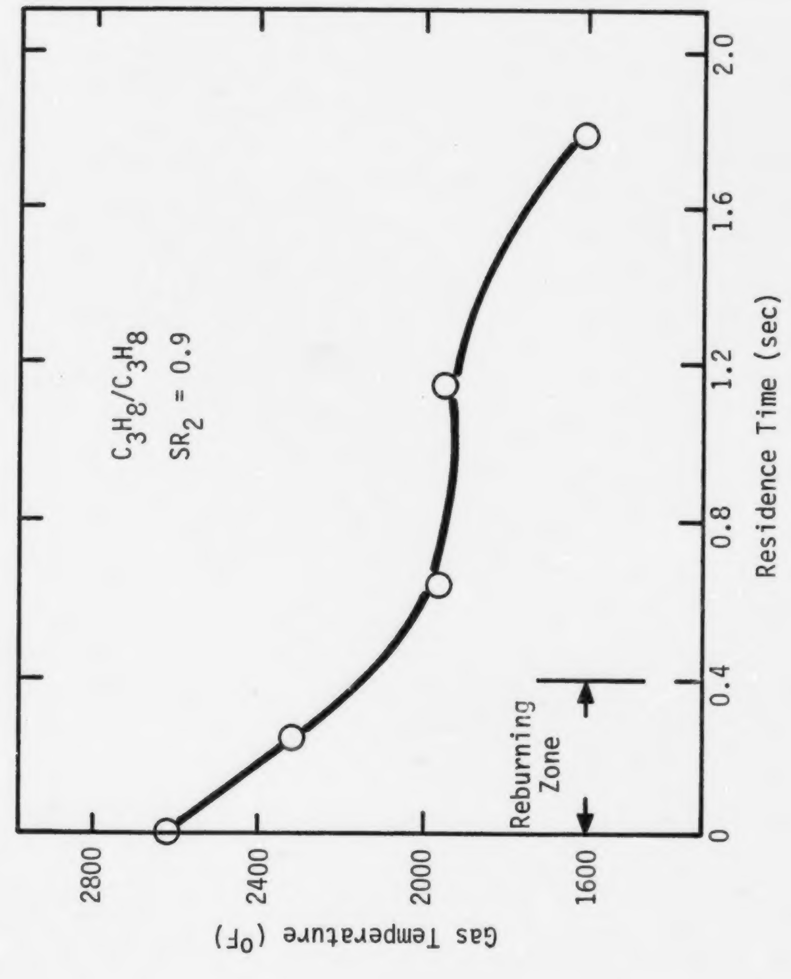

Figure 11-2. Time-temperature profile at baseline conditions.

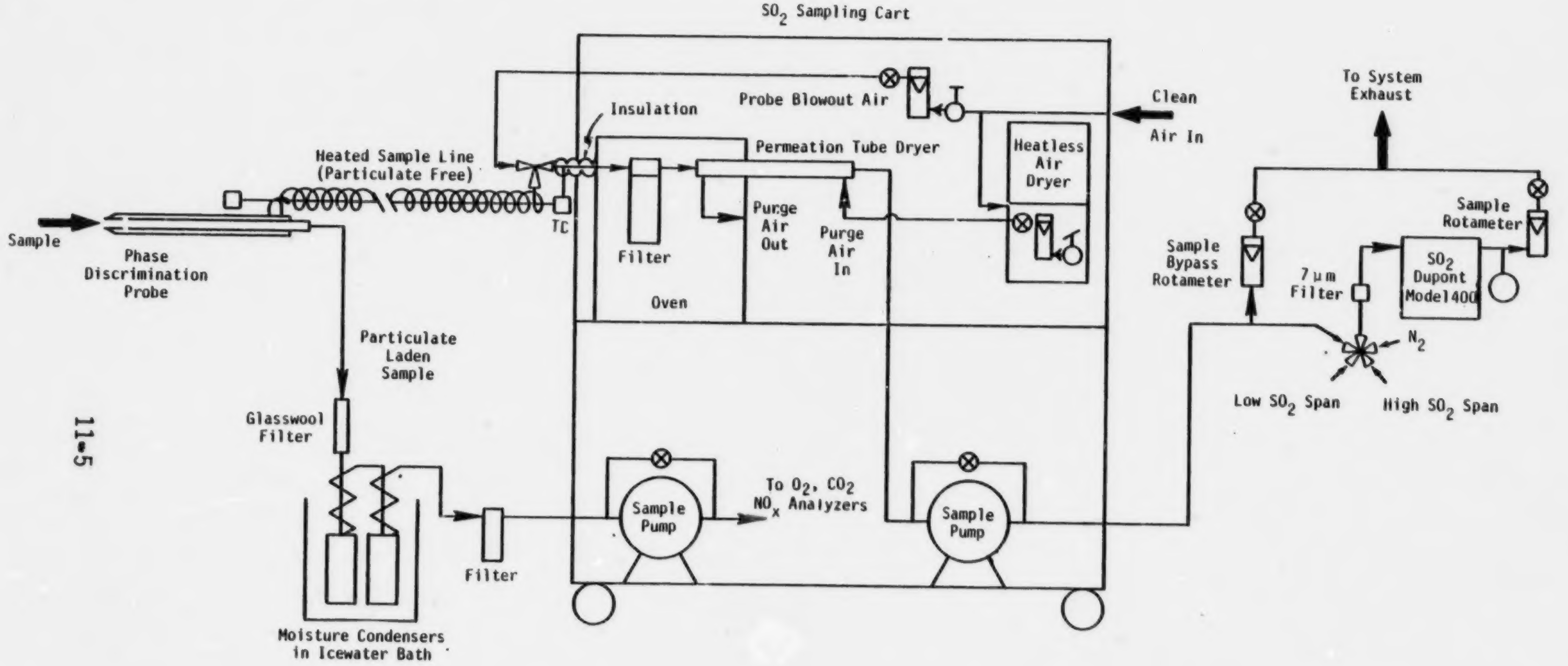
SO2 Sampling Cart
Probe Blowout Air
Clean
Air In
To System
Exhaust
Insulation
Permeation Tube Dryer
Heatless
Air
Dryer
Heated Sample Line
(Particulate Free)
Sample
Phase
Discrimination
Probe
TC
Filter
Oven
Purge
Air
Out
Purge
Air
In
Sample
Rotameter
Sample
Bypass
Rotameter
7 µm
Filter
SO2
Dupont
Model 400
N2
Low SO2 Span
High SO2 Span
Particulate
Laden
Sample
Glasswool
Filter
Moisture Condensers
in Icewater Bath
Filter
Sample
Pump
To O2, CO2
NOx Analyzers
Sample
Pump

Figure 11-3. Continuous monitoring gas sampling system.

To obtain representative calcined sorbent samples for surface area measurements it requires that the sampling system be kept above the dew point to avoid condensation and below about 315°C to prevent recarbonation. Either hydration or recarbonation would result in a loss of the surface area of the calcined. The sorbent sampling system illustrated in Figure 11-4 was fabricated and a series of shakedown experiments were conducted. The calcined sorbent was collected by pulling the sample through the probe where the sorbent-laden gas was immediately diluted with nitrogen at the probe tip. Dilution with nitrogen lowered the partial pressure of the water vapor in the gas which aided in avoiding any condensation of the vapor in the sampling system. The sample was transferred through a heated line into a total filter located inside an isothermal oven. Gas temperatures were measured at the probe tip, at the exit of the heated line, and immediately downstream of the total filter. Sampling was conducted for approximately 20 minutes with a total sample flowrate of approximately 90 SCFH. Sorbent was injected into the combustor at a feedrate of approximately 6 grams/minute. After the sample was collected the sample line was closed and a nitrogen purge was introduced to remove any moisture in the gas surrounding the filter while the filter was allowed to cool. The sorbent sample was removed from the filter and transferred to a sample vial which was initially evacuated and then filled with nitrogen after the sample was inserted. The stored sample was analyzed for BET surface area on a Quantachrom Quantasorb surface area analyzer.

The shakedown experimental work focused on the effects of temperatures in the sampling system and the amount of nitrogen introduced as diluent. Table 11-1 lists the results from the sorbent sampling system shakedown tests. The data was obtained from injecting Vicron with the burnout air and sampling the calcined sorbent at a distance of 188 cm from the top of the combustor (where the gas temperature was 1172 K). The combustor was operated at the baseline condition with the exception that the lower auxiliary burners were not fired. The results in Table 11-1 show that as long as every part of the system was maintained above the dew point (approximately 100°C) surface areas results were consistent (see Tests 1 and 5). If the temperature fell below the dew point anywhere in the system, the surface areas were markedly

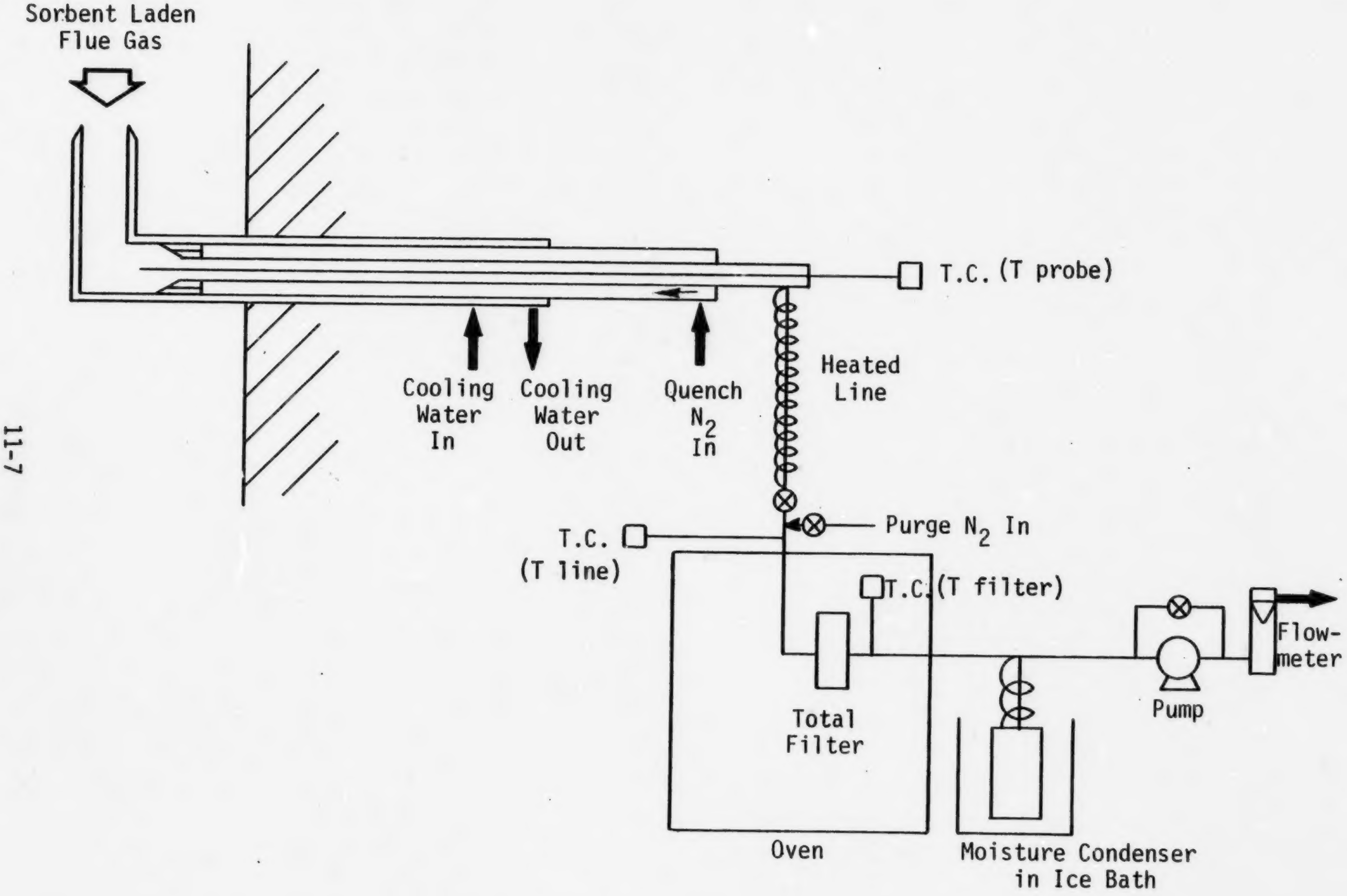
Sorbent Laden
Flue Gas
Cooling Water In
Cooling Water Out
Quench N_2 In
Heated Line
T.C. (T probe)
Purge N_2 In
T.C. (T line)
T.C. (T filter)
Total Filter
Oven
Moisture Condenser in Ice Bath
Pump
Flow-meter

Figure 11-4. Sorbent sampling system.

TABLE 11-1. SORBENT SAMPLING SYSTEM SHAKEDOWN RESULTS

Test #	Temperature (^{o}C)			N_2 dilution N_2: Sample	Surface Area (m^2/g)
	Probe	Line	Filter		
1	293	119	208	1:5	14.7
2	245	78	51	1:5	5.1
3	80	53	38	2:5	5.7
4	117	78	185	2:5	10.1
5	272	111	137	1:5	15.0

lower, presumably due to the hydration effects (see Tests 2, 3, and 4). Increasing the diluent flow rates resulted in temperatures dropped below the dew point (Tests 3 and 4), and lower surface areas were measured. Therefore, for this test program, all parts of the sorbent sampling system were maintained above 100°C, and a 1:5 nitrogen to sample dilution ratio was employed.

Experiments were also conducted to determine if the surface area of the sorbent was affected by storage in the sample vials over a period of time. To investigate this, the surface area of a sorbent sample taken immediately from the collection filter was determined. A portion of the same sample was stored in a vial under nitrogen and analyzed one day later and then one week later. No change in the surface area of the sample as a function of storage time was noted.

12.0 SORBENT PROPERTIES

12.1 Sorbent Composition

Three sorbents, a limestone, a dolomite, and a hydrated lime, were utilized in the SO_2 capture experiments. The physical properties of the sorbents are listed in Table 12-1.

12.2 Sorbent Surface Area

Experiments were performed to determine the calcination characteristics of sorbents injected into the CTT at reburning conditions. More specifically, the effects of peak calcination temperature, cooling rate, and residence time needed to be quantified. Studies were conducted with Vicron limestone injected with the reburning fuel at the baseline operating conditions (C_3H_8/C_3H_8 reburning) with the exception that no SO_2 was doped into the combustor. The effects of sorbent particle residence time and cooling rate on sorbent surface area are presented in the left graph of Figure 12-1. The residence time data was obtained by sampling the sorbent at different axial locations along the combustor. The cooling rate data was obtained by varying the time/temperature profile, which was accomplished by firing or not firing the lower auxiliary burners. The two temperature profiles are shown in the right graph of Figure 12-1. The data obtained indicated that the surface area did not depend on the residence time of the sorbent particles (at least above 0.4 sec) or on the thermal history of the particles. The percent calcination of the sorbent did slightly increase with residence time (percent calcination values are in parentheses).

The influence of peak calcination temperature on limestone surface area is presented in Figure 12-2. The data, obtained from sequentially injecting Vicron with the reburning fuel, and then with burnout air, at the two temperature profiles in Figure 12-1. The data indicated that the surface area decreased with increasing peak temperatures. As expected, the calcination of the sorbent increased at higher peak temperatures. The composite plot of surface area vs. peak calcination temperature on the right

TABLE 12-1. SORBENT PROPERTIES

Sorbent	Vicron 45-3	Dolomite	Hydrated Lime
Petrographic Characterization:			
Type	Calcite	Dolomite	Hydrated Lime
Composition	$CaCO_3$	$CaCO_3$+$MgCO_3$	$Ca(OH)_2$
Grain Size, μm	500-700	<100	30
Top Size, μm	40-45		
Mean Size, μm	11-12	34-40	11-12
Bottom Size, μm	.3-.8	1.0	.3
Density, g/cm^3	2.757	2.855	2.350
Oil Absorption	14		
Uncalcined S. A., m^2/g	.6-.9	.6	12.1-13.5
Ignition Weight Loss, % (1000°C)	41.0-44.0	44.2-47.1	25.3
Hydration Weight Gain (1000°C)	33.08	67.5	
Chemical Composition, %			
Ca	39.2	21.0	51.0
Al	0.07	0.09	0.26
Si	0.07	0.37	0.80
Fe	0.037	0.102	0.22
Na	0.022	0.033	
Mg	0.485	12.1	
K	0.011	0.039	0.51
Cr	0.006	0.27	

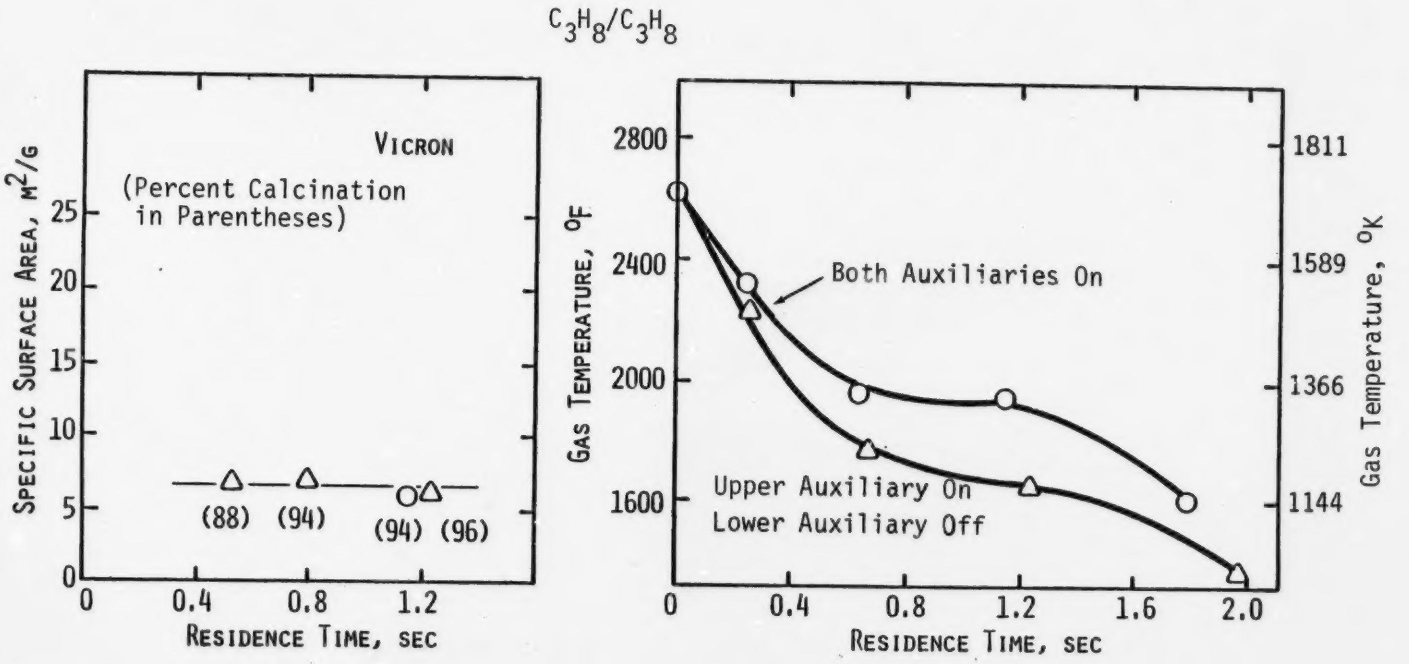

Figure 12-1. Vicron surface area as a function of residence time and cooling rate.

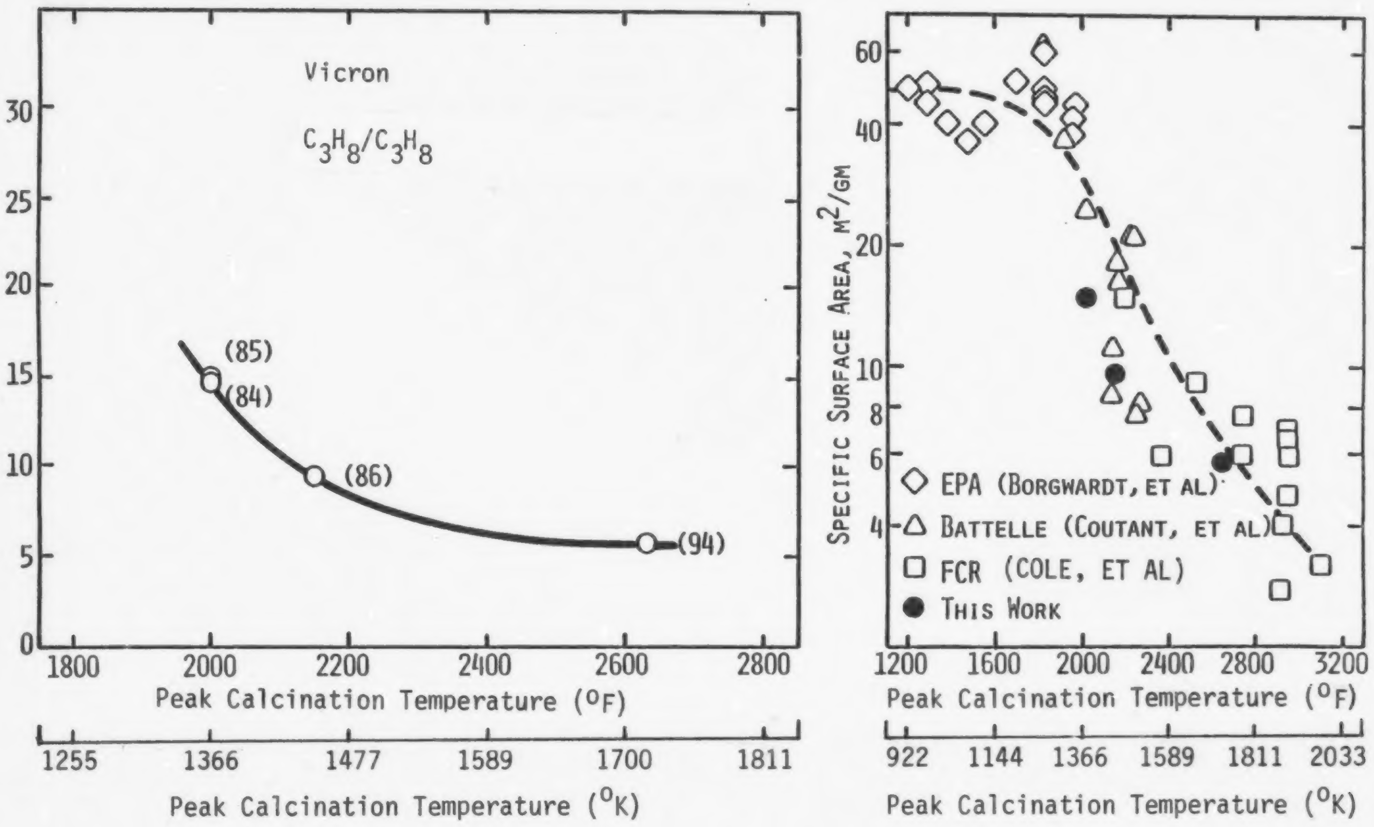

Figure 12-2. Limestone surface area as a function of peak calcination temperature.

side of Figure 12-2 compares surface areas measured during this work to surface areas measured by Borgwart, et al (1982), Contant, et al (1971), and Cole, et al (1983). The surface areas measured from sorbent calcination in the CTT correlate fairly well with the previous data.

Surface area data for all three sorbents used in this study are presented in Figure 12-3. The dolomite had significantly larger surface area than either the limestone or hydroxide. As was noted with the limestone, a similar increase in surface area with decreasing peak calcination temperature was observed for the dolomite. The surface area of the hydrated lime was less sensitive to temperature. The percent calcination of all sorbents was highest at the high peak calcination temperature. This effect was due to the higher temperature and longer residence time in the reactor.

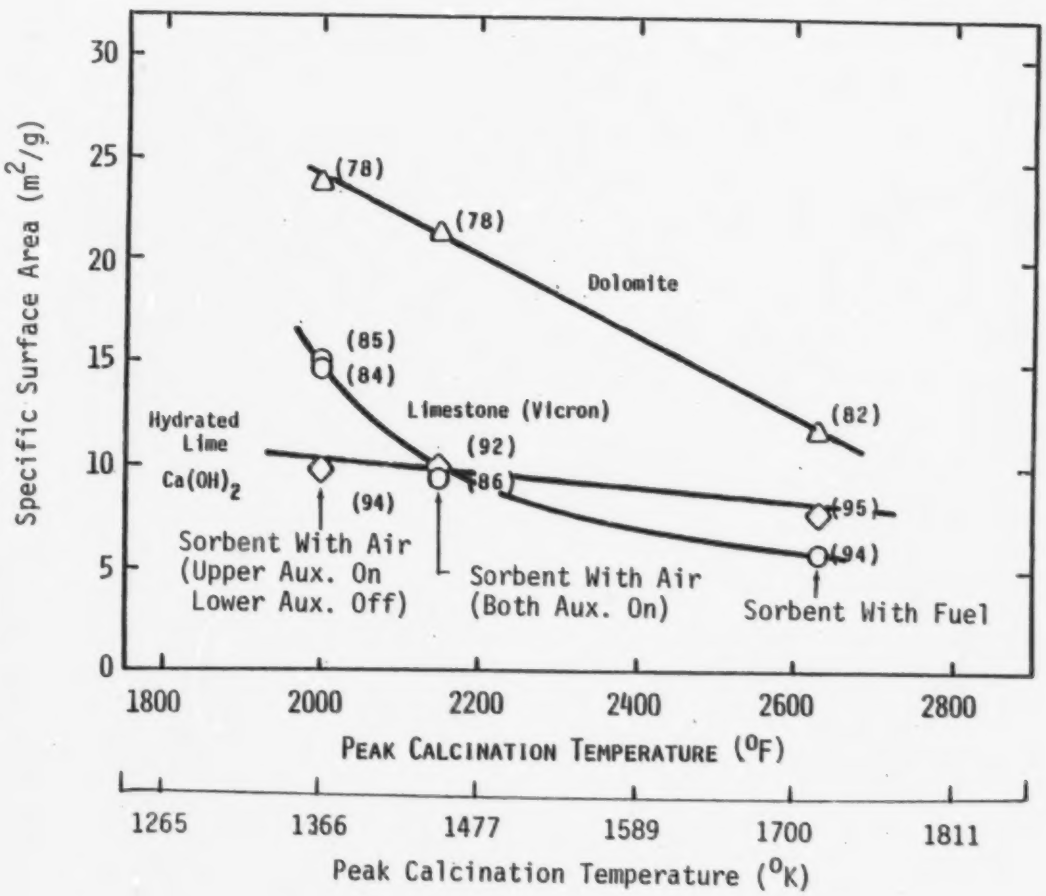

C_3H_8/C_3H_8

Figure 12-3. Sorbent surface area as a function of peak calcination temperature.

13.0 PARAMETRIC SCREENING STUDIES

The parametric screening studies were conducted at the baseline combustor operating conditions. Limestone was used as the baseline sorbent for all tests. Sorbent injection feedrates corresponding to molar calcium-to-sulfur ratios of 1 and 2 were used.

13.1 Impact on Reburning Effectiveness

Initially, exhaust NO_x concentrations were measured to identify the impacts of sorbent injection and SO_2 on the effectiveness of NO_x reduction with reburning. Table 13-1 shows these results. No significant effects were observed with the presence of SO_2 or the sorbent in the system.

13.2 Reburning Zone Stoichiometry

The influence of the reburning zone stoichiometry on the SO_2 capture efficiency is presented in Figure 13-1. At all stoichiometries, sorbent injection with the burnout air was more effective than with the reburning fuel. The improved capture obtained with air injection was attributed to the higher sorbent surface area. As the reburning zone stoichiometry was increased, better capture was exhibited at either injection location. This effect is believed due to increased sulfation zone residence time. As SR_2 increased, the total volumetric flow rate in the reactor decreased, resulting in longer residence time as shown in Figure 13-2. Consequently, the extent of sulfation increased with SR_2.

As the Ca/S ratio was increased better captures were obtained due to the availability of more reactive sorbent. The observed trends were similar at both Ca/S ratios.

13.3 SO_2 Partial Pressure

The influence of initial SO_2 concentration on sorbent utilization is presented in Figure 13-3. No effect on the percent SO_2 captured by the

Figure 13-1. INFLUENCE OF SO_2 AND SORBENT ON REBURNING EFFECTIVENESS IN NO_x REDUCTION

			$(NO_x)_{ex}/(NO_x)_p$, Percent			
			SR_2			
	$(SO_2)_p$	Ca/S	1.1	1.0	0.9	0.8
	0	-	100	65	37	46
	1940	0	100	62	37	43
Sorbent with Fuel	1940	1.0	100	57	36	46
	1940	2.0	100	59	34	44
Sorbent with Air	1940	1.0	99	62	38	43
	1940	2.0	99	62	38	42

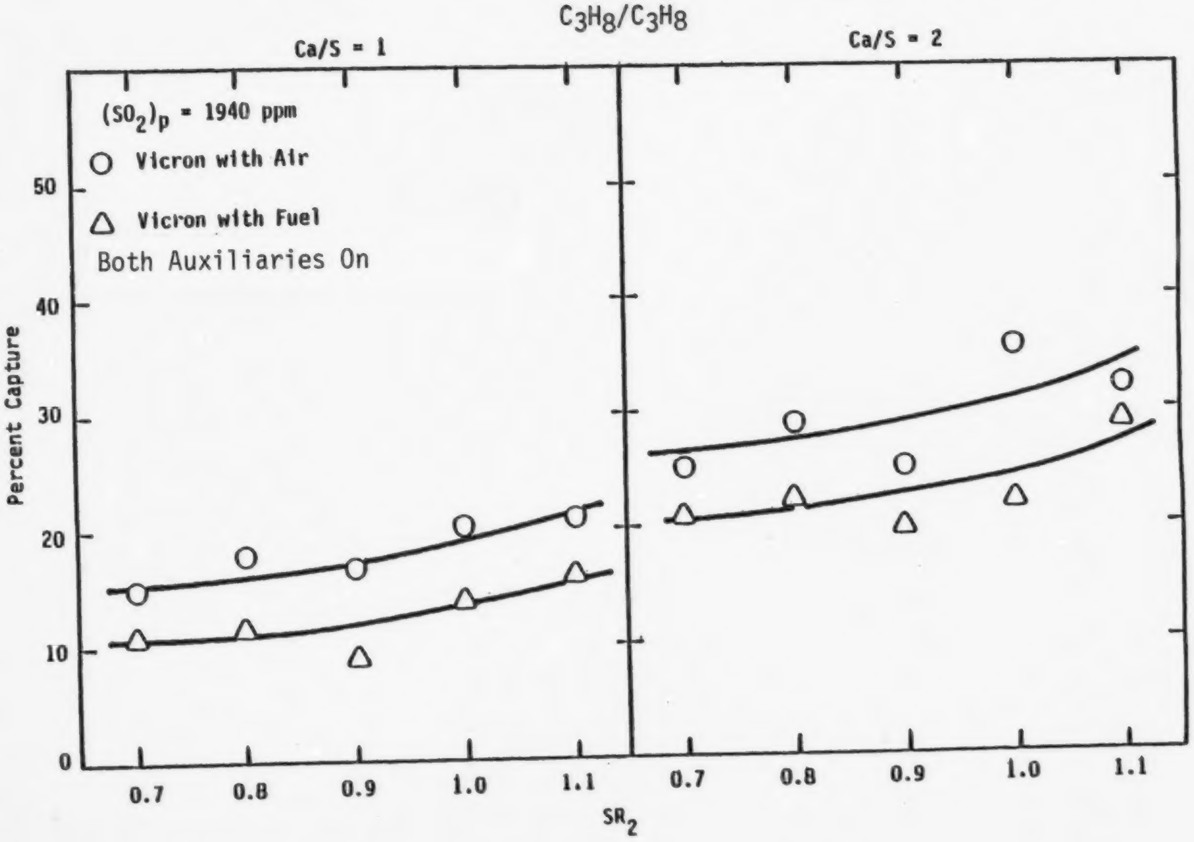

Figure 13-1. Influence of reburning zone stoichiometry on SO_2 capture.

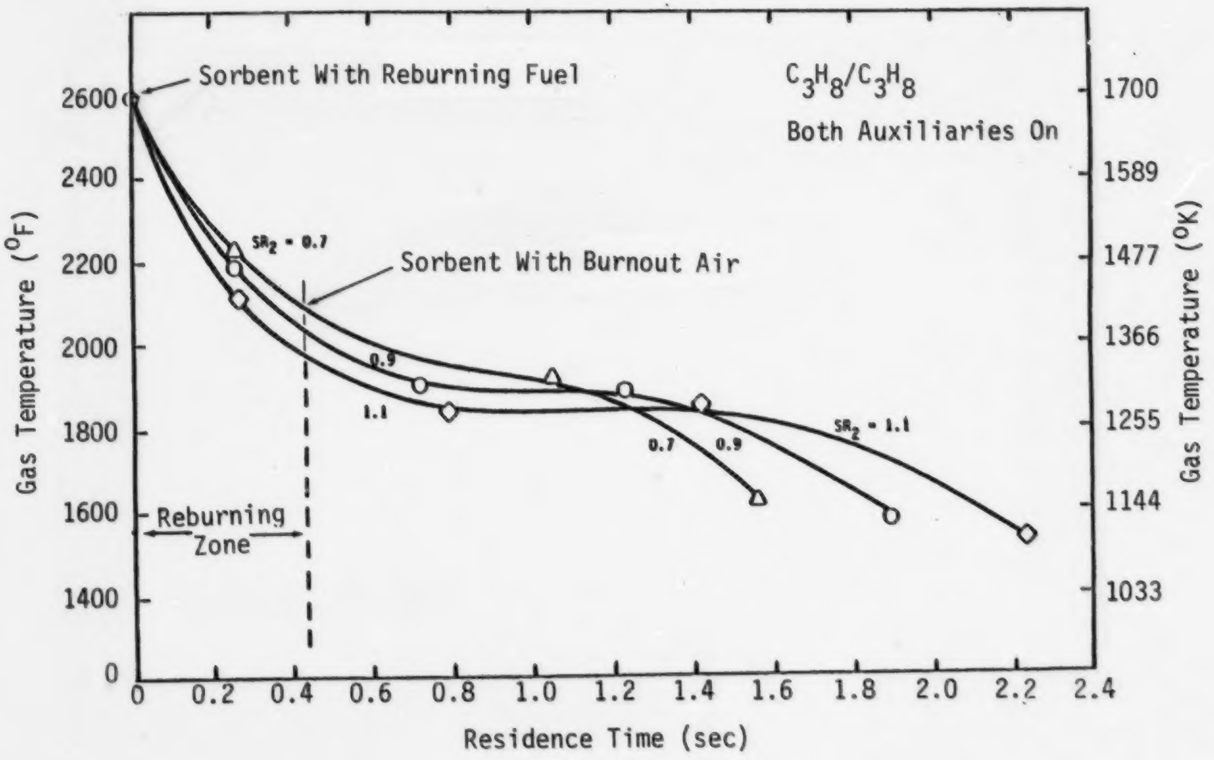

Figure 13-2. Time/temperature histories at three SR_2 values.

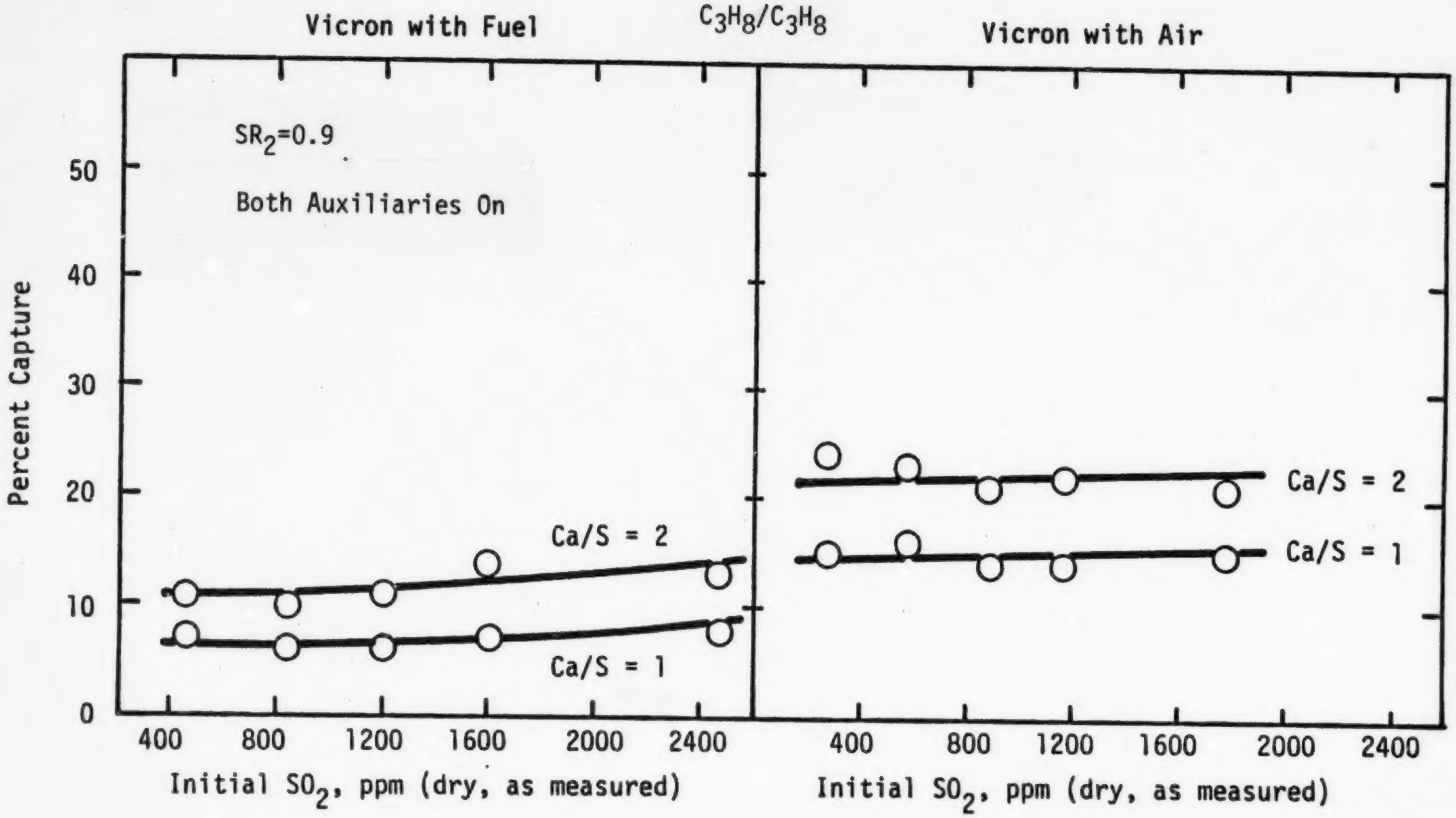

Figure 13-3. Sulfur captures as a function of initial SO_2 concentrations.

sorbent was observed over the range of initial SO_2 concentrations tested. From these data the overall reaction appeared to be independent of SO_2 concentrations above about 400 ppm. Figure 13-4 shows the comparison of these data with the model predictions. As discussed in the Appendix, disagreement was found at low-SO_2 concentrations where the reaction rate should be limited by diffusion.

13.4 Sulfur Speciation

To investigate the effect of sulfur speciation on SO_2 capture, identical amounts of sulfur were either injected in the main burner zone as SO_2 or added as H_2S to the fuel-rich reburning zone. The capture data for Vicron injected with the burnout air is presented in Figure 13-5. No difference in the SO_2 capture was noted with the sorbent injection with the air. This result was expected because the H_2S in the rich reburning zone was immediately oxidized to SO_2 in the burnout zone. The sorbent was insensitive to the original source of sulfur because all sulfur was present as SO_2. When Vicron was injected with the reburning fuel, better capture was noted when the sulfur was present as H_2S. As the reburning zone became richer, better captures were observed (see Figure 13-6). However, this case represents an extreme where all sulfur was reburning fuel sulfur. In a practical situation, the reburning fuel would supply only about 10 to 20 percent of the total sulfur into the system. Under these conditions, rich capture would be insignificant.

13.5 Burnout Zone Stoichiometry

In order to determine the effect of variable excess air on SO_2 capture by sorbent injection an experiment was conceived which would allow for direct data comparison with no residence time effect. The burnout zone stoichiometry was varied by the addition of pure O_2 with the burnout air such that the total volumetric flowrate of burnout air plus O_2 remained constant. Performing the experiment in this manner effectively held the sulfation zone residence time constant while allowing the percent O_2 in the exhaust to be varied. Figure 13-7 illustrates the effect of variable SR_3 on SO_2 capture

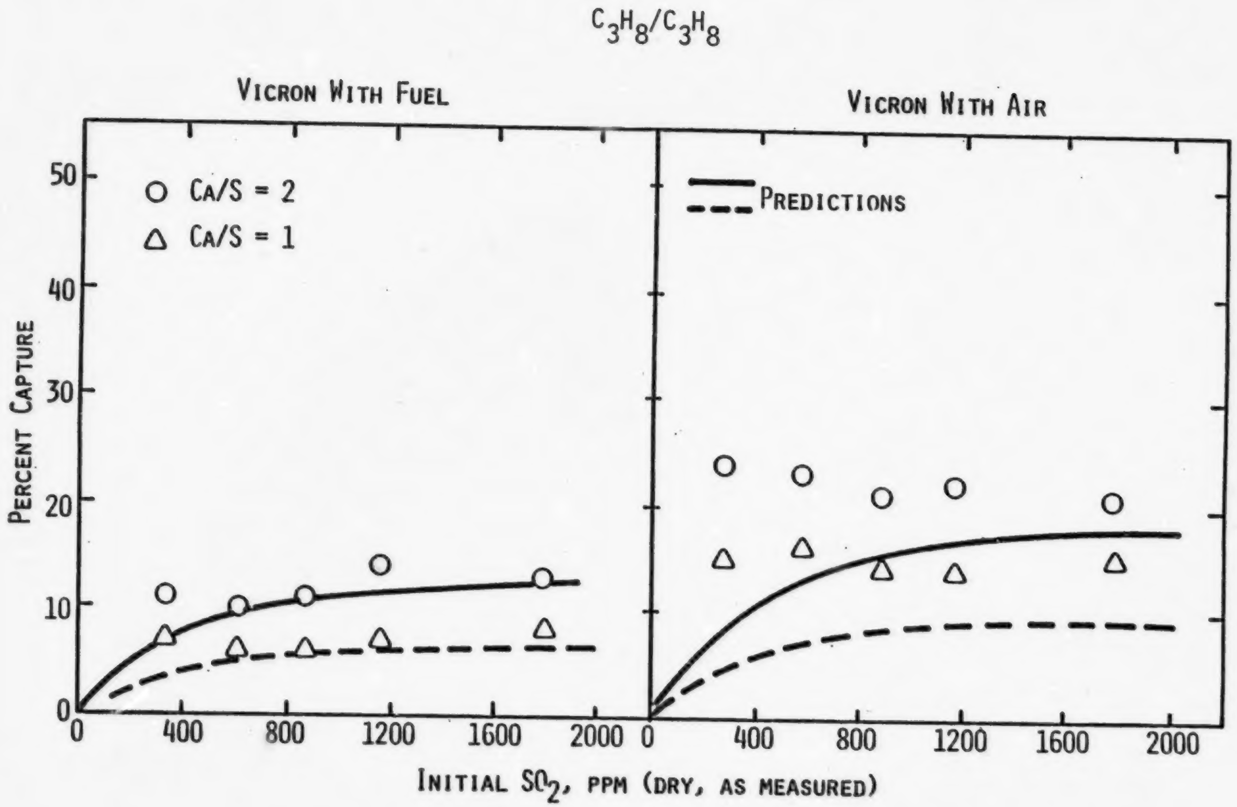

Figure 13-4. Model predictions.

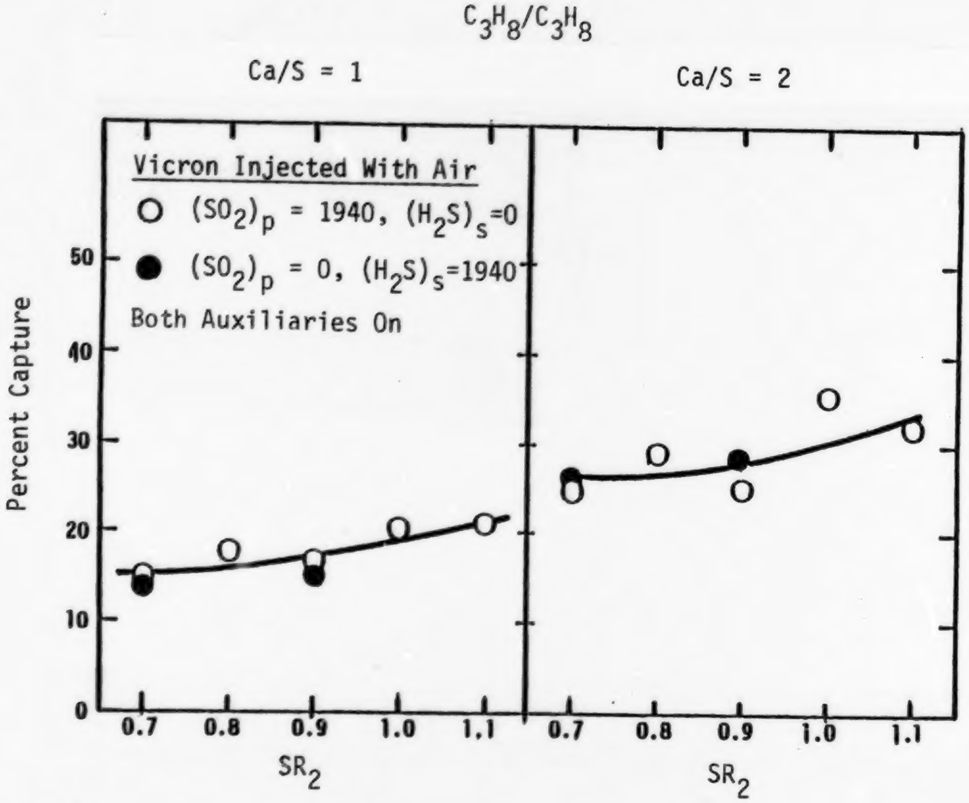

Figure 13-5. Impact of initial forms of sulfur.

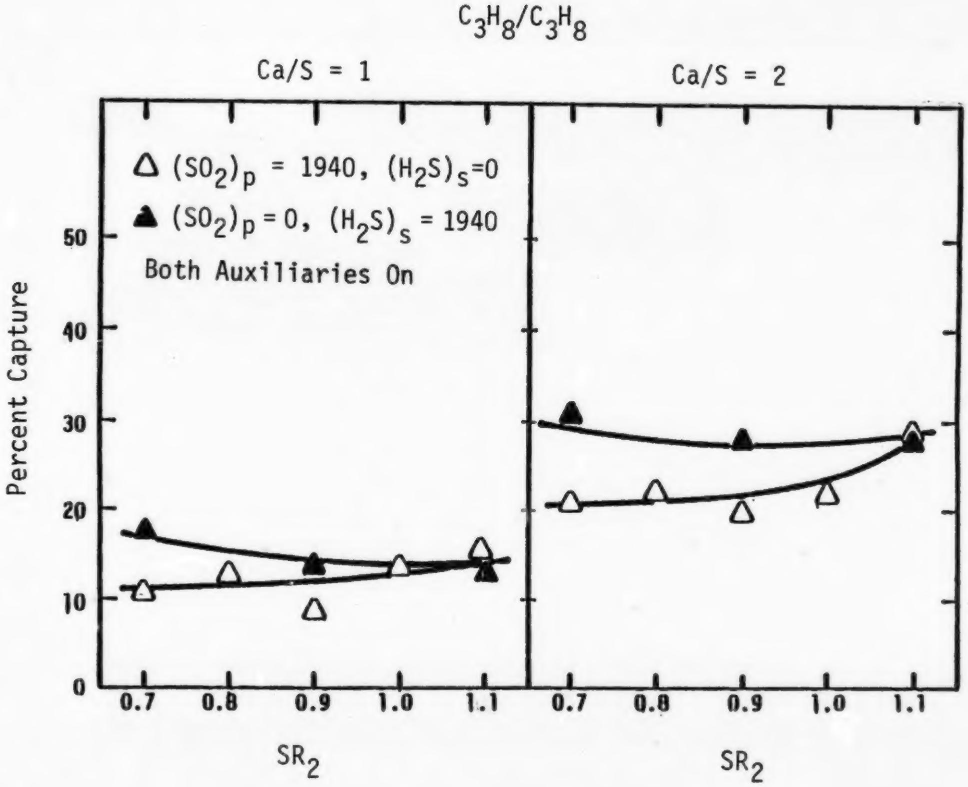

Figure 13-6. Impact of initial forms of sulfur.

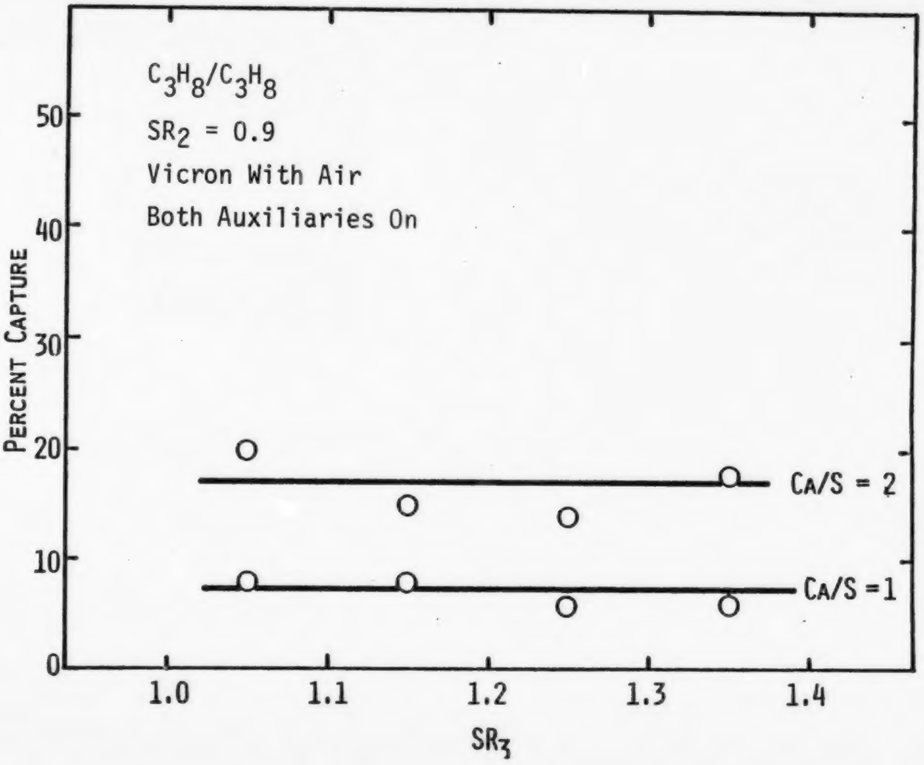

Figure 13-7. Effect of burnout zone stoichiometry.

for Vicron injected with the burnout air at a constant SR_2 of 0.9. No effect on SO_2 capture was noted.

14.0 SORBENT COMPOSITION EFFECTS

This section addresses the influence of calcintion and sulfation parameters on the SO_2 capture effectiveness for the three sorbents described in Section 3.0.

14.1 Injection Location and Calcination Temperature

The influence of injection location on SO_2 capture for the various sorbents is presented in Figure 14-1. For both Vicron and dolomite, better captures were obtained when the sorbents were injected with the burnout air. The increased capture was due to the higher sorbent surface area which was obtained by injecting the sorbent at a lower temperature (see Figure 12-3). However, the hydrated lime exhibited an opposite trend. Slightly better capture was obtained when the hydrated lime was injected with the reburning fuel. Because the surface area of the hydrated lime remained essentially constant with respect to injection temperature, the better capture was probably a result of longer residence time in the sulfation reaction zone. Figure 14-2 shows the time/temperature profile at the baseline condition with the shaded area representing the sulfation window. By injecting the sorbent with the fuel a somewhat longer residence time in the sulfation window was obtained.

The crossplot of Figure 14-1 illustrates the influence of sorbent type at the two injection locations (see Figure 14-3). For injection with the fuel, dolomite showed the best capture, followed by the hydrated lime, with Vicron the poorest of the three sorbents. For air injection, dolomite was far better than either the hydrated lime or Vicron, which were equally as effective. Combining the capture data in Figure 14 -3 with the sorbent surface area datain Figure 14-3, a composite plot was made illustrating that the capture effectiveness of all sorbents can be correlated solely in terms of surface area (see Figure 14-4). This suggested that the additional sulfation reaction time obtained by injecting sorbent with the fuel generally had a small effect in comparison with the overall surface area.

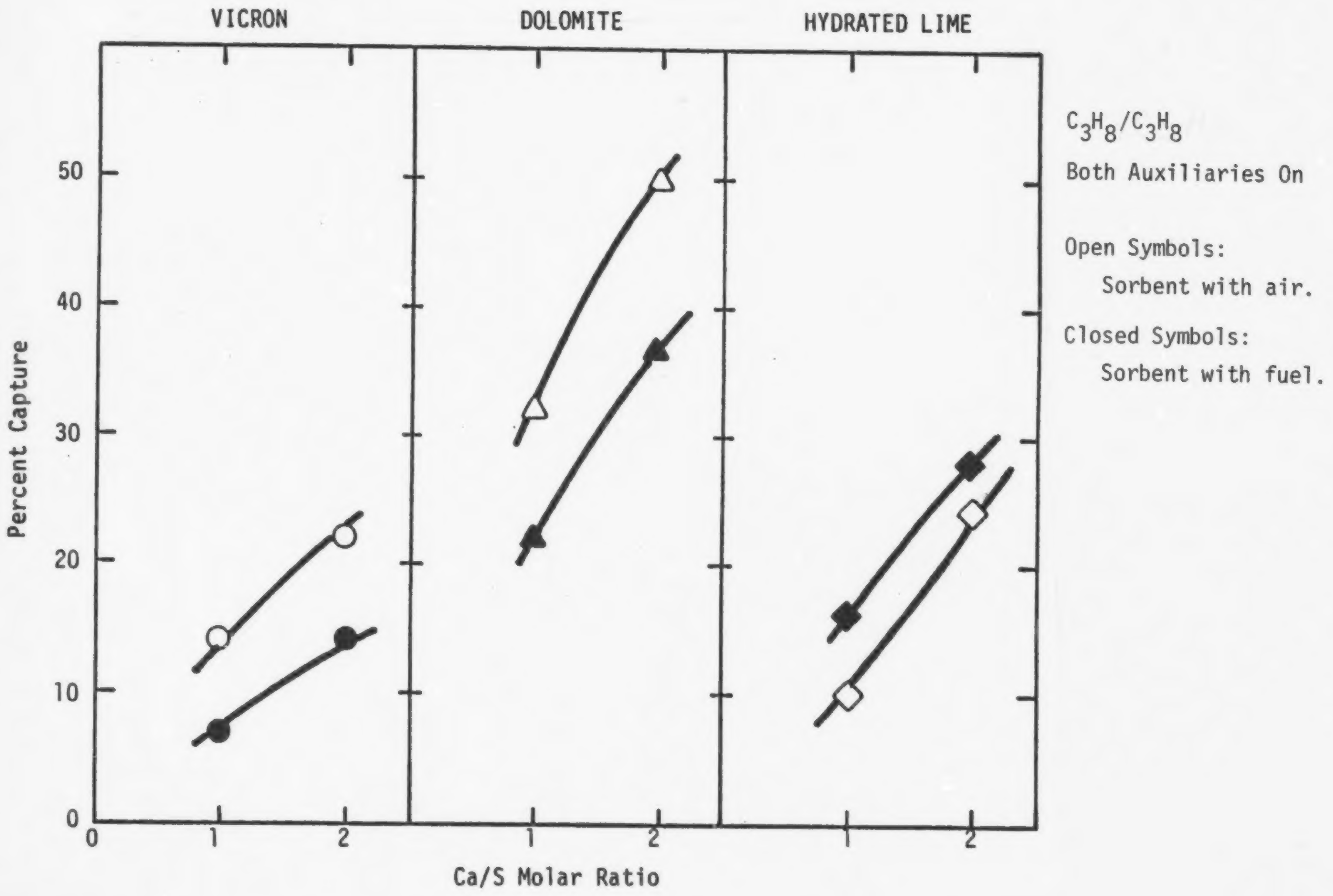

Figure 14-1. Influence of sorbent injection location.

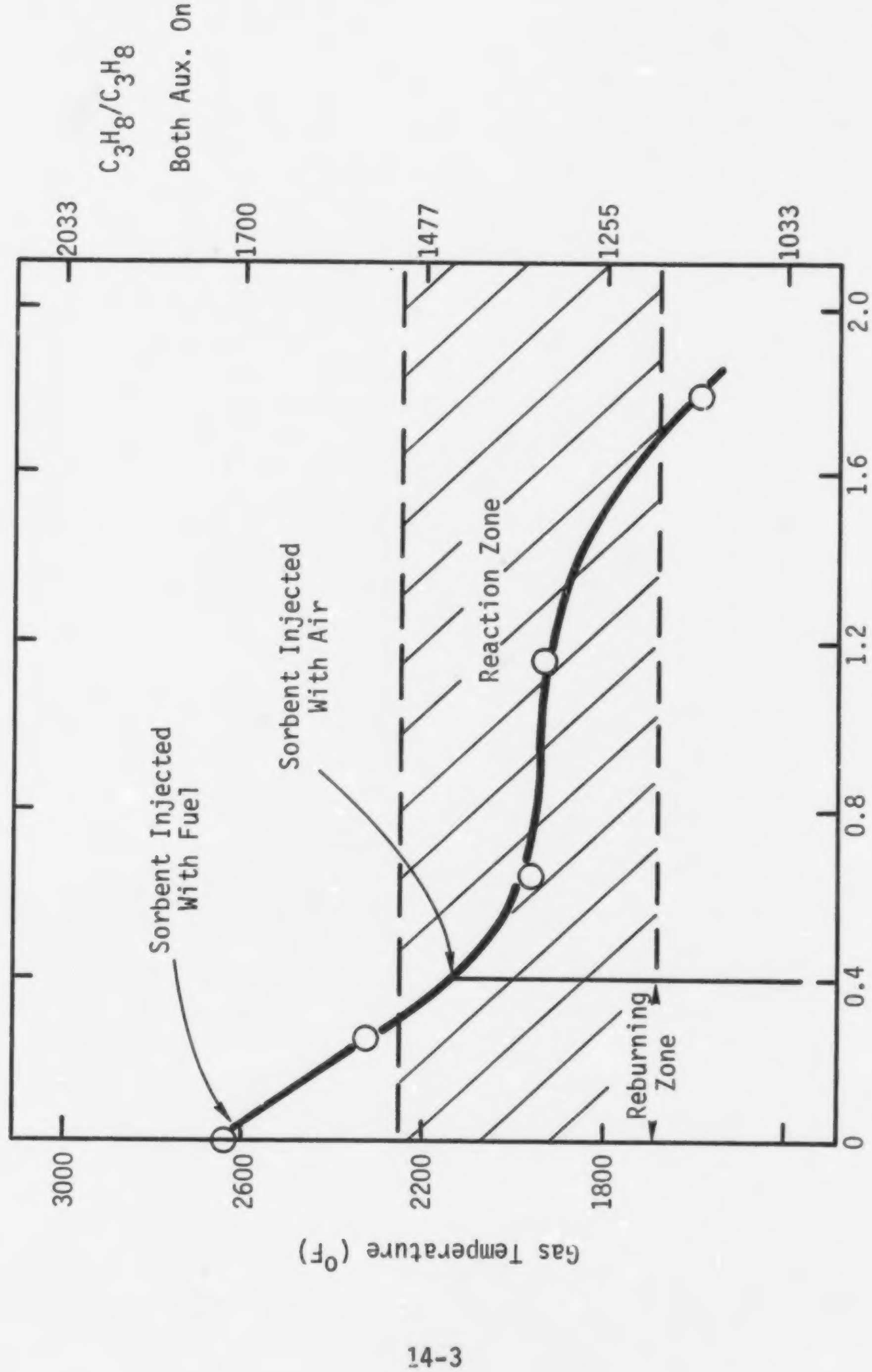

Figure 14-2. Time/temperature profile at baseline condition.

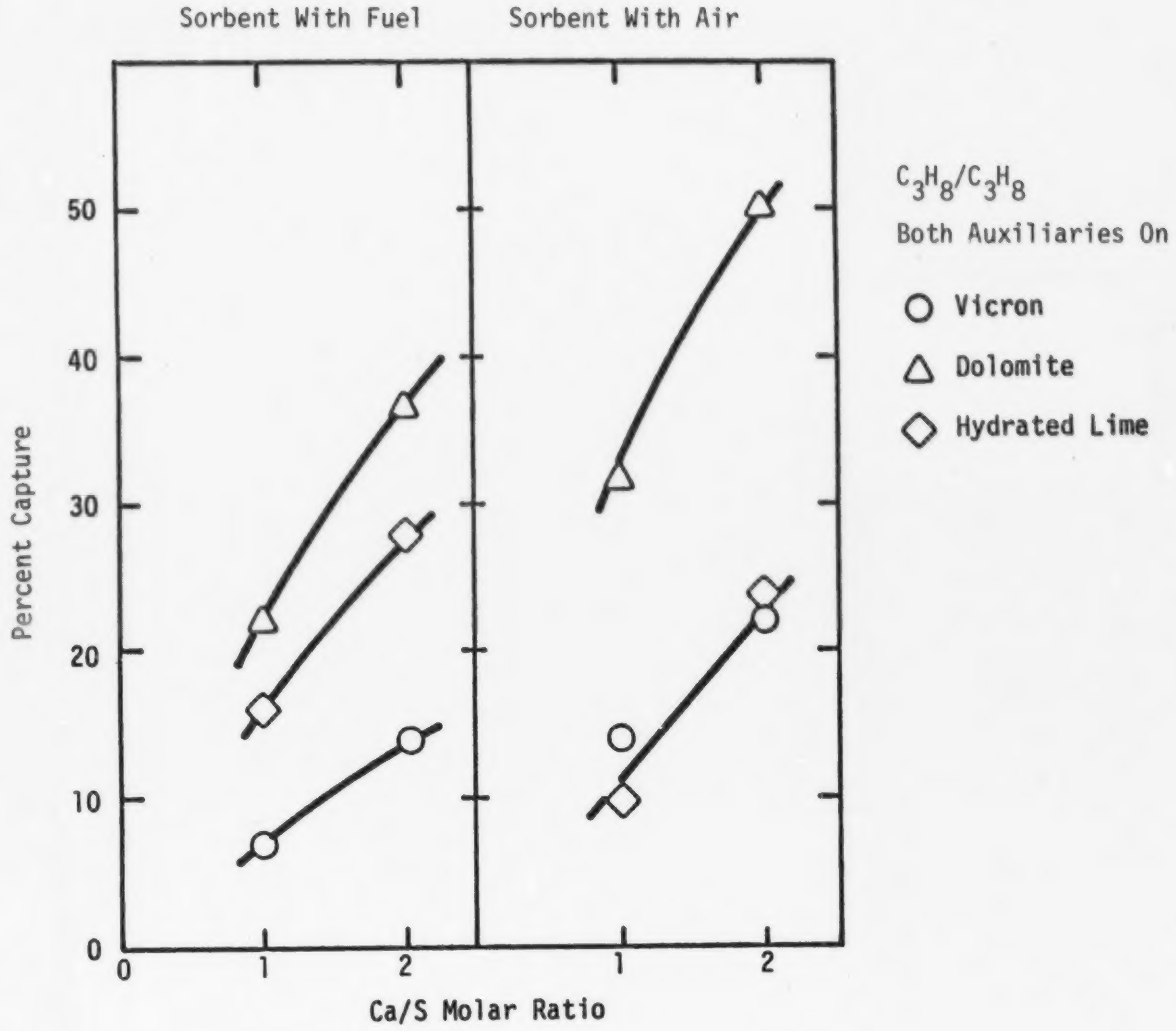

Figure 14-3. Comparison of sorbent type.

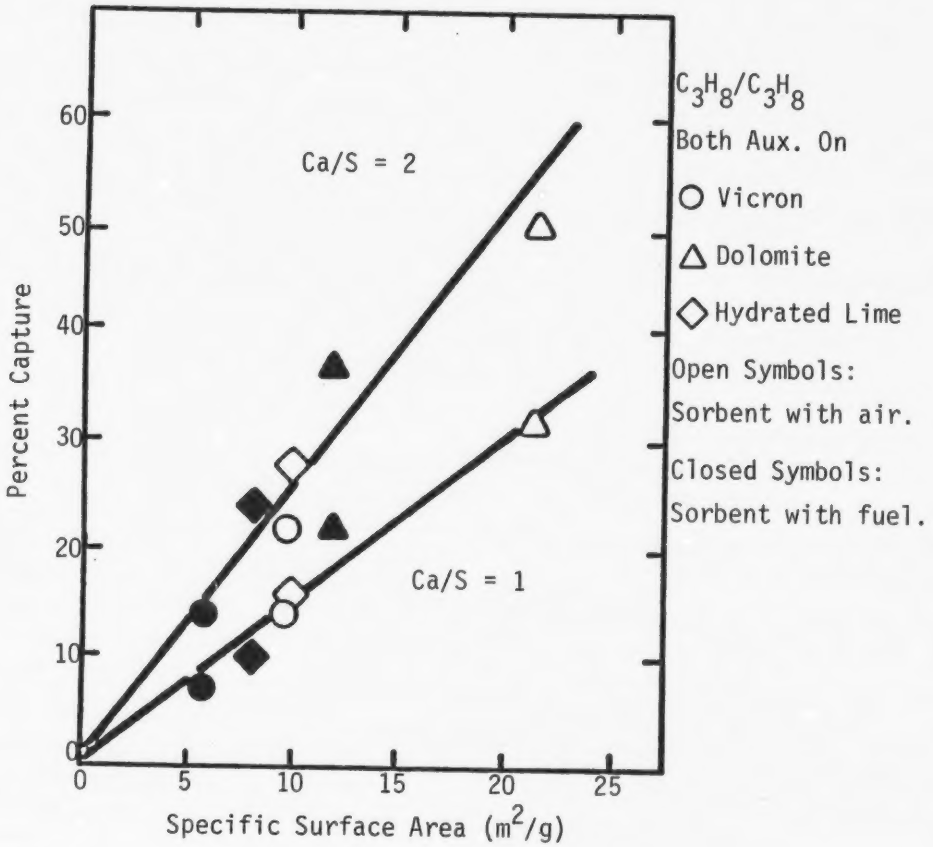

Figure 14-4. Capture vs. sorbent surface area.

Based on the measured surface area and the time/temperature profile, the two sulfation models (see Section 1.2) were used to predict the captures. As shown in Figure 14-5, the predictions of the models bracket the measurements fairly well.

14.2 Influence of Reaction Time/Temperature

The influence of the sulfation zone time/temperature history on SO_2 capture was investigated by injecting sorbent with the reburning fuel at two thermal profiles (both auxiliary burners on and upper on, and lower off, see Figure 14-6). The resulting capture data for the three sorbents are presented in Figure 14-7. Dolomite exhibited the only significant reaction temperature effect, the hotter profile (both auxiliary burners on) was significantly better than the cooler profile. Vicron and hydrated lime showed essentially no reaction temperature dependence. Figure 14-8 summarizes all the data obtained at both thermal profiles and compares with model predictions. The measured captures with Vicron and the dolomite agreed reasonably well with model predictions. However, for the hydrated lime, the measured captures were higher than the predicted values, particularly at low sulfation temperatures.

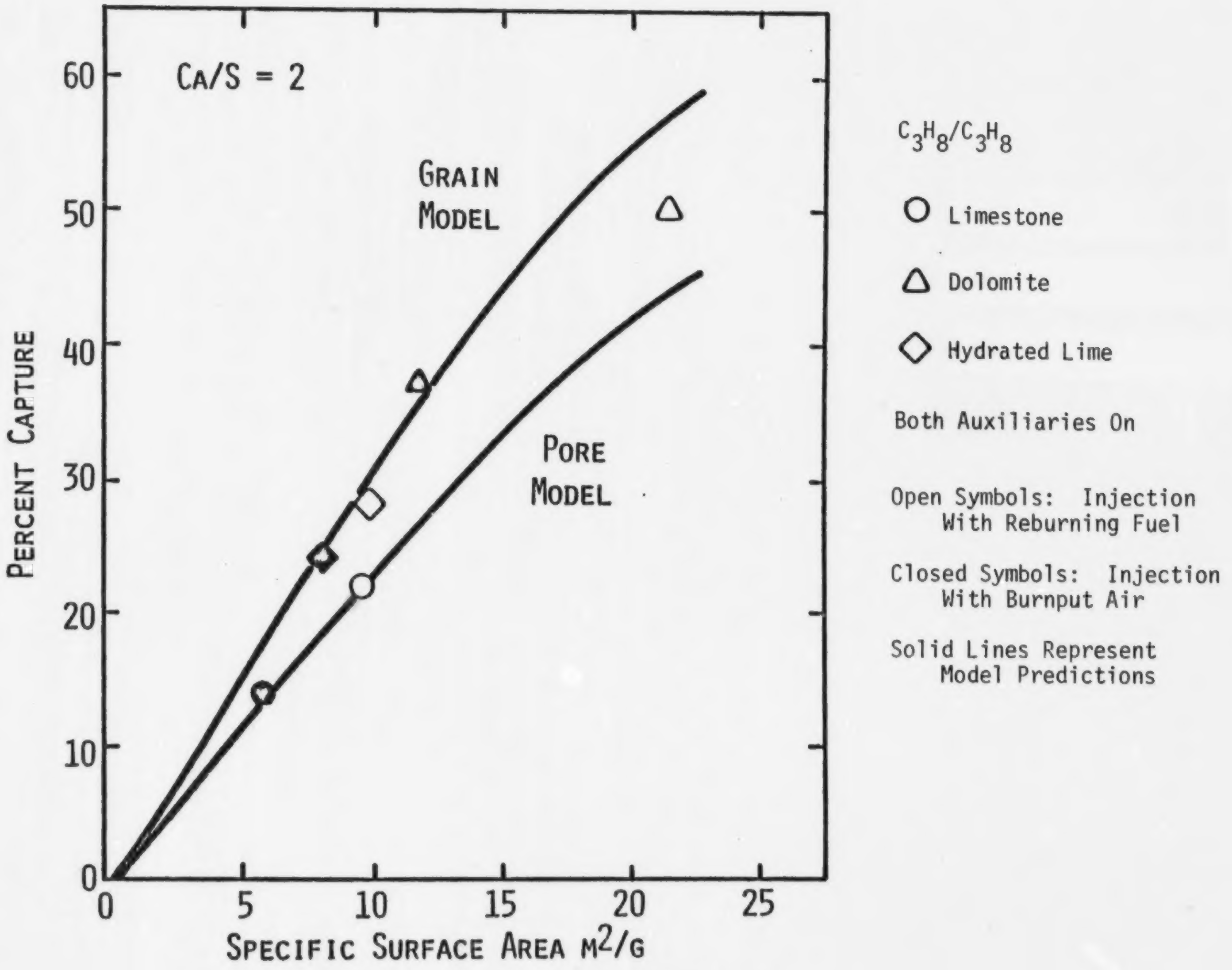

Figure 14-5. Model predictions.

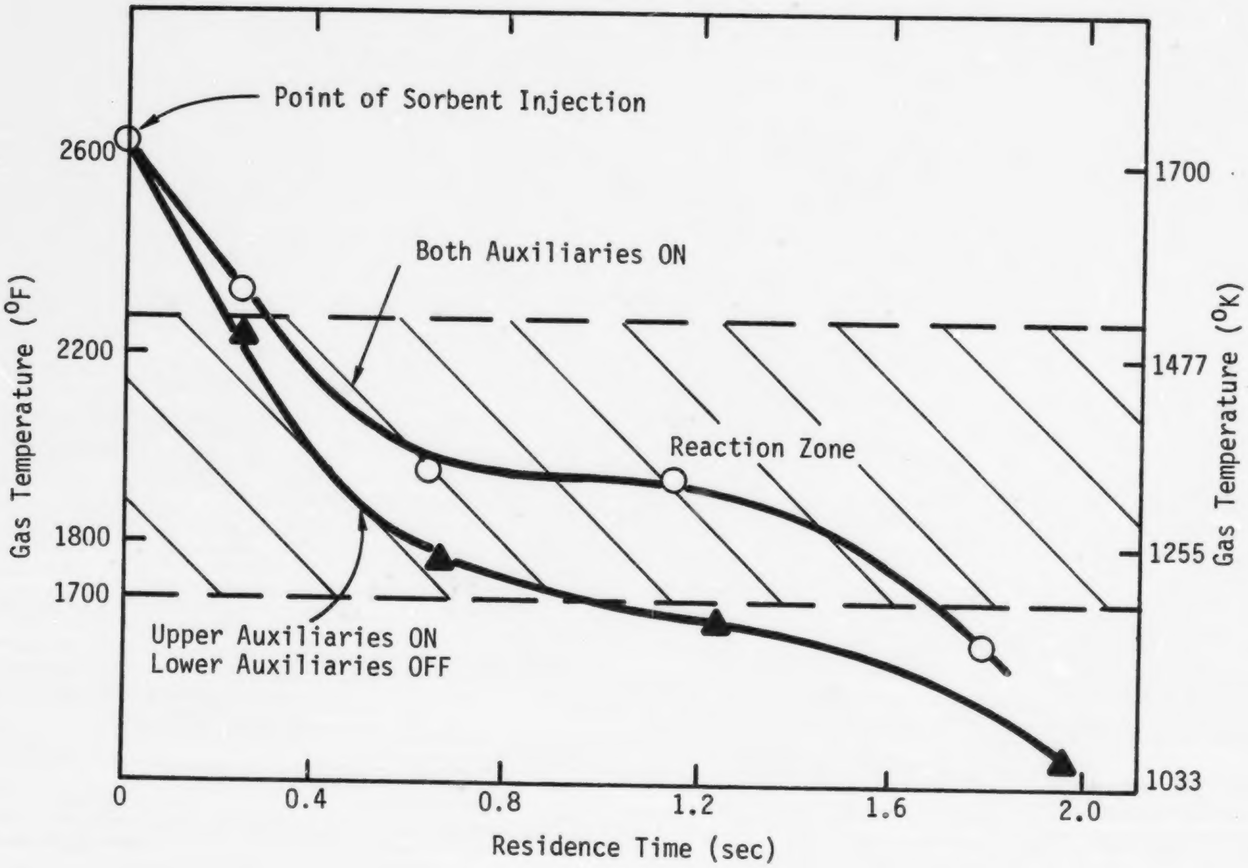

Figure 14-6. Reaction zone temperature profiles.

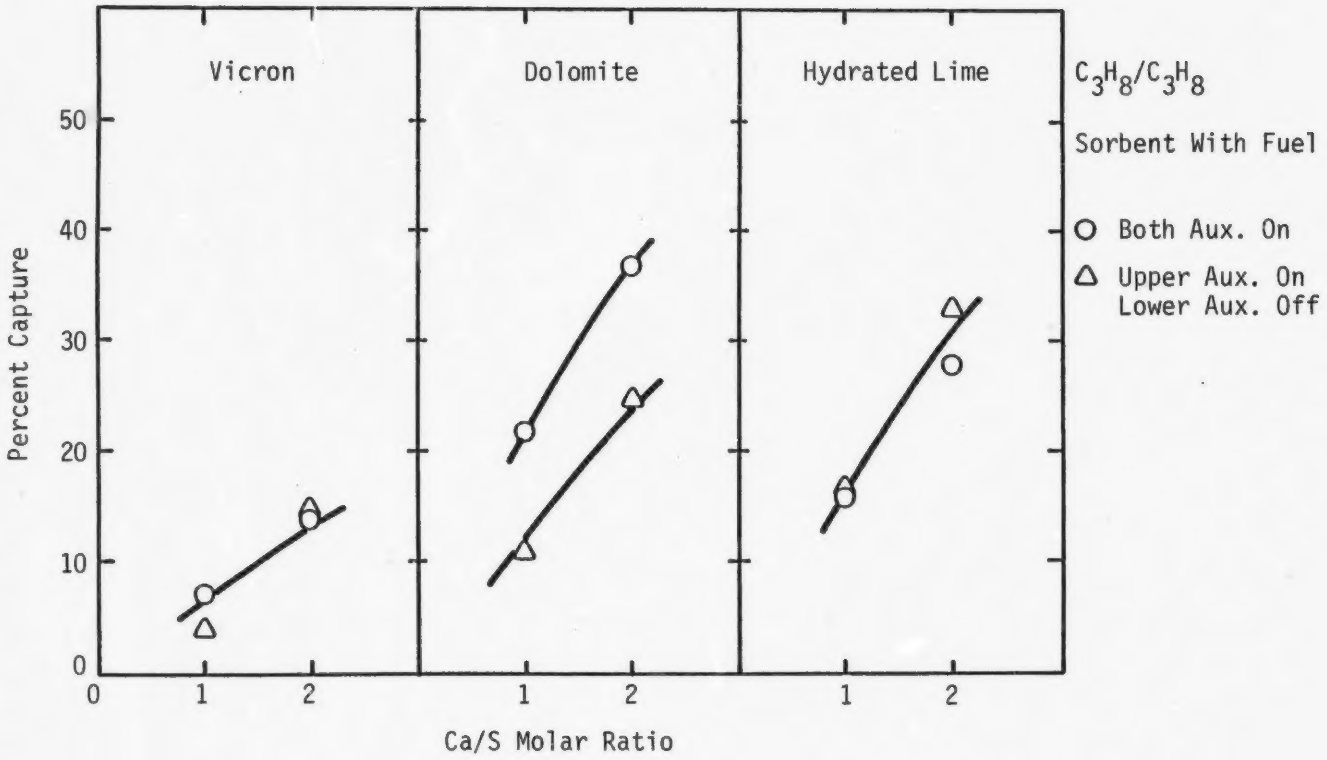

Figure 14-7. Reaction zone temperature effects.

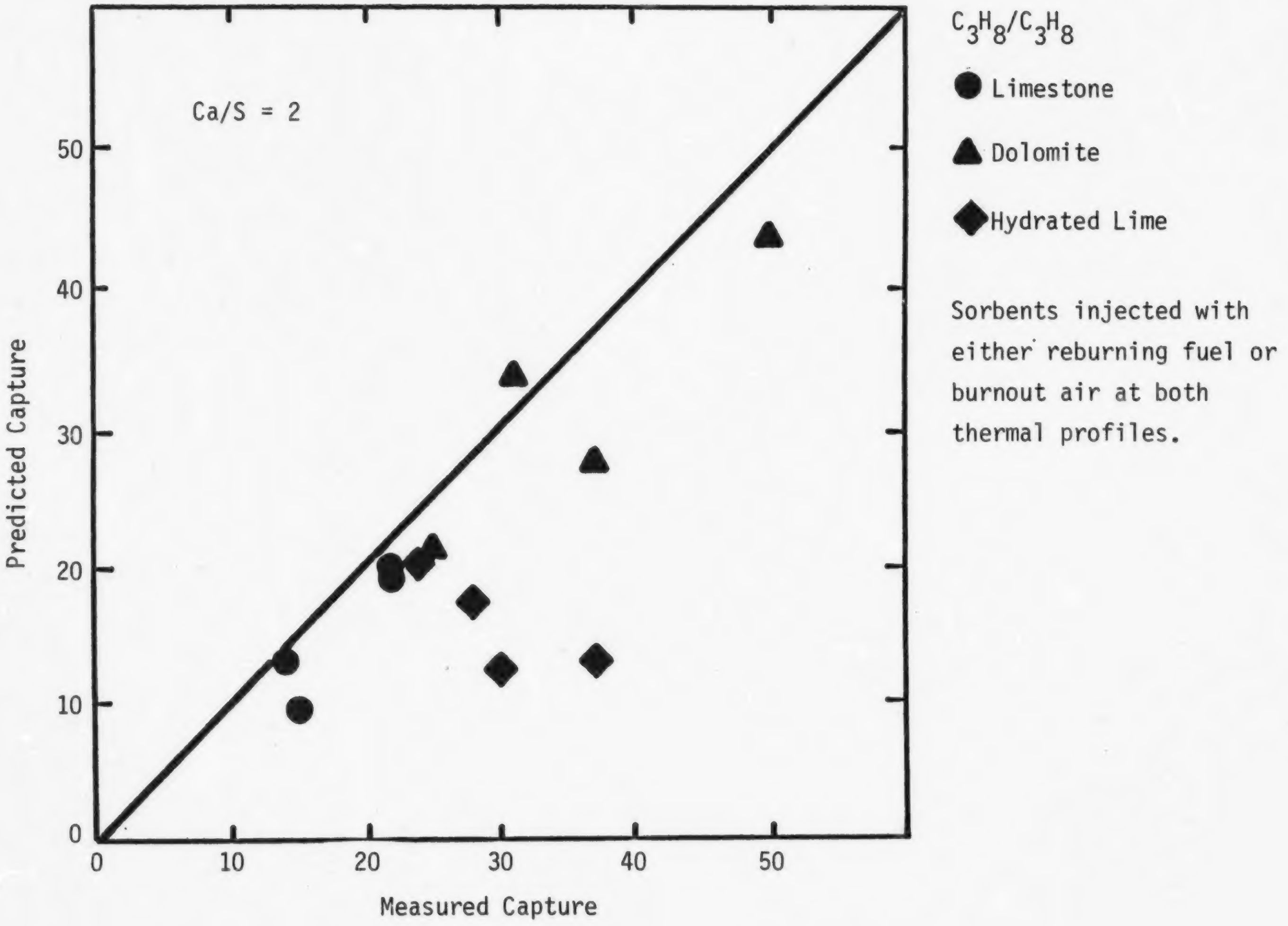

Figures 14-8. Comparison of model predictions with observed SO_2 captures.

15.0 FUEL COMPOSITION EFFECTS

15.1 Injection Location

SO_2 capture experiments were conducted under reburning conditions with Indiana coal fired as both primary and reburning fuels. The influence of sorbent injection location on SO_2 capture is presented in Figure 15-1. No difference between injection locations was noted for the Vicron. The dolomite was slightly better when injected with the air and the hydroxide was significantly better when injected with the air. It is noted that the hydroxide showed better capture when injected with the fuel in a propane flame (see Figure 14-1).

15.2 Thermal Effects

The effects of variable reaction zone temperature are illustrated in Figure 15-2. Vicron and the hydrated lime showed no sulfation zone temprature effect while slightly better capture was obtained with the dolomite at colder sulfation conditions. The capture data with coal did not correlate with the surface area data obtained from the propane reburning studies, however. The reaction zone temperature data with coal did follow the trends observed with the propane data except for the dolomite, which experienced an opposite trend as the propane data.

15.3 Comparison of Coal and Gas

A composite plot illustrating the effects of Vicron injected with the fuel and air for three sets of primary/reburning fuels is presented in Figure 6-3. The SO_2 capture was fairly independent of fuel composition when the Vicron was injected with the air. However, the C_3H_8/C_3H_8 data indicated poorer capture than either the C_3H_8/Indiana or Indiana/Indiana data when Vicron was injected with the reburning fuel. Detailed examination of the thermal profiles shown in Figure 15-4 indicated that with coal, the sorbent injection temperature was higher (which would have produced a lower sorbent surface area and hence lower capture) and the temperature profile in the

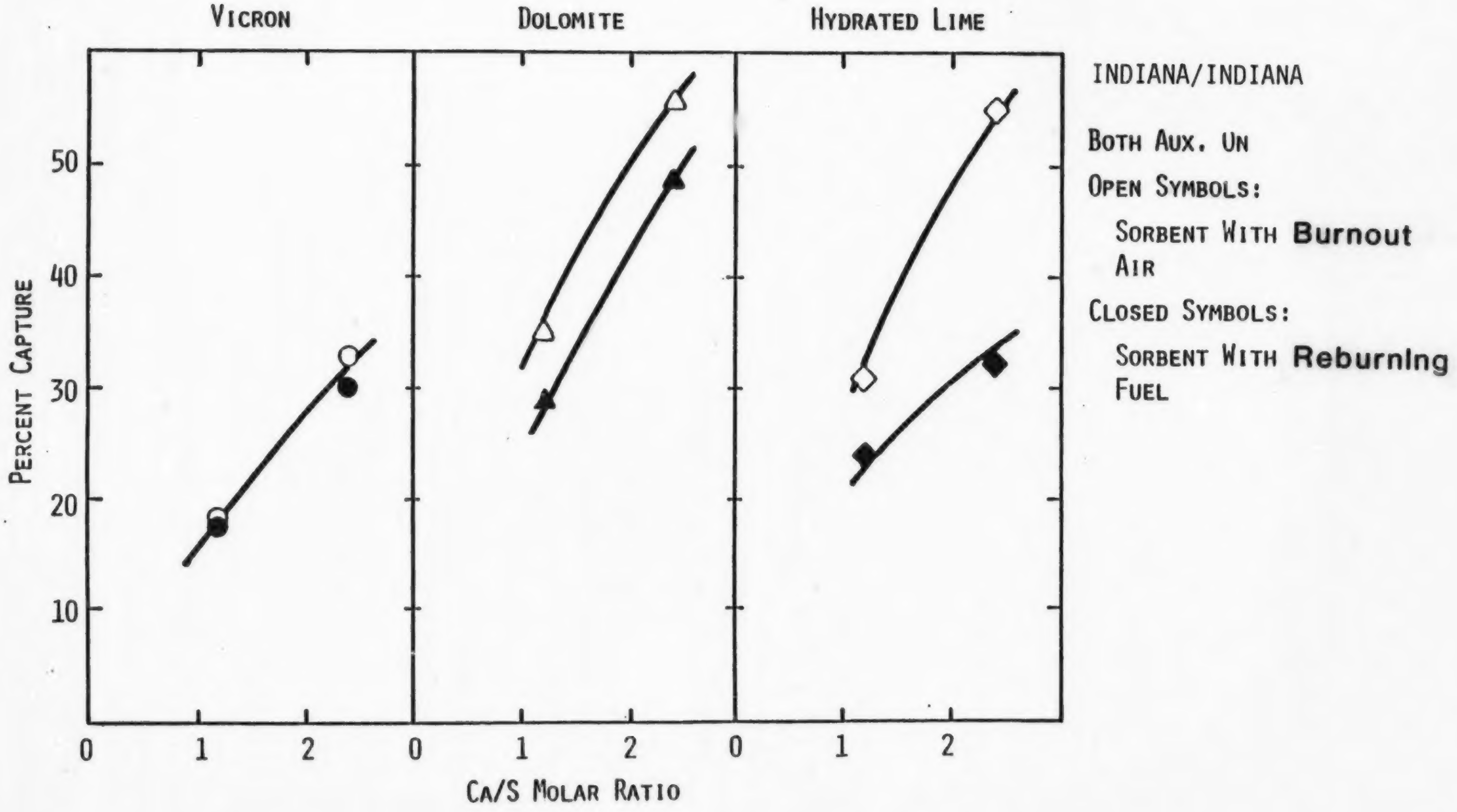

Figure 15-1. Influence of sorbent injection location.

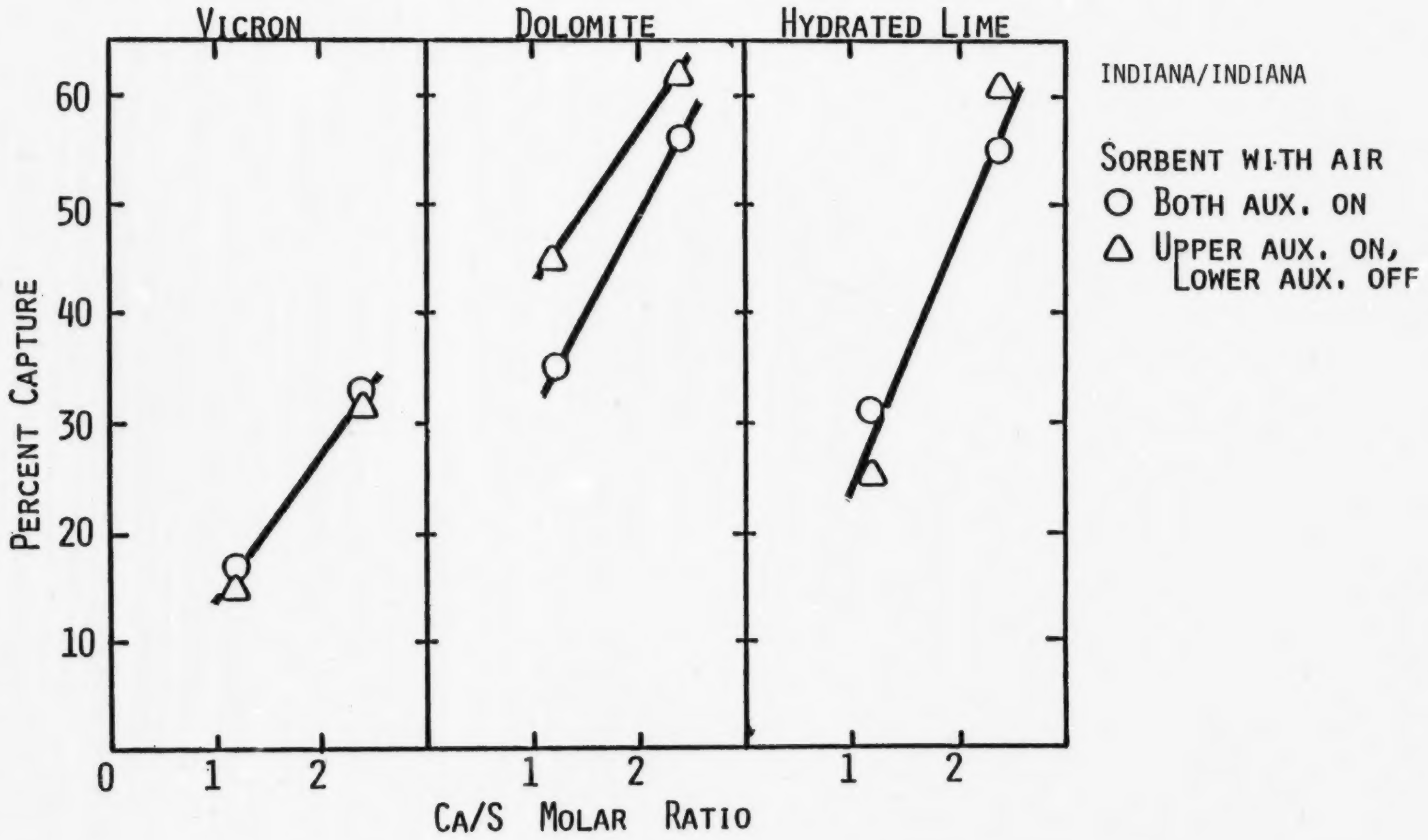

Figure 15-2. Reaction zone temperature effects.

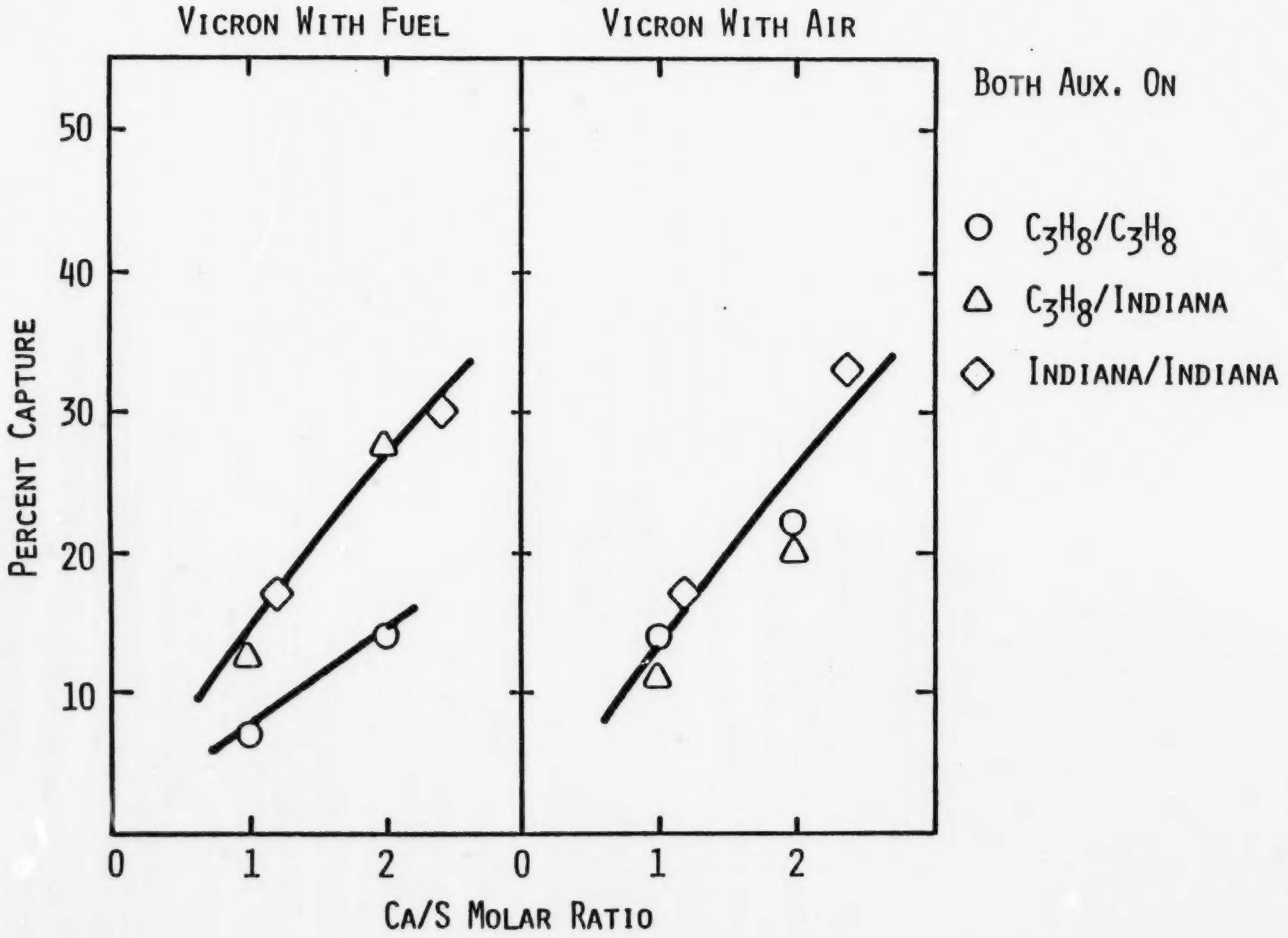

Figure 15-3. Comparison of coal and gas.

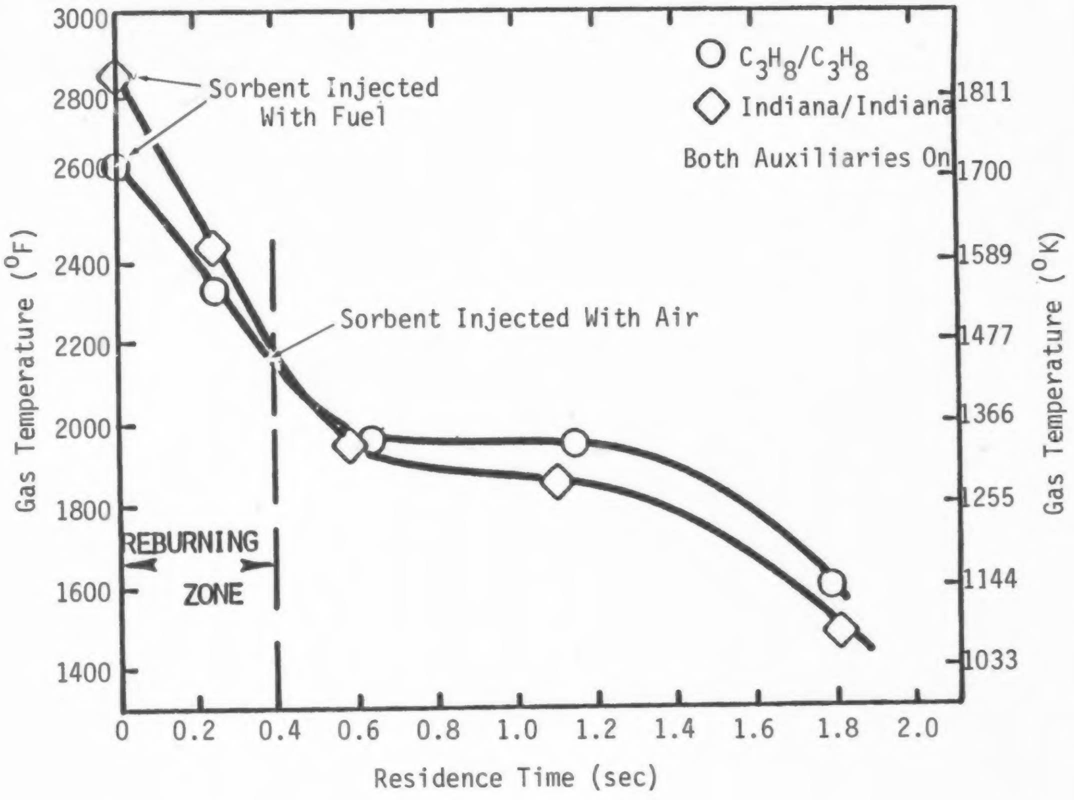

Figure 15-4. Time temperature profiles of propane and Indiana coal.

sulfation window was lower (which also would have decreased sulfur capture with coal).

Figure 15-5 compares sulfur captures obtained with Indiana coal with those obtained with propane for the three sorbents. In general, the Indiana coal consistently gave better captures than propane regardless of the sorbent type, the injection location, or the thermal history. These results suggest that the coal minerals might be responsible for the increased sulfur capture observed in these experiments.

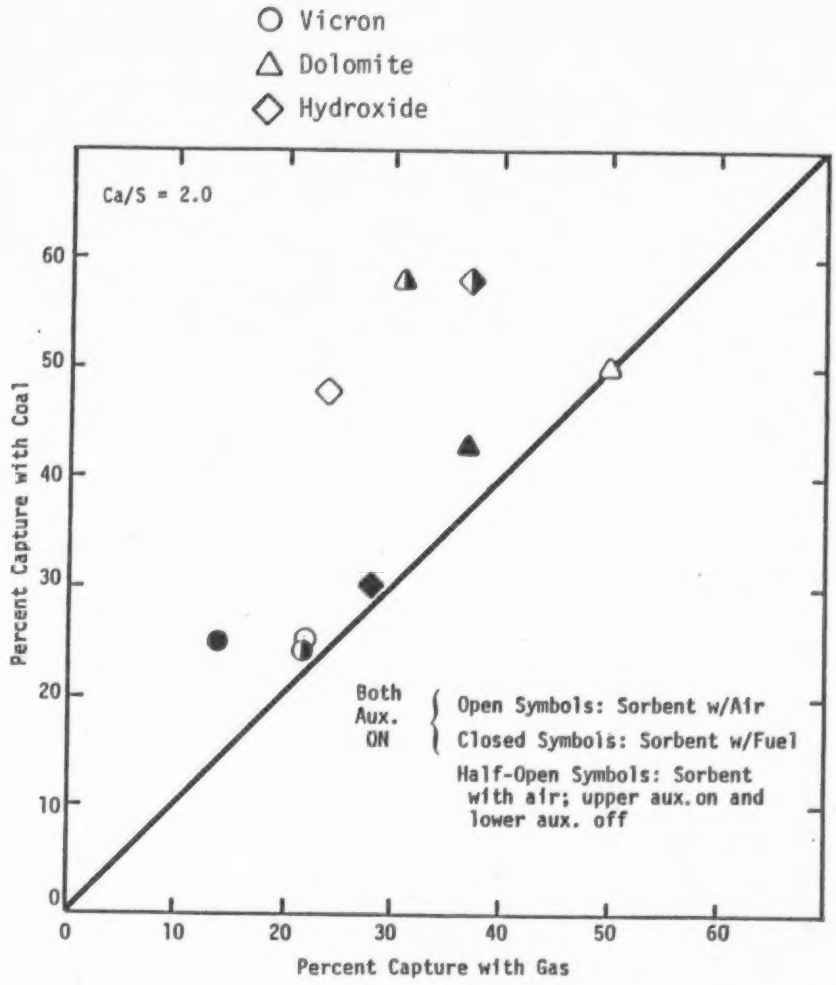

Figure 15-5. Comparison between coal and gas.

16.0 CONCLUSIONS

The conclusions obtained from the SO_2 capture by sorbent injection as applied to a reburning system were as follows:

- Sorbent surface area decreased with increasing peak calcination temperature.
- SO_2 capture was relatively insensitive to reburning zone and burnout zone stoichiometries.
- Sorbent injection with the burnout air was generally preferred due to increased surface area.
- SO_2 capture was only weakly dependent on SO_2 concentration.
- Capture with dolomite was higher than with Vicron or hydroxide due to increased surface area.
- Capture with Indiana coal was equivalent or superior to that obtained with propane.
- Sulfation models are capable of predicting capture data of doped propane.

17.0 REFERENCES

Bhatia, S. K. D. D. Perlmutter. The Effect of Pore Structure on Fluid Solid Reactions: Application of the SO_2-Lime Reaction. AIChE J., Vol. 27, No. 2, 1981. p. 226.

Borgwardt, R. H., G. R. Gillis, and N. F. Roache. IERL-RTP Research on Sulfur Capture in LIMB. Joint EPA/EPRI Symposium on Stationary Combustion NO_x Control. Dallas, Texas, November 3, 1982.

Chen, S. L., Heap, M. P., Pershing, D. W., and Martin, G. G. "Influence of Coal Composition on the Fate of Volatile and Char Nitrogen During Combustion." Nineteen Symposium (International) on Combustion, The Combustion Institute, Pittsburgh, Pennsylvania, 1982.

Chen, S. L., W. D. Clark, M. P. Heap, D. W. Pershing and W. R. Seeker "NO_x Reduction by Reburning with Gas and Coal - Bench Scale Studies" Proceedings of the Joint Symposium on Stationary Combustion NO_x Control, Dallas, Texas, 1982.

Cole, J. A., W. D. Clark, M. P. Heap, J. C. Kramlich, S. Samuelsen, W. R. Seeker. Fundamental Studies of Sorbent Calcination and Sulfation for SO_2 Control from Coal-Fired Boilers. Task Report EPA Contract No. 68-02-3633, October, 1983.

Coutant, R. W., R. Simon, B. Campbell, and R. E. Barrett, Investigation of the Reactivity of Limestone and Dolomite for Capturing SO_2 from Flue Gas (Final Report). EPA report APTD 0802 (NTIS PB 204-385), U.S. EPA, Industrial Environmental Research Laboratory, Research Triangle Park, NC, October 1971.

Lyon, R. K., and Longwell, J. P., Paper Presented at EPRI NO_x Control Technology Seminar, San Francisco, California, 1976.

Overmoe, B. J., Chen, S. L. Pershing, D. W., Seeker, W. R., Heap, M. P., and Johnson, T. R. "Influence of Steam and Flue Gas Addition on NO_x Formation from Australian Brown Coal." Western States Section/The Combustion Institute, Boulder, Colorado, 1984.

Reed, R. D. Process for the Disposal of Nitrogen Oxide. John Zinc Company, U.S. Patent 1274637, 1969.

Seeker, W. R., Samuelsen, G. S., Heap, M. P., and Trolinger, J. D. "The Thermal Decomposition of Pulverized Coal Particles." Eighteen Symposium (International) on Combustion, The Combustion Institute, Pittsburgh, Pennsylvania, 1980.

Takahashi, Y., et al. Development of Mitsubishi "MACT" In-Furnace NO_x Removal Process. Presented at U.S.-Japan NO_x Information Exchange, Tokyo, Japan, May 25-30, 1981.

Wendt, J. O. L., C. V. Sternling, and M. A. Matovich. Fourteenth Symposium (International) on Combustion, The Combustion Institute, 1973. p. 897.

APPENDIX A: QUALITY ASSURANCE

The collection and analysis of quality data is key to the success of this program. In order to ensure that the data quality is commensurate with the program objectives, many quality assurance measures have been taken in all phases of the program. The program QA objectives for precision and accuracy are listed in Table A-1. These objectives were based on the program requirements and the precision and accuracy levels achievable by the selective measurements methods. Table A-1 also shows references to standard measurements procedures or measurement validation studies, and the experimental conditions under which each measurement was performed. The procedures and measurements which have not been standardized by EPA or ASTM are described in detail in this appendix.

A.1 Sampling Procedures

Table A-2 summarizes the sampling procedures for each measurement. This table includes sampling location selection criteria, sampling procedures, and sampling frequency.

Continuous Monitoring Instrumentation

Figure A-1 shows a schematic diagram of the continuous monitoring system for NO, NO_x, CO, CO_2, and O_2. This system was specifically designed to monitor emissions from the combustor exhaust. All components in contact with the sample were stainless steel or Teflon to insure sample integrity and corrosion resistance. The gas sample was provided to the instruments by a sample conditioning system consisting of a pump, moisture condenser and particulate filters.

Figure A-2 shows a diagram of the continuous monitoring system for exhaust SO_2 measurements. A phase discrimination probe was used to separate the majority of the particulate from the sample gas stream. The SO_2 gas sample in the nearly particulate-free stream was transported in a heated Teflon line maintained above 115°C under vacuum to a heated filter followed

TABLE A-1. PROGRAM OBJECTIVES FOR MEASUREMENT PRECISION, AND ACCURACY

MEASUREMENT PARAMETER (Method)	REFERENCE	EXPERIMENTAL CONDITIONS	PRECISION RELATIVE STANDARD DEVIATION	ACCURACY
Fuel Composition:				
Carbon (Perkin-Elmer 240 B)		Coal	2%	2%
Hydrogen			5%	5%
Nitrogen			10%	10%
Ash			10%	10%
Moisture			10%	10%
Sulfur (Leco SC32)			10%	10%
Heating Value (Calorimeter)	ASTM D2015		2%	2%
Fuel Size Distribution (Wire Cloth Sieves)	ASTM D197	Pulverized Coal	2%	3%
Fuel Flow Rate/Distribution (Weigh Feeders)		Coal	2%	2%
Combustion Air Flow Rate/ Distribution (Laminar Flow Elements or Rotameters)	EPA Method 2	Ambient Air	5%	10%
Combustion Air Temperature (Thermocouple)	EPA Method 2	Ambient Air	1%	1.5%
Exhaust Gas Composition:				
NO, NO_2 (chemiluminescent)	EPA Performance Specification 2	Combustion Exhaust Gas	2%	20%
O_2 (paramagnetic)	EPA Performance Specification 3			
CO (infrared)	EPA Performance Specification 3			
CO_2 (infrared)				
SO_2 (ultraviolet)	EPA Performance Specification 2			
Hydrocarbons (heated flame ionization)				
SO_3 (controlled condensation)	Sulfuric Acid Emissions, IERL Contract 68-02-2165, Task No.13		20%	20%
N_2O (ECD)	Geo. Res. Ltrs. Vol 3, No.5, 1976		5%	5%
Particulate (EPA Method 5)	EPA 600/4-76-004		10%	
Moisture (EPA Method 4)	EPA 600/4-76-004		2%	5%
In-Furnace HCN, NH_3 (water-quenched probe specific ion electrode)		Furnace Gas	10%	10%
Furnace Gas Temperature (suction pyrometer)		Furnace Gas	5%	5%

TABLE A-1. PROGRAM OBJECTIVES FOR MEASUREMENT, PRECISION, AND ACCURACY (Concluded)

MEASUREMENT PARAMETER (Method)	REFERENCE	EXPERIMENTAL CONDITIONS	PRECISION RELATIVE STANDARD DEVIATION	ACCURACY
Particulate Composition:				
Carbon Hydrogen Nitrogen Ash (Perkin-Elmer 240 B)	Instrument Instruction Manual	Flyash	10%	10%
Calcium (EDTA Titration)	ASTM D2795			
Sulfur (Leco SC32)				
Sorbent Composition:				
Calcium Sodium Magnesium Potassium (atomic absorption)	ASTM D3682	Sorbent	5%	5%
Sorbent Flow Rate (volumetric feeder)		Sorbent	2%	2%
Sorbent Size Distribution (x-ray sedimentation)	Instrument Instruction Manuals	Sorbent	2%	2%
Sorbent Surface Area (BET analysis)		Sorbent	5%	5%

TABLE A-2. SAMPLING PROCEDURES

MEASUREMENT PARAMETER	SAMPLING LOCATION SELECTION CRITERIA	SAMPLING PROCEDURE	SAMPLING FREQUENCY	REFERENCE
Fuel Composition	EPA Level I Solid Sampling Procedures	Shovel Grap Sample	1/Batch or Daily	EPA 600/7-78-201, p.105
Fuel Size Distribution	ASTM D 197	Multiple System Grab Sample	1/Batch or Daily	ASTM D 197
Fuel Flow Rate/Distribution	Based on Burner Design	All Fuel Flow Measured	Continuous	
Combustion Air Flow Rate/Distribution	Based on Burner Design	All Air Flow Measured	Continuous	
Combustion Air Temperature	Based on Burner Design	In-line Thermocouple	Continuous	
Exhaust Gas Composition:				
NO, NO_2	EPA Performance Specifications for Continuous Monitors	Extractive (see text)	Continuous	Federal Register, Vol. 44, No.197, October 10, 1979, pp. 58602-58636
O_2				
CO				
CO_2				
SO_2				
Hydrocarbons				
SO_3	EPA Process Measurement Procedures, Sulfuric Acid Procedures	EPA Process Measurement Procedures, Sulfuric Acid Procedure	At Selected Conditions	EPA IERL Contract No.68-02-2165, Task No.13
N_2O	EPA Performance Specifications for Continuous Monitors	Cyrogenic Concentration (see text)	At Selected Conditions	Federal Register, Vol. 44, No.197, October 10, 1979, pp. 58602-58636
Particulate	EPA Method 1	EPA Method 5	At Selected Conditions	Federal Register, Vol. 42, No.160, August 18, 1977, pp. 41754-41788
Moisture		EPA Method 4		

TABLE A-2. SAMPLING PROCEDURES (Concluded)

MEASUREMENT PARAMETER	SAMPLING LOCATION SELECTION CRITERIA	SAMPLING PROCEDURE	SAMPLING FREQUENCY	REFERENCE
In-Furnace HCN, NH_3	Traverse Furnace Before and After Reburning	Water-cooled Probe Impinger Collection (see text)	At Selected Conditions	"Industrial Flames Vol. I., Measurements in Flames", International Flame Research Foundation, 1972.
Furnace Gas Temperature	Selected Locations Throughout Furnace	Suction Pyrometer (see text)	At Selected Conditions	
Particulate Composition	EPA Method 1	Use EPA Method 5 Particulate Sample	At Selected Conditions	
Sorbent Composition, Size Distribution, Surface Area	EPA Level I Solid Sampling Procedures	Shovel Grab Sample	Daily	EPA 600/7-78-201, p.105
Sorbent Flow Rate	Prior to Injection in Furnace	All Sorbent Flow Measured	Continuous	

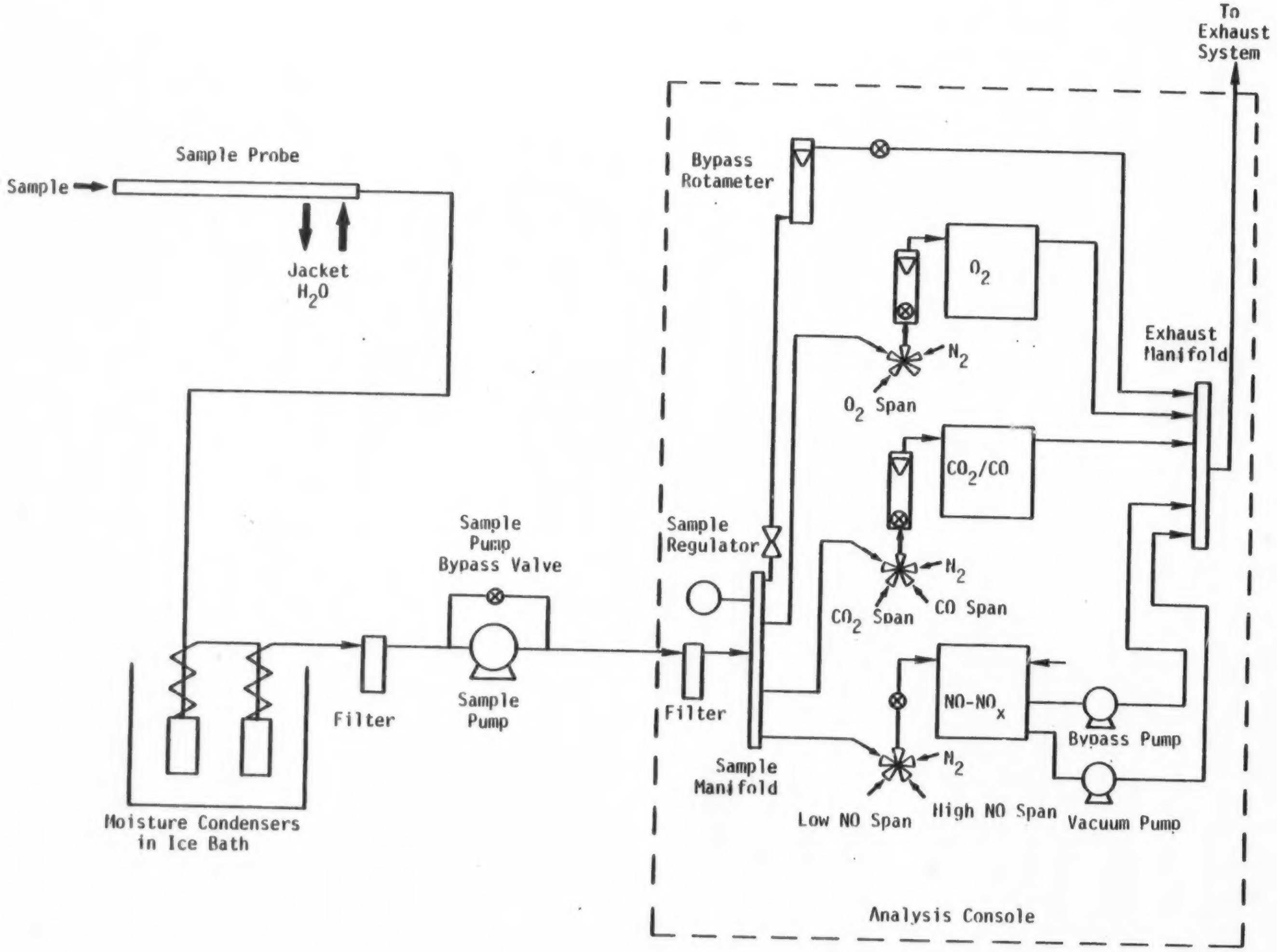
To Exhaust System
Sample Probe
Sample
Jacket H_2O
Bypass Rotameter
O_2
N_2
O_2 Span
Exhaust Manifold
CO_2/CO
Sample Regulator
Sample Pump Bypass Valve
N_2
CO_2 Span
CO Span
Filter
Sample Pump
Filter
$NO-NO_x$
Bypass Pump
Sample Manifold
N_2
Low NO Span
High NO Span
Vacuum Pump
Moisture Condensers in Ice Bath
Analysis Console

Figure A-1. Continuous Monitoring Sampling System

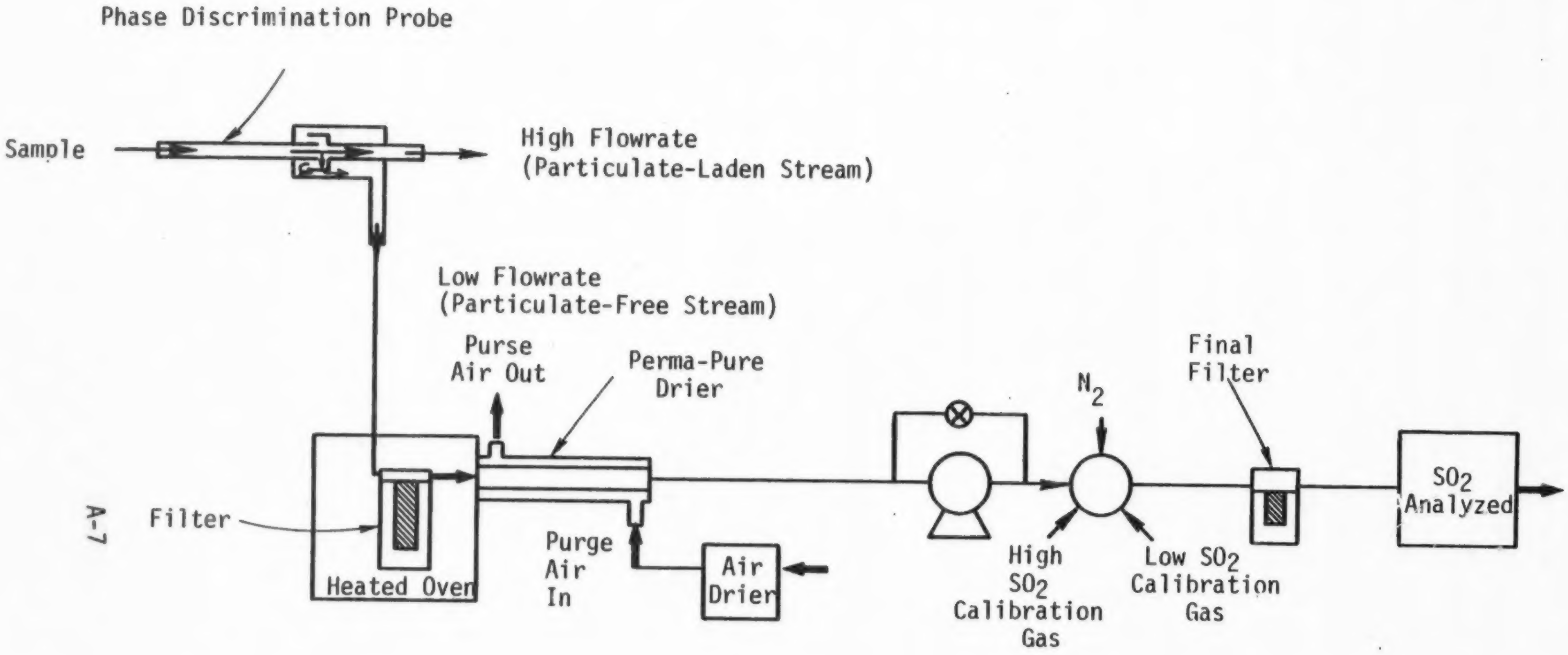
Phase Discrimination Probe
Sample
High Flowrate
(Particulate-Laden Stream)
Low Flowrate
(Particulate-Free Stream)
Purse
Air Out
Perma-Pure
Drier
Filter
Heated Oven
Purge
Air
In
Air
Drier
N_2
High
SO_2
Calibration
Gas
Low SO_2
Calibration
Gas
Final
Filter
SO_2
Analyzed

Figure A-2. SO_2 Continuous Monitoring System by a permeation tube drier. The permeation tube drier selectively removed water vapor from the gas sample. Dry air was used as the dry gas medium in the permeation drier. The sample was then pressurized and delivered to the analyzer. SO_2 concentration was measured using a non-dispersive ultraviolet instrument manufactured by DuPont.

HCN and NH_3

Sampling of HCN and NH_3 at exit of the reburning zone was performed with the sampling train represented in Figure A-3. A water spray probe as shown in Figure A-4, was used. Gas phase HCN and NH_3 species were collected in a gas washing unit which consisted of an impinger in series with a fritted glass bubbler. The impinger and the bubbler contained an absorbing solution of lead carbonate and sodium carbonate.

N_2O

Measurements of N_2O was made with the sampling train shown in Figure A-5. The sample was collected in a Tedlar bag. A gas tight syringe was then used to withdraw a sample from the bag fir direct injection into a gas chromatographer.

Solids Species

An elbow-shaped water quench probe was used for collecting solid samples isokinetically. This probe is similar to the one shown in Figure A-4 except that the water cooling jacket had been replaced with a layer of insulating ceramic fiber which minimized thermal disturbances resulting from the cooling probe. Figure A-6 shows the schematic of the sampling system.

In-Furnace Gas Temperature

High-temperature gas measurements within furnaces are subject to large inaccuracies due to the effects of thermal couple radiation loss. Therefore, in-furnace gas temperatures were measured using a suction pyrometer system as

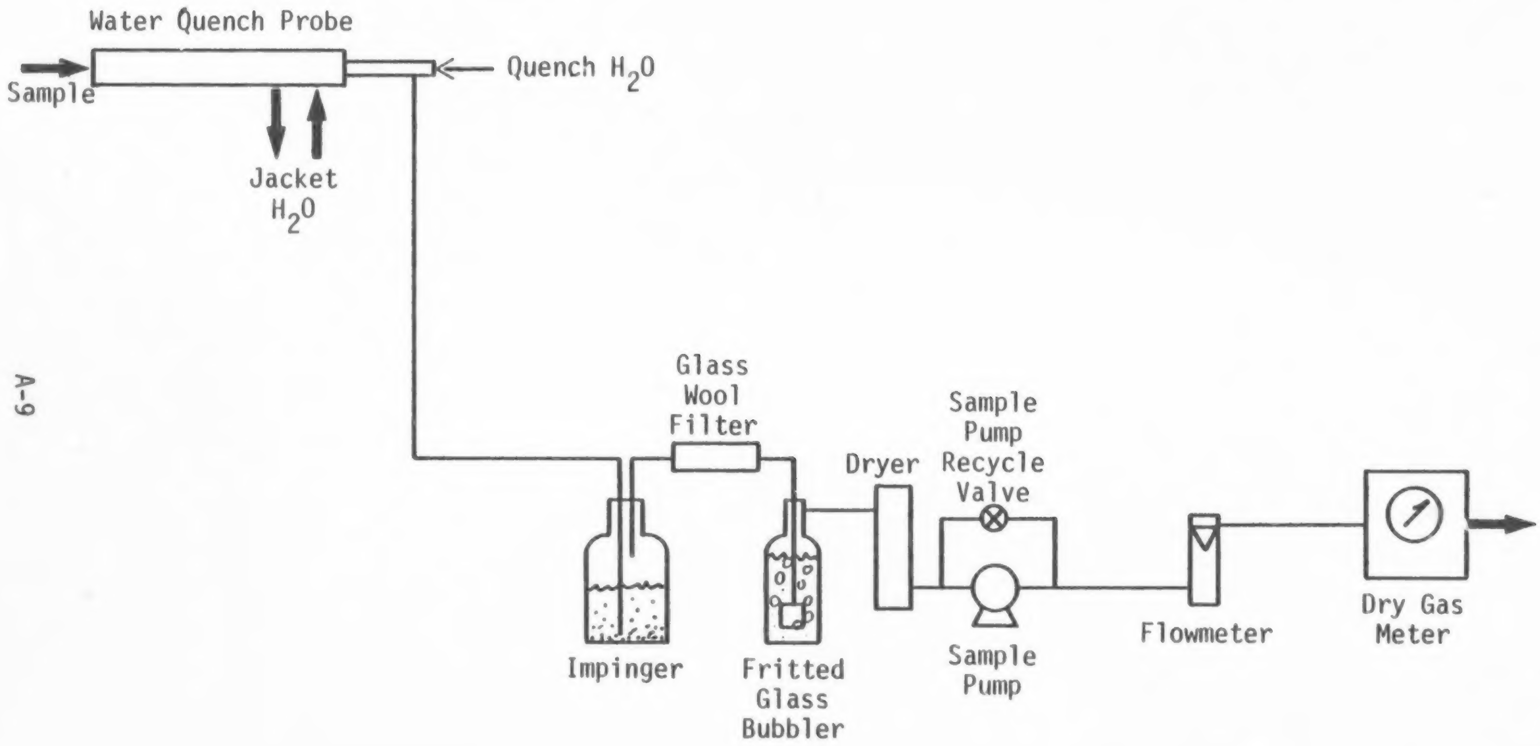
Water Quench Probe
Sample
Quench H_2O
Jacket H_2O
Glass Wool Filter
Dryer
Sample Pump Recycle Valve
Impinger
Fritted Glass Bubbler
Sample Pump
Flowmeter
Dry Gas Meter

Figure A-3. HCN and NH_3 sampling train.

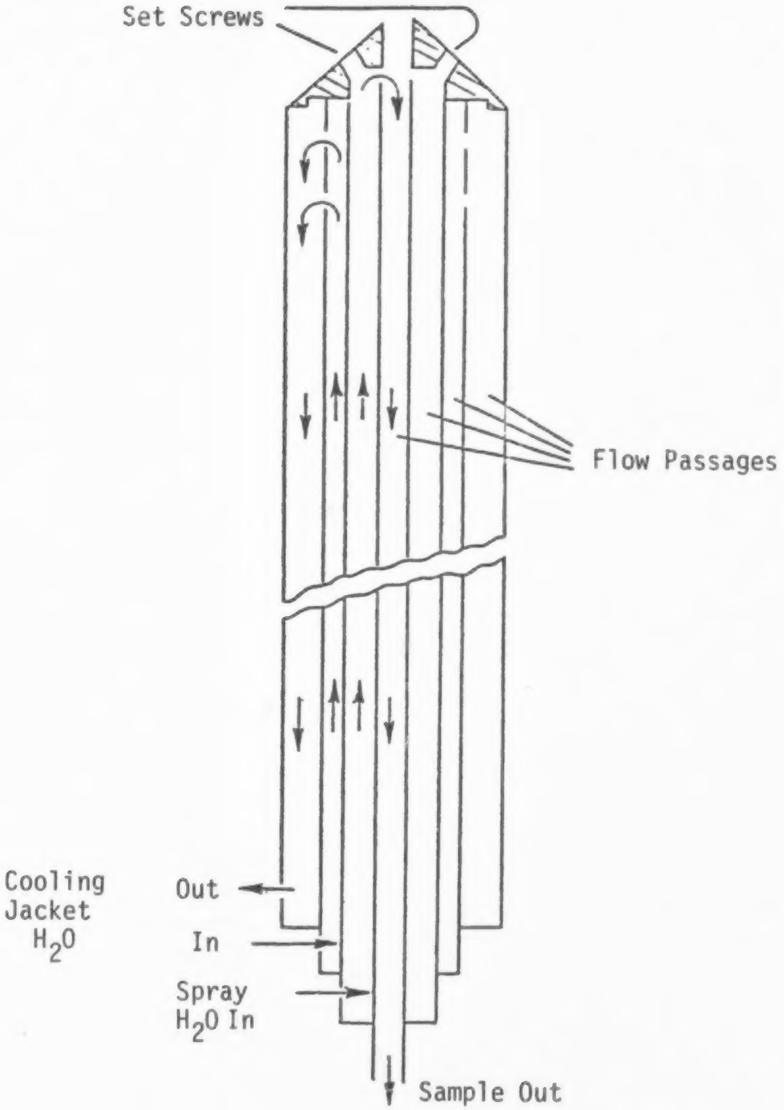
Set Screws
Flow Passages
Cooling Jacket H_2O
Out
In
Spray H_2O In
Sample Out

Figure A-4. Schematic of water-spray probe.

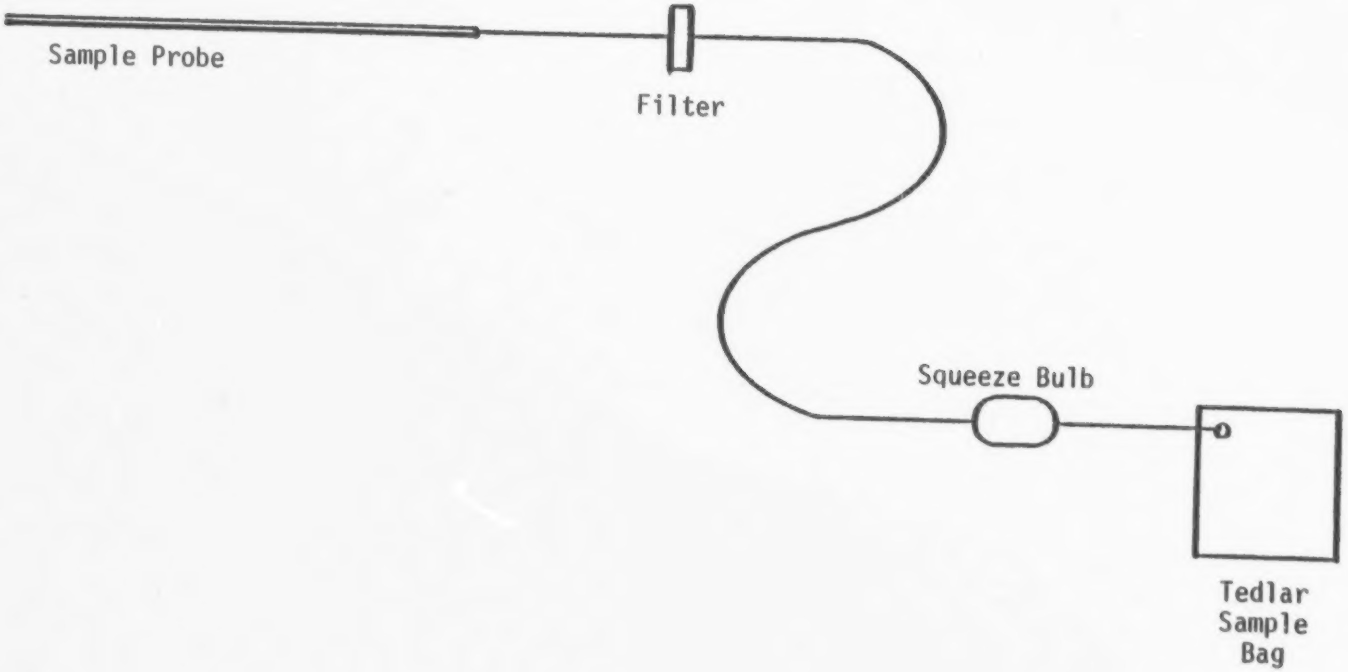
Sample Probe
Filter
Squeeze Bulb
Tedlar
Sample
Bag

Figure A-5. N_2O sampling train.

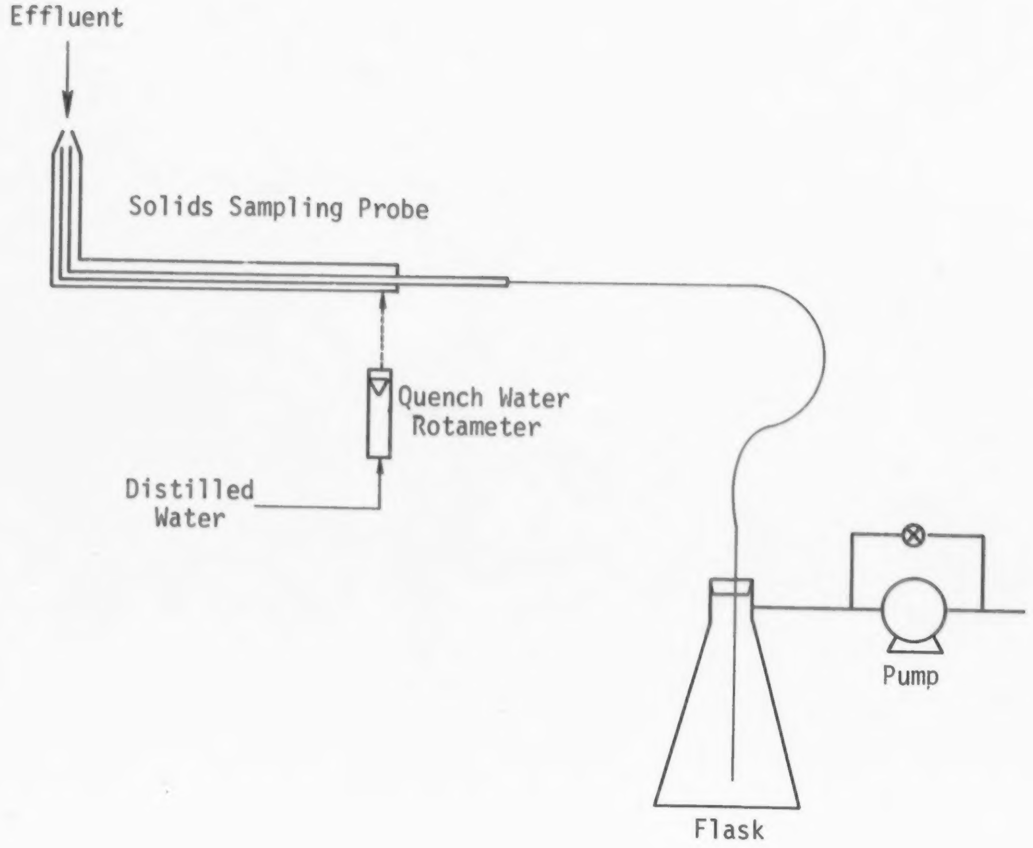
Effluent
Solids Sampling Probe
Quench Water
Rotameter
Distilled
Water
Flask
Pump

Figure A-6. Solids sampling system.

shown in Figure A-7. The suction pyrometer consisted of a high-temperature thermocouple (B type) in a porous ceramic radiation shield. The pyrometer was placed in the gas stream with the opening in the alumina sheath pointing downstream. A high flow rate of furnace gas was withdrawn through the sheath and over the thermocouple to increase convective heat transfer to the thermocouple and reduce radiation loss. As the gas flow rate was increased, the gas temperature increased to a constant value, indicating no additional reduction in radiation loss. Figure A-8 shows the results of the educator pressure (a measure of suction flow rate) calibration. A suction pressure of 40 psig was adopted for all the temperature measurements.

A.2 Calibration Procedures

Calibration procedures and frequency for each measurement system are listed in Table A-3. As shown in the table, standard calibration procedures were used for each system. Each system was calibrated at the frequency shown in the table to insure the accuracy of the measurement were traceable to the calibration standards.

Each of the continuous monitoring instruments was calibrated with three gases: a zero gas and two span gases. Table A-4 lists the span gases used to calibrate instruments.

A.3 Analytical Procedures

Analytical procedures for each measurement are listed in Table A-5. EPA standard procedures were used, where appropriate. Where possible, the remaining measurements used other standard procedures, as shown in the table. Nonstandard procedures are described in the following sections.

Continuous Monitoring Instrumentation

Continuous monitoring instrumentation used to analyze NO, NO_x, CO, CO_2, O_2, SO_2, and hydrocarbon concentrations is described in Table A-6. These instruments were specifically selected to provide the highest sensitivity and

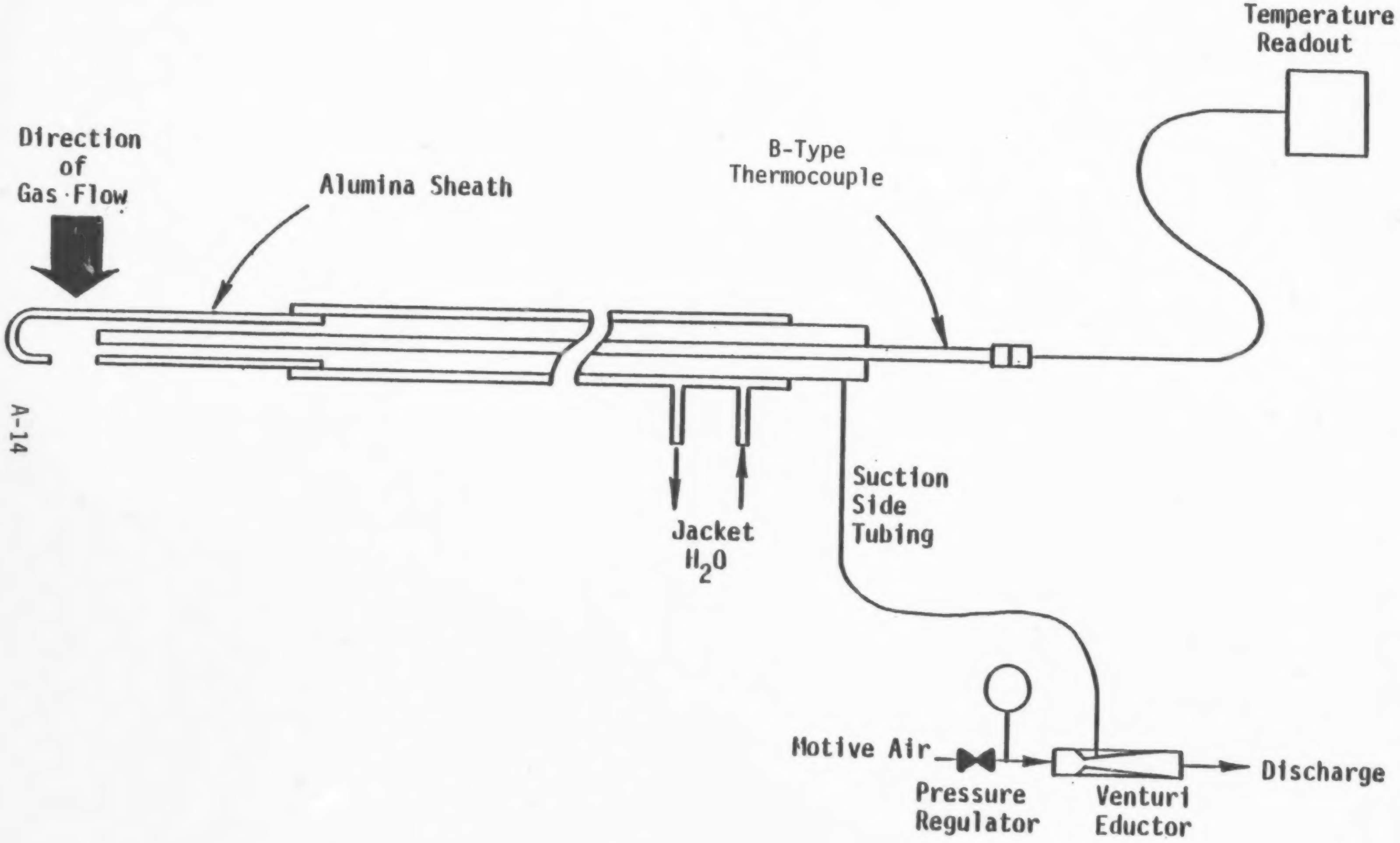
Direction of Gas·Flow
Alumina Sheath
B-Type Thermocouple
Temperature Readout
Jacket H_2O
Suction Side Tubing
Motive Air
Pressure Regulator
Venturi Eductor
Discharge

Figure A-7. Gas temperature measurement system.

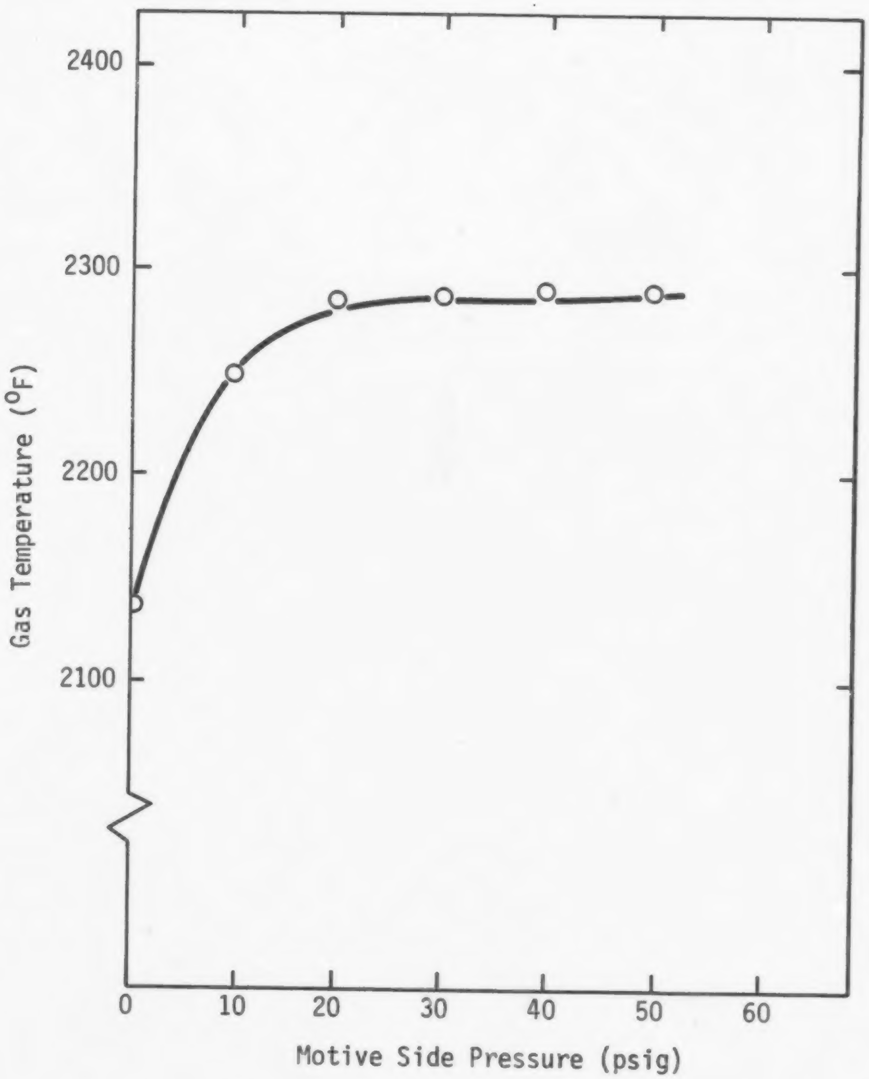

Figure A-8. Suction pyrometer aspirator pressure calibration.

TABLE A-3. CALIBRATION PROCEDURES

MEASUREMENT PARAMETER	CALIBRATION PROCEDURE	CALIBRATION FREQUENCY	CALIBRATION STANDARD	REFERENCE
Fuel Composition:				
Carbon	Standard Samples	Daily	Known quantity of 100% acetanilide	Perkin Elmer 240 B Operating Manual
Hydrogen				
Nitrogen				
Ash				
Moisture				
Sulfur	Standard Sample	Daily	Certified sulfur standards	Leco SC 32 Operating Manual
Fuel Size Distribution	Compare results to standard glass beads	Bi-annually	NBS SRM Glass Beads	ASTM E 11
Fuel Flowrate/ Distribution	Weigh feed over time with independent balance	Monthly	Standard Weights	
Combustion Air Flowrate/Distribution	Compare with EPA Method 2 or dry gas meter	Bi-annually	EPA Method 2 or calibrated dry gas meter	Federal Register, Vol. 42, No. 160, August 18, 1977 pp. 41754-41788
Combustion Air Temperature	Compare to standard thermometer	Monthly	ASTM Thermometer	EPA Method 2
Exhaust Gas Composition				
NO, NO_2	Compare to standard compressed gas	Daily	EPA Protocol 1 Gases or custom gas blends. See Section 10.0	EPA EMSL Protocol No. 1, June 1, 1978
O_2				
CO				
CO_2				
SO_2				
Hydrocarbons				

TABLE A-3. CALIBRATION PROCEDURES (Continued)

MEASUREMENT PARAMETER	CALIBRATION PROCEDURE	CALIBRATION FREQUENCY	CALIBRATION STANDARD	REFERENCE
Exhaust Gas Composition (Continued)				
SO_3	Compare to standard acid	Daily	Gravimetrically prepared standard solution	"Process Measurement Procedures, Sulfuric Acid Emissions," IERL Contract No. 68-02-2165, Task No. 13, February 1977
N_2O	Compare to standard compressed gas	Daily	Gas certified against Gas Manufacturers Primary Standard (GMPS)	Geophysical Research Letters, Vol. 3, No. 5, May 1976
Particulate:				
Gas Meter	Compare to wet test meter	Before and after each test series	Wet test meter	Federal Register, Vol. 42, No. 197, October 10, 1979 pp. 58602-58636
Pitot	EPA Method 2		Standard Pitot	
Nozzle	EPA Method 5		Micrometer	
Thermocouple	EPA Method 2		ASTM Thermometer	
Balance	Compare to standard weights	Daily	Class 5 Weights	
HCN, NH_3	Standard solutions	Daily	Gravimetrically prepared standard solutions	
Furnace Gas Temperature	Compare to standard thermocouple	Monthly	NBS Standard Thermocouple	EPA Method 2
Particulate Composition C, H, N	Compare to standard samples	Daily	Known quantity of 100% acetanilide	Perkin Elmer 240 B Operating Manual
Sorbent Composition	Compare to standard samples	Daily	Certified sulfur standards	Leco SC 32 Operating Manual

TABLE A-3. CALIBRATION PROCEDURES (Concluded)

MEASUREMENT PARAMETER	CALIBRATION PROCEDURE	CALIBRATION FREQUENCY	CALIBRATION STANDARD	REFERENCE
Sorbent Size Distribution	Compare to standard glass beads	Once for each set of measurements	NBS standard glass beads	
Sorbent Surface Area		Daily	Known quantity of N_2	Quantasorb Surface Area Analyzer Operating Manual
Sorbent Flowrate	Weigh feed over measured time with independent balance	Daily	Standard weights	

TABLE A-4. CALIBRATION GASES

Gas	Concentration	Percent of Full-Scale	Balance Gas	Grade
NO	710 ppm	71	Nitrogen	Certified Standard
NO	150 ppm	60	Nitrogen	Certified Standard
SO_2	2784 ppm	70	Nitrogen	Certified Standard
SO_2	403 ppm	10	Nitrogen	Certified Standard
CO	2100 ppm	84	Nitrogen	Certified Standard
CO	1200 ppm	80	Nitrogen	Certified Standard
CO_2	12%	30	Nitrogen	Certified Standard
CO_2	5%	13	Nitrogen	Certified Standard
O_2	10%	40	Nitrogen	Certified Standard
O_2	21%	84	Nitrogen	Certified Standard
CO	10%	100	Nitrogen	Certified Standard

TABLE A-5. ANALYTICAL PROCEDURES

MEASUREMENT PARAMETER	ANALYTICAL PROCEDURE	REFERENCE
Fuel Composition		
Carbon Hydrogen Nitrogen Ash Moisture	Sample combusted, interferences absorbed, and elements detected by thermal conductivity	Perkin Elmer 240 B Operating Manual
Sulfur	Sample combusted and resulting SO_2 detected by infrared	Leco SC 32 Operating Manual
Heating Value	Adiabatic Bomb Calorimeter	ASTM D-2015
Fuel Size Distribution	Sieve Analysis	ASTM D-197
Combustion Air Flowrate/Distribution	Rotameter or pressure differential across laminar flow elements	Dwyer Rotameter or inclined manometer operating instructions
Combustion Air Temperature	Thermocouple	EPA Method 2
Exhuast Gas Composition:		
NO, NO_2	Chemiluminescent Analyzer	Teco Model 10 Operating Manual
O_2	Paramagnetic Analyzer	Taylor OA 570 Operating Manual
CO, CO_2	Infrared Analyzer	Anarad AR 500 Operating Manual
SO_2	Ultraviolet Analyzer	DuPont 400 Operating Manual
Hydrocarbons	Heated Flame Ionization	Beckman 402 Operating Manual

TABLE A-5. ANALYTICAL PROCEDURES (Continued)

MEASUREMENT PARAMETER	ANALYTICAL PROCEDURE	REFERENCE
Exhaust Gas Composition (Continued)		
SO_3	Barium Perchlorate/ Thorim Titration	EPA Method 8
N_2O	Gas Chromatography/ECD	Geophys. Res. Ltrs. Vol 3, #5, May 1976
Particulate	Gravimetric	EPA Method 5
Moisture	Gravimetric	EPA Method 4
In Furnace HCN, NH_3	Specific Ion Electrode	See Text
Furnace Gas Temperature	Suction Pyrometer	
Particulate Composition		
Carbon Hydrogen Nitrogen Ash	Sample combusted, interferences absorbed, and elements detected by thermal conductivity	Perkin Elmer 240 B Operating Manual
Calcium	Chelatometric Titration	ASTM D 2795
Sulfur	Sample combusted, and resulting SO_2 detected by infrared	Leco SC 32 Operating Manual
Sorbent Composition		
Calcium Sodium Magnesium Potassium	Atomic Absorption	ASTM D 3682

TABLE A-5. ANALYTICAL PROCEDURES (Concluded)

MEASUREMENT PARAMETER	ANALYTICAL PROCEDURE	REFERENCE
Sorbent Flowrate	Volumetric	
Sorbent Size Distribution	X-Ray Diffraction	Micromeritics Sedigraph Operating Manual
Sorbent Surface Area	Condensation of N_2 on sample followed by desorption and analysis of N_2 by thermal conductivity	Quantasorb Surface Area Analyzer Operating Manual

TABLE A-6. CONTINUOUS GAS ANALYSIS INSTRUMENTS

Gas Measured	Detection Principle	Manufacturer	Model No.	Range
NO, NO_2	Chemiluminescent	Thermo Electron Corp. (TECO)	10 AR	0-1000 ppm
CO	Nondispersive Infrared (NDIR)	Anarad, Inc.	AR500R	0-500 ppm
CO_2	Nondispersive Infrared (NDIR)	Anarad, Inc.	AR500R	0-25%
O_2	Paramagnetic	Taylor Servomex	OA-272	0-10%
SO_2	Nondispersive Ultraviolet (NDUV)	DuPont	400	0-5000 ppm
H_xC_y	Flame Ionization (Heated)	Beckman Instruments, Inc.	402	500 ppm (C_3H_8)

minimum interferences possible. Test data from the instrument were continuously recorded with a strip chart recorder to provide permanent documentation of test results.

N_2O

N_2O samples were analyzed by gas chromatography using an electron capture detector. The gas chromatograph was operated with an argon/5 percent methane carrier gas and separation was achieved using a 2 m x 3 mm (o.d.) Porasil B column. Results were presented as N_2O concentrations in ppm by volume. The method was calculated by analyzing standard mixtures of N_2O in N_2.

HCN and NH_3

HCN and NH_3 sample solutions were analyzed by specific ion electrodes immediately after sampling to avoid complexation of cyanide ions with lead ions in the sample solutions. An Orion Model 95-10 ammonia electrode was first used to detect NH_3 after the pH of the solution had been adjusted to 13 to convert the ammonium ions to NH_3 gas. An Orion Model 94-06 cyanide ion electrode was then used to detect HCN. Electrical potentials generated within the electrodes were proportional to the species concentrations and were measured with an Orion Model 901 Digital Ionalyzer. Calibration curves were developed using standard solutions to relate electrical potential to species concentrations.

A.4 Data Reduction, Validation and Reporting

After raw data were collected from various experiments, a fair amount of data reduction was required before results could be reported in their final form. Equations used to calculate results for each of the measurements are discussed below. Many of the results were obtained directly from the measurements and thus did not require calculations.

1. Fuel and Particulate Analysis for Carbon, Hydrogen, Nitrogen

The data consist of millivolt responses from the analyzer. These millivolt responses are converted to micrograms using a graphical calibration curve generated with three standards. Weight percent is then calculated for each element, knowing the total sample weight as follows:

$$\text{Element Weight \%} = \frac{\text{Element Weight}}{\text{Total Sample Weight}} \times 100$$

2. Fuel Size Distribution

Analytical data consist of weights of each size fraction which are converted to percent weight less than each size fraction from the equation:

$$\text{Fraction Weight \%} = \frac{\text{Fraction Weight}}{\text{Total Sample Weight}} \times 100$$

Results are presented graphically plotting cumulative weight percent against particle size. Figure A-9 shows an example of the coal size analysis results for one of the coals tested in the program.

3. Fuel Flowrate/Distribution

Fuel flowrate is obtained directly from the weigh feeder and is averaged over each test period.

4. Combustion Air Flowrate/Distribution

Combustion air flowrate is read directly from rotameters or is calculated from pressure drop measured across laminar flow elements based on the equation:

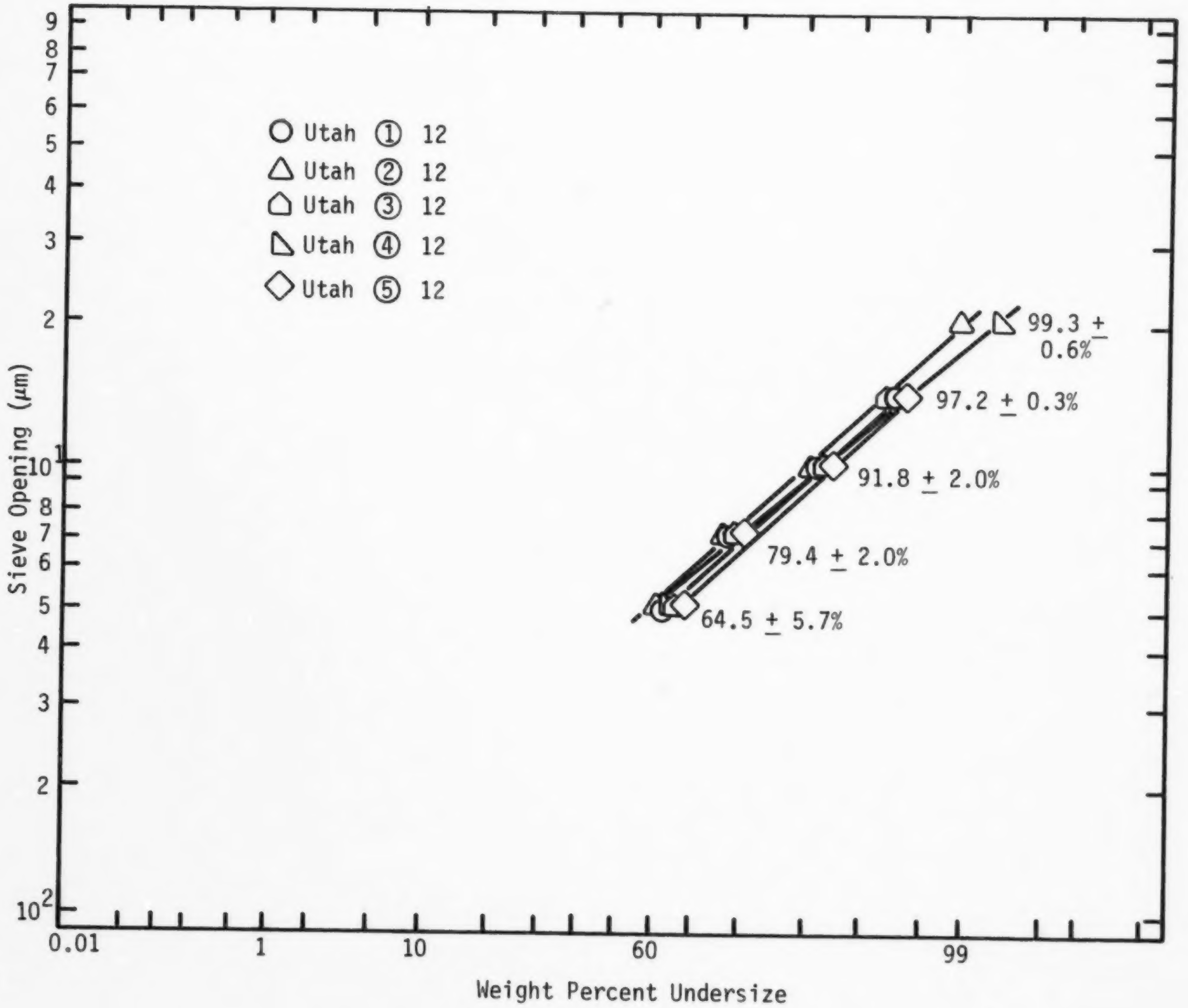

Figure A-9. Replicate coal size distributions.

$$Q = K\left(\frac{\Delta P}{T}\right)^{1/2}$$

where Q is the flowrate, K is a calibration factor determined for each flow element, P is the pressure drop measured across the element and T is the absolute temperature.

5. Sorbent Composition: Ca, Na, Mg, K

Sorbent composition is measured by atomic absorption with the results obtained as weight of each element based on a calibration curve from the analysis and calibration curves. Results are converted to weight percent based on this weight and the total sample weight.

6. Sorbent Flowrate

Sorbent flowrate is read directly from a volumetric feeder and averaged over each test period. Flowrate is converted to mass flowrate based on the sorbent density.

7. Sorbent Size Distribution

Sorbent size distribution is plotted directly as size against cumulative weight percent by a Micromeritics Sedigraph Analyzer. Figure A-10 shows an example of the size distribution of a sorbent (Vicron 45-3) used in the program.

8. Sorbent Surface Area

Sorbent surface area is measured by a BET Quantasorb Analyzer. This analyzer measures the quantity of nitrogen condensed on the sample surface by thermal conductivity based on calibration standards. This quantity of nitrogen is converted to surface area based on a monolayer of nitrogen condensed on the sample and the

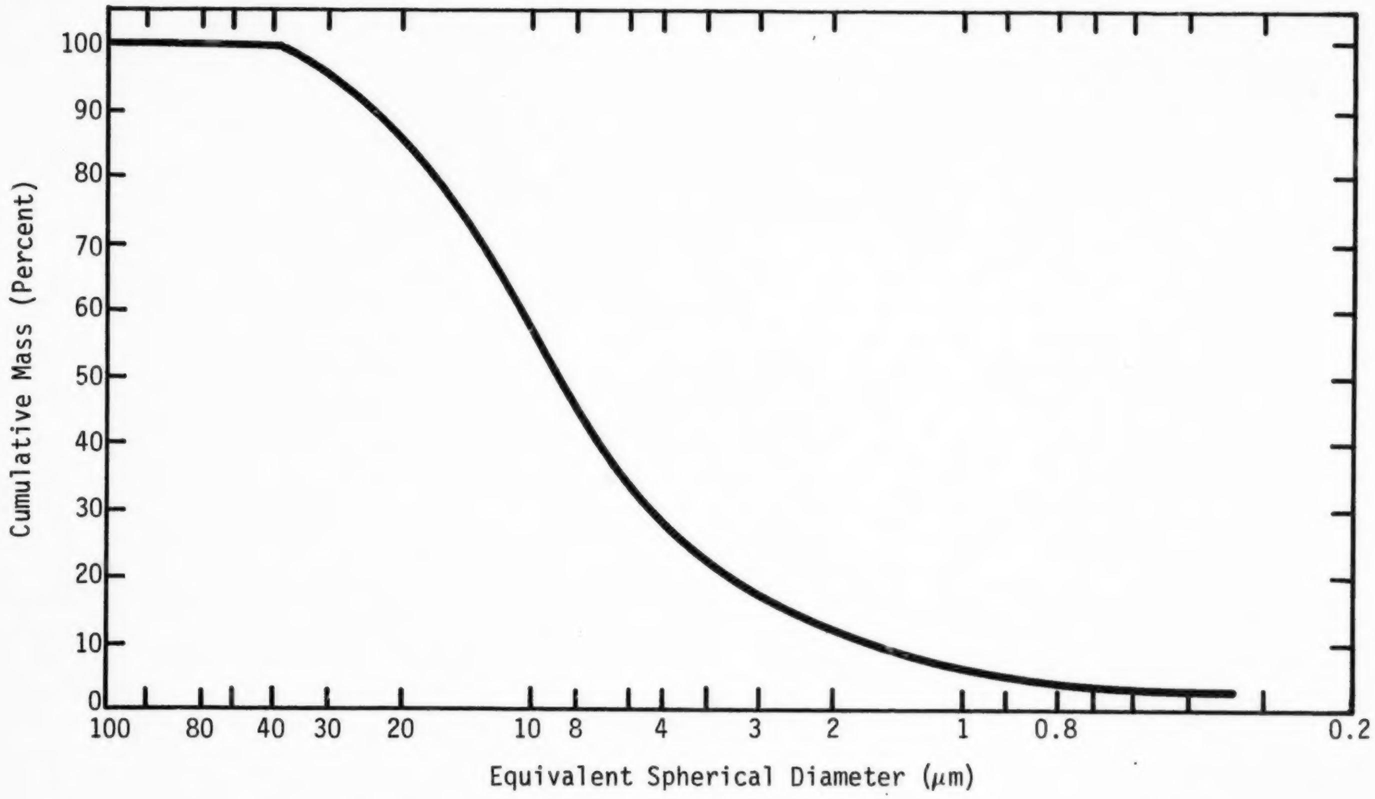

Figure A-10. Size distribution of Vicron 45-3.

known volume of nitrogen molecules following the instrument manufacturer's instructions.

9. Combustion Air, Furnace Gas, and Exhaust Gas Temperatures

Temperatures are measured by thermocouples and provide results in units of degrees centigrade which can then be converted to other temperature scales, as required. Figure A-11 shows an example of the gas temperatures measured by a B-type thermocouple with a suction pyrometer.

10. Residence Time

Residenct times are calculated by assuming a one-dimensional flow in the furnace. Based on the measured temperatures, the bulk mean residence time of the reburning zone (τ_2) was calculated by using the following equation:

$$\tau_2 = \frac{\overline{V}}{\dot{\overline{V}}} \left(\frac{T_o}{T_m} \right)$$

where $\overline{V}$ = Volume of reburning zone, ft^3

$\dot{\overline{V}}$ = Volumetric flow rate of gas, SCF-S

T_o = 530°R

T_m = Bulk mean gas temperature

= $1/2\ (T_1 + T_2)$

T_1 and T_2 are center line temperatures measured at the exit of the primary and reburning zones, respectively.

11. In-Furnace NH_3, HCN

NH_3 and HCN are measured by specific ion electrodes with results as ppm, liquid based on calibration standards. Results are converted to gas concentrations using the form and equations shown

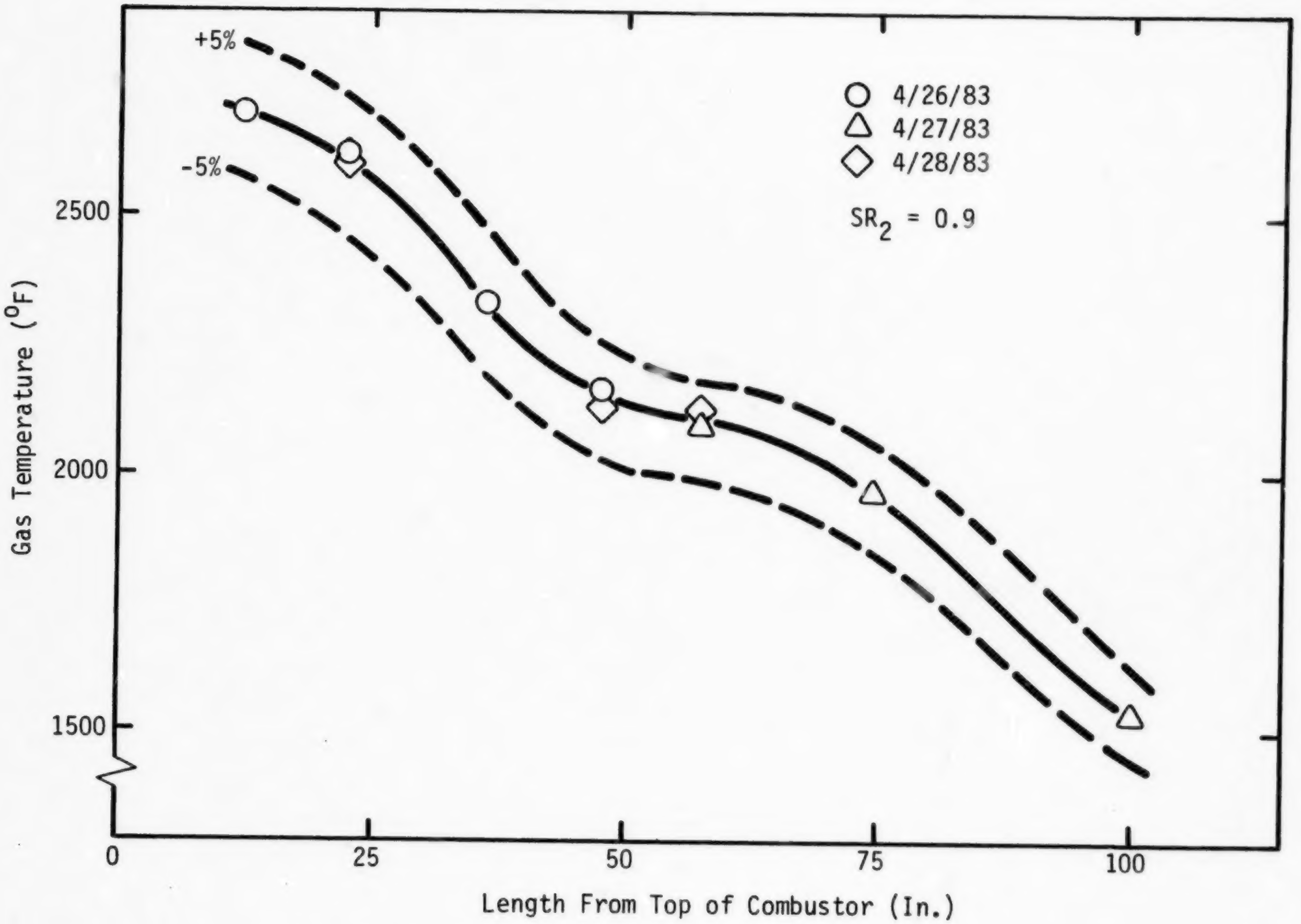

Figure A-11. Precision of gas temperature measurements.

in Figure A-12. A-13 shows an example of the XN species concentrations, presented as percent of the primary NO_x. These values had been corrected for dilution, followed the method discussed in Appendix B.

12. Exhaust Gas Composition: N_2O

N_2O is measured by electron capture detector, with data obtained as peak areas from an automatic integrator. Results are converted to concentration (ppm) based on a ratio of peak areas of the sample to a calibration standard.

13. Exhaust Gas Composition--NO, NO_x, O_2, CO, CO_2, SO_2

The above gas compositions are measured as chart divisions on a strip chart recorder. The measured divisions are converted to concentration (ppm or percent) based on calibrations with certified gases. The measured NO_x values (in PPMV) are then corrected for dilution, using the method described in Appendix B, and reported in terms of the molar ratio (in percent) of NO_x at the exit of the primary zone. An example of the exhaust NO_x emissions is presented in Figure A-14. The reproducibility of these data are also included.

SO_2 capture with sorbent injection is defined as:

$$\text{Percent Capture} = \frac{(SO_2)_1 \quad (SO_2)_2}{(SO_2)_1} \times 100\%$$

where $(SO_2)_1$ = SO_2 concentration without sorbent, ppm

$(SO_2)_2$ = SO_2 concentration with sorbent injection, ppm

Date			
Sample No.			
Sample Volume (ft^3)			
Average Meter Temperature Tm (^oR)			
Barometric Pressure P_{bar} ("H_G)			
Average Orifice Pressure ΔH("H_2O)			
Standard Gas Sample Volume: $Vm\ (STD)(L) = \frac{(17.64)(28.32)Vm}{Tm} \cdot \left(P_{bar} + \frac{\Delta H}{13.6}\right)$			
CN^- (ppm liquid)			
$CN^-\ (u\ell\ gas) = mgCN^- \cdot \frac{24.04}{26} \cdot 10^3$			
$HCN\ (ppm\ gas) = \frac{u\ell CN^-}{Vm(STD)(L)}$			
NH_4 + (ppm liquid)			
$NH_4^+\ (u\ell\ gas) = mg\ NH_4^+ \cdot \frac{24.04}{18} \cdot 10^3$			
$NH_3\ (ppm\ gas) = \frac{u\ell NH_4^+}{Vm(STD)(L)}$			

Figure A-12. Calculation of HCN and NH_3 results.

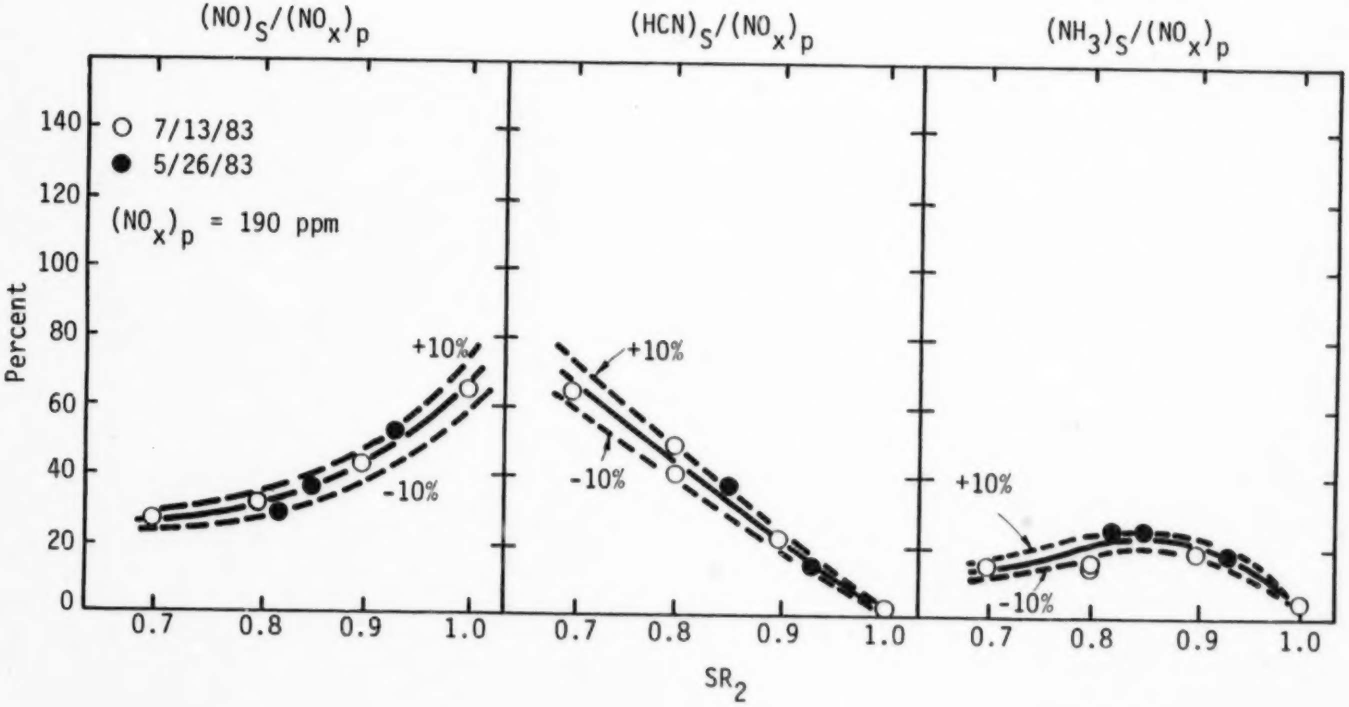

Figure A-13. XN concentrations at exit of reburning zone.

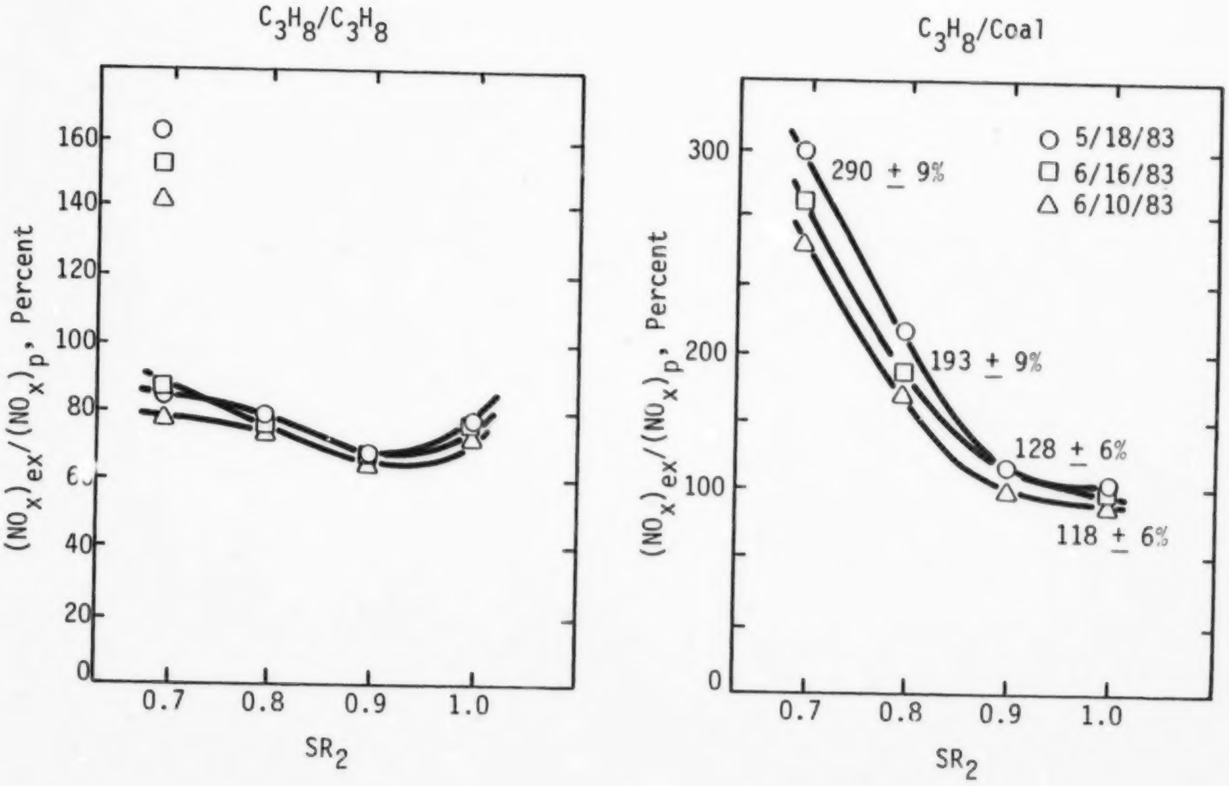

Figure A-14. NO_x emissions with reburning.

Figure A-15 shows an example of the capture data obtained and their reproducibility.

A.5 Quality Assurance Audits

Internal Audit

The internal systems audit, performed by the quality assurance officer at EER, involved reviewing sampling and analytical procedures with the measurement personnel, inspecting the test equipment, and reviewing measurement and quality control documentation. The current precision and accuracy of each measurement were also reviewed. The results of the systems audit showed that the overall measurement quality was acceptable and no major quality problems existed. The precision and accuracy of the measurements are summarized in Table A-7. Each measurement was within the precision and accuracy goals presented in the Quality Assurance Plan except N_2O. However, the N_2O procedure has just recently been developed, and measurements have not yet been made on this program.

A performance evaluation if the NO_x, O_2, and CO_2 continuous monitoring instrumentation was also conducted to determine overall system accuracy. Instrument measurements were compared to EPA Reference Methods. Results of this evaluation are summarized in Table A-8. The evaluation showed acceptable accuracy for each of the instruments.

Systems Audit by EPA

On August 31, 1983, a systems audit was conducted by Ms. Judy Ford of IERL-RTP and Dr. David Taylor of S-Cubed. The purpose of the audit was to evaluate the work performed on EPA contract 68-02-3925 as well as evaluate the analytical facilities and overall research capabilities of EER.

A presentation was made to the auditors by EER focusing on the following topics:

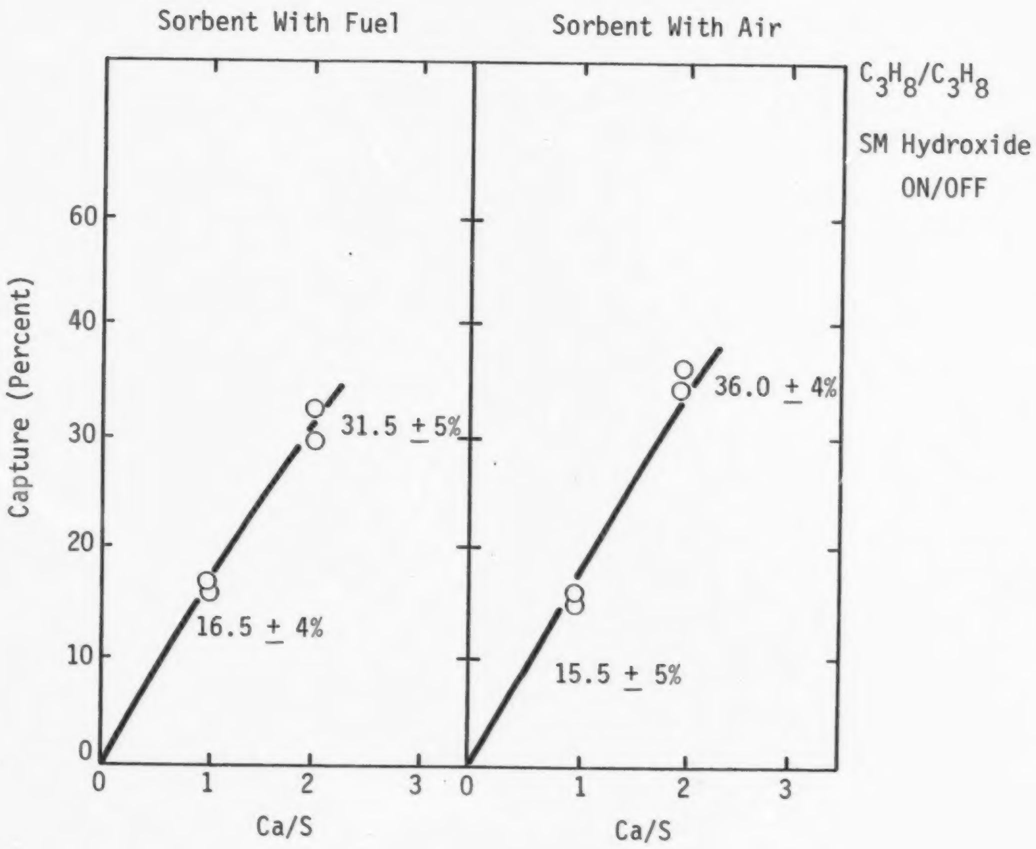

Figure A-15. SO_2 capture data.

TABLE A-7. COMPARISON OF MEASUREMENT PRECISION AND ACCURACY WITH PROGRAM GOALS

MEASUREMENT	PRECISION (%)		ACCURACY (%)	
	ACTUAL	GOAL	ACTUAL	GOAL
CARBON } PERKIN-ELMER 240 B	.24	2	0.8	2
HYDROGEN	1.38	5	0.6	5
NITROGEN	2.13	10	1.9	10
ASH	0.33	10	1.42	10
MOISTURE	2.55	10	8.71	10
SULFUR - LECO SC32	2.36	10	0.55	10
HEATING VALUE - CALORIMETER	--	2	0.39	2
FUEL SIZE - SIEVES	2.0	2	2.0	3
COMBUSTION AIR - ROTAMETER	0.04	5	3.1	10
NO_x - CHEMILUMINESCENT	0.3	2	12.3	20
O_2 - PARAMAGNETIC	0.2	2	13.1	20
CO - INFRARED	0.5	2	No STD	20
CO_2 - INFRARED	0.1	2	2.5	20
SO_2 - ULTRAVIOLET	0.3	2	10.2**	20
SO_3 - CONTROLLED CONDENSATION	*	20	4.3	20
N_2O - ECD / GC	6	5	20	5
HCN } SPECIFIC ION ELECTRODE	2.38	10	0.8	10
NH_3	0.94	10	0.9	10
FURNACE GAS TEMPERATURE } SUCTION PYROMETER	1	5	1.7	5

*Not measured **Similar sampling system

TABLE A-8. COMPARISON OF CONTINUOUS MONITORING INSTRUMENTATION WITH EPA REFERENCE METHODS

Instrument	Instrument Reading	Reference Method Results	Relative Accuracy	95% Confidence Interval
NO_x	195 ppm	187 ppm	4.3%	3.4%
O_2	2.13%	2.2%	1.4%	6.5%
CO_2	12.40%	12.23%	1.4%	1.2%

- The process of in-furnace NO_x reduction by reburning and how it may be applied to full-scale combustion systems.

- The Task 2 program objectives and responsibilities.

- A tour of the combustor and laboratory facilities which included examples of data acquisition techniques.

- Results of an internal systems audit performed by the quality assurance officer at EER. This internal audit addressed precision and accuracy measurements of the analytical equipment as well as data acquisition techniques.

- Specific examples of data reduction.

- Changes needed in the QA plan.

The follow-up report submitted by the auditors indicated that the quality assurance program and experimental program at EER was, in general, very good. No major problems were identified during the course of the audit and there were no major recommendations for improvement.

APPENDIX B: DILUTION CORRECTION CALCULATIONS

In order to directly compare NO_x concentrations measured in the combustor effluent to NO_x concentrations in the primary zone, a dilution correction was employed as part of the data reduction procedure. The correction factor adjusts for the dilution effect of increased load with respect to the primary NO_x concentration. Derivation of the dilution correction factor as well as the general performance calculations used in the experimental work follow.

As explained in Section 4 of this report, the reburning process was divided into three zones: the primary, reburning, and burnout zones. Conceptually, the three zones may be considered as separate reactors each with its individual feed and exit streams as shown in Figure B-1. In the primary zone air (A_1) and fuel (F_1) mixed and reacted, the product of which mixes and reacts with reburning fuel (F_2) and transport medium ($(N_2)_2$) in the reburning zone. The reburning zone effluent combines with the burnout air (A_3) in the burnout zone and reacts to the final products (see nomenclature section for definition of symbols) form.

This derivation assumes the following reactions go to completion when in the presence of an oxidizing atmosphere:

$$C + O_2 \longrightarrow CO_2 \tag{1}$$

$$H + 1/4\ O_2 \longrightarrow H_2O \tag{2}$$

$$S + O_2 \longrightarrow SO_2 \tag{3}$$

$$O \longrightarrow 1/2\ O_2 \tag{4}$$

$$N \longrightarrow 1/2\ N_2 \tag{5}$$

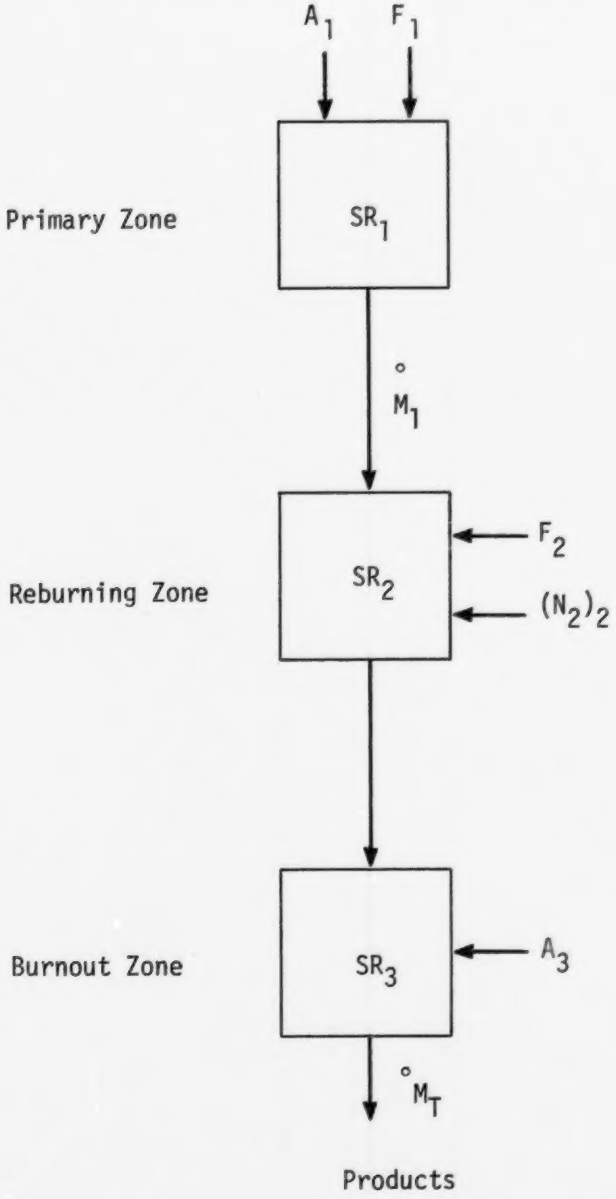
A1
F1
Primary Zone
SR1
°M1
F2
Reburning Zone
SR2
(N2)2
Burnout Zone
SR3
A3
°MT
Products

Figure B-1. Conceptual Layout of the Reburning Process

Primary Zone

The lb. moles O_2 required to burn one pound of primary fuel is calculated from

$$\left(\frac{C_1}{12} + \frac{H_1}{4} + \frac{S_1}{32} - \frac{O_1}{32}\right) / 100 = R_1 \qquad (6)$$

The primary fuel feed rate is calculated from

$$\frac{(FR)_1}{(HV)_1} = F_1 \qquad (7)$$

The theoretical air required in the primary zone is found to be

$$R_1 \cdot F_1 \cdot 3.76 = (TA)_1 \qquad (8)$$

Total primary air is

$$(TA)_1 \cdot SR_1 = A_1 \qquad (9)$$

The lb.moles dry effluent from the primary per pound of primary fuel is calculated from

$$R_1 \cdot 3.76 + \frac{C_1}{12} + \frac{N_1}{28} + \frac{S_1}{32} \; / \; 100 + R_1 \cdot 4.76 \; (SR_1{}^{-1}) = M1 \qquad (10)$$

and the molar flowrate of exhaust gas from the primary zone is

$$M_1 \cdot F_1 = M_1 \qquad (11)$$

Reburning Zone

The reburning zone stoichiometry is defined as

$$\frac{A_1}{(TA)_T} = SR_2 \qquad (12)$$

where

$$(TA)_T = (TA)_1 + (TA)_2 \qquad (13)$$

Rearranging (12) and substituting (9) and (13) yields

$$(TA)_1 \cdot \left(\frac{SR_1}{SR_2} - 1\right) = (TA)_2 \qquad (14)$$

The pound moles O_2 required to burn one pound reburning fuel is found from

$$\left(\frac{C_2}{12} + \frac{H_2}{4} + \frac{S_2}{32} - \frac{O_2}{32}\right) / \ 100 = R_2 \qquad (15)$$

Therefore, the air required to burn one pound of reburningfuel is

$$R_2 \cdot 4.76 \cdot 387 = [TA]_2 \qquad (16)$$

Which enables the calculation of the reburning fuel feedrate by

$$\frac{(TA)_2}{[TA]_2} = F_2 \qquad (17)$$

Burnout Zone

The total required pound moles of O_2 needed to combust both F_1 and F_2 is

$$\left(\frac{\mathring{C}_T}{12} + \frac{\mathring{H}_T}{4} + \frac{\mathring{S}_T}{32} + \frac{\mathring{O}_T}{32}\right) / \ 100 = R_T \qquad (18)$$

and the total dry effluent from the process is calculated from

$$R_T \cdot 3.76 + \left(\frac{C_T}{12} + \frac{N_T}{28} + \frac{S_T}{32}\right) / 100 + \mathring{R}_T \cdot 4.76 \cdot (SR_3 - 1) + (\mathring{N}_2)_2 = \mathring{M}_T \tag{19}$$

Where:

$$\mathring{C}_T = \sum_1^2 F_i C_i \tag{20}$$

$$\mathring{H}_T = \sum_1^2 F_i H_i \tag{21}$$

$$\mathring{N}_T = \sum_1^2 F_i N_i \tag{22}$$

$$\mathring{S}_T = \sum_1^2 F_i O_i \tag{23}$$

$$\mathring{O}_T = \sum_1^2 F_i O_i \tag{24}$$

A_3 may be calculated from

$$SR_3 \cdot (TA)_T - A_1 = A_3 \tag{25}$$

Calculation of Dilution Factor

The dilution correction is calculated from

$$M_T/M_1 = N \tag{26}$$

and is a function of reburning zone stoichiometry. For the baseline firing conditions (C_3H_8/C_3H_8 reburning), the following dilution correction factors were calculated:

SR_2	N
1.0	1.33
0.9	1.47
0.8	1.64
0.7	1.87

For example,

If a concentration of 200 ppm NO_x is measured in the exhaust and the primary NO_x concentration is 570 ppm (both are on a dry, as measured, basis), at an SR_2 of 0.9,

$$\left(\frac{200}{570} \cdot 1.47\right) \cdot 100 = 52 \text{ percent} \tag{27}$$

or 52 percent of the primary NO_x was measured in the exhaust. Which corresponds to

$$100 - 52 = 48 \text{ percent} \tag{28}$$

48 percent chemical reduction of the primary NO_x by the reburning process.

Calculation of Theoretical Gas Concentrations

The theoretical combustion gas concentrations may be calculated, on a dry basis, by the following equations:

Primary zone:

$$\text{Percent } O_2\text{, dry} = \frac{(SR_1 - 1) \cdot R_1}{M_1} . 100 \tag{29}$$

$$\text{Percent } CO_2\text{, dry} = \frac{C_1/12}{M_1} . 100 \tag{30}$$

Total gas concentrations:

$$\text{Percent } O_2\text{, dry} = \frac{(SR_3-1) \cdot R_T}{M_T} \cdot 100 \qquad (31)$$

$$\text{Percent } CO_2\text{, dry} = \frac{C_T/12}{M_T} \cdot 100 \qquad (32)$$

NOMENCLATURE

Symbol	Definition	Units
A_1	Primary air flowrate	SCFM
A_3	Burnout air flowrate	SCFM
C_i	Weight percent carbon in i^{th} fuel	Weight percent
$\mathring{C}_T$	Total carbon input to system	Lb. carbon/minute
F_1	Primary fuel feedrate	Lb.//min.
F_2	Reburning fuel feedrate	Lb./min.
$(FR)_1$	Primary zone firing rate	Btu/min.
H_i	Weight percent hydrogen in i^{th} fuel	Weight percent
H_T	Total hydrogen input to system	Lb. hydrogen/min.
$(HV)_1$	Heating value of primary fuel	Btu/lb. dry fuel
M_1	Lb.moles dry effluent per pound of primary fuel	Lb.moles/lb.fuel
$\mathring{M}_1$	Primary zone effluent flowrate (dry)	Lb.moles/min.
$\mathring{M}_T$	Total effluent flowrate (dry)	Lb.moles/min.
N_i	Weight percent of nitrogen in i^{th} fuel	Weight percent
$(\mathring{N}_2)_2$	Transport nitrogen flowrate	Lb.moles/min.
$\mathring{N}_T$	Total nitrogen input to system	Lb.nitrogen/min.
η	Dilution correction factor	-
O_i	Weight percent of oxygen in i^{th} fuel	Weight percent
$\mathring{O}_T$	Total oxygen input to system	Lb. oxygen/min.
R_1	O_2 required by primary fuel	Lb.moles O_2/lb.fuel
R_2	O_2 required by reburning fuel	Lb.moles O 2/lb.fuel

NOMENCLATURE (Continued)

Symbol	Definition	Units
$\overset{\circ}{R}_T$	Total oxygen required by system	Lb.moles/min.
S_1	Weight percent sulfur in i^{th} fuel	Weight percent
$\overset{\circ}{S}_T$	Total sulfur input to system	Lb. sulfur/min.
SR_1	Primary zone stoichiometric ratio	-
SR_2	Reburning zone stoichiometric ratio	-
SR_3	Burnout zone stoichiometric ratio	-
$(TA)_1$	Primary zone stoichiometric ratio	SCFM
$[TA]_2$	Required air per pound of dry reburning fuel	SCF/lb
$(TA)_2$	Reburning fuel theoretical air	SCFM
$(TA)_T$	Total theoretical air	SCFM

APPENDIX C: COMPOSITE PROCESS MODEL FOR NO_x REDUCTION BY REBURNING

A composite process model for prediction of NO_x reduction by reburning is being developed at EER. The general objectives which the model is designed to meet are: 1) to assist the experimenter in planning experiments and in understanding and correlating data; 2) to identify important parameters and predict their effects; and 3) to estimate reburning efficiency in practical applications and to identify changes in design or operation which may be most effective in improving reburning efficiency.

To be useful, the model must be easy to use and to modify, and it must be broadly applicable. It must use commonly available or easily estimated input data; it should allow areas of interest to be isolated so that individual trends are not obscured by the composite predictions; and it should allow correlation of data taken from a range of scales, fuels, and operating conditions.

This section briefly discusses the composite model and its components, compares predicted and measured trends for the CTT, and states conclusions thus far obtained from the modeling effects.

Model Description

A modular approach to composite model development provides the most effective means of satisfying these objectives and goals. Such a composite modular model is shown conceptually in Figure C-1. Boxes in the figure represent input, intermediate, or output data and the lines represent submodels. Working portions of the model are designated by bold lines. In its present form, the model takes fuel-lean primary combustion products, adds nitrogen-doped gaseous secondary fuel, and calculates soot concentration, equilibrium H_2 and H_2O concentrations, and concentrations of fixed nitrogen species emitted from the fuel-rich secondary flame. Nitrogen processing in

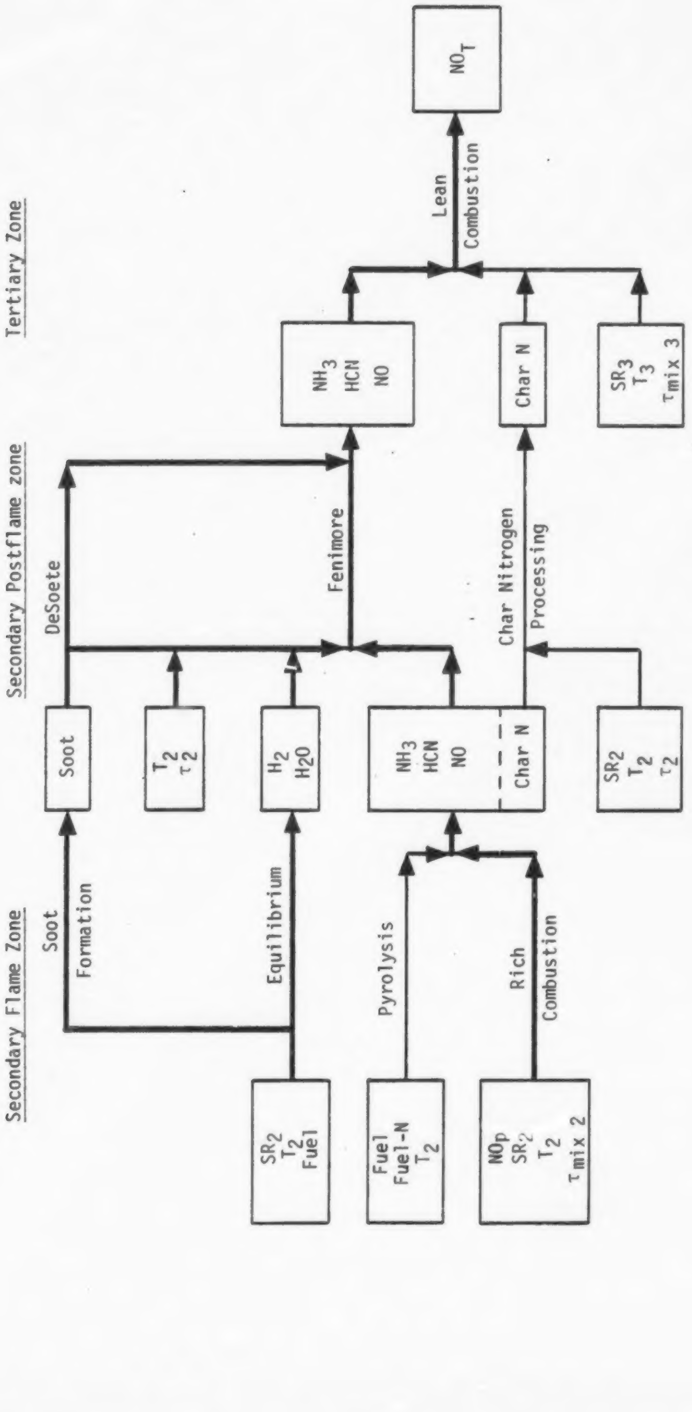
Secondary Flame Zone
Secondary Postflame zone
Tertiary Zone
SR_2 T_2 Fuel
Fuel Fuel-N T_2
NO_p SR_2 T_2 $\tau_{mix\ 2}$
Soot Formation
Equilibrium
Pyrolysis
Rich Combustion
Soot
T_2 τ_2
H_2 H_2O
NH_3 HCN NO
Char N
SR_2 T_2 τ_2
DeSoete
Fenimore
Char Nitrogen Processing
NH_3 HCN NO
Char N
SR_3 T_3 $\tau_{mix\ 3}$
Lean Combustion
NO_T

Figure C-1. Composite process model.

the postflame secondary is calculated using a combination of homogeneous and heterogeneous kinetics. Finally, NO emitted after tertiary burnout is calculated using an empirical correlation. The pyrolysis and char nitrogen processing portions of the model necessary to describe reburning with coal have not as yet been addressed. Description of the working modules will proceed from the back end forward, more or less in the same order in which they were developed.

The lean combustion module predicts tertiary NO concentration from NH_3, HCN, and NO concentrations emitted from the secondary. An empirical correlation is used, originally developed to predict NO concentrations emitted from the lean stage of rich/lean staged coal combustion (Overmoe et al 1983). The formula is as follows:

$$(NO_x)_{ex} = 0.81\ SR_2\ (NO)_s + \frac{0.36\ [(HCN)_s + (NH_3)_s]}{1 + 0.0024\ [(HCN)_3 + (NH_3)_s]}$$
$$+ 0.27\ (\mathrm{Char\ N})_s \sqrt{1-SR_2} + 53$$

where all concentrations are ppm dry, corrected to stoichiometric conditions. The char nitrogen term becomes zero when gaseous fuels are used.

The secondary postflame module uses homogeneous and heterogeneous kinetics to describe changes in HCN, NH_3, and NO concentrations. The homogeneous reaction rates of Fenimore (1979), shown in Table C-1, are used in a manner similar to that described by Glass and Wendt (1982). At low NO concentrations, homogeneous kinetics alone are insufficient to describe mesured NO decline in the postflame zone. The heterogeneous reaction rates for NO reactions on soot reported by de Soete (1982) are used as shown in Table C-2. In combination, the homogeneous and heterogeneous kinetics describe a situation where HCN is converted to NH_3 which reacts with NO to form N_2. Under most situations examined, the postflame model predicted declining HCN and NO concentrations and rising NH_3 concentrations. Hydrogen and water concentrations necessary for the postflame kinetics are calculated from Carbon and

TABLE C-1. FENIMORE HOMOGENEOUS KINETICS

$HCN + OH \xrightarrow{K_1} NH_2 + CO$	$K_1 = 10^{12}\ [HCN]\ [OH]\ \frac{Mole}{cm^3\ sec}$
$NH_2 + NO \xrightarrow{K_2} N_2 + H_2O$	$K_2 = 5 \times 10^{12}\ [NO][NH_2]\ \frac{Mole}{cm^3\ sec}$
$N + OH \xrightarrow{f(K_2)} NO + H$	$K_3 = K_2 \times 700\ \frac{[H_2O]}{[NO]}\ exp\ \frac{-50\ K_{cal}}{R_T}$
$2H_2O \overset{K_{OH}}{\rightleftharpoons} H_2 + 2OH$	$K_{OH} = 2.841 \times 10^7\ exp\ \frac{-138\ K_{cal}}{R_T}$
$OH + NH_3 \overset{K_{NH_3}}{\rightleftharpoons} NH_2 + H_2O$	$K_{NH_3} = 1.66\ ex\{\ \frac{12\ K_{cal}}{R_T}$

TABLE C-2. DE SOETE HETEROGENEOUS KINETICS

1. $NO + a\ (-C) \rightarrow 0.5\ N_2 + (2a - 1)\ CO + (1 - a)\ CO_2$ $(0.5 \leqslant a \leqslant 1)$	$V_1 = 1.3 \times 10^{10} \exp\left[-22550(\pm 2500)/T\right]\ X_{NO}^{0.75}$
2. $NO + a\ (-C) + b\ (-H) \rightarrow NH_3 + \left(\frac{b - 5}{2} + 2a\right) CO + \left(\frac{5 - b}{2} - a\right) CO_2 + \frac{b - 3}{2} H_2O$ $(0 \leqslant a \leqslant 1\ ;\ 5 \geqslant b \geqslant 3)$	$V_2 = 1.9 \times 10^{6} \exp\left[-14300(\pm 1500)/T\right]\ X_{NO}^{0.7}$
4. $NO + nNH_3 \rightarrow \left(\frac{1 + n}{2}\right) N_2 + H_2O + \left(\frac{3n - 2}{2}\right) H_2$	$V_4 = 6 \times 10^{8} \exp\left[-11500(\pm 1500)/T\right]\ X_{NO}\ X_{NH_3}$
5. $NH_3 + (-C) \rightarrow HCN + H_2$	$V_5 = 6 \times 10^{6} \exp\left[-16600(\pm 1500)/T\right]\ X_{NH_3}$
11. $NO + 2.5\ H_2 \rightarrow NH_3 + H_2O$	$V_{11} = 1.3 \times 10^{10} \exp\left[-17100(\pm 2500)/T\right]\ X_{NO}^{0.5}\ X_{H_2}$
13. $NH_3 \rightarrow 0.5\ N_2 + 1.5\ H_2$	$V_{13} = 5.3 \times 10^{8} \exp\left[-18600(\pm 1300)/T\right]\ X_{NH_3}$
14. $NO + H_2 \rightarrow 0.5\ N_2 + H_2O$	$V_{14} = 6.8 \times 10^{8} \exp\left[-13260(\pm 1500)/T\right]\ X_{NO}\ X_{H_2}$

Soot concentrations necessary for the kinetics are presently set to values necessary to allow the model to accurately reproduce bench-scale data for NO decline in the postflame secondary at low NO concentrations.

The rich combustion model is a very simple empirical correlation which predicts the distribution of nitrogen species entering the postflame secondary. Twenty-five percent of the total fixed nitrogen entering the secondary is converted to NO and seventy-five percent is converted to HCN.

This 25/75 split is assumed to be independent of the source of the fixed nitrogen: either primary NO or secondary fuel nitrogen. The split was chosen to provide the best fit to measured data as the composite mode was applied to 24 bench scale data points taken over a range of stoichioimetries, NO concentrations, secondary fuel concentrations, and residence times. The rich combustion process is assumed to take 300 milliseconds, thus the postflame reactions do not begin until 300 milliseconds into the secondary. This time was chosen to allow the postflame model to reproduce intermediate NH_3 measurements without using unrealistic (negative) initial NH_3 concentrations.

Model Applications

The model was applied to 24 gaseous fuel data points listed in Table C-3. Secondary stoichiometry ranged from 0.7 to 0.9; primary NO concentration ranged from 190 to 630 ppm; secondary fuel nitrogen ranged from 0 to 1.58 percent; and secondary residence time ranged from 400 to 750 milliseconds. Temperature varied with stoichiometry as did H_2 and H_2O concentrations. Figure C-2 compares predicted and measured exhaust NO concentrations. Predictions generally agreed quite well with measurements. Specific trends were predicted with reasonable accuracy as well. Figure C-3 shows that secondary stoichiometry has only a small effect on reburning efficiency (defined as one minus the molar ratio of exhaust NO to primary NO) for nitrogen-free secondary fuels, but reburning efficiency decreases as the secondary becomes richer for nitrogen-containing fuels because a greater proportion of the fuel bypasses the primary, losing one opportunity to decrease its fixed nitrogen content. This effect becomes even more

TABLE C-3. TEST CONDITIONS

Secondary Stoichiometric Ratio	Primary NO (ppmd,stoic)	Secondary Fuel Nitrogen (wt %)	Secondary Residence Time (msec)	Secondary Temperature		Secondary Hydrogen Concentration	Secondary Water Concentration	Secondary Soot Concentration (cm^2/cm^3)
				400 msec (^{o}K)	750 msec (^{o}K)			
0.7	190	0	400	1456	1339	0.029	0.132	5.6
0.7	190	0	750	1456	1339	0.029	0.132	5.6
0.7	190	1.58	400	1456	1339	0.029	0.132	5.6
0.7	190	1.58	750	1456	1339	0.029	0.132	5.6
0.7	630	0	400	1456	1339	0.029	0.132	5.6
0.7	630	0	750	1456	1339	0.029	0.132	5.6
0.7	630	1.58	400	1456	1339	0.029	0.132	5.6
0.7	630	1.58	750	1456	1339	0.029	0.132	5.6
0.8	190	0	400	1483	1339	0.025	0.135	7.1
0.8	190	0	750	1483	1339	0.025	0.135	7.1
0.8	190	1.58	400	1483	1339	0.025	0.135	7.1
0.8	190	1.58	750	1483	1339	0.025	0.135	7.1
0.8	630	0	400	1483	1339	0.025	0.135	7.1
0.8	630	0	750	1483	1339	0.025	0.135	7.1
0.8	630	1.58	400	1483	1339	0.025	0.135	7.1
0.8	630	1.58	750	1483	1339	0.025	0.135	7.1
0.9	190	0	400	1528	1367	0.018	0.144	5.7
0.9	190	0	750	1528	1367	0.018	0.144	5.7
0.9	190	1.58	400	1528	1367	0.018	0.144	5.7
0.9	190	1.58	750	1528	1367	0.018	0.144	5.7
0.9	630	0	400	1528	1367	0.018	0.144	5.7
0.9	630	0	750	1528	1367	0.018	0.144	5.7
0.9	630	1.58	400	1528	1367	0.018	0.144	5.7
0.9	630	1.58	750	1528	1367	0.018	0.144	5.7

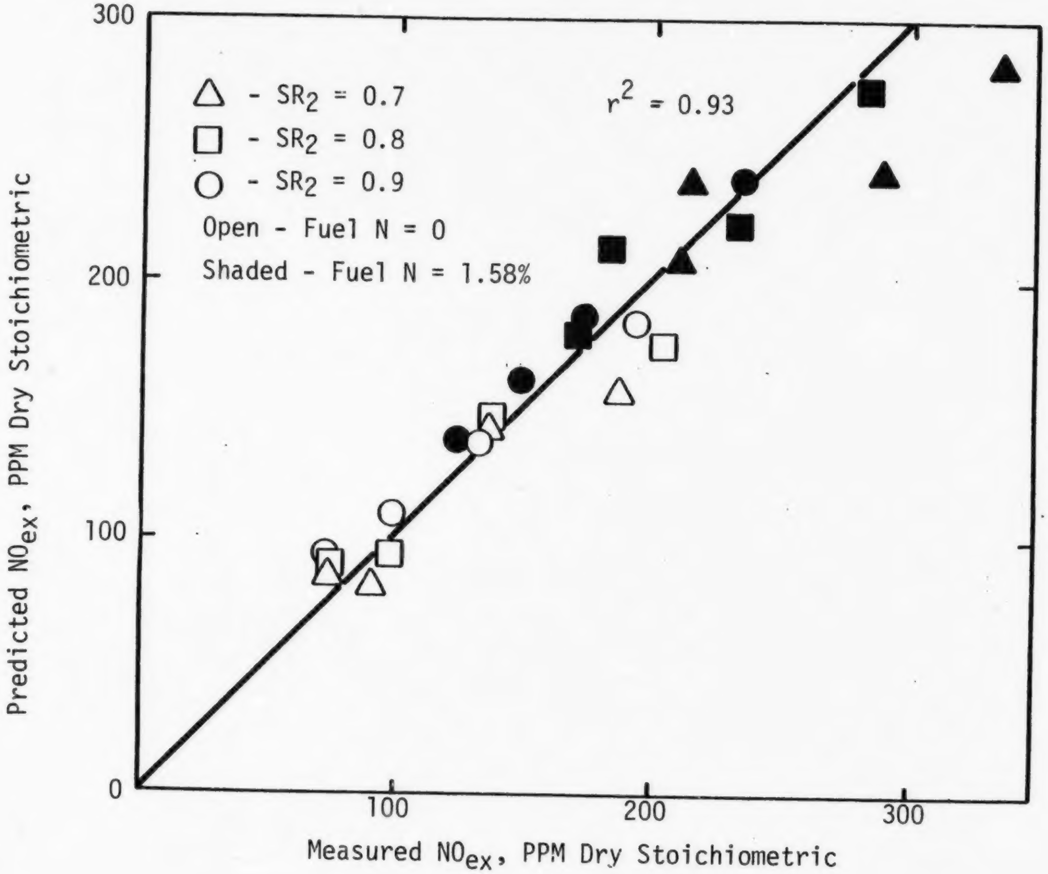

Figure C-2. Composite model verification

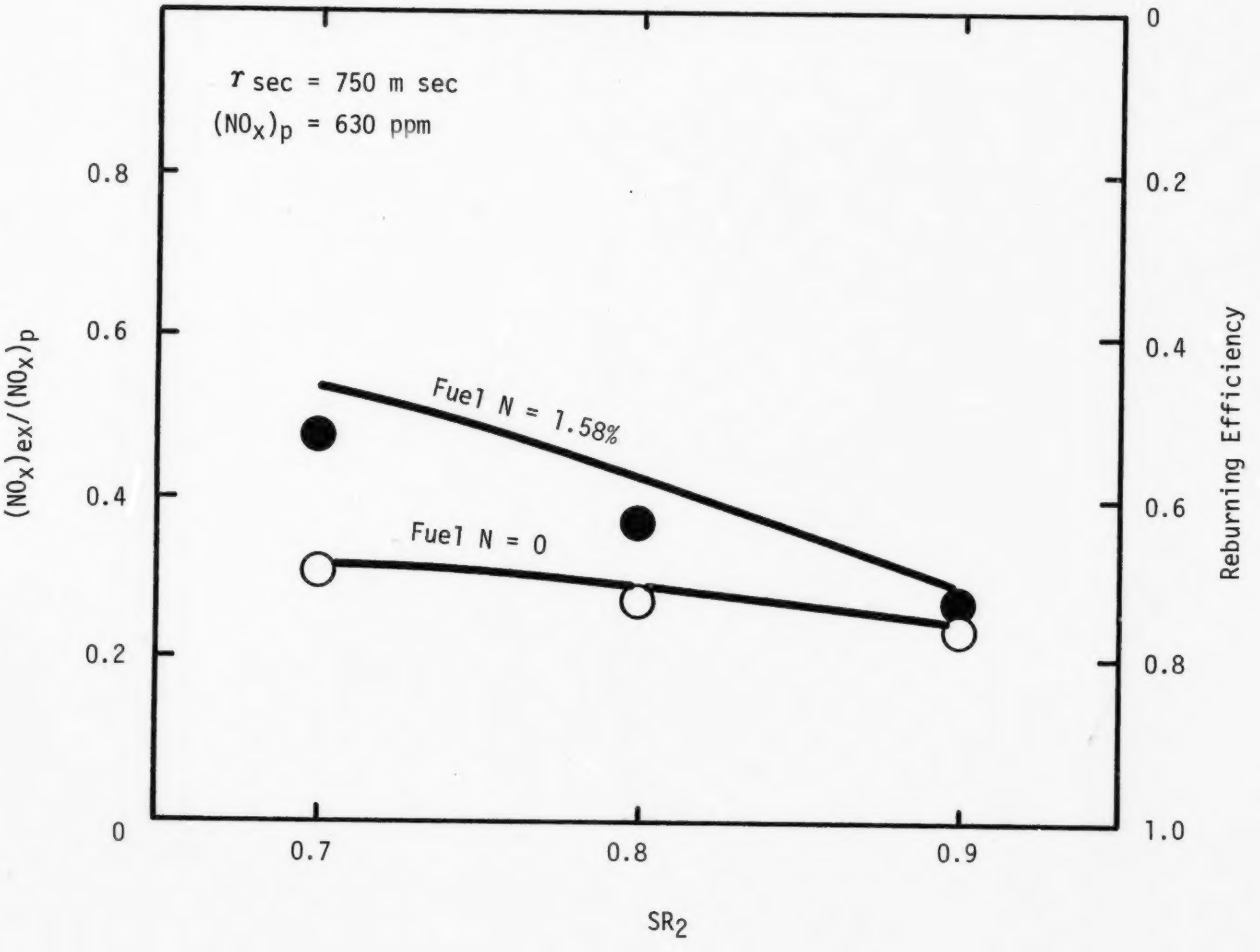

Figure C-3. Effect of SR_2

pronounced at low primary NO concentrations, representative of low-NO_x primary burners. Figure C-4 shows that reburning efficiency increases with increasing primary NO concentration. Concentration is important in both the postflame secondary model and in the lean combustion model. The effect of secondary fuel nitrogen content is shown in Figure C-5. Secondary fuel nitrogen content has only a small impact on reburning efficiency for high-to-intermediate NO_x primary burners, but reburning efficiency decreases sharply with increasing secondary fuel nitrogen for primary NO_x concentrations representative of low-NO_x primary burners. Figure C-6 shows the effect of secondary residence time. The first 300 milliseconds are considered part of the rich combustion zone where 75 percent of the total fixed nitrogen is converted to HCN and 25 percent is converted to NO. As the secondary residence time increases beyond 300 milliseconds, reburning efficiency increases but at a decreasing rate. This is due primarily to declining temperatures in the secondary. Postflame reactions are expected to be more important in hotter secondaries with a lower quench rate.

Conclusions

The composite model in its present form is a useful tool to assist in analyzing, interpreting, and extrapolating data for gas-fired reburning applications. In order for the model to be applicable to coal-fired reburning, submodels are required describing nitrogen speciation in pyrolysis and describing char nitrogen processing. In addition, several areas of the present model could be improved. The rich combustion model, the lean combustion model, and the soot formation model are, at present, simple empirical curve fits to a limited data set. At a minimum, these submodels should be tested and tuned to fit a much broader data set, adding whatever parameters are necessary. Ideally, global kinetics should be applied to 87ese submodels, although such an approach may prove impractical in a mixing-limited flame.

References

DeSoete, G. G. Mechanisms of Nitric Oxide Reduction on Solid Particles. Fundamental Combustion Research Applied to Pollution Formation, Final

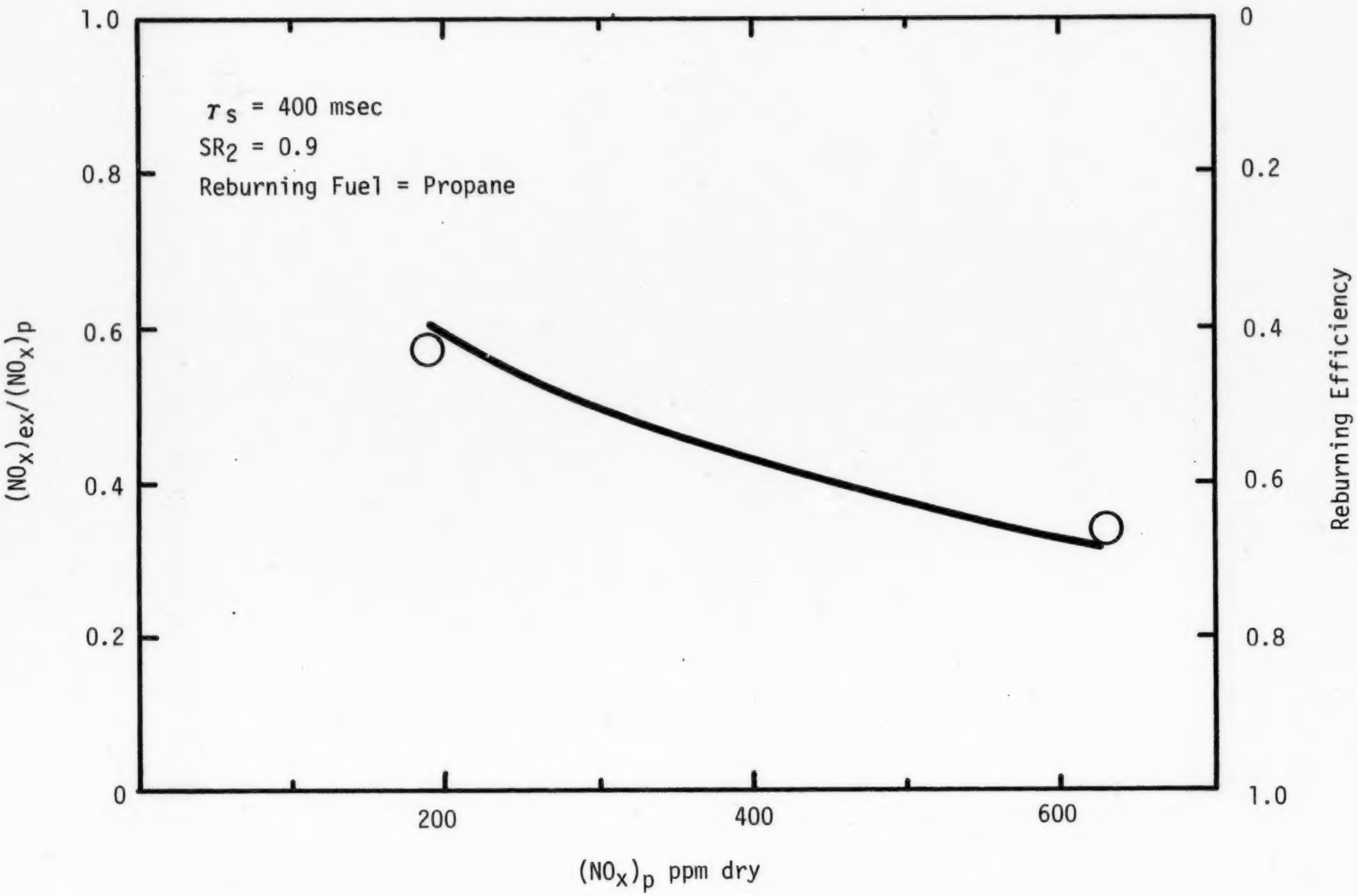

Figure C-4. Effect of primary NO concentration.

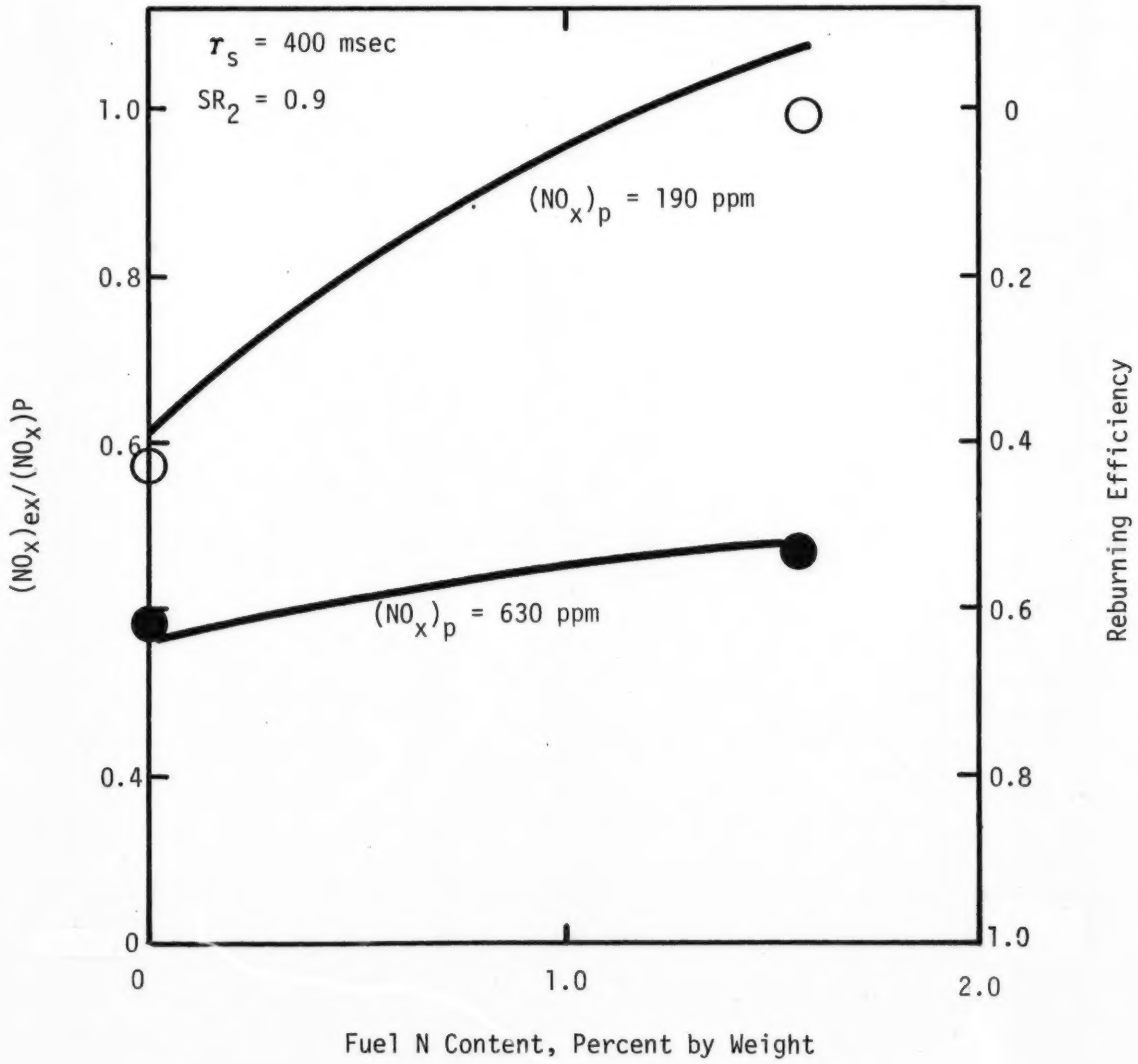

Figure C-5. Effect of fuel N content.

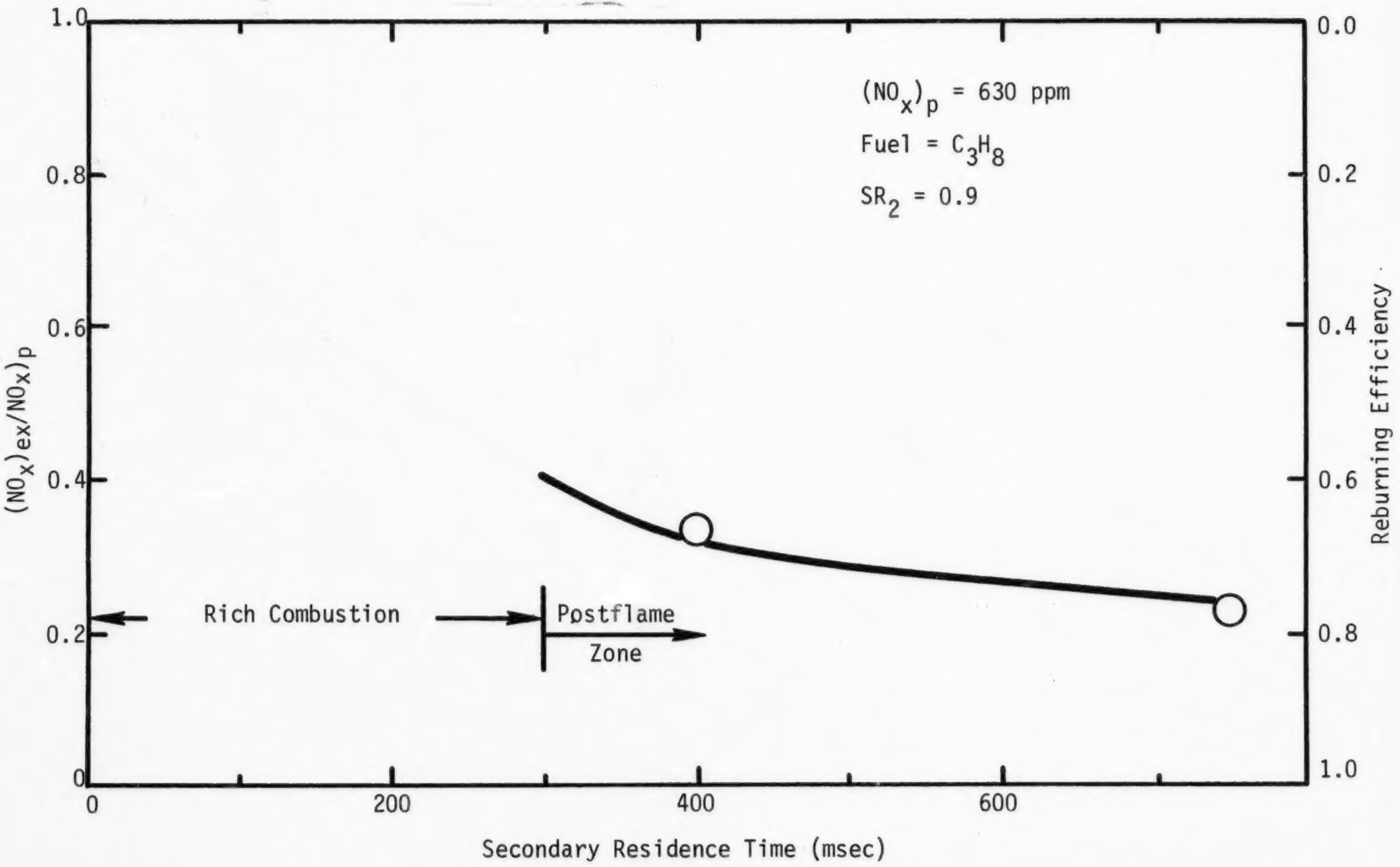

Figure C-6. Effect of secondary residence time.

Report, Volume II--Physics and Chemistry of Two-Phase Systems, Section C, Heterogeneous NO Reduction. Prepared by W. R. Seeker, M. P. Heap, and T. J. Tyson, EPA Contract No. 68-02-2631, 1982.

Fenimore, C. P. Studies of Fuel-Nitrogen Species in Rich Gas Flames. Seventeenth Symposium (International) on Combustion, The Combustion

APPENDIX D: SULFUR CAPTURE MODEL

The capture of sulfur by solid sorbents injected directly into the furnace is a complex process. Modeling helps to understand and clarify the parameters involved in the sulfur capture process. The general approach has been to divide the process into the two zones of sorbent activation and sorbent sulfation as shown in Figure D-1, and to model each zone separately. The first zone, sorbent activation, includes the processes which ultimately govern sorbent reactivity and sulfation capacity; these processes include: particle heat-up, calcination, and deactivation as a result of over-heating and/or reactions with minerals in the coal ash. The second zone, sulfate formation, includes the processes which control sulfate formation, including: gas phase diffusion of SO_2 to the sorbent particle surface, diffusion within the particle pores, chemisorption, reaction with the solid, diffusion through the reactant layer, blockage of the pores due to sulfate formation, and the thermal stability limits of the sulfate.

D.1 Sorbent Activation Model

Sorbent activation has been studied in detail under EPA contract 68-02-3633-as described by Cole, et al. (1983). This section is a brief summary of the major conclusions concerning sorbent activation.

The rate at which a sorbent particle calcines depends upon the heat capacity of the particle, convective heat transfer between the particle and the surrounding gas, radiative heat transfer between the particle and the walls of the combustion system, and heat consumption in the endothermic calcination process. Within the ranges of interest, particle heat-up is generally dominated by convection; and both heat-up and calcination are essentially complete within 1 to 10 milliseconds. Thus, unless low temperatures or large particles are encountered, calcination is fast compared to sulfation.

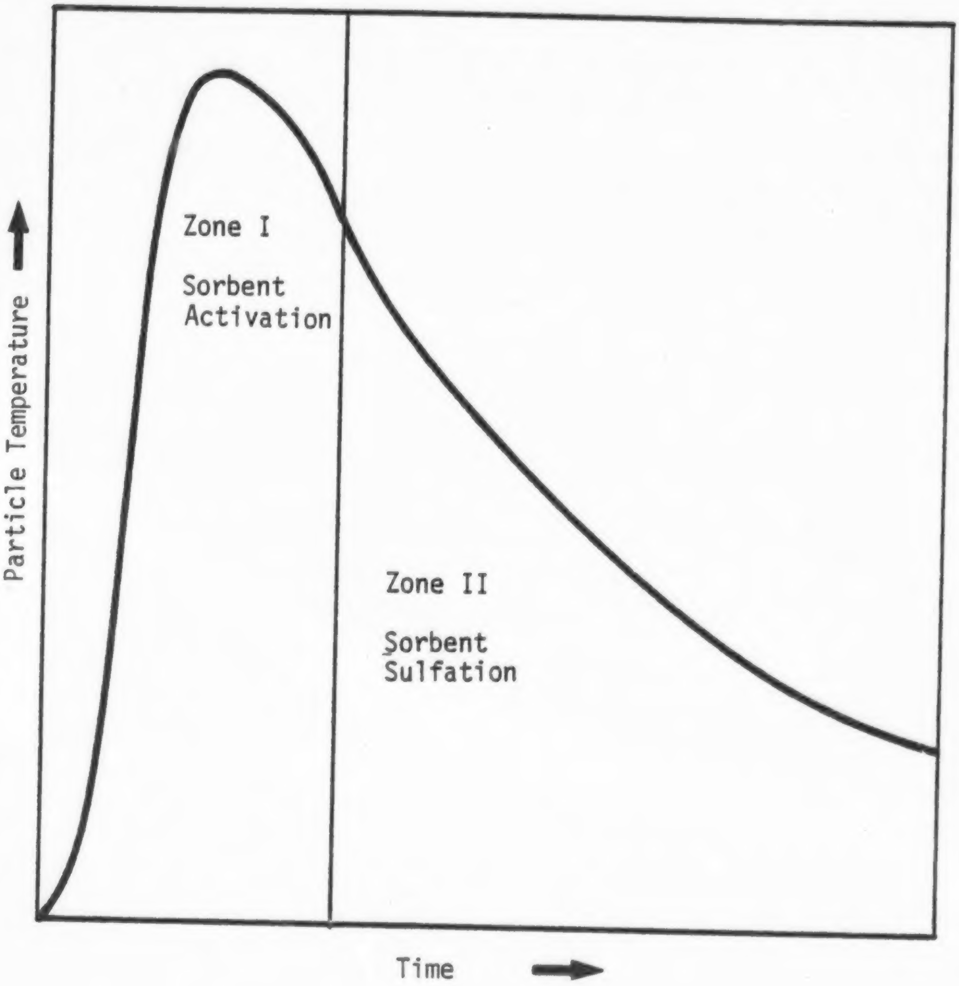

Figure D-1. Zone approach to sulfur capture model.

As a sorbent particle calcines, its internal surface area increases due to the conversion of $CaCO_3$ to less bulky CaO. At high temperatures, the internal surface area decreases as sintering or deadburning results in pore closure. A fundamental model describing the growth and decay of surface area has not yet been developed; however, a simple empirical curve fit relating ultimate surface area to peak particle temperature appears to be an adequate substitute. Figure D-2 shows such a correlation for limestone.

Thus the sorbent activation model is very simple. Particle heat-up and complete calcination is assumed to occur instantaneously resulting in a particle surface area which depends on the peak temperature which the particle encounters.

D.2 Sorbent Sulfation Model

Two basic methods of modeling the SO_2-lime (CaO) reaction are currently available, having been developed by various workers to model reactions occurring in fluidized-bed combustors. The two main approaches to modeling the sulfation processes are:

The grain model which treats the sorbent as single calcium oxide particles made up of tiny, nonporous micro-pellets; where reaction with CaO occurs. As reaction proceeds, a shell of reaction product uniformly accumulates around the surface of the CaO micro-pellets. Further reaction occurs only after gas diffuses through the pore structure of the particle and then through the reaction product layer around the micro-pellets to the inner core of the fresh, unreacted calcium/oxide which gradually shrinks in size until only a pellet of reaction product remains (Hartman, 1976).

The pore model (developed by Bhatia and Perlmutter, 1981) which treats the particles as spheres enveloping a random distribution of cylindrical pores which provide the overall particle surface area. A computer program of this random pore model applied to the SO_2-lime reaction has been coded for use at EER. This section describes the pore model, and outlines the

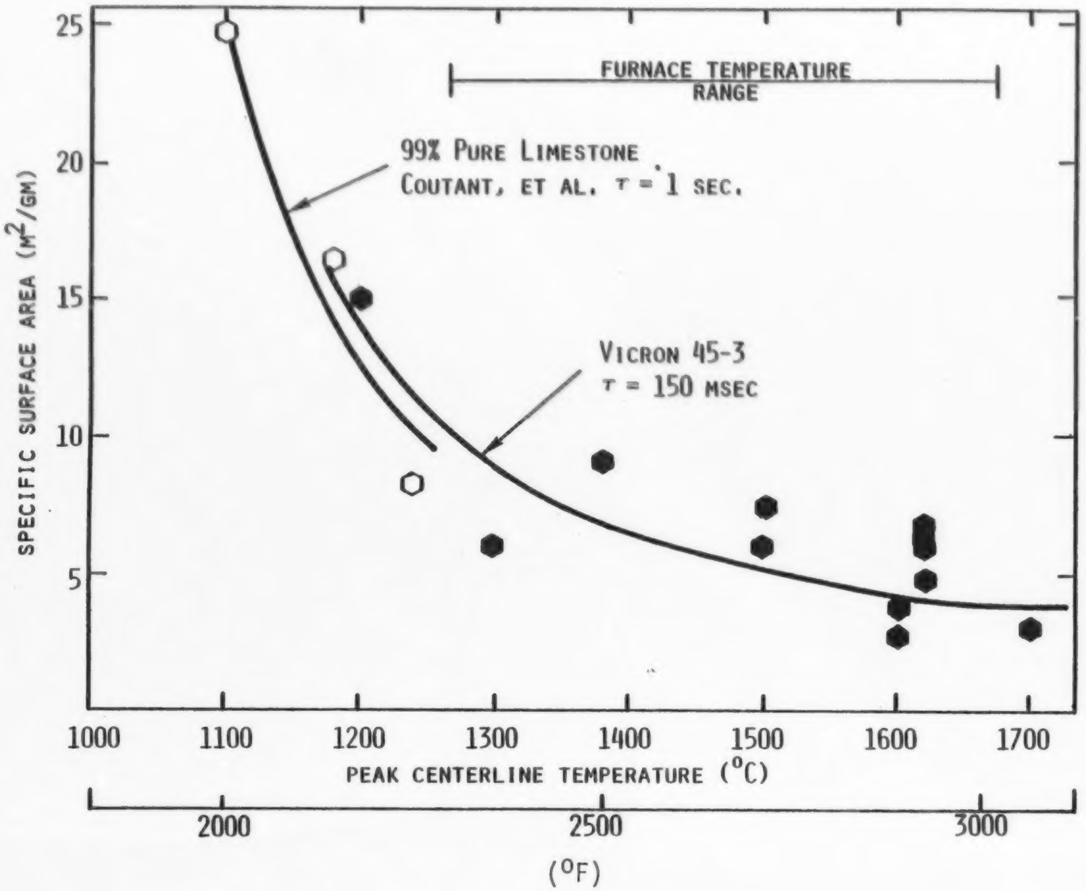

Figure D-2. Effect of peak temperature on sorbent surface area.

procedures used to verify the model and to identify the most sensitive parameters.

Pore Model Description

The model considers the internal structure of the particle to be given by a set of overlapping, random-size, cylindrical pores. The reaction is initiated at the pore surface and a layer of reaction product (calcium-sulfate) forms around the pore. This reaction product (calcium-sulfate) forms around the pore. This reaction product layer separates the pore surface and the solid reactant surface. The gas (SO_2) must diffuse through the product layer to the surface of the solid reactant (CaO) where the sulfation reaction takes place. The model also considers boundary layer diffusion and pore diffusion of the gas reactant. The model scheme for a single particle is shown conceptually in Figure D-3.

The order of the chemical reaction with respect to SO_2 concentration is a subject of current debate. Borgwardt(1970) originally observed a first-order dependence; however, most EER data correlates better with zro-order kinetics.

The resulting governing equations for first-order kinetics are (see list of nomenclature at the back of this appendix:

$$\frac{1}{r^2}\frac{\partial}{\partial r}\left(D_e r^2 \frac{\partial C}{\partial r}\right) = \frac{p(1-\epsilon_0)}{Mb}\frac{dX}{dt} \qquad (1)$$

and

$$\frac{dX}{dt} = \frac{K_s S_0 C\,(1-X)\sqrt{1-\Psi\ln(1-X)}}{(1-\epsilon_0)\quad 1+\frac{\beta Z}{\varphi}\left(\sqrt{1-\varphi\ln(1-x)}-1\right)} \qquad (2)$$

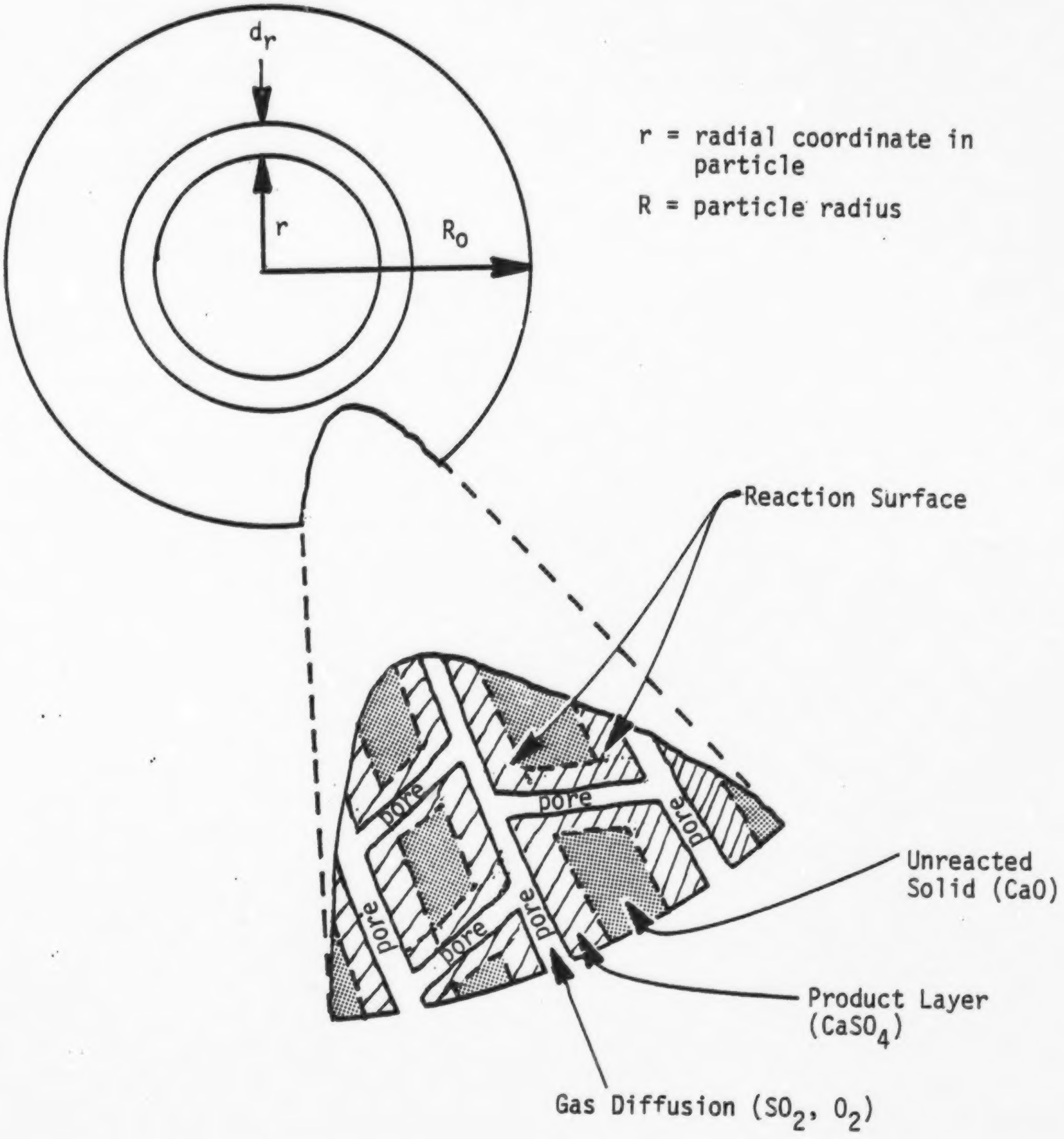
d_r
r
R_o
Reaction Surface
pore
pore
pore
pore
pore
pore
Unreacted Solid (CaO)
Product Layer ($CaSO_4$)
Gas Diffusion (SO_2, O_2)

r = radial coordinate in particle

R = particle radius

Figure D-3. Conceptual illustration of pore model for CaO/SO_2 reaction.

Equation 1 describes the diffusion of gaseous reactant into the pore while Equation 2 gives the local rate of conversion (accounting for the effect of the product layer diffusional resistance).

The boundary conditions are:

$$\frac{\partial C}{\partial r} = 0 \qquad \text{at } r = 0 \tag{3}$$

and

$$D_e \frac{C}{r} = k_b \left(C_\infty - C\right) \qquad \text{at } r = R \tag{4}$$

where k_b is the boundary layer mass transfer coefficient and C is the concentration of gas reactant at the free stream. The governing equations, (1) and (2) and the boundary condition equations (3) and (4) constitute the complete system for the pore model. These equations are nondimensionalized and solved numerically in the following manner:

- Equation (1) and boundary condition (3) and (4) are integrated numerically by finite-difference method to give the intraparticle concentration distribution.

- Equation (2) is simultaneously integrated (using a fourth-order Runge-Kutta scheme) to give local conversion.

Pore Model Verification

In order to test the program, the SO_2-lime reaction calculations, identical to those performed by Bhatia & Perlmutter (1981) were repeated. The results of these calculations (presented in terms of overall lime conversion as a function of time for various temperatures) are plotted in Figure D-4. For comparison, Bhatia & Perlmutter's results and Borgwardt's data (1970) are also shown in Figure D-4. The calculations and the data are in reasonable agreement. Slight discrepancies between the EER calculations and Bhatia's calculations may be attributed to the differences in numerical method

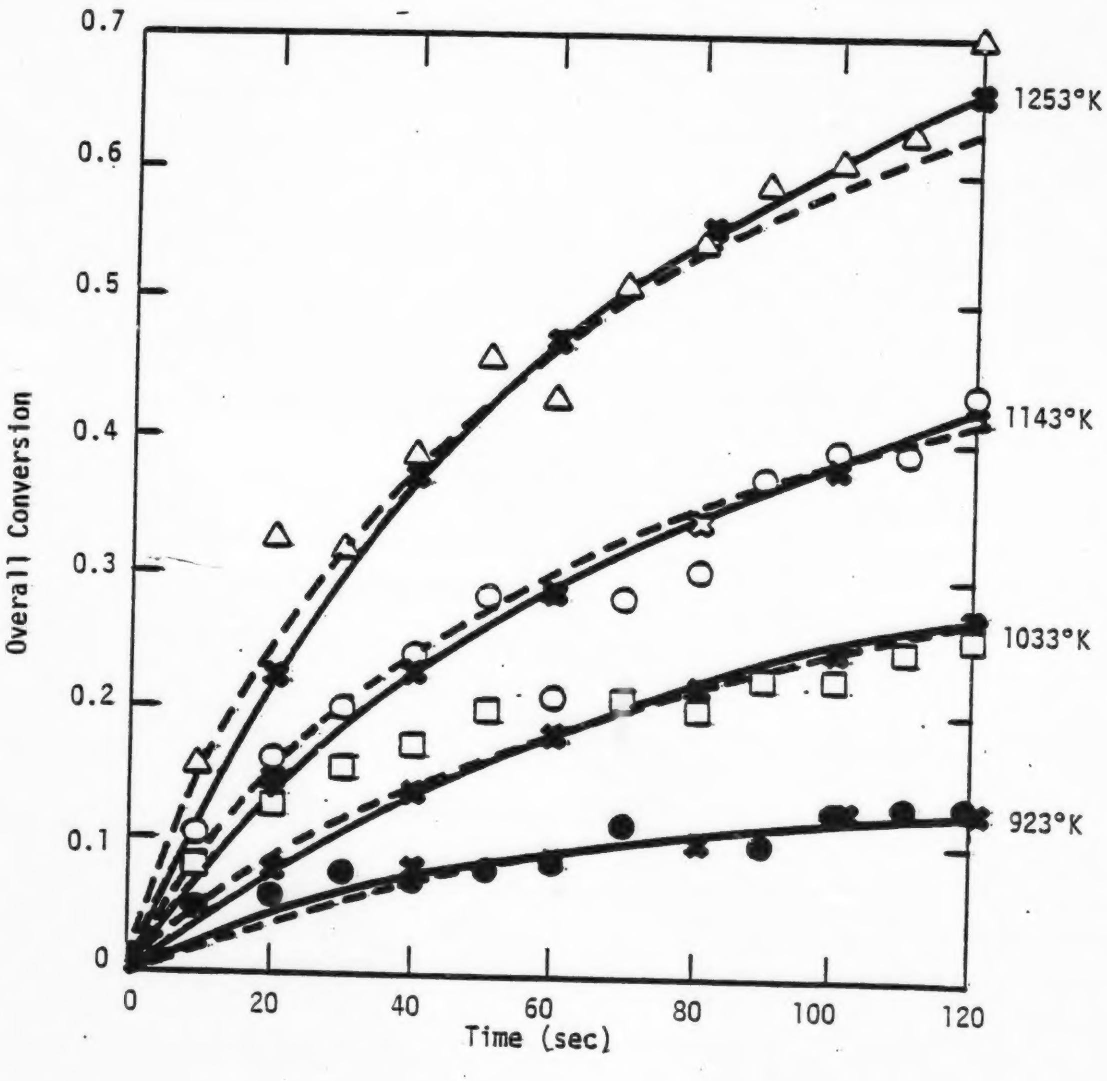

Figure D-4. Application of random pore model to data of Borgwardt (1970). Solid lines represent the current model calculations, dotted lines represent Bhatia & Perlmutter's calculations (1981).

solution. The calculations assumed first-order SO_2 dependence and constant free-stream SO_2 concentrations (3000 ppm) at constant temperature (indicated). It should be noted that these data can be fit equally well with zero-order kinetics.

A second verification of the pore model was achieved by comparing pore model pedictions with those of the grain model developed concurrently at the University of Utah by Silcox and Pershing. Figure D-5 shows that, under similar conditions, the pore model and the grain model are in excellent agreement.

Sensitivity Study

In order to identify the most sensitive model parameters, calculations were performed by varying input parameters about the baseline values listed in Table D-1. First-order kinetics were assumed for these sensitivity studies, but the conclusions should qualitatively apply to zero-order kinetics as well, except when SO_2 concentration is the parameter of interest.

Three independent parameters are necessary to define the pore structure. Pore length, surface area, and porosity have been chosen as inputs to the model, but mean pore radius and/or the spread in the pore size distribution may be substituted for any of the three. Thus, in the sensitivity study, when any one of these five parameters is varied with two others held constant, the remaining two variables are dependent and cannot be held constant. Figure D-6 shows the predicted effect of particle surface area at two porosities. The spread in the log-normal pore size distribution is held constant. Total pore length increases and particle radius decreases with increasing surface area. Under these conditions, sulfur capture is quite sensitive to pore structure parameters, increasing with increasing porosity.

Sulfur capture is only moderately dependent on temperature as shown in Figure D-7. Capture increases with increasing temperature due to increasing rates of reaction and diffusion until the equilibrium cur-off temperature is reached. At temperatures above the equilibrium limit, it is assumed that no

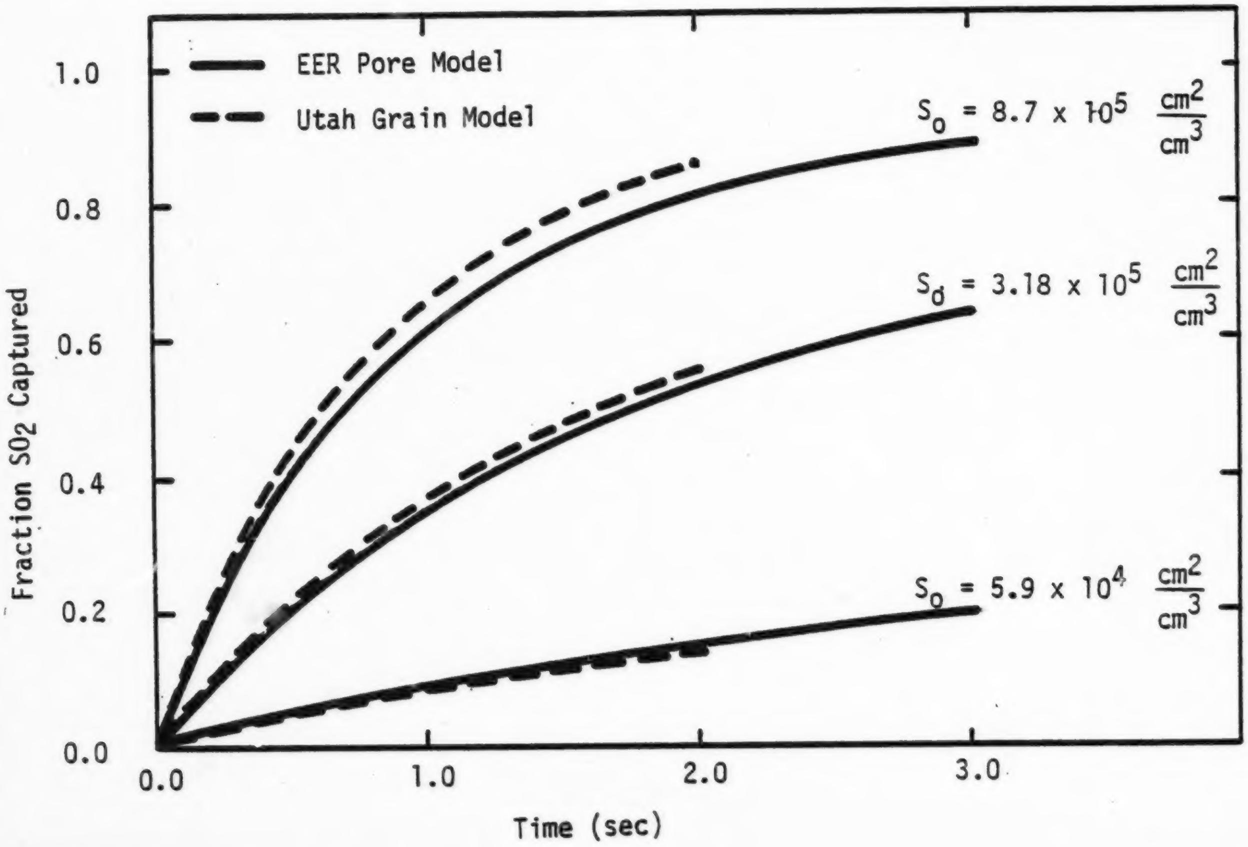

Figure D-5. Model comparison.

TABLE D-1. BASELINE CONDITIONS

Ro Particle Radius = 5.5 m

Lo Initial Pore Length = 7.55×10^8 cm/cm^3

So Initial Surface Area = 5.9×10^4 cm^2/cm^3

ϵ_o Initial Porosity = 0.55 cm^3/cm^3

Wo Initial Mass Fraction CaO = 0.97

ρ_b Initial Bulk Density = 1.59 g/cm^3

Sh Sherwood Number = 1×10^6 Infinite

Co Initial Gas Phase SO_2 Concentration = 3000 ppm

Ca/S Ratio = 2.0

T Isothermal Temperature = 1422 ^{o}K

K_s Kinetic Rate Constant

$$K_s = \frac{1890\ \text{cm}^4}{\text{mole sec}}\ \exp\ \frac{-13500\ \text{cal}}{\text{RT mole}}$$

Dp Diffusivity through Product Layer

$$Dp = 0.0528\ \frac{\text{cm}^2}{\text{sec}}\ \exp\ \frac{-28000\ \text{cal}}{\text{RT mole}}$$

Do Diffusivity through Pores

$$Do = \frac{1}{(1/D_a) + (1/DK_0)}$$

where

$$D_a = \exp\,[\underset{2}{1.66}\ \ell n(T) - 11.3]\ \text{cm}^2/\text{sec}$$

$$DK_o = 9700\ \frac{\text{cm}^2}{\text{sec}}\ \left(2\ \epsilon_o/S_o\right)\ \ T/M$$

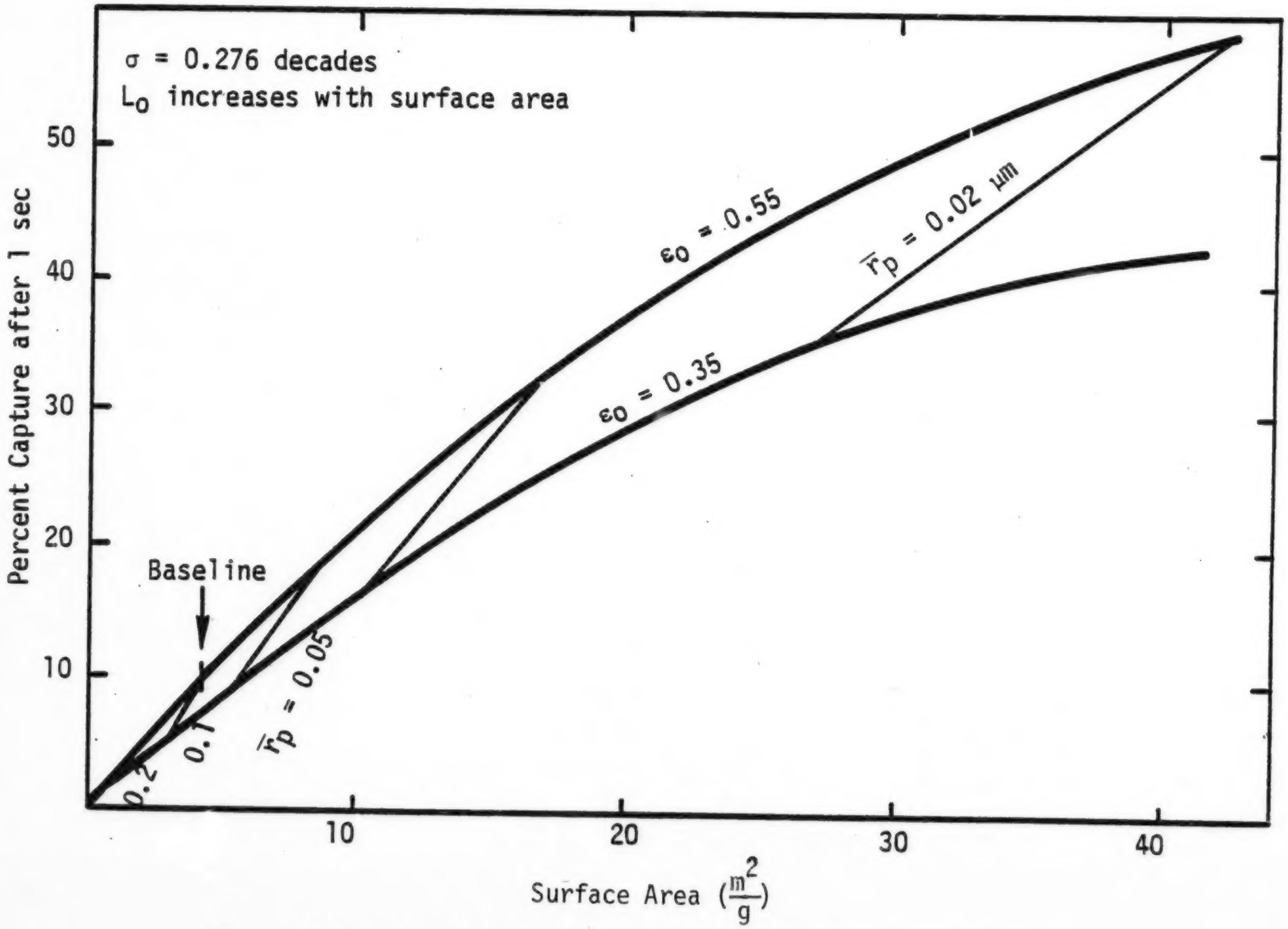

Figure D-6. Predicted effect of pore structure parameters.

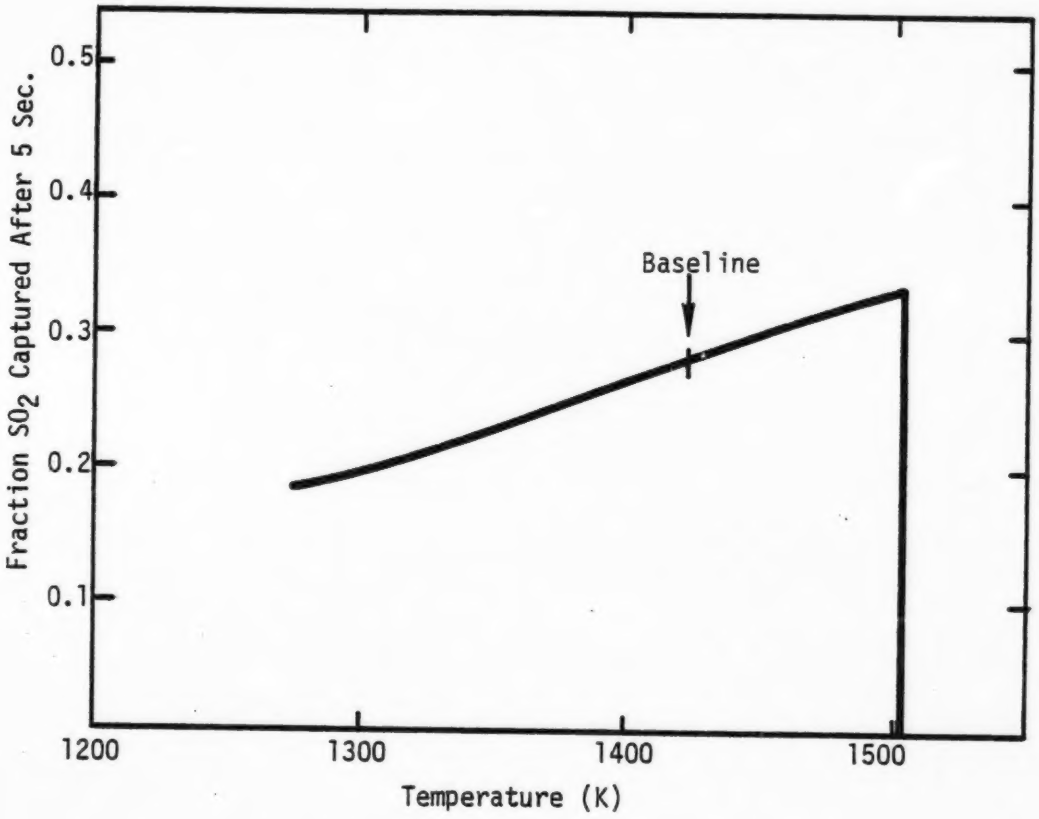

Figure D-7. Predicted effect of temperature.

reaction occurs. This assumption does not allow for the regeneration of CaO at above-equilibrium temperatures. Such a modification to the model would require detailed data for the backward reaction rates which are currently unavailable.

Effects of calcium-to-sulfur ratio and SO_2 concentration are shown in Figures D-8 and D-9. SO_2 capture increases with increasing Ca/S and with increasing SO_2 concentration. The predicted concentration effect is much stronger than most of of the data indicates suggesting that the assumed first-order dependence of intrinsic reaction are on SO_2 concentration may be incorrect. Comparison of zero-order predictions with EER reburning data are shown in Figure D-10. The predictions agree very well with the measurements at SO_2 concentrations above 600 ppm where the sulfation reaction is mostly under chemical control and SO_2 concentration has little effect on capture. However, at low SO_2 concentrations where the reaction rate should be limited by diffusion, a strong effect of SO_2 concentration on capture is predicted, but no effect is measured. Two possible explanations for this disagreement are: 1) The reaction is limited by diffusion of some other species besides SO_2 (perhaps oxygen), or 2) Control of sorbent feed rate is not fine enough to obtain accurate results at low-SO_2 concentrations (low Ca feed rates).

Parameters which have lesser effects on sulfur capture include intrinsic rate constant, product layer diffusivity, particle density, particle CaO content, particle size, and Sherwood Number as shown in Figures D-11 through D-15. Other parameters which had no effect on sulfur capture under investigated conditions were SO_2 diffusivity and Knudson diffusivity.

D.3 Sulfur Capture Model--Conclusions

A fairly simple model of sulfur capture has been produced. The model divides the process into two steps--sorbent activation and sorbent sulfation. The sorbent activation step is empirical. Results from recent studies of flash limestone calcination were used to derive a prediction of sorbent surface area from the peak temperature seen by the sorbent. Particle calcination is assumed to be instantaneous and the model does not account for any

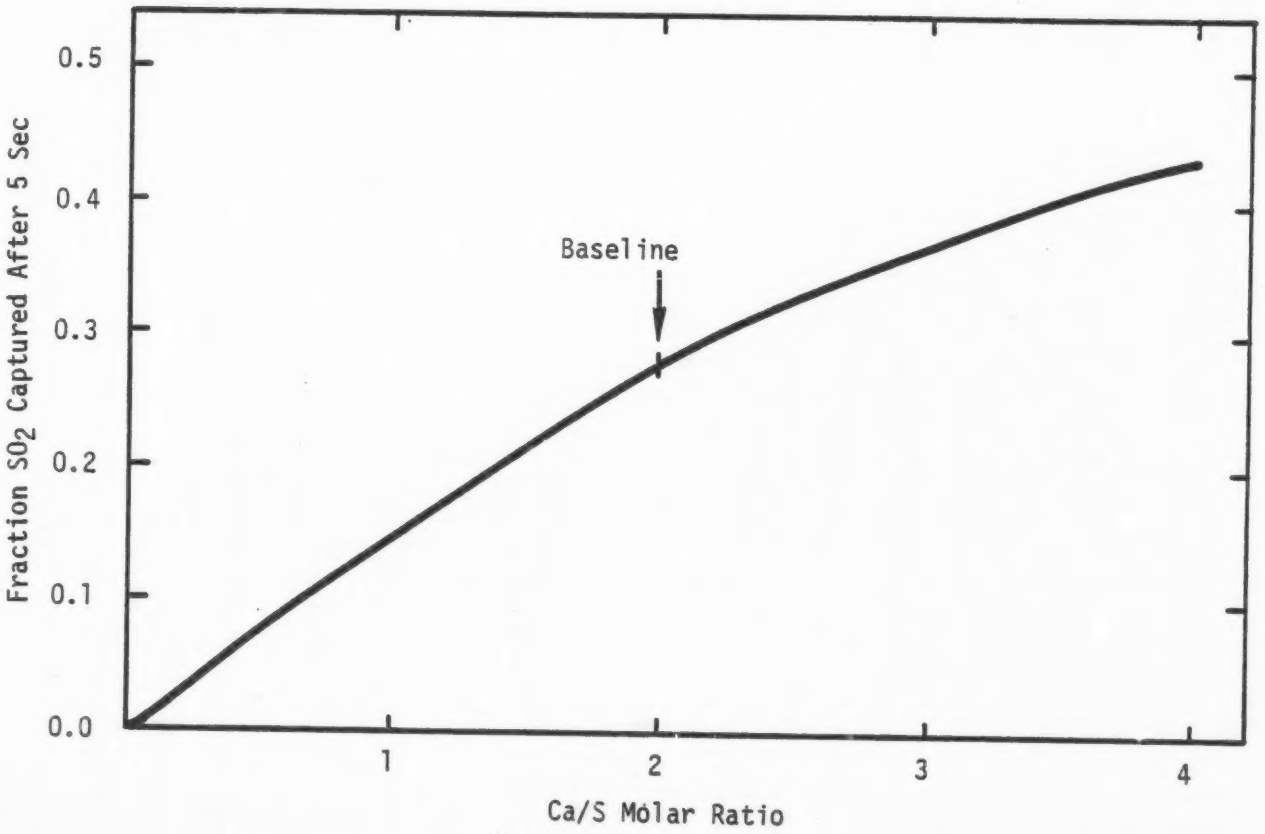

Figure D-8. Predicted effect of Ca/S ratio.

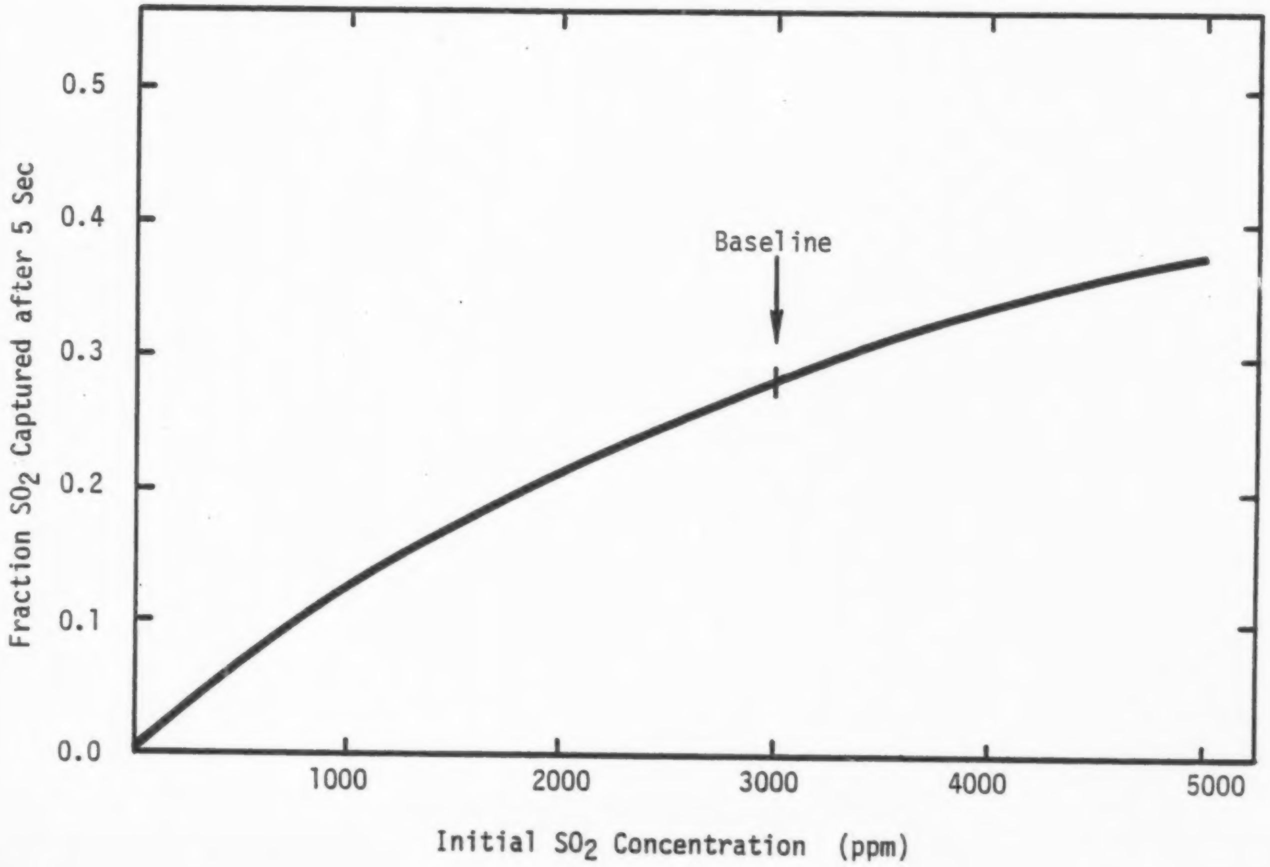

Figure D-9. Predicted effect of SO_2 concentration.

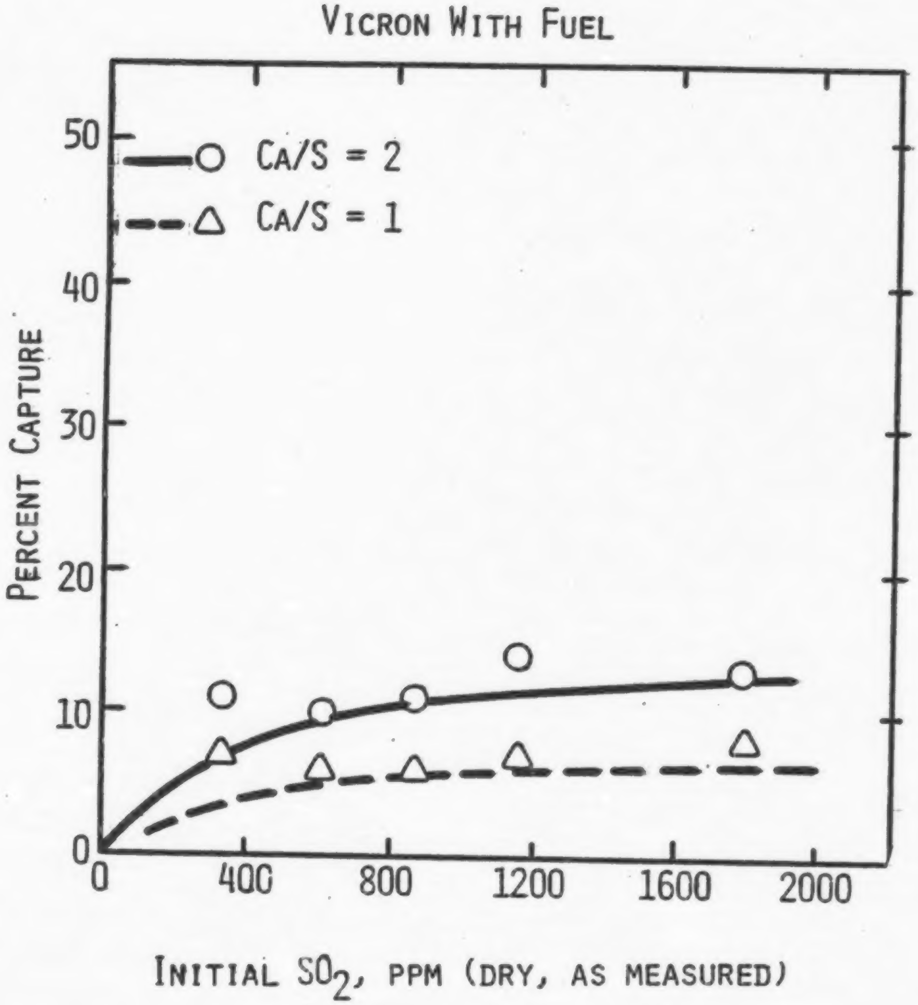

Figure D-10. Effect of SO_2 concentration (the lines represent model predictions with zero order kinetics).

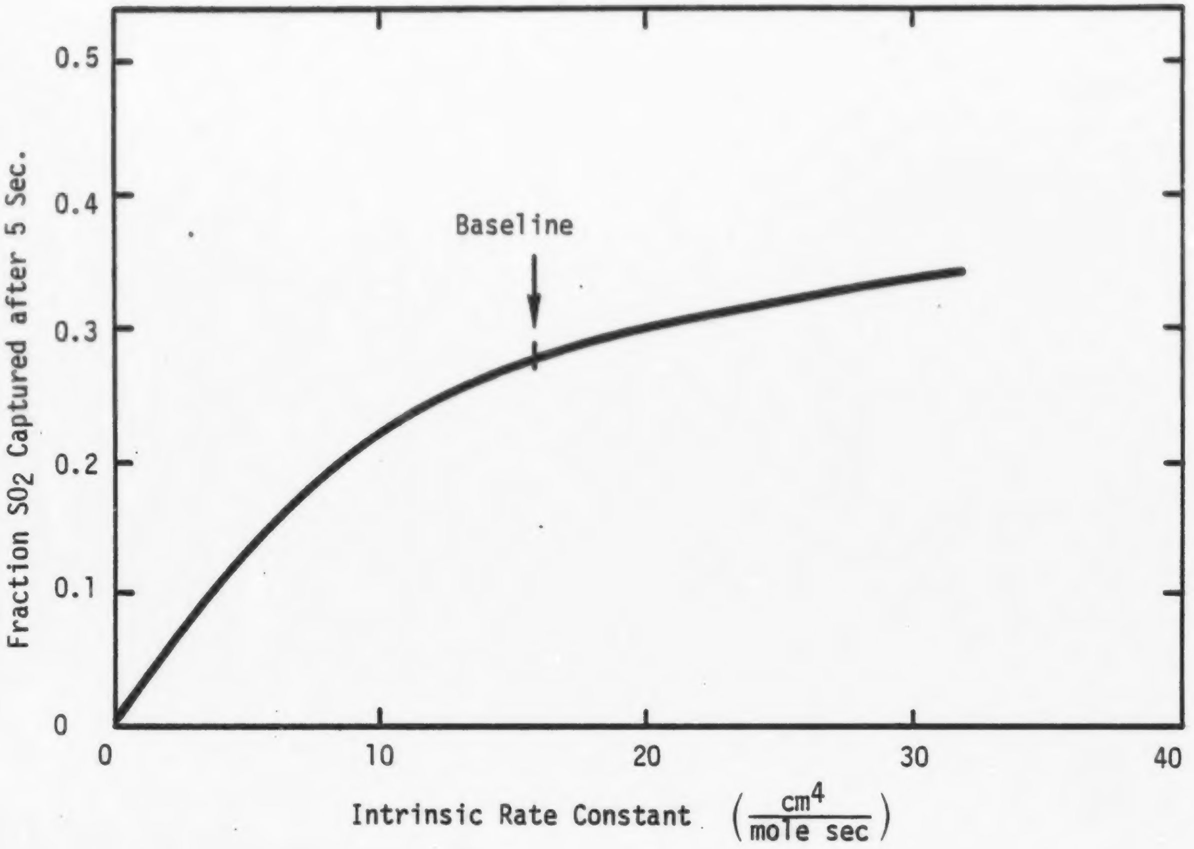

Figure D-11. Predicted effect of intrinsic rate constant.

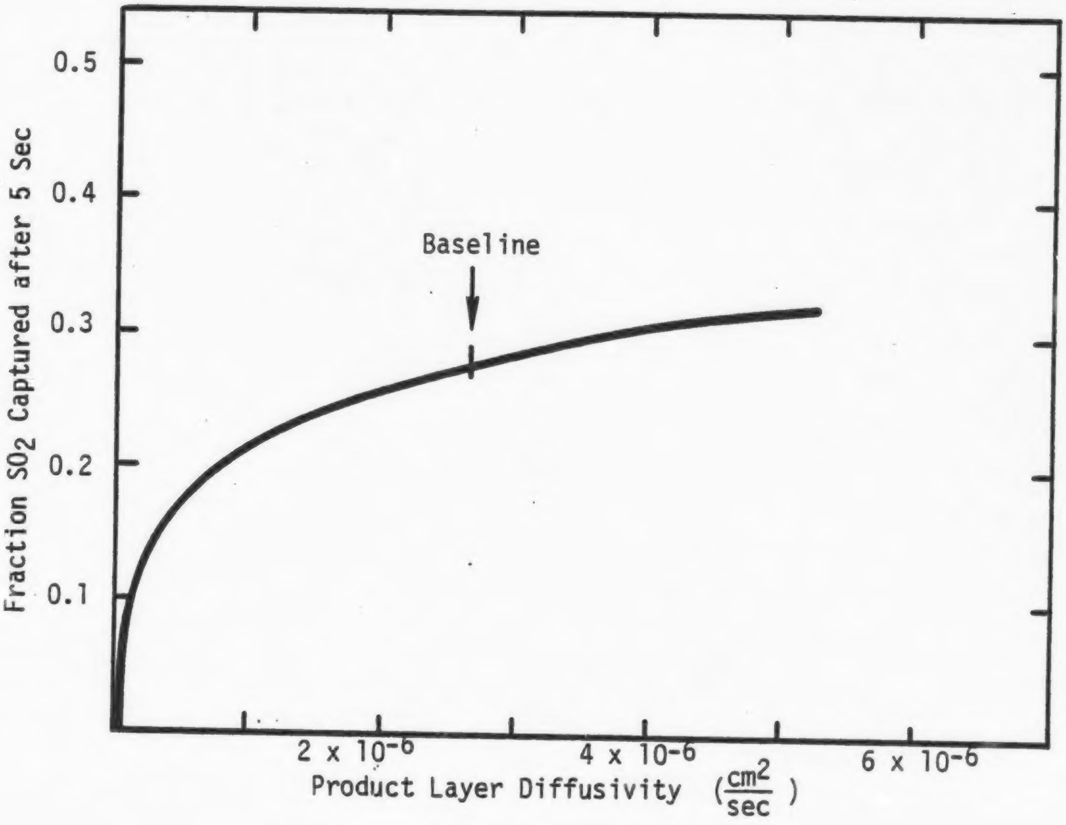

Figure D-12. Predicted effect of product layer diffusivity.

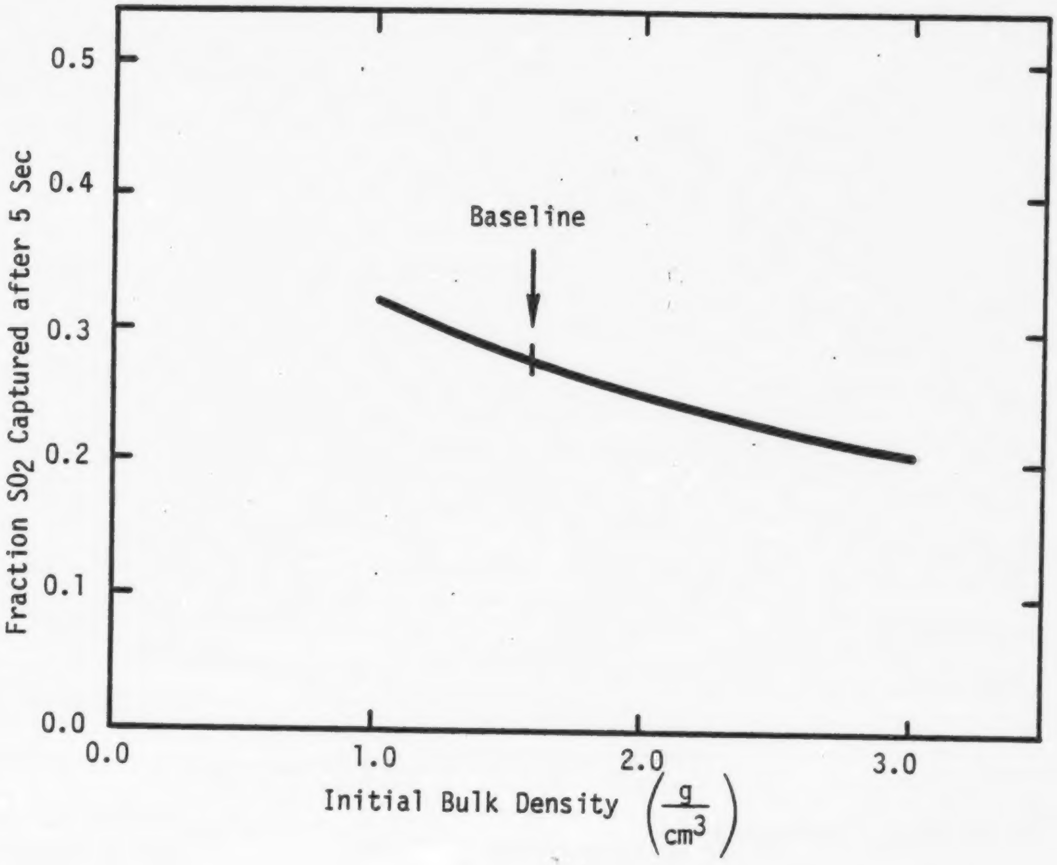

Figure D-13. Predicted effect of particle density.

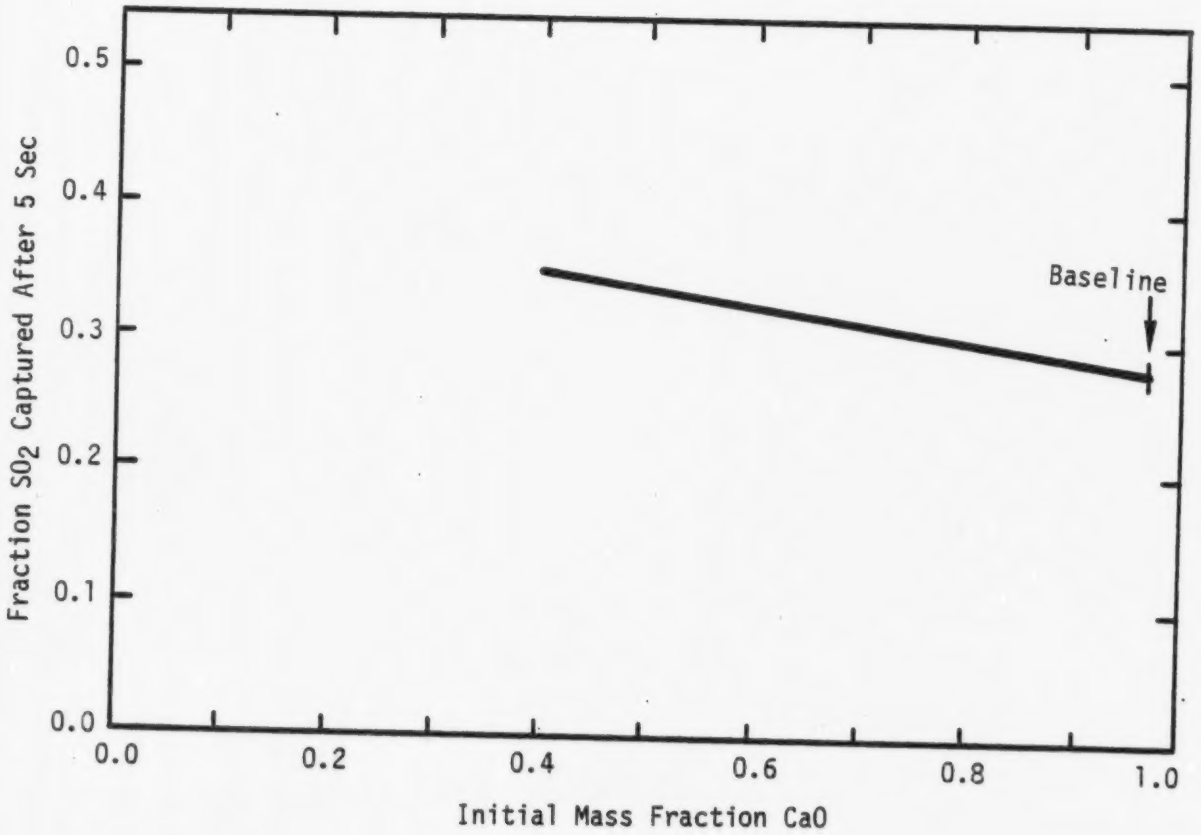

Figure D-14. Predicted effect of particle CaO content.

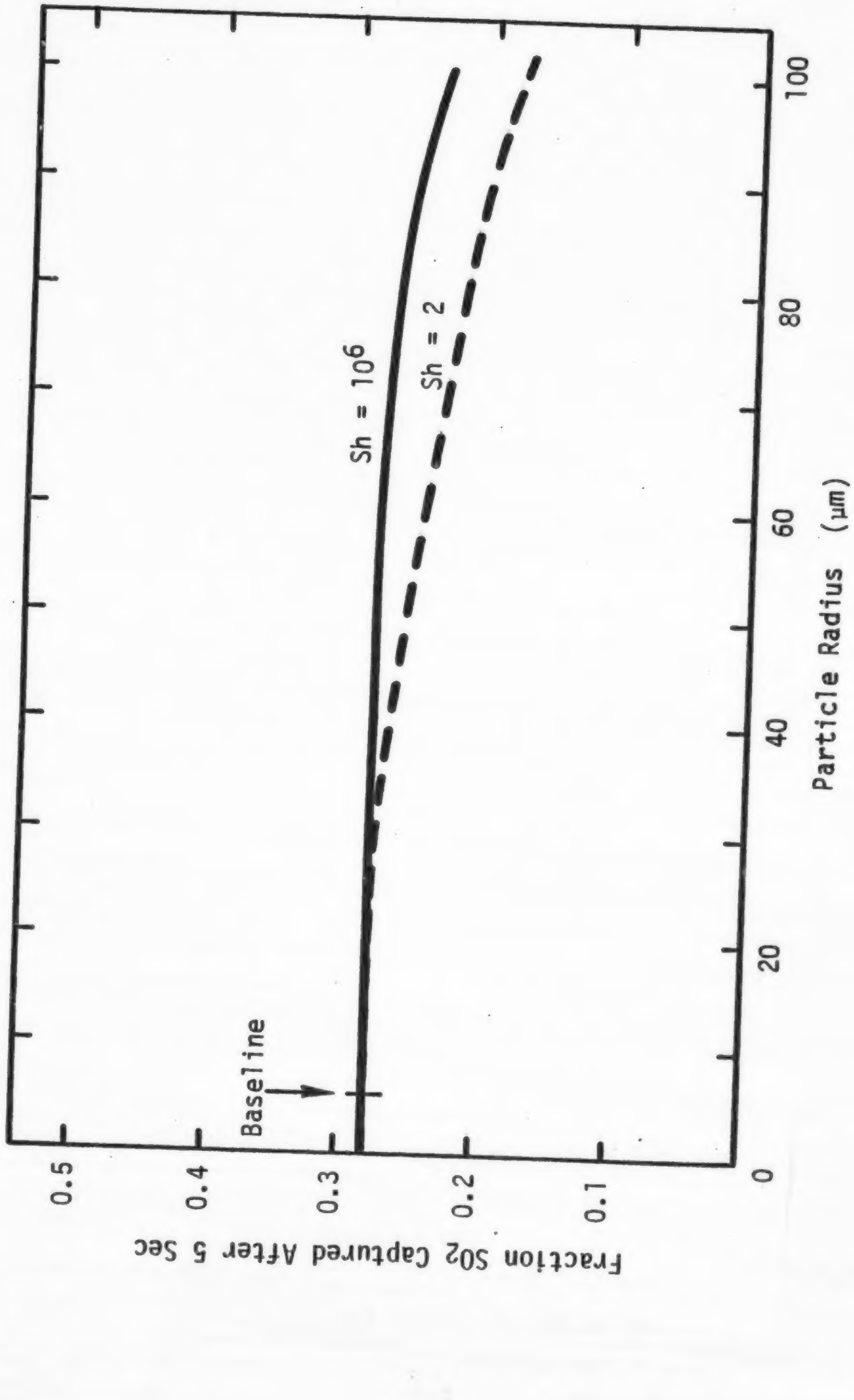

Figure D-15. Predicted effect of particle size.

effects of time-at-temperature on sorbent surface area. A pore model of the sulfation process is used. The pore model considers diffusion of SO_2 into the sorbent pores, chemisorption and reaction with the solid, diffusion of SO_2 through the sulfate layer, pore blockage and the limits of sulfate stability.

The sulfation portion of the model was tested against the original development of the pore model, against a grain type model applied by a group at the University of Utah (Silcox, et al.) and against sulfation data obtained by Borgwardt all with good agreement.

The sensitivity of the model to various parameters including pore-size characteristics, surface area, temperature, calcium-to-sulfur ratio, the selected intrinsic rate constant (derived from kinetic data and subject to some variation in interpretation), sulfate product layer diffusivity and Sherwood number (which influences the SO_2 concentration gradient at the particle surface) was tested. The parameters which had a significant effect on capture were the porosity/pore size/surface area of the sorbent (these are interrelated) and to a lesser extent, time, temperature, SO_2 concentration and Ca/S ratio.

The sulfation portion of the model is probably adequate for the model application needs. The sorbent activation portion of the model is the best currently available, but is over-simplified and should be refined as data on the effects of calcination conditions and input sorbent characteristics becomes available.

NOMENCLATURE

a = stoichiometric coefficient for SO_2

b = stoichiometric coefficient for C_a

C = local concentration of SO_2 (mole/cm^3)

D_e = effective diffusivity of SO_2 in pores (cm^2/sec)

D_p = effective diffusivity of SO_2 in product layer (cm^2/sec)

L_o = total length of pore system per unit volume (cm/cm^3)

K_s = rate constant for surface reaction cm^4/mole-sec

M = Molecular weight of CaO (9/mole)

r = distance from the particle center (cm)

R = particle radius

S_o = initial pore surface area per kunit volume (cm^2/cm^2)

t = time (sec)

X = local conversion

Z = ratio of volume of solid phase after reaction to that before reaction

$$\beta = \frac{2K_s\ a\ \rho\,(1-\epsilon_o)}{M\ b\ D_p\ S_o}$$

E_o = Initial porosity (cm^3/cm^3)

W_o = Mass fraction of CaO in initial solid particle

$$\psi = \frac{4\pi\ L_o\ (1 - \epsilon_o)}{\nu\ S_o^2}$$

ρ = Mass of CaO per unit volume of solid phase